

AD-A274 137



AFIT/GE/ENG/94M-01

DTIC
ELECTE
DEC 27 1993
S E D

AUTOMATION OF FORMATION FLIGHT CONTROL

THESIS

Vincent P. Reyna
First Lieutenant, USAF

AFIT/GE/ENG/94M-01

93-31041



19380

Approved for public release; distribution unlimited

93 12 22 1 54

The views expressed in this thesis are those of the author and do not reflect the official policy or position of the Department of Defense or the U. S. Government.

Accession For	
NTIS CRA&I	<input checked="" type="checkbox"/>
DTIC TAB	<input type="checkbox"/>
Unannounced	<input type="checkbox"/>
Justification	
By	
Distribution /	
Availability Codes	
Dist	Avail and/or Special
A-1	

DTIC QUALITY INSPECTED 2

AFIT/GE/ENG/94M-01

AUTOMATION OF FORMATION FLIGHT CONTROL

THESIS

**Presented to the Faculty of the Graduate School of Engineering
of the Air Force Institute of Technology**

Air University

**In Partial Fulfillment of the
Requirements for the Degree of
Master of Science in Electrical Engineering**

**Vincent P. Reyna, B.S. Astronautical Engineering
First Lieutenant, USAF**

March, 1994

Approved for public release; distribution unlimited

Acknowledgements

I am indebted to Dr Meir Pachter and Dr John J. D'Azzo for their help and guidance through the course of this research. The problem of Automated Formation Flight Control is quite an interesting one. Their insights helped me considerably. They taught me to think critically about problems, instead of blindly applying theories and mathematics in a mechanical manner. I will always be grateful for their patience with me.

I also want to thank my Parents, Jim and Gloria. They do not live nearby, nor do I see them more than twice a year. However, their encouragement and prayers helped more than they know.

Most importantly, I would like to thank my wife, Lorraine. She has always been there when I needed her, even though she had studies of her own. She understood when I worked late and on weekends. She was grateful for whatever time we had together while this thesis was in preparation. She taught me to take one day at a time. Her kind of selfless person is rare in life. I love her very much.

Vincent P. Reyna

Table of Contents

	Page
Acknowledgements	ii
List of Figures	vii
List of Tables	xiii
List of Symbols	xv
Abstract	xix
 I. Introduction To Formation Flight Control Thesis	 1-1
1.1 Overview of Thesis	1-1
1.2 Formation Flight Control Motivation	1-2
1.3 Background Information For Thesis Effort	1-2
1.4 Summary of the Current Literature	1-6
1.5 Research Objective and Questions	1-6
1.6 Assumptions	1-7
1.7 Scope	1-8
1.8 Figures of Merit	1-9
1.9 Materials and Equipment	1-9
1.10 Conclusion	1-9
 II. Literature And Concept Review	 2-1
2.1 Equation of Coriolis	2-1
2.2 Intraformation Positioning System (IFPS)	2-2
2.3 Decoupling of Output: Porter's Design Method	2-3
2.4 AFIT Theses	2-5
2.5 Conclusion	2-5

	Page
III. Model and Simulation Development	3-1
3.1 Aircraft Models	3-1
3.2 Aircraft Sensor Measurements	3-5
3.3 Formation Coordinate System	3-5
3.4 Kinematic Equations	3-6
3.5 Initial Conditions	3-10
3.6 Simulation Overview	3-10
3.7 Two Dimensional Controller Development	3-12
3.7.1 PI Controller and Linear Mixer	3-12
3.8 Three Dimensional Controller Development	3-13
3.8.1 PI Control Laws for Three Dimensional Case	3-14
IV. Horizontal Formation Flight Control - Analysis	4-1
4.1 Theoretical Development	4-1
4.1.1 Y-Channel	4-7
4.1.2 X-Channel	4-12
4.2 Gain Envelopes	4-17
4.2.1 Buzogany's Test Case Plotted Inside Stability Envelope	4-27
4.2.2 Gain Envelope Conclusion	4-31
4.3 Pole Placement Through Controller and Linear Mixer Gain Ad-	
justment	4-32
4.3.1 Linear Mixer Gain Adjustment	4-35
4.3.2 Trial and Error: Mixer Gains	4-38
4.3.3 Varying Y-Channel PI Controller Gains Only	4-41
4.3.4 Varying X-Channel PI Controller Gains Only	4-44
4.3.5 Trial and Error: PI Controller Gains	4-44
4.3.6 Comparison of New Dimensional Gains With Those of	
Dargan's	4-47

	Page
4.4 Dimensional Eigenvalue Comparison	4-50
4.4.1 Plots of Linear System Response To A Unit Step . .	4-55
4.5 Conclusion	4-55
V. Three Dimensional Energy Excursion Minimizing Maneuvers	5-1
5.1 Development	5-2
5.1.1 Difference Between The New Approach and Previous (Busogany's) Approach	5-9
5.1.2 Static Stability Analysis	5-12
5.1.3 Dynamic Stability Analysis	5-13
5.2 Mathematical Analysis of Three Dimensional Maneuvers . .	5-15
5.3 Graphical Comparison of Implementations: Energy Excursion Minimizing and Energy Conserving	5-18
5.4 Energy Excursion Minimizing Maneuvers Simulation	5-18
5.5 Dimensional Eigenvalue Analysis	5-21
5.5.1 Nonlinear Three Dimensional Maneuvers Simulation	5-24
5.6 New Approach To V_{W_c}	5-28
5.7 Dimensional Eigenvalue Analysis For New V_{W_c}	5-29
5.7.1 Nonlinear Simulations With New V_{W_c}	5-32
5.8 Conclusions	5-34
VI. Comparison of Two Dimensional and Three Dimensional Maneuvers . .	6-1
6.1 Nonlinear Simulations	6-1
6.2 Discussion	6-1
6.3 Conclusion	6-9
VII. Analysis and Conclusions	7-1
7.1 Objectives of Research Met	7-1
7.1.1 Horizontal Formation Flight Control - Analysis . . .	7-1

	Page
7.1.2 Three Dimensional Energy Excursion Minimizing Ma- neuvers	7-2
7.1.3 Comparison Of Formulations	7-2
7.2 Conclusions and Lessons Learned	7-3
7.3 Recommendations For Further Study	7-4
7.4 Summary	7-6
Appendix A. Dimensional Plant Matrices	A-1
A.1 Chapter IV Dimensional Models	A-1
A.1.1 Y-Channel	A-1
A.1.2 X-Channel	A-1
A.2 Chapter V Dimensional Model	A-2
Appendix B. Stability Equations From Chapter V	B-1
Appendix C. Y and X Channel Stability Constraints Plotted Separately .	C-1
Appendix D. Energy Minimizing Maneuvers Without e_w in V_w	D-1
D.1 Static Stability Analysis	D-2
D.2 Dynamic Stability Analysis	D-2
Bibliography	BIB-1
Vita	VITA-1

List of Figures

Figure	Page
1.1. Trail Formation [2:Figure 1.1]	1-3
1.2. Diamond Formation [2:Figure 1.2]	1-4
1.3. Diamond Formation Heading Change Maneuver	1-5
1.4. Trail Formation Altitude Change Maneuver [2:Figure 1.4]	1-5
1.5. Trail To Diamond Formation Change Maneuver [2:Figure 1.5]	1-6
2.1. Inertial And Rotating Frames of Reference [2:Figure 1.7]	2-2
2.2. Output Feedback Tracking System With PI Controller [5:Figure 20.1] .	2-4
2.3. Output Feedback Tracking System With PI Controller Utilising Measurement Matrix To Correct For Irregular Plant [5:Figure 20.4]	2-4
3.1. First Order Models Used In Simulations	3-3
3.2. Simulation of C-130A and C-130B Aircraft Channels	3-4
3.3. Inertial Reference Frame and Separation Distances [2:Figure 2.3] . . .	3-6
3.4. Wing's Rotating Reference Frame and Separation Distances [2:Figure 2.4]	3-7
3.5. Relative Motion Diagram [2:Figure 2.5]	3-8
3.6. Upper and Lower Tier Implementation Strategy	3-11
4.1. Formation Geometry	4-2
4.2. Nondimensional Y-Channel Constraints	4-21
4.3. Nondimensional Y-Channel Envelope: Stability Between the Surfaces .	4-22
4.4. Nondimensional X-Channel Constraints	4-23
4.5. Nondimensional X-Channel Envelope: Stability Between the Surfaces .	4-24
4.6. Nondimensional Y-Channel, Buzogany's Case: No Mixer, $\alpha = 45^\circ$; Shaded Region Denotes Stability	4-25
4.7. Nondimensional X-Channel, Buzogany's Case: No Mixer, $\alpha = 45^\circ$; Shaded Region Denotes Stability	4-26

Figure	Page
4.8. Buzogany's Case (No Mixer): Nondimensional Stability Envelopes With Test Case Plotted (See Figure 4.6 to Examine Entire Buzogany Y-Channel Envelope)	4-29
4.9. Nondimensional Y Stability Envelope With Test Case Plotted	4-30
4.10. Nondimensional X Stability Envelope With Test Case Plotted	4-30
4.11. Nondimensional Y Stability Envelope With Test Case Plotted and k_ψ Varied	4-31
4.12. Nondimensional X Stability Envelope With Test Case Plotted and k_ψ Varied	4-32
4.13. Comparison of Linear and Rate-Limited Velocity Responses [2:Figure 5.2]	4-34
4.14. Linear System: Y-Channel, ψ_w Heading Step Response, Poles and Residues Versus k_ψ	4-36
4.15. Linear System: X-Channel, V_w Velocity Step Response, Poles and Residues Versus k_ψ	4-37
4.16. C-130A: Diamond Formation, 10 Degree Heading Change, Time Response Comparison of Buzogany's (solid line) and New Gains (dashed line)	4-39
4.17. C-130A: Diamond Formation, 25 $\frac{ft}{sec}$ Velocity Change, Time Response Comparison of Buzogany's (solid line) and New Gains (dashed line)	4-40
4.18. Linear System: Y-Channel, ψ_w Heading Step Response, Poles and Residues Versus Controller Gains, $\frac{k_{xz}}{k_{yi}} = 100$	4-42
4.19. Linear System: X-Channel, V_w Heading Step Response, Poles and Residues Versus Controller Gains, $\frac{k_{xz}}{k_{yi}} = 100$	4-43
4.20. C-130A: Diamond Formation, 10 Degree Heading Change, Time Response Comparison of Figure 4.16 (solid line) and New PI Gains (dashed line)	4-45
4.21. C-130A: Diamond Formation, 25 $\frac{ft}{sec}$ Velocity Change, Time Response Comparison of Figure 4.17 (solid line) and New Gains (dashed line)	4-46
4.22. C-130B: Diamond Formation, 30 Degree Heading Change, Time Response Comparison Of Dargan/Buzogany Gains For Mixer And PI Controller (solid line) And New PI Gains (dashed line). First-Order Models Are Used	4-48

Figure	Page
4.23. C-130B: Diamond Formation, 25 $\frac{ft}{sec}$ Velocity Change, Time Response Comparison Of Dargan/Buzogany Gains For Mixer And PI Controller (solid line) And New PI Gains (dashed line). First-Order Models Are Used	4-49
4.24. C-130B: Diamond Formation, 30 Degree Heading Change, Time Response Comparison Of Dargan/Buzogany Gains For Mixer And PI Controller (solid line) And New PI Gains (dashed line). First-Order Models Are Used. $k_s = 3$	4-51
4.25. C-130B: Diamond Formation, 25 $\frac{ft}{sec}$ Velocity Change, Time Response Comparison Of Dargan/Buzogany Gains For Mixer And PI Controller (solid line) And New PI Gains (dashed line). First-Order Models Are Used. $k_s = 3$	4-52
4.26. (Linear System) TOP: New ψ_w Response to a Unit Step Disturbance (ψ_{Lc}) with Mixer and PI Controller; BOTTOM: Buzogany's ψ_w Response to a Unit Step Disturbance (ψ_L) with Mixer Only	4-56
4.27. (Linear System) TOP: New V_w Response to a Unit Step Disturbance (V_{Lc}) with Mixer and PI Controller; BOTTOM: Buzogany's V_w Response to a Unit Step Disturbance (V_L) with Mixer Only	4-57
4.28. Linear System: V_w Response to a Unit Step Disturbance ($d\psi$)	4-58
5.1. Comparison of $v(t)$ (solid line) and $h(t)$ (dotted line)	5-11
5.2. Energy Conservation: Buzogany's Three Dimensional Maneuvers Simulation Formulation, With the Aircraft Specific Energy Rate = 0	5-17
5.3. Energy Excursion Minimization: New Three Dimensional Maneuvers Simulation Formulation	5-17
5.4. Nonlinear Simulation, C-130A Aircraft: Comparison of Buzogany's Implementation (solid line) and New Implementation (dashed line) in Equation (5.23)	5-19
5.5. Nonlinear Simulation, C-130A Aircraft, With Velocity and Altitude Error Signal Limiters Eliminated: Comparison of Buzogany's Implementation (solid line) and New Implementation (dashed line) in Equation (5.23)	5-20

Figure	Page
5.6. XZ-Channel, Wing Velocity Response, Dimensional Poles and Residues versus Controller Gains, $\frac{k_{asy}}{k_{asyV}} = 100$	5-23
5.7. C-130A: Diamond Formation, 10° Side Step Heading Change. Nonlinear Simulation: Energy Conserving Implementation (solid line) and Energy Excursion Minimizing Implementation (dashed line)	5-25
5.8. C-130A: Diamond Formation, 90° Heading Change. Nonlinear Simulation: Energy Conserving Implementation (solid line) and Energy Excursion Minimizing Implementation (dashed line)	5-26
5.9. C-130A: Diamond Formation, 25 $\frac{ft}{sec}$ Velocity Change. Nonlinear Simulation: Energy Conserving Implementation (solid line) and Energy Excursion Minimizing Implementation (dashed line)	5-27
5.10. XZ-Channel, Wing Velocity Response, Dimensional Poles and Residues versus Controller Gains, $\frac{k_{asy}}{k_{asyV}} = 100$	5-30
5.11. C-130A: Nonlinear Simulation, Response To A 10° Side Step Heading Change: Energy Conserving Implementation (solid line) and Energy Excursion Minimizing Implementation (dashed line)	5-35
5.12. C-130A: Nonlinear Simulation, Response To A 90° Step Heading Change: Energy Conserving Implementation (solid line) and Energy Excursion Minimizing Implementation (dashed line)	5-36
5.13. Diamond Formation 90° Heading and Formation Change Utilizing Energy Conserving/Excursion Minimizing [2:Figure 6.6]	5-37
5.14. C-130A: Nonlinear Simulation, Response To A 25 $\frac{ft}{sec}$ Step Velocity Change: Energy Conserving Implementation (solid line) and Energy Excursion Minimizing Implementation (dashed line)	5-38
5.15. C-130A: Nonlinear Simulation, Response To A 100 ft Step Altitude Change: Energy Conserving Implementation (solid line) and Energy Excursion Minimizing Implementation (dashed line)	5-39
6.1. C-130A: Diamond Formation, 10° Side Step Heading Change. Nonlinear Simulation: Energy Conserving Implementation (solid line), Energy Minimizing Implementation (dashed line), and Two Dimensional Implementation (dotted line)	6-2

Figure	Page
6.2. C-130A: Diamond Formation, 90° Heading Change. Nonlinear Simulation: Energy Conserving Implementation (solid line), Energy Minimizing Implementation (dashed line), and Two Dimensional Implementation (dotted line)	6-3
6.3. C-130A: Diamond Formation, 25 $\frac{ft}{sec}$ Velocity Change. Nonlinear Simulation: Energy Conserving Implementation (solid line), Energy Minimizing Implementation (dashed line), and Two Dimensional Implementation (dotted line)	6-4
6.4. C-130A: Nonlinear Simulation, Response To A 100 ft Step Altitude Change: Energy Conserving Implementation (solid line), Energy Minimizing Implementation (dashed line), and Two Dimensional Implementation (dotted line)	6-5
C.1. Plot of the Nondimensional Y-Channel Stability Constraint for Row s^3 of the Routhian Array (Equation (4.84))	C-2
C.2. Plot of the Nondimensional Y-Channel Stability Constraint for Row s^2 of the Routhian Array (Equation (4.85))	C-3
C.3. Plot of the Nondimensional Y-Channel Stability Constraint for Row s^1 of the Routhian Array (Equation (4.86))	C-4
C.4. Plot of the Nondimensional Y-Channel Stability Constraint for Row s^0 of the Routhian Array (Equation (4.87))	C-5
C.5. All of the Nondimensional Y-Channel Stability Constraints	C-6
C.6. Nondimensional Y-Channel Envelope: Stability Between the Surfaces	C-7
C.7. Plot of the Nondimensional X-Channel Stability Constraint for Row s^3 of the Routhian Array (Equation (4.88))	C-8
C.8. Plot of the Nondimensional X-Channel Stability Constraint for Row s^2 of the Routhian Array (Equation (4.89))	C-9
C.9. Plot of the Nondimensional X-Channel Stability Constraint for Row s^1 of the Routhian Array (Equation (4.90))	C-10
C.10. Plot of the Nondimensional X-Channel Stability Constraint for Row s^0 of the Routhian Array (Equation (4.91))	C-11
C.11. All of the Nondimensional X-Channel Constraints	C-12

Figure

Page

C.12. Nondimensional Y-Channel Envelope: Stability Between the Surfaces .

C-13

List of Tables

Table	Page
3.1. Aircraft Rate Limits and Model Time Constants [2:Table 2.1]	3-2
4.1. Y-Channel Routhian Array	4-11
4.2. X-Channel Routhian Array	4-15
4.3. Test Case: Formation, Aircraft Parameters, and Pertinent Gains . . .	4-28
4.4. Values of Test Case Plotted in 3-Dimensional Nondimensional Stability Envelopes	4-29
4.5. Variance of Nondimensional Mixer Gains for Plots	4-31
4.6. Dimensional Mixer Gains	4-40
4.7. Dimensional PI Controller Gains Used In Simulations	4-41
4.8. Adjusted Dimensional PI Controller Gains Used In Simulations To Achieve Better Performance	4-44
4.9. Dargan's Dimensional Gains (See Also Table 4.10 For Adjusted k_p) . .	4-47
4.10. Adjusted Gain To Refine Response of Figure 4.22	4-50
4.11. Mixer and PI Controller Gains Used In Dimensional Eigenvalue Comparisons	4-53
5.1. XZ-Channel Routhian Array	5-14
5.2. PI Controller Values For Equation (5.23) and Nonlinear Simulation Shown in Figures 5.7 - 5.9	5-24
5.3. PI Controller Values For Equation (5.64) and Nonlinear Simulations Using New V_{W_c} : Heading Changes In Figures 5.11 and 5.12	5-32
5.4. PI Controller Values For Equation (5.64) and Nonlinear Simulation Using New V_{W_c} : Velocity Change In Figure 5.14	5-33
5.5. PI Controller Values For Equation (5.64) and Nonlinear Simulation Using New V_{W_c} : Altitude Change In Figure 5.15	5-33
6.1. Gains Used In Nonlinear Simulations To Compare All Three Methods For Heading, Velocity, and Altitude Changes In Figures 6.1 - 6.4 . . .	6-6

Table	Page
D.1. XZ-Channel Routhian Array	D-3

List of Symbols

Symbol		Page
ψ_L	lead aircraft heading	1-6
V_L	lead aircraft velocity	1-6
ψ_{Lc}	lead aircraft heading command	1-7
V_{Lc}	lead aircraft velocity command	1-7
\dot{R}_i	velocity of object in frame i	2-1
\dot{R}_p	velocity of object in frame p	2-1
ω_{ip}	angular velocity of frame p with respect to i	2-1
R_p	position of object in frame p	2-2
$x(t)$	state vector	2-3
A	plant matrix	2-3
B	input matrix	2-3
$u(t)$	input vector	2-3
$y(t)$	output vector	2-3
C	output matrix	2-3
τ_v	time constant of velocity channel	3-1
τ_ψ	time constant of heading channel	3-1
τ_h	time constant of altitude channel	3-1
V_{WL}^W	velocity of the lead aircraft with respect to the wing, in the wing's reference frame	3-7
ω_W^W	angular velocity of the wing in the wing's reference frame	3-7
R_{WL}^W	position of lead aircraft with respect to wing in the wing's reference frame	3-7
R_W^W	position of wing aircraft in its own reference frame	3-7
V_W^W	inertial velocity of wing aircraft in its own reference frame	3-7
V_L^W	inertial velocity of lead aircraft in the wing's reference frame	3-7
ψ_B	heading error	3-8

Symbol		Page
V_L^L	inertial velocity of the lead aircraft in its own frame of reference . . .	3-8
$\dot{\psi}$	heading rate	3-10
\dot{z}^W	altitude rate	3-10
z	$z_c^W - z^W$, x separation error	3-12
V_E	velocity error signal	3-12
k_V	velocity error mixer gain	3-12
k_z	x separation error mixer gain	3-12
k_{zp}	z-channel proportional gain	3-13
k_{zi}	z-channel integral gain	3-13
y	$y_c^W - y^W$, y separation error	3-13
k_ψ	heading error mixer gain	3-13
k_y	y separation error mixer gain	3-13
k_{yp}	y-channel proportional gain	3-13
k_{yi}	y-channel integral gain	3-13
z	$z_c^W - z^W$, z separation error	3-13
k_{zp}	z-channel proportional gain	3-13
k_{zi}	z-channel integral gain	3-13
k_{zzp}	zz-channel proportional gain	3-14
k_{zzi}	zz-channel integral gain	3-14
e_W	specific energy of an aircraft	3-14
h_W	perturbation away from nominal for wing altitude	3-14
τ_{V_W}	time constant of wing velocity channel	3-14
τ_{h_W}	time constant of wing altitude channel	3-14
g	acceleration of gravity	3-14
V_o	nominal velocity of the formation	3-14
k_{zspv}	zz-channel, altitude error proportional gain	3-14
k_{zsiw}	zz-channel, altitude error, integral gain	3-14

Symbol		Page
h_e	$h_L - h_W$, altitude error	3-15
z_o	nominal x separation	4-2
y_o	nominal y separation	4-2
α	separation angle	4-2
τ_{V_W}	the velocity time constant of the wing	4-3
τ_{ψ_W}	the heading time constant of the wing	4-3
τ_{V_L}	the velocity time constant of the lead	4-3
τ_{ψ_L}	the heading time constant of the lead	4-3
l	characteristic length of the nominal formation separation	4-4
\bar{t}	characteristic time	4-4
V_o	nominal formation velocity	4-4
\hat{z}	nondimensional x separation error	4-4
\hat{y}	nondimensional y separation error	4-5
\hat{z}_o	nondimensional nominal x separation	4-5
\hat{y}_o	nondimensional nominal y separation	4-5
\hat{V}_W	nondimensional wing velocity	4-5
\hat{V}_{W_c}	nondimensional commanded wing velocity	4-5
\hat{V}_L	nondimensional lead velocity	4-5
\hat{V}_{L_c}	nondimensional commanded lead velocity	4-5
$\hat{\tau}_{V_W}$	nondimensional wing velocity time constant	4-5
$\hat{\tau}_{\psi_W}$	nondimensional wing heading time constant	4-5
$\hat{\tau}_{V_L}$	nondimensional lead velocity time constant	4-5
$\hat{\tau}_{\psi_L}$	nondimensional lead heading time constant	4-5
Γ	disturbance input matrix	4-6
D	disturbance input vector	4-6
Y	output vector	4-6
C	output matrix	4-6

Symbol		Page
X_y	augmented y-channel state vector	4-9
A_y	augmented y-channel plant	4-9
Γ_y	augmented y-channel input matrix	4-9
D_y	augmented y-channel input vector	4-9
Y_y	augmented y-channel output vector	4-9
C_y	augmented y-channel output matrix	4-9
X_x	augmented x-channel state vector	4-14
A_x	augmented x-channel plant	4-14
Γ_x	augmented x-channel input matrix	4-14
D_x	augmented x-channel input vector	4-14
Y_x	augmented x-channel output vector	4-14
C_x	augmented x-channel output matrix	4-14
T	aircraft's thrust	5-6
D	aircraft's drag	5-6
m	aircraft's mass	5-6
h_e	$h_L - h_W =$ altitude error	5-6
k_{zspv}	nondimensional, three dimensional altitude error, proportional gain .	5-6
k_{zsiV}	nondimensional, three dimensional altitude error, integral gain	5-6
X_{zscd}	augmented zz -channel state vector	5-8
A_{zscd}	augmented zz -channel plant matrix	5-8
Γ_{zscd}	augmented zz -channel input matrix	5-8
D_{zscd}	augmented zz -channel input vector	5-9
Y_{zscd}	augmented zz -channel output vector	5-9
C_{zscd}	augmented zz -channel output matrix	5-9

Abstract

The research contained in this thesis continues to explore the concepts of Automated Formation Flight Control documented in three previous AFIT theses. The generic formation analyzed consists of a Leader and Wingman, with the Wingman referencing its maneuvers off of Leader maneuvers. Specifically, planar formation flight control concerning only heading and velocity changes is considered. Next, the vertical separation constraint is relaxed to allow wing maneuvers outside of the flight plane of the lead in order to minimize the energy expended by the wing in a maneuver. Analysis of the two forms of formation flight control investigated in this thesis reveals the close relationship between formation geometry, aircraft time constants, controller gains, formation performance, and control system stability. Integral control action is determined to be necessary for formation flight control. Nonlinear simulations are accomplished on a digital computer to validate the analysis of the automated formation flight control system. Comparisons are made between the two forms of formation flight control considered, and a third, energy conserving maneuvers, in order to determine which is best for each phase of flight.

AUTOMATION OF FORMATION FLIGHT CONTROL

I. Introduction To Formation Flight Control Thesis

1.1 Overview of Thesis

This thesis effort is different than other theses in the area of flight control. Its purpose is not to synthesize a controller to provide desirable flying qualities of an aircraft. Instead, the emphasis is on controlling a formation of aircraft equipped with flight control systems. This is a high level control problem.

The first chapter provides an introduction to the Automatic Formation Flight Control problem analyzed in this research. It gives the background, the assumptions, the research questions answered, and the scope of the thesis.

The second chapter reviews the literature pertaining to the formation flight control problem. It gives a brief overview of related work and discusses the relevance of this thesis.

The third chapter provides a "blueprint" of the model and simulation development used in this thesis. It is hoped, that on reading this chapter and understanding the intricacies of the simulation models, one will be able to reproduce the simulations performed in this thesis.

The fourth chapter begins the new research into the area of Automatic Formation Flight Control by extending Buzogany's research from December of 1992. It is the development of the analytical formulation for the formation flight controller, using two dimensional maneuvers (i.e., the wing aircraft follows lead aircraft maneuvers, maintaining the same altitude as the lead). The difference between last year's approach and this year's is the inclusion of additional measurements, i.e., the heading error and velocity error, and the use of a linear mixer. This mandates the incorporation of the lead aircraft states into the system model. Previously, the lead aircraft states were assumed to be the disturbances affecting/driving the formation flight control system. Now, the lead aircraft commands play the role of disturbances driving the formation flight control system.

The fifth chapter extends the energy conserving maneuvers concept first investigated by Buzogany and explores energy excursion minimizing maneuvers. In Buzogany's thesis, the wing aircraft was allowed to moderate its speed by making excursions outside the flight plane of the lead aircraft, in order that the specific energy of the wing be maintained at a constant level. However, wing aircraft capability is decreased because only formation heading changes could be made. Now, the wing aircraft is still allowed to deviate from the lead's flight plane, however, it now can make velocity and altitude changes in addition to heading changes, while at the same time minimizing the specific energy excursions.

The sixth chapter compares the three concepts of formation flight control investigated in this and previous theses. The relative advantages of each method are ascertained.

The final chapter summarizes the finding of this research, provides conclusions, and makes recommendations for further research.

1.2 Formation Flight Control Motivation

Air Force Airborne Special Operations Forces must be able to operate in hostile environments in order to successfully complete their mission. In addition to weather, terrain avoidance, and enemy opposition, their missions may require formation flights, composed of dissimilar aircraft, flying at low altitudes in close proximity to each other. The increased additional pilot workload imposed on pilots in these situations is known to result in pilot fatigue and decreased mission effectiveness. Some reliable and safe form of automatic formation control, similar to an automatic pilot, would be beneficial. Hence, the need to decrease pilot work load is the impetus for research into the area of Automatic Formation Flight Control. This technology will increase aircraft safety during prolonged missions.

1.3 Background Information For Thesis Effort

C-130 aircraft, models A and B, are the aircraft models employed in this research. They are chosen for the following reasons:

1. C-130s currently participate in Special Operations Missions

2. C-130s were used in the previous three thesis efforts in this area, thus providing a baseline by which new research can be compared

Two generic formations were investigated in previous thesis efforts and are reviewed in this chapter. These formations are the trail and diamond formations illustrated in Figures 1.1 and 1.2, respectively.

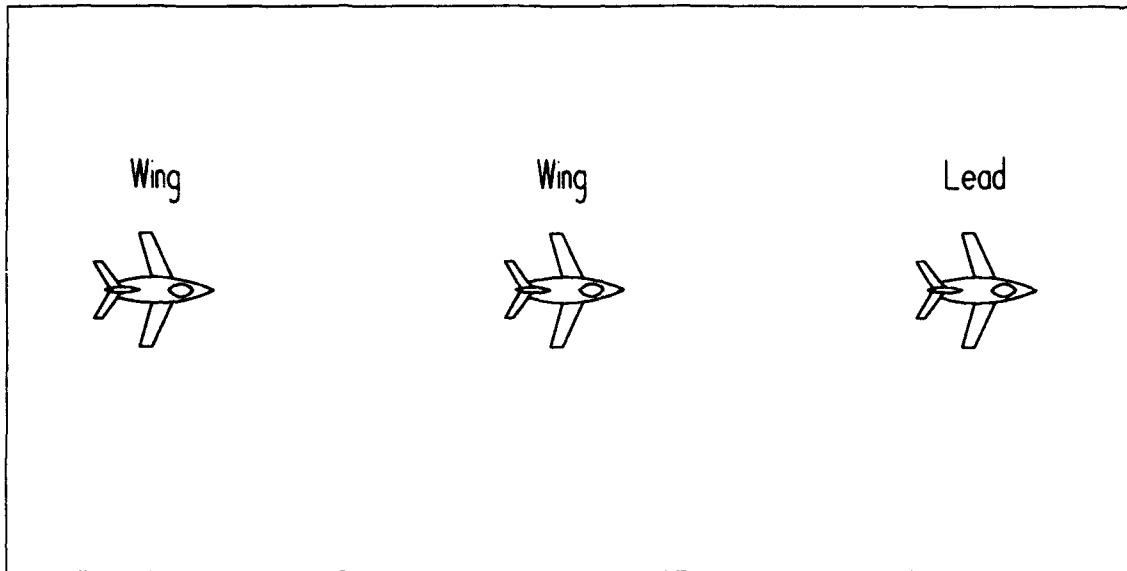


Figure 1.1 Trail Formation [2:Figure 1.1]

The formations chosen have good operational characteristics. The trail formation reduces the probability of detection by hostile ground forces since a minimum amount of land is traversed by the aircraft in formation. In contrast, the diamond formation will over-fly a larger patch of the earth, however, it provides good visibility between various aircraft [2:page 1-2].

A formation is not a static entity. Throughout the course of a mission, a typical aircraft formation will make several maneuvers, initiated by the lead aircraft, that the wing aircraft must also make while still maintaining the formation. Typical maneuvers include changes in velocity, heading, altitude, or a combination thereof. An example of these maneuvers is illustrated in Figures 1.3 and 1.4, where a diamond formation heading change and a trail formation altitude change are respectively shown. In addition, the formation geometry may not remain constant throughout the flight. It is quite possible

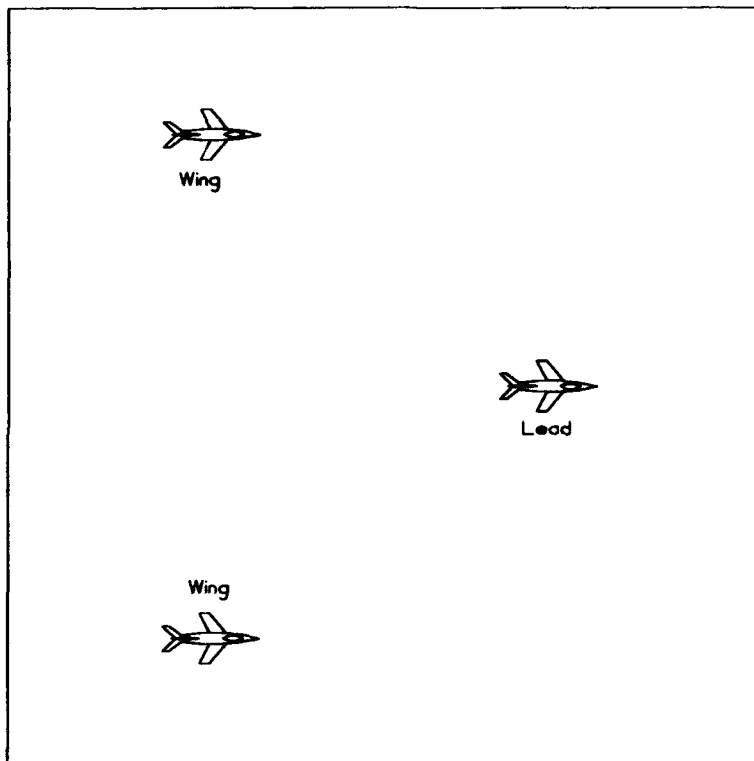


Figure 1.2 Diamond Formation [2:Figure 1.2]

that the formation geometry will change as the threat changes. An example of this is shown in Figure 1.5 [2:page 1-3].

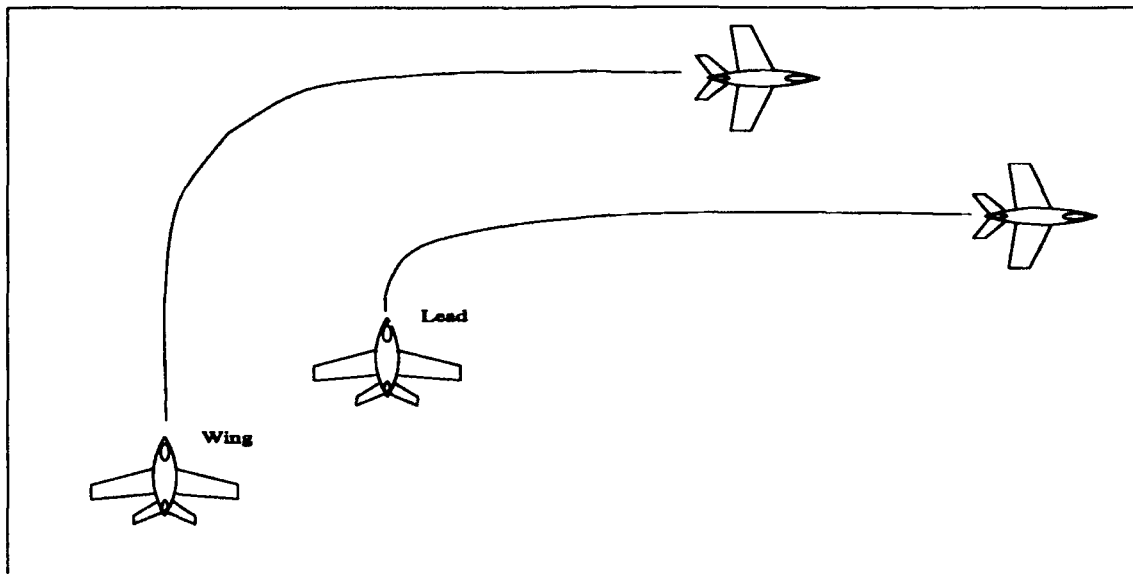


Figure 1.3 Diamond Formation Heading Change Maneuver

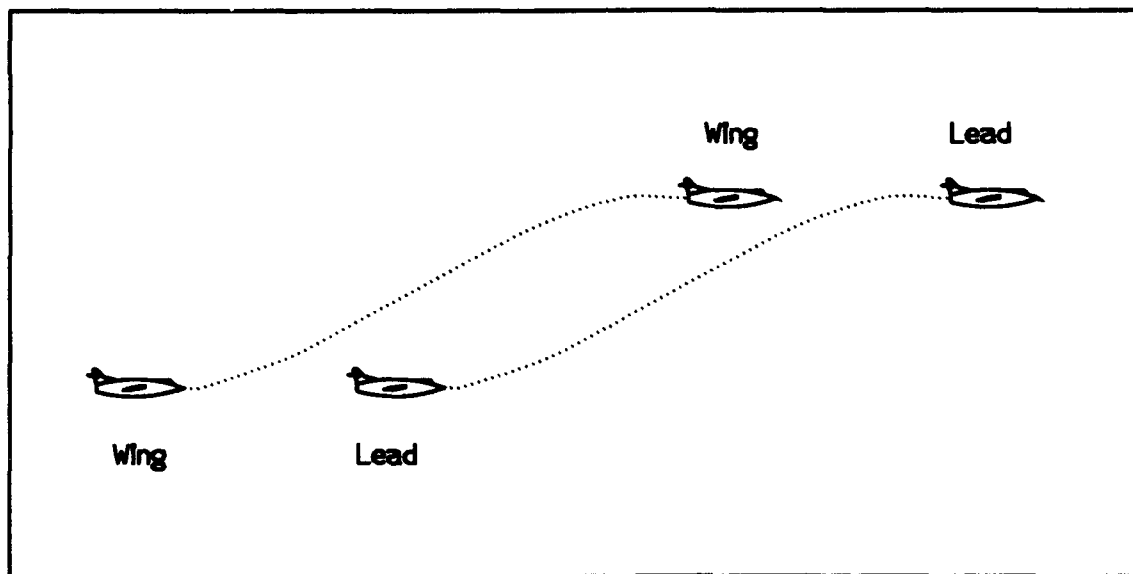


Figure 1.4 Trail Formation Altitude Change Maneuver [2:Figure 1.4]

This research is particularly concerned with the diamond formation. It was used extensively by Buzogany. Since Buzogany's thesis is used as a baseline, the diamond formation is simulated exclusively, due to time constraints.

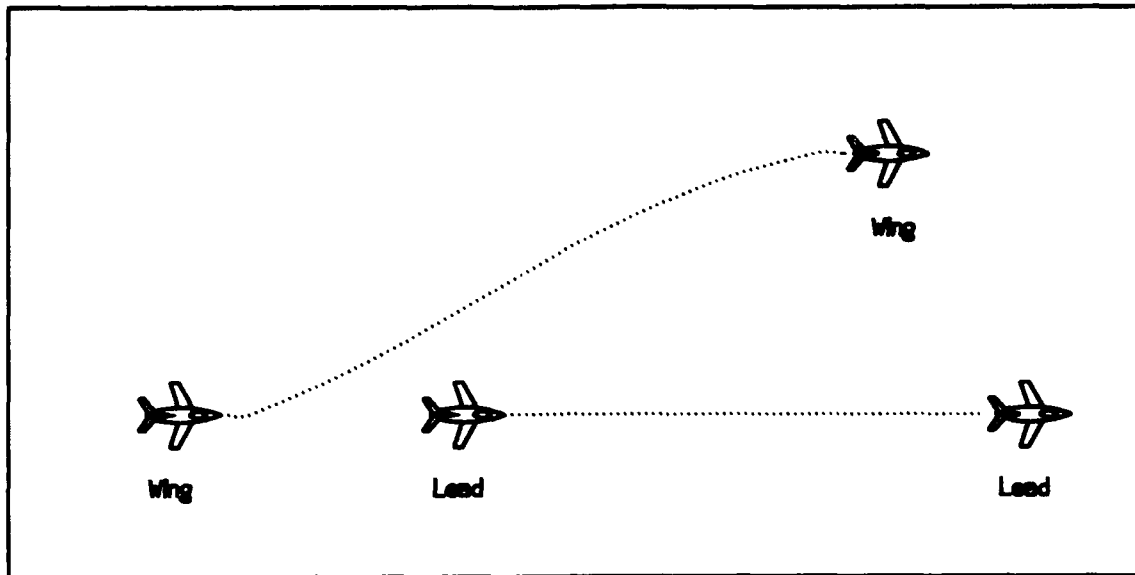


Figure 1.5 Trail To Diamond Formation Change Maneuver [2:Figure 1.5]

1.4 Summary of the Current Literature

See Chapter II.

1.5 Research Objective and Questions

The thrust of the current research into Formation Flight Control is to continue the work initiated by Rohs, Dargan, and Buzogany. This entails enhancing the modelling complexity of formation flight control, performing the required analysis, and concept validation that includes nonlinear computer simulations of the Formation Flight Control System. The following questions are answered in this research effort:

1. In previous research, it was assumed the lead aircraft states, ψ_L and V_L , the heading and velocity of the lead aircraft, were not measurable by the wing, and were the disturbances driving the formation flight control system. How is performance affected when:
 - (a) the lead aircraft states, ψ_L and V_L , are observables incorporated into the formation flight control model

- (b) the lead aircraft commands, ψ_L , and V_L , are the disturbances of the Formation Flight Control System?
- 2. Can a dominant pole be found through gain adjustments of the controller that will achieve "good" formation response to commanded inputs (See Section 1.8 for definition of "good")?
- 3. Is there a graphical way to investigate the stability of two dimensional maneuvers?
- 4. Previous research investigated the concept of three dimensional, energy conserving maneuvers. The concept is valid for heading change maneuvers only. It cannot perform formation energy change maneuvers adequately. Is it possible to enable a formation to do heading, velocity, and altitude changes while minimizing wing aircraft specific energy or excursions?
- 5. Compare the formation flight control concepts of:
 - (a) Two Dimensional (Planar) Formation Flight Control
 - (b) Energy Conserving
 - (c) Energy Excursion Minimizing

1.6 Assumptions

The assumptions need to be stated clearly in order to give the reader a complete picture of the problem. There are many assumptions necessary for this problem. This thesis effort is a building block. It adopts many of the same assumptions used in previous theses. In time, an effort such as this might result in an operational system using the concepts outlined in this thesis. If an operational implementation is ever to be attained, small stepping stones like this thesis need to be placed in order to provide a path toward a "real world" system. The assumptions are:

- 1. Each aircraft in the formation has the following autopilots in place:
 - (a) Mach-Hold Autopilot
 - (b) Heading-Hold Autopilot

(c) Altitude-Hold Autopilot

All aircraft in the formation are coordinated. A coordinated aircraft allows pilots to bank-to-turn without the problems associated with side slip velocity and adverse yaw. In other words, the flight control system works the rudder for the pilot in a turning condition to provide coordination [3:page 55].

2. No communication is necessary between the aircraft in the formation in order for the formation flight control system to work.
3. Each wing aircraft possesses a perfect on-board sensor capable of providing precise, real-time, position information with respect to the lead aircraft in the formation. No data delay is assumed.
4. Initial conditions for all simulations are straight and level flight in a constant formation.
5. Wing aircraft are controlled by the automatic formation flight control system. They automatically track maneuvers made by the lead aircraft.
6. In order for an analysis to be undertaken, the standard "small perturbations" flight control assumptions must be made: aircraft can be modelled by a linear system, the earth is flat, etc. Aircraft are highly nonlinear systems. Nonlinearities, such as kinematics, induced nonlinearities and saturations do play a prominent roll in formation flight control. A time invariant aircraft's only changing parameters are its inputs of thrust, and control surface deflection. Now the aircraft model will only respond to control inputs and not changing aircraft parameters. These are valid assumptions because the analysis time of interest is typically anywhere from 1 - 100 seconds after a maneuver has been performed. During this time the center of gravity is not moving a noticeable amount, nor does the aircraft's mass significantly change.

1.7 Scope

This research will use first-order models developed by Rohs [10] and Dargan [4]. The second-order models developed by Buzogany will not be used but will be recommended as

an extension to the analyses presented in this thesis. Both linear and nonlinear simulations are performed in order to validate and "fine tune" linear analyses.

1.8 Figures of Merit

There are no established "flying qualities" requirements for formation flight control. Safe maneuvering in a formation entails avoidance of other aircraft or the ground. Beyond this, there is a need for wing aircraft to be able to follow the lead. Additionally, large maneuver command inputs can produce unstable responses due to the nonlinear saturations in the system [2:page 2-14]. These common sense requirements can now be put into more technical specifications:

- Automatic Formation Flight Control System must be able to track commanded inputs with zero steady state error (i.e., wing aircraft follow the lead aircraft)
- The system must have "good" transient behavior (i.e., avoid collisions between aircraft)
- The system must be able to handle large command inputs [4:page 3-36] [2:page 2-14]

1.9 Materials and Equipment

A Sun Sparc Station 2 is the only hardware needed for this effort. In addition, a control system analysis software package is needed. Matlab 4.0 by Mathworks is the recommended software. This equipment is provided by the Department of Electrical and Computer Engineering in the Navigation and Flight Control Lab, Room 131, and in Room 2001, Building 641, Air Force Institute of Technology. In addition, the thesis document is written in \LaTeX , on a Unix platform (i.e, the Sun Sparc Station 2).

1.10 Conclusion

This thesis effort helps continue the development of Formation Flight Control. By alleviating pilot workload, Formation Flight Control will make aircraft missions more effective and safer for both aircrew and aircraft participating in war time missions.

II. Literature And Concept Review

This chapter explores the literature pertaining to the concept of Automatic Formation Flight Control. Its purpose is to inform the reader on research and concepts that directly apply to this research.

2.1 Equation of Coriolis

Similar to pilots flying in formation off the lead aircraft, an Automated Formation Flight Control system needs a frame of reference. Therefore, it is logical that all relevant commands to the formation be referenced to the lead aircraft. To accomplish this task, a rotating coordinate system is affixed to and centered upon the wing aircraft.

With different coordinate frames moving relative to each other, the Equation of Coriolis is used to express one frame's coordinates in terms of another. Blakelock states this equation in the following manner: "The motion of an object as viewed from a reference frame is equal to the motion as seen from the moving frame, plus the motion resulting from the relative angular velocity of the moving frame with respect to the reference frame" [1:page 489]. This fundamental mathematical theorem is the basis for any research in this area. It will allow the Formation Flight Control System to resolve all the aircraft data from the planes in formation to the reference coordinate system. Therefore, position, velocity, and acceleration of each aircraft in formation can be determined. Without this information, Formation Flight Control is not possible. In equation form, the Equation of Coriolis is [1:page 490]:

$$\dot{R}_i = \dot{R}_p + \omega_{ip} \times R_p$$

where (See Figure 2.1) [1:page 490].

\dot{R}_i = the vector velocity of the point in the i reference frame

\dot{R}_p = the vector velocity of the point in question as seen from the p reference frame

ω_{ip} = the angular velocity of the p reference frame with respect to the i reference frame

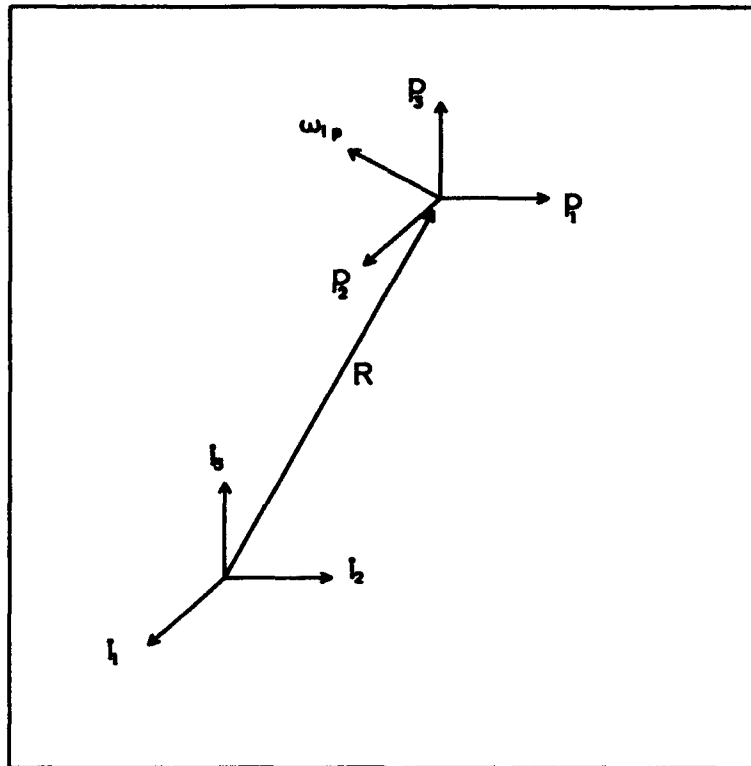


Figure 2.1 Inertial And Rotating Frames of Reference [2:Figure 1.7]

R_p is the position vector of a point in the p frame

2.2 Intraformation Positioning System (IFPS)

The Flight Dynamics Lab (WL/FIGS) is currently in the process of demonstrating a type of Formation Flight Control System. This system is a manual control system with the pilot of the wing aircraft flying a trajectory dictated by the flight computer [9]. The wing's trajectory is computed by determining how far away the wing is from the lead. When this is determined, the lead's trajectory is given to the wing through the Heads-Up Display (HUD) so the wing pilot can maintain formation by flying according to information displayed on the HUD[9]. There are no provisions for automatic control of the formation [9].

2.3 Decoupling of Output: Porter's Design Method

Decoupling of outputs in a multivariable control system is extremely desirable. If all the states of a system are accessible, output decoupling may be achieved. However, it is not always easy to gain access to all of the states of a system. The feedback loop of any aircraft is not a wire connected to the output of the aircraft. On the contrary, sensors provide the necessary feedback in order to close the loop. It would be better if output decoupling could take place with a smaller number of outputs, thus the inaccessible states would not be needed. A control design method which uses only output feedback to generate an error vector avoids the requirement for measuring or reconstructing the entire state vector. Dr. Brian Porter developed a method of designing a high gain proportional plus integral (PI) controller which produces output decoupling and leads to very fast tracking of the command input by the output. The standard MIMO (multiple-input, multiple-output) plant is represented by the following state and output equations [2:page 1-12] [4:page 2-4] [5:page 660]:

$$\dot{\mathbf{x}}(t) = \mathbf{A}\mathbf{x}(t) + \mathbf{B}\mathbf{u}(t) \quad (2.1)$$

$$\mathbf{y}(t) = \mathbf{C}\mathbf{x}(t) \quad (2.2)$$

where,

$\mathbf{x}(t)$ = state vector

\mathbf{A} = plant matrix

\mathbf{B} = input matrix

$\mathbf{u}(t)$ = input vector

$\mathbf{y}(t)$ = output vector

\mathbf{C} = output matrix

According to the D'Azzo and Houpis classical textbook [5:page 660], this design is dependent upon the first Markov parameter. The first Markov parameter is equal to the

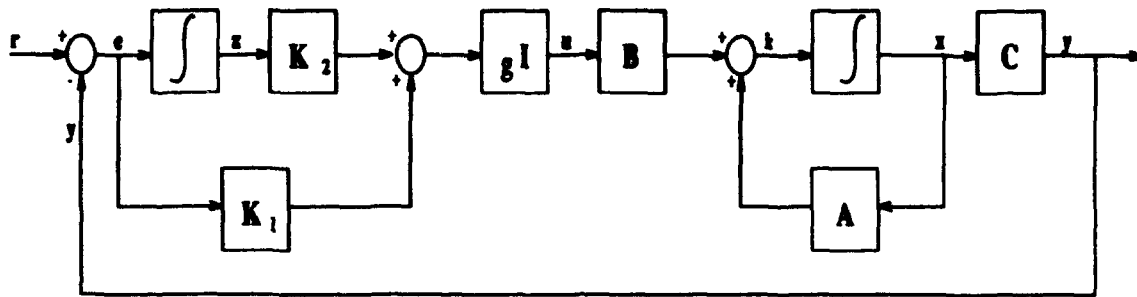


Figure 2.2 Output Feedback Tracking System With PI Controller [5:Figure 20.1]

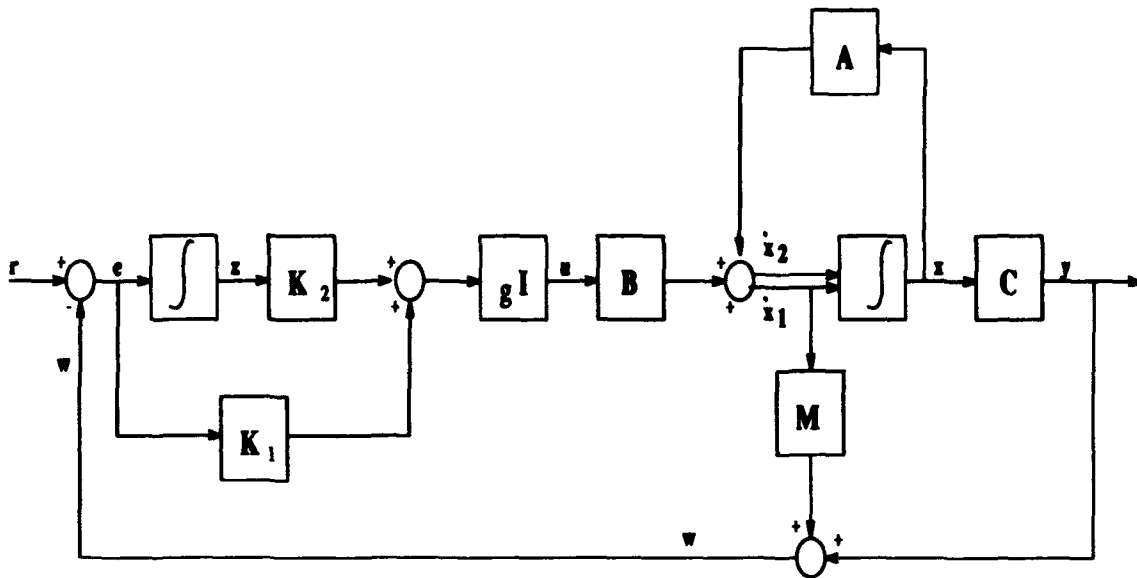


Figure 2.3 Output Feedback Tracking System With PI Controller Utilising Measurement Matrix To Correct For Irregular Plant [5:Figure 20.4]

matrix product CB . The rank of this product indicates whether the plant is one of two types: 1) If CB has full rank, the plant is considered regular, and 2) otherwise, the plant is considered irregular. Regular plants have a proportional plus integral (PI) control law implemented in the forward path of the control system operating on error taken from the input minus the output. Irregular plants have a PI controller augmented with an inner-loop providing extra measurements for control purposes [2:page 1-12] [4:page 2-4] [5:page 660]. Figures 2.2 and 2.3 show regular and irregular plants with their respective implemented PI controllers. These Figures are taken from Figures 20.1 and 20.4 of D'Asso and Houpis [5].

2.4 AFIT Theses

Three AFIT theses have described the topic of Formation Flight Control. The first was presented in March of 1991. These works are the most current documented research on this topic [9]. This thesis activity was sponsored by the Flight Dynamics Lab to look into the feasibility of Automatic Formation Flight Control.

Rohs' thesis was the first (March 1991). His research lays the groundwork for the investigation of Automatic Formation Flight Control. He concluded that manual flight control system, such as the IFPS, could not guarantee formation maintenance and could result in a collision [10:page 100]. Some form of feedback was necessary to prevent the outmaneuvering of a less capable aircraft [10:page 100]. Feedback of aircraft errors with respect to the formation makes possible automatic dissimilar aircraft formation flight.[10:page 100].

Dargan (December 1991) furthered this work by investigating different feedback parameters to control the formation. He concluded that velocity and heading feedback could be used to keep the required separation distances between aircraft [4:page 6-3]. The feedback gains were experimentally determined and consisted of a mix of separation and maneuver error [4:page 6-3].

Busogany was the last thesis student to tackle this problem (December 1992). He developed more accurate aircraft models and extended the investigation of this problem by looking at large heading changes and how they affect formation maintenance [2:page 8-5]. In addition, he examined the case of multiple wing formations [2:page 8-5]. He found that the Automatic Formation Flight Control System performed well for multiple wing aircraft[2:page 8-4]. His research is the basis of the work proposed in this document.

2.5 Conclusion

The majority of the work accomplished in Automatic Formation Flight Control has been research performed at the Air Force Institute of Technology. The ongoing Flight Dynamics Lab effort concerns open loop control, while the AFIT research is focused on closed loop performance. The concepts and research outlined in this chapter give a brief

overview of the pertinent aspects of this research problem. The present research will contribute to this body of knowledge.

III. Model and Simulation Development

This chapter provides the necessary information to reproduce the results in this thesis. It is written to give the reader a brief overview of the simulation, which is implemented in Matlab. This chapter reviews each segment of the simulation and gives an overview of the actual implementation. Control Strategies are also discussed.

3.1 Aircraft Models

Previous research by Rohs [10] and Dargan [4] developed first-order aircraft models that were incorporated by Busogany [2] into his thesis. These models approximate the response of a C-130H aircraft with Mach-Hold, Altitude-Hold, and Heading-Hold automatic pilots in place [2:page 2-2]. Because of the three axes autopilots working in concert, the aircraft will generally behave like an overdamped first or second-order system because of the compensation each autopilot provides. Three distinct channels are considered: velocity, heading, and altitude. They are given in Equations (3.1) - (3.3).

$$\frac{V(s)}{V_c(s)} = \frac{\frac{1}{\tau_v}}{s + \frac{1}{\tau_v}} \quad (3.1)$$

$$\frac{\psi(s)}{\psi_c(s)} = \frac{\frac{1}{\tau_\psi}}{s + \frac{1}{\tau_\psi}} \quad (3.2)$$

$$\frac{h(s)}{h_c(s)} = \frac{\frac{1}{\tau_h}}{s + \frac{1}{\tau_h}} \quad (3.3)$$

where,

τ_v = time constant of velocity channel

τ_ψ = time constant of heading channel

τ_h = time constant of altitude channel

Table 3.1 shows the model time constants for Equations (3.1) - (3.3). It also provides the upper and lower limits for the rate limiters employed in the nonlinear models. *It is important to realize that this table will not exactly match Table 2.1 in Busogany's thesis.*

Table 2.1 in Buzogany's thesis lists the Upper Altitude Rate Saturation Limit as $8.5 \frac{ft}{sec}$. However, in his simulations he implemented this as $8 \frac{ft}{sec}$. This has been determined through inspection of his simulation implementation in Matrixx, System Build and its resulting plots. Since Buzogany's thesis is considered a baseline for this thesis effort, the Upper Altitude Rate Saturation Limit is implemented as $8 \frac{ft}{sec}$ in simulations and is listed as such in Table 3.1. This will not match Table 3.1, page 3-3 of Dargan [4], nor Table 2.1, page 2-4 of Buzogany [2]. A similar situation exists for the limits on the Velocity Error in Table 3.1. These were not listed in Dargan's Table 3.1 or Buzogany's Table 2.1. The values are taken from Buzogany's simulation of the Velocity models (Dargan only showed his C-130B models in his thesis and the Upper and Lower Limits on the Velocity Error match those of Buzogany). The time responses of C-130A and B aircraft channels listed in Table 3.1 are in Figure 3.2.

Table 3.1 Aircraft Rate Limits and Model Time Constants [2:Table 2.1]

Aircraft	Parameter	Lower Limit	Upper Limit	τ_v	τ_ψ	τ_h
C-130A				$\frac{1}{3}$ sec	$\frac{1}{1.5}$ sec	2 sec
	Velocity	$304 \frac{ft}{sec}$	$422 \frac{ft}{sec}$			
	Velocity Error	$-5 \frac{ft}{sec^2}$	$2.5 \frac{ft}{sec^2}$			
	Heading Error	$-3 \frac{deg}{sec}$	$3 \frac{deg}{sec}$			
	Altitude Error	$-42 \frac{ft}{sec}$	$8 \frac{ft}{sec}$			
C-130B				$\frac{1}{3}$ sec	$\frac{1}{1.5}$ sec	2 sec
	Velocity	$304 \frac{ft}{sec}$	$422 \frac{ft}{sec}$			
	Velocity Error	$-5 \frac{ft}{sec^2}$	$2.5 \frac{ft}{sec^2}$			
	Heading Error	$-4.7 \frac{deg}{sec}$	$4.7 \frac{deg}{sec}$			
	Altitude Error	$-42 \frac{ft}{sec}$	$8 \frac{ft}{sec}$			

In addition to the first-order models developed by Rohs, Buzogany developed second-order models by simulating the linear bare aircraft state space models and equipped these with the three basic autopilots (Mach-Hold, Altitude-Hold, and Heading-Hold) [2:page 2-4]. The method by which he accomplished this is documented in Appendices A and B of his thesis [2]. Because of time constraints and to limit the scope of this thesis, first-order models are used in analysis and simulation. However, the inclusion of the second-order models in the analysis and simulations is a logical extension of the research in this thesis.

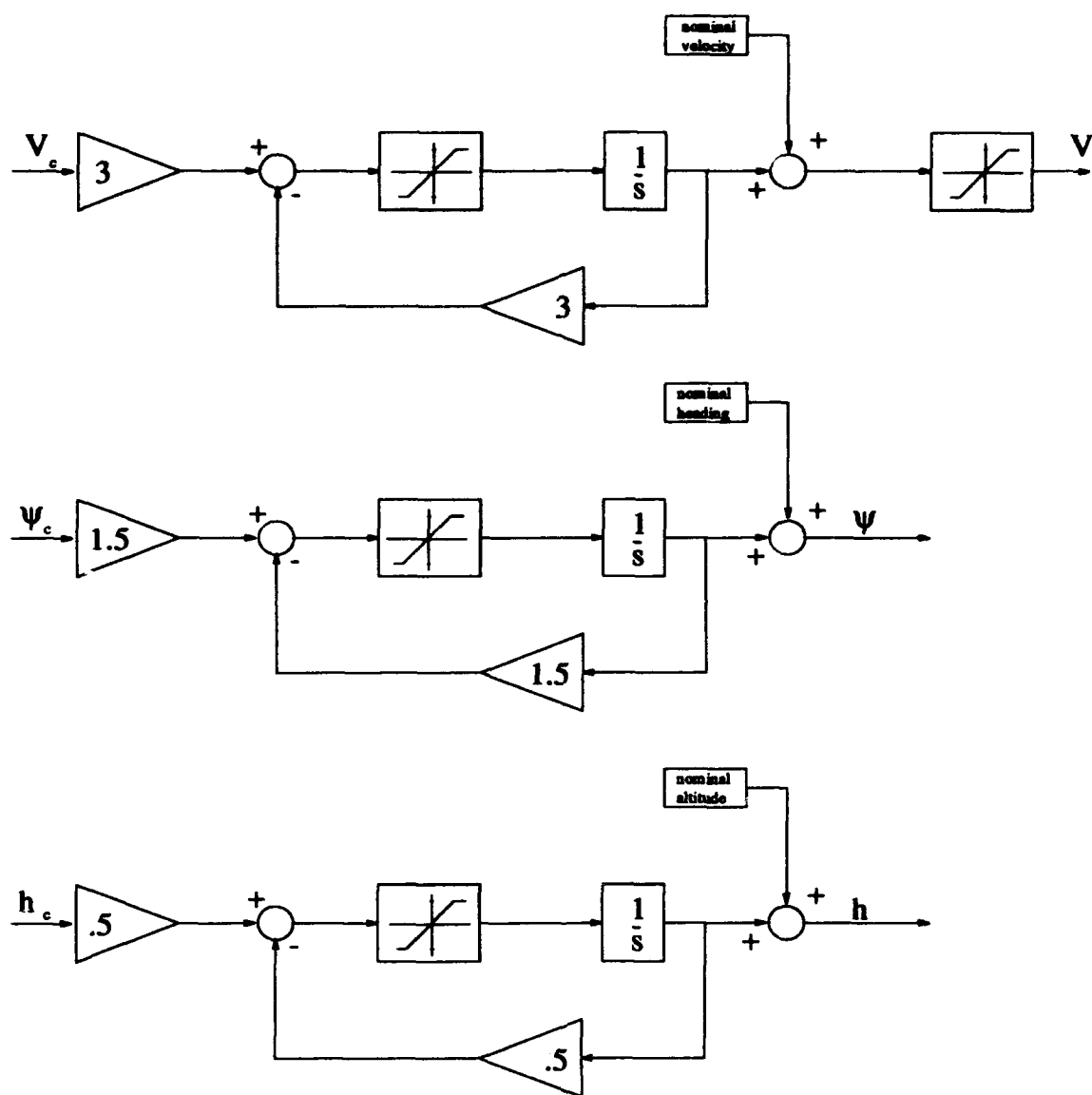


Figure 3.1 First Order Models Used In Simulations

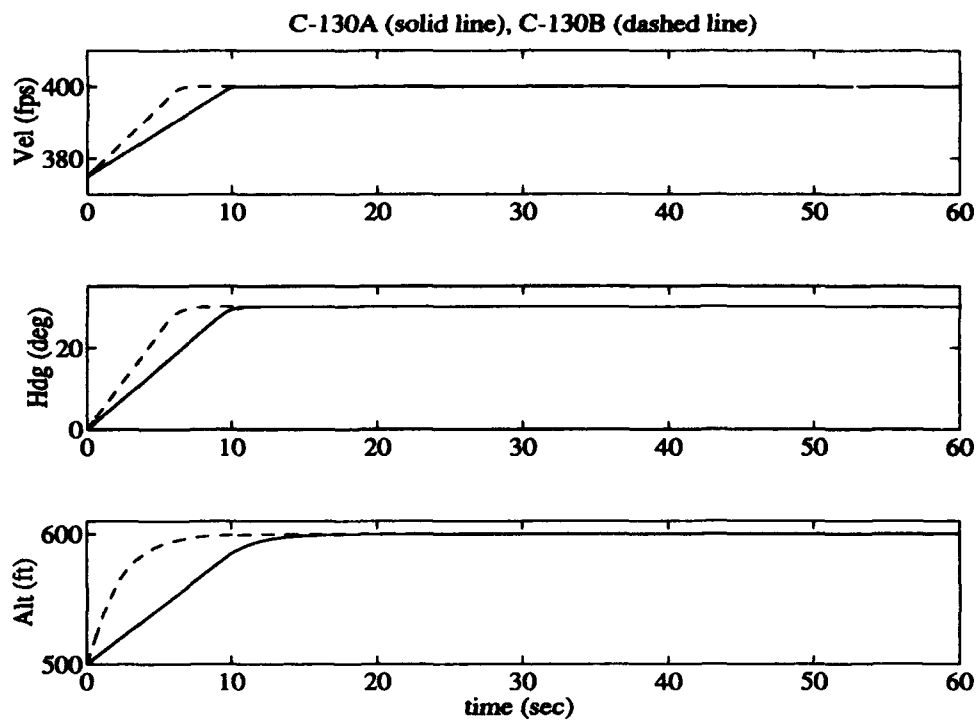


Figure 3.2 Simulation of C-130A and C-130B Aircraft Channels

3.2 Aircraft Sensor Measurements

Feedback is an inherent part of any robust control system. Feedback entails measurements of the output which are subtracted from the command signal and allow an error signal to be created. Driving this error signal to zero is the fundamental part of feedback control. The feedback for an Automatic Formation Flight Control system is provided by sensor(s) on board each wing aircraft. These sensors must be capable of providing position and velocity information of the lead aircraft with respect to the wing [2:page 2-5] [4:page 3-8]. An actual sensor will have dynamics and a time delay associated with its operation. This will further complicate the Formation Flight Control System, by making it more unstable. In this analysis, the sensors are assumed to be ideal (i.e., no dynamics, no time delay, unit gain). Another problem with aircraft sensor measurements is the transmission of each sensor's information to the Formation Flight Controller. There is already a time delay before the information is transmitted. Thus, the time delay associated with data transmission also contributes to the instability of the system. This research effort considers ideal sensors and no time delay associated with the data transmission is assumed.

3.3 Formation Coordinate System

This thesis uses the same formation coordinate system as discussed in Section 3.4 of Dargan's thesis [4] and Section 2.3 of Buzogany's thesis [2]. It is restated here for completeness.

This research uses two coordinate frames:

1. Inertial coordinate frame
2. Rotating reference frame centered on the wing aircraft

[2:page 2-6] [4:page 3-8]

The inertial frame is depicted in Figure 3.3. It has latitude, longitude, and altitude as its axes and has a stationary origin [2:page 2-6] [4:page 3-9].

The rotating aircraft reference frame is attached to the wing aircraft and is depicted in Figure 3.4. The wing aircraft provides the origin for the frame. The x axis is in the

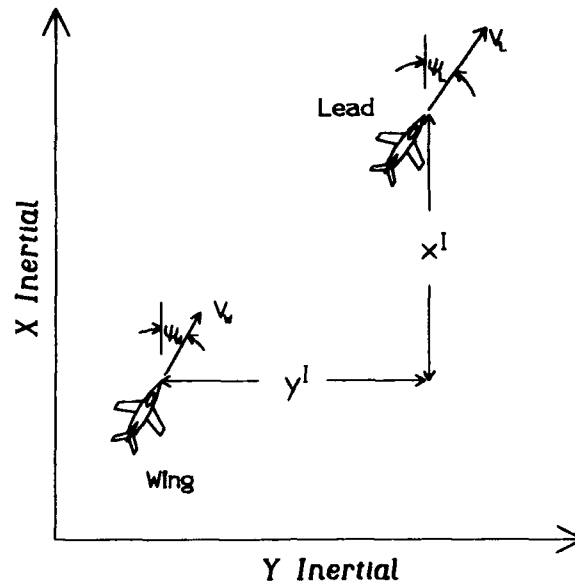


Figure 3.3 Inertial Reference Frame and Separation Distances [2:Figure 2.3]

direction of the aircraft's flight direction (i.e., aligned with velocity vector), the y axis points out the right wing, and the z axis points down, toward the earth [2:page 2-6] [4:page 3-9]. Relative position between the wing and lead aircraft is easily obtained using the wing aircraft rotating reference frame. In addition, the distance measurements provided by the actual on board sensors would provide information in a similar manner as the rotating reference frame [4:page 3-9].

3.4 Kinematic Equations

Mathematical expressions must be derived to determine the relative separations between the lead and wing aircraft. This has already been done by Dargan and repeated by Buzogany [4:pages 3-12 to 3-21] [2:pages 2-6 to 2-10]. It is repeated under the assumption that the reader does not have adequate knowledge of the kinematic development leading to the x and y separation equations. The separation equations yield information that on-board sensors would provide in a "real world" implementation of a formation flight control system [4:page 3-12]. Specifically, they provide the x and y separation distances between lead and wing with respect to the wing aircraft [2:page 2-6].

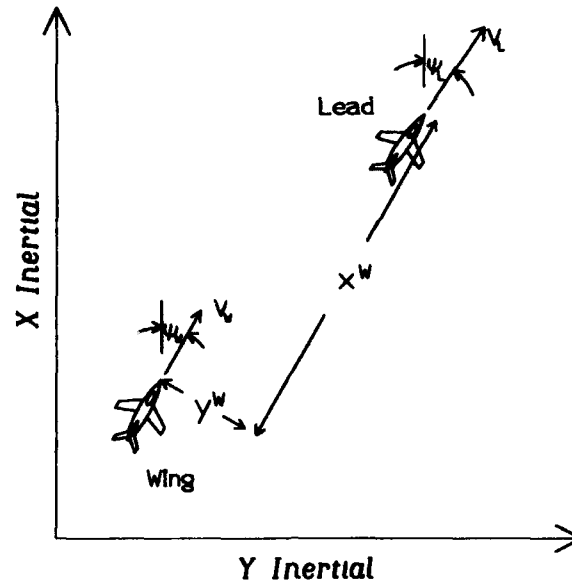


Figure 3.4 Wing's Rotating Reference Frame and Separation Distances [2:Figure 2.4]

Using the Equation of Coriolis (See Chapter II), the velocity of the lead with respect to the wing has been found by Dargan as [4:Equation (3.11)]

$$V_{WL}^W = \underbrace{V_L^W - \omega_W^W \times R_{WL}^W}_{\text{lead velocity in wing's frame}} - \underbrace{V_W^W + \omega_W^W \times R_W^W}_{\text{wing velocity in wing's frame}} \quad (3.4)$$

where,

V_{WL}^W = velocity of the lead aircraft with respect to the wing, in the wing's reference frame

ω_W^W = angular velocity of the wing in the wing's reference frame

R_{WL}^W = position of lead aircraft with respect to wing in the wing's reference frame

R_W^W = position of wing aircraft in its own reference frame

V_W^W = inertial velocity of wing aircraft in its own reference frame

V_L^W = inertial velocity of lead aircraft in its own reference frame

Figure 3.5 shows the basis for development of the pertinent kinematic equations. In Figure 3.5, the following observations can be made (See [2:page 2-9]):

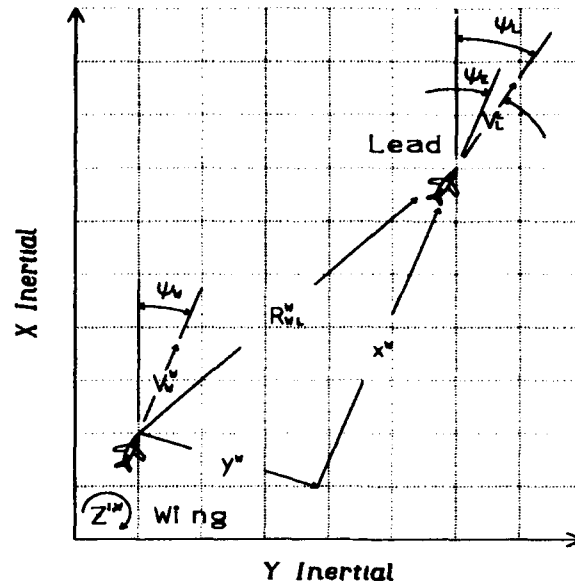


Figure 3.5 Relative Motion Diagram [2:Figure 2.5]

$$\psi_E = \psi_L - \psi_W, \quad \omega_W^W = \begin{bmatrix} 0 \\ 0 \\ \dot{\psi}_W \end{bmatrix}, \quad R_{WL}^W = \begin{bmatrix} x^W \\ y^W \\ z^W \end{bmatrix}, \quad R_W^W = \begin{bmatrix} 0 \\ 0 \\ 0 \end{bmatrix} \quad (3.5)$$

$$V_W^W = \begin{bmatrix} V_W \\ 0 \\ 0 \end{bmatrix}, \quad V_L^L = \begin{bmatrix} V_L \\ 0 \\ 0 \end{bmatrix}$$

where,

ψ_E = heading error

V_L^L = inertial velocity of the lead aircraft in its own frame of reference

Due to $R_W^W = 0$, Equation (3.4) can be rewritten as [4:Equation (3.12)]

$$V_{WL}^W = V_L^W - \omega_W^W \times R_{WL}^W - V_W^W \quad (3.6)$$

All terms of the right hand side of Equation (3.6) are known with the exception of V_L^W . In order to determine this, a Direction Cosine Matrix needs to be determined

to rotate V_L^L into the wing rotating reference frame, thus yielding V_L^W . By inspection of Figure 3.5, Dargan found the Direction Cosine Matrix to be [4:Equation (3.8)]:

$$C_L^W = \begin{bmatrix} \cos \psi_B & -\sin \psi_B & 0 \\ \sin \psi_B & \cos \psi_B & 0 \\ 0 & 0 & 1 \end{bmatrix} \quad (3.7)$$

Premultiplying V_L^W by C_L^W yields the following equation [4:Equation (3.9)] [2:Equation (2.8)],

$$V_L^W = C_L^W V_L^L = \begin{bmatrix} V_L \cos \psi_B \\ V_L \sin \psi_B \\ 0 \end{bmatrix} \quad (3.8)$$

With V_L^W determined, Equation (3.6) can have its variables substituted for the expressions in Equations (3.5) and (3.8) to yield [4:Equation (3.13) and (3.14)] [2:Equation (2.10)],

$$V_{WL}^W = \begin{bmatrix} V_L \cos \psi_B \\ V_L \sin \psi_B \\ 0 \end{bmatrix} - \begin{bmatrix} 0 \\ 0 \\ \dot{\psi}_W \end{bmatrix} \times \begin{bmatrix} x^W \\ y^W \\ z^W \end{bmatrix} - \begin{bmatrix} V_W \\ 0 \\ 0 \end{bmatrix} + \begin{bmatrix} 0 \\ 0 \\ \dot{\psi}_W \end{bmatrix} \times \begin{bmatrix} 0 \\ 0 \\ 0 \end{bmatrix} \quad (3.9)$$

$$V_{WL}^W = \begin{bmatrix} V_L \cos \psi_B \\ V_L \sin \psi_B \\ 0 \end{bmatrix} - \begin{bmatrix} -\dot{\psi}_W y^W \\ \dot{\psi}_W x^W \\ 0 \end{bmatrix} - \begin{bmatrix} V_W \\ 0 \\ 0 \end{bmatrix} \quad (3.10)$$

Separating the components in Equation (3.10) yields the following equations:

$$\dot{x}^W = V_L \cos \psi_B + \dot{\psi}_W y^W - V_W \quad (3.11)$$

$$\dot{y}^W = V_L \sin \psi_B - \dot{\psi}_W x^W \quad (3.12)$$

$$\dot{z}^W = 0 \quad (3.13)$$

In this research effort, x and y separation distances are fed back for comparison purposes. In the simulation the separations distances are found by integrating Equations (3.11) and (3.12). Since the only angular rate used in this simulation is $\dot{\psi}$, there is no component of velocity in the z^W direction, thus, $\dot{z}^W = 0$ [4:page 3-16]. Future research efforts may want to explore this area.

3.5 Initial Conditions

In this thesis, all simulations are performed with the following initial conditions:

- 0° magnetic heading on inertial axes
- 375 $\frac{ft}{sec}$ formation flight velocity
- 500 ft separation in x^W and y^W directions
- 500 ft altitude (for three dimensional maneuvers)

These initial conditions are chosen because Buzogany used these in his simulations and his thesis is the baseline by which this research effort is proceeding.

3.6 Simulation Overview

Previous research into this topic at the Air Force Institute of Technology (AFIT) has been conducted using Matrix₂. Because of availability, convenience, and quality, Matlab and its program for simulating nonlinear dynamic systems, Simulink, is chosen as the software for simulations performed in this thesis. This necessitates the need to reproduce Buzogany's results, where appropriate, before extending his research. A large amount of time has been spent in providing a quality simulation that not only matches past results, but is implemented in a control analysis program that is now the AFIT standard.

The simulation is implemented as done previously in Dargan and Buzogany. A two tiered control strategy is employed. The upper tier is for controlling the entire formation. Its commands are issued by the pilot in the lead aircraft. The lower tier is for controlling the

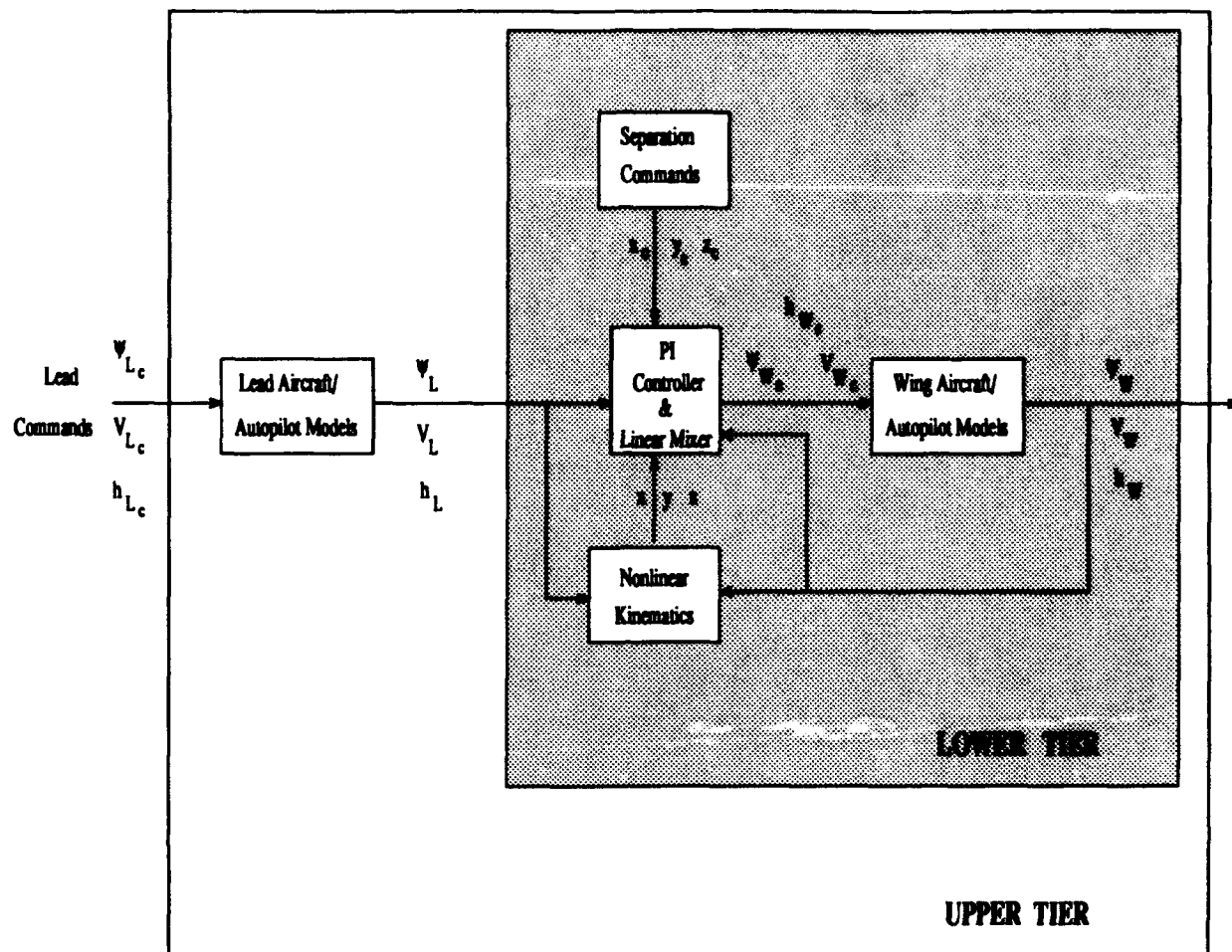


Figure 3.6 Upper and Lower Tier Implementation Strategy

individual aircraft within the formation. The individual wing aircraft command originates in the PI controller of each wing aircraft [4:page 3-11] [2:page 2-10]. A pictorial illustration of this concept is shown in Figure 3.6

Two simulations are developed in this thesis. The first is a Two Dimensional maneuvers simulation in which the wing aircraft follows the lead maneuvers without leaving the lead's flight plane. The second is a Three Dimensional maneuvers simulation in which the wing aircraft is allowed to leave the lead's flight plane in order that the excursions of the wing's specific energy are minimized.

3.7 Two Dimensional Controller Development

Previous research explored both PI control and PI control enhanced with a linear mixer. Analysis was accomplished, however, with just the PI controller in place. In this research, the analysis is extended to include a PI controller and a linear mixer in place. Both types of controller are simulated; however, the thrust of the investigation pertains to the inclusion of a linear mixer in the simulation.

In Busogany's analysis, the variables available for feedback were separation (x or y depending on the channel). In the present analysis, a mix of separation and maneuver error (velocity error for the z channel and heading error for the y channel) is available for feedback.

3.7.1 PI Controller and Linear Mixer. A controller uses the error between the command and the output and drives this to zero. The error is a mixture of separation error (x or y separation errors) and channel maneuver error (heading or velocity errors). The controller is the PI controller, which commands the wing aircraft to nullify the error. Obviously, only the velocity and heading channels are controlled using this two dimensional formation flight control system [2:page 2-12].

The control law perturbation equations for the two dimensional case are developed in Chapter IV and are presented here as in Busogany [2:Equations (2.20) and (2.21)]:

$$V_{Wc} = k_{xp}(k_v V_B + k_x x) + k_{xi} \int_0^t (k_v V_B + k_x x) dt \quad (3.14)$$

$$\psi_{Wc} = k_{yp}(k_\psi \psi_B + k_y y) + k_{yi} \int_0^t (k_\psi \psi_B + k_y y) dt \quad (3.15)$$

where in Equation (3.14),

$x = x_c^W - x^W$, x separation error [units: ft]

$V_B = V_L - V_W$, velocity error signal [units: $\frac{ft}{sec}$]

k_v = velocity error mixer gain [units: sec]

k_x = x separation error mixer gain [units: 1 for this research effort (See Chapter IV)]

k_{zp} = z-channel proportional gain [units: sec]

k_{zi} = z-channel integral gain [units: sec²]

in Equation (3.15),

$y = y_c^W - y^W$, y separation error [units: ft]

$\psi_B = \psi_L - \psi_W$, heading error [units: $\frac{rad}{sec}$]

k_ψ = heading error mixer gain [units: ft]

k_y = y separation error mixer gain [units: 1 for this research effort (See Chapter IV)]

k_{yp} = y-channel proportional gain [units: $\frac{1}{ft}$]

k_{yi} = y-channel integral gain [units: $\frac{sec}{ft}$]

Additionally, a control law commanding an altitude change was developed by Dargan and presented by Busogany as [2:Equation (2.17)] [4:Equation (4.1)]

$$h_{W_c} = \underbrace{k_{zp}z + k_{zi} \int_0^t z dt}_{\text{no mixer; only } z \text{ error available}} \quad (3.16)$$

where,

$z = z_c^W - z^W$, z separation error [units: ft]

k_{zp} = z-channel proportional gain [units: unit-less]

k_{zi} = z-channel integral gain [units: $\frac{1}{sec}$]

3.8 Three Dimensional Controller Development

Previously, Busogany kept the specific energy of the wing aircraft constant by allowing the aircraft the ability to deviate outside of the lead aircraft's flight plane in response to velocity changes, thereby, maintaining a constant specific energy level (i.e., trading kinetic for potential energy). Chapter V extends Busogany's research by investigating if allowing specific energy changes less than those made in two-dimensional maneuvers can have the benefit of improved energy consumption with better capabilities. This is done by formulating an altitude and velocity command.

3.8.1 PI Control Laws for Three Dimensional Case. Busogany developed an altitude command in response to x separation error. This allows for the wing aircraft's speed modulation and at the same time energy conserving maneuvers to take place (i.e., the specific energy of a wing aircraft remains at its nominal value during a maneuver).

In energy excursion minimising maneuvers, the wing aircraft's energy perturbations are minimized throughout the course of a maneuver and are preferably approximately zero. This necessitates the use of a velocity control law in addition to the altitude control law to minimize the swings in the specific energy state of the wing aircraft and at the same time to afford formation speed increases. The two control laws for energy minimizing maneuvers are:

$$h_{W_c} = k_{zsp}x + k_{zsi} \int_0^t x \, dt \quad (3.17)$$

$$V_{W_c} = \left(\frac{e_W}{V_o} + \frac{g}{V_o} h_W \left[\frac{\tau_{V_W}}{\tau_{h_W}} - 1 \right] - \frac{g}{V_o} \frac{\tau_{V_W}}{\tau_{h_W}} h_{W_c} \right) + k_{zspv} h_e + k_{zsi_v} \int_0^t h_e \, dt \quad (3.18)$$

where, in Equation (3.17),

k_{zsp} = zz -channel proportional gain [units: unit-less]

k_{zsi} = zz -channel integral gain [units: $\frac{1}{sec}$]

and in Equation (3.18)

e_W = specific energy of an aircraft [units: $\frac{ft^2}{sec^2}$]

h_W = perturbation away from nominal for wing altitude [units: ft]

τ_{V_W} = time constant of wing velocity channel [units: sec]

τ_{h_W} = time constant of wing altitude channel [units: sec]

g = acceleration of gravity [units: $\frac{ft}{sec^2}$]

V_o = nominal velocity of the formation [units: $\frac{ft}{sec}$]

k_{zspv} = zz -channel, altitude error proportional gain [units: $\frac{1}{sec}$]

k_{zsi_v} = zz -channel, altitude error, integral gain [units: $\frac{1}{sec^2}$]

$h_e = h_L - h_W$, altitude error [units: ft]

Additionally, a velocity control law is formulated without e_W . This control law is

$$V_{W_e} = \left(\frac{g}{V_o} h_W \left[\frac{\tau_{V_W}}{\tau_{h_W}} - 1 \right] - \frac{g}{V_o} \frac{\tau_{V_W}}{\tau_{h_W}} h_{W_e} \right) + k_{sspv} h_e + k_{ssiv} \int_0^t h_e dt \quad (3.19)$$

This development is discussed in more detail in Chapter V.

IV. Horizontal Formation Flight Control - Analysis

This chapter develops the derivation of a linear and parameterised MIMO plant. It is used to analytically determine the PI control and linear mixer gains for the formation flight control problem. Analysis is constrained to the flight plane of the aircraft (i.e., velocity and heading channels). A three dimensional analysis is considered in a later chapter.

4.1 Theoretical Development

Following Buzogany's research, the investigation of the linearized formation flight control model proceeds as follows:

1. Formation geometry is outlined and geometric parameters are identified
2. Linearized equations for the aircraft models and aircraft kinematics are developed and nondimensionalized
3. The x and y -channels are decoupled and augmented using a PI control law.
4. The augmented state equations are analyzed for steady-state error and stability
5. The stability envelopes for each channel parameters are plotted and analyzed to show where acceptable gains may be picked
6. Trial and error process of picking gains exercising the nonlinear simulation
7. Varying gains and analyzing the poles and residues of the pertinent responses of the two channels

[2:page 5-1]

Figure 4.1 illustrates the formation geometry for a two aircraft formation. By inspection of Figure 4.1, the formation parameters are l , the separation distance ($\sqrt{x_0^2 + y_0^2}$), and α , the formation angle [2:pages 5-1 and 5-2].

The Cartesian separation distances can be found in Buzogany [2][Eqs (5.1) and (5.2)]

$$x_o = l \cos \alpha \quad (4.1)$$

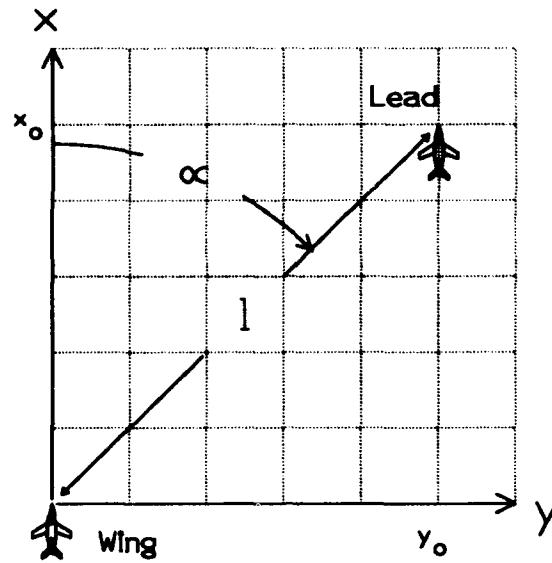


Figure 4.1 Formation Geometry

$$y_o = l \sin \alpha \quad (4.2)$$

where,

x_o = nominal x separation

y_o = nominal y separation

α = separation angle = $\arctan \left(\frac{y_o}{x_o} \right) \rightarrow$ without loss of generality, $0 \leq \alpha \leq \frac{\pi}{2}$

Equations (4.1) and (4.2) relate the key formation parameters to the separation distances.

First-order aircraft models are used to simplify the analysis. In addition, the analysis results can be compared to results obtained by Buzogany [2]. Equations (4.3) - (4.7) are the first-order C-130 aircraft models used in prior research by Rohs [10], Dargan [4], and Buzogany [2].

$$\dot{V}_W = -\frac{1}{\tau_{V_W}} V_W + \frac{1}{\tau_{V_W}} V_{W_c} \quad (4.3)$$

$$\dot{\psi}_W = -\frac{1}{\tau_{\psi_W}} \psi_W + \frac{1}{\tau_{\psi_W}} \psi_{W_c} \quad (4.4)$$

$$\dot{V}_L = -\frac{1}{\tau_{V_L}} V_L + \frac{1}{\tau_{V_L}} V_{L_o} \quad (4.5)$$

$$\dot{\psi}_L = -\frac{1}{\tau_{\psi_L}} \psi_L + \frac{1}{\tau_{\psi_L}} \psi_{L_o} \quad (4.6)$$

$$\dot{h}_W = -\frac{1}{\tau_{h_W}} h_W + \frac{1}{\tau_{h_W}} h_{W_o} \quad (4.7)$$

where

τ_{V_W} = the velocity time constant of the wing

τ_{ψ_W} = the heading time constant of the wing

τ_{V_L} = the velocity time constant of the lead

τ_{ψ_L} = the heading time constant of the lead

The nonlinear kinematic equations relating the x and y separation between the lead and wing aircraft are given by Buzogany [2:Equations (5.6) and (5.7)]

$$\dot{x} = V_L \cos \psi_B + \dot{\psi}_W y - V_W \quad (4.8)$$

$$\dot{y} = V_L \sin \psi_B - \dot{\psi}_W x \quad (4.9)$$

Because Equations (4.8) and (4.9) are nonlinear, they are linearized about a steady-state operating point using small angle approximations and the method of small perturbations. This results in the linear equations found by Buzogany [2:Equations (5.8) and (5.9)]

$$\dot{x} = V_L + \dot{\psi}_W y_o - V_W \quad (4.10)$$

$$\dot{y} = V_L \psi_B - \dot{\psi}_W x_o \quad (4.11)$$

Substituting Equations (4.1) - (4.6) into Equations (4.10) and (4.11) yields the equations Buzogany found in his research [2:Equations (5.10) and (5.11)]

$$\dot{z} = V_L + \left[-\frac{1}{\tau_{\psi W}} \psi_W + \frac{1}{\tau_{\psi W}} \psi_{W_c} \right] l \sin \alpha - V_W \quad (4.12)$$

$$\dot{y} = V_L(\psi_L - \psi_W) - \left[-\frac{1}{\tau_{\psi W}} \psi_W + \frac{1}{\tau_{\psi W}} \psi_{W_c} \right] l \cos \alpha \quad (4.13)$$

Simplifying the analysis, Equations (4.3) - (4.6) and Equations (4.12) - (4.13) are nondimensionalized using the following definitions:

$$l \triangleq \sqrt{x_o^2 + y_o^2} \quad (4.14)$$

$$\bar{t} \triangleq \frac{l}{V_o} \quad (4.15)$$

where,

l = characteristic length of the nominal formation separation

\bar{t} = characteristic time

V_o = nominal formation velocity

(Buzogany [2])

l , \bar{t} , and V_o are used to nondimensionalize Equations (4.3) - (4.6) and (4.12) - (4.13). Each variable in these equations is nondimensionalized and then substituted back into the original equation in order to yield the final nondimensional equation. The nondimensional variables are denoted by the caret superscript, " $\hat{\cdot}$ ". They are as follows:

$$\begin{aligned} \hat{x} &= \frac{x}{l} & \hat{y} &= \frac{y}{l} & \hat{x}_o &= \frac{x_o}{l} = \cos \alpha \\ \hat{y}_o &= \frac{y_o}{l} = \sin \alpha & \hat{V}_W &= \frac{V_W}{V_o} & \hat{V}_{W_c} &= \frac{V_{W_c}}{V_o} \\ \hat{\tau}_{V_W} &= \frac{\tau_{V_W}}{\bar{t}} & \hat{\tau}_{\psi_W} &= \frac{\tau_{\psi_W}}{\bar{t}} & \hat{V}_L &= \frac{V_L}{V_o} \\ \hat{\tau}_{V_L} &= \frac{\tau_{V_L}}{\bar{t}} & \hat{\tau}_{\psi_L} &= \frac{\tau_{\psi_L}}{\bar{t}} \end{aligned} \quad (4.16)$$

where,

\hat{x} = nondimensional x separation error

- \hat{y} = nondimensional y separation error
 \hat{z}_o = nondimensional nominal x separation
 \hat{y}_o = nondimensional nominal y separation
 \hat{V}_W = nondimensional wing velocity
 \hat{V}_{W_c} = nondimensional commanded wing velocity
 \hat{V}_L = nondimensional lead velocity
 \hat{V}_{L_c} = nondimensional commanded lead velocity
 $\hat{\tau}_{V_W}$ = nondimensional wing velocity time constant
 $\hat{\tau}_{\psi_W}$ = nondimensional wing heading time constant
 $\hat{\tau}_{V_L}$ = nondimensional lead velocity time constant
 $\hat{\tau}_{\psi_L}$ = nondimensional lead heading time constant

The resulting nondimensionalized equations are as follows (4.16). (The “~” notation is no longer used. It is considered extraneous notation. Therefore, all remaining variables in this section are considered to be nondimensional):

$$\dot{z} = -V_W - \frac{\sin \alpha}{\tau_{\psi_W}} \psi_W + \frac{\sin \alpha}{\tau_{\psi_W}} \psi_{W_c} + V_L \quad (4.17)$$

$$\dot{V}_W = -\frac{1}{\tau_{V_W}} V_W + \frac{1}{\tau_{V_W}} V_{W_c} \quad (4.18)$$

$$\dot{y} = \left[\frac{\cos \alpha}{\tau_{\psi_W}} - 1 \right] \psi_W - \frac{\cos \alpha}{\tau_{\psi_W}} \psi_{W_c} + \psi_L \quad (4.19)$$

$$\dot{\psi}_W = -\frac{1}{\tau_{\psi_W}} \psi_W + \frac{1}{\tau_{\psi_W}} \psi_{W_c} \quad (4.20)$$

$$\dot{V}_L = -\frac{1}{\tau_{V_L}} V_L + \frac{1}{\tau_{V_L}} V_{L_c} \quad (4.21)$$

$$\dot{\psi}_L = -\frac{1}{\tau_{\psi_L}} \psi_L + \frac{1}{\tau_{\psi_L}} \psi_{L_c} \quad (4.22)$$

Equations (4.17) - (4.22) are put into state variable form. The MIMO linearized and nondimensionalized state variable representation of the plant, inputs, outputs, and disturbances are represented by the following equations:

$$\dot{X} = AX + BU + \Gamma D \quad (4.23)$$

$$Y = CX \quad (4.24)$$

therefore,

$$\begin{aligned} \dot{X} = \begin{bmatrix} \dot{x} \\ \dot{V}_W \\ \dot{y} \\ \dot{\psi}_W \\ \dot{V}_L \\ \dot{\psi}_L \end{bmatrix} &= \begin{bmatrix} 0 & -1 & 0 & -\frac{\sin \alpha}{\tau_{\phi W}} & 1 & 0 \\ 0 & -\frac{1}{\tau_{VW}} & 0 & 0 & 0 & 0 \\ 0 & 0 & 0 & \left(\frac{\cos \alpha}{\tau_{\phi W}} - 1\right) & 0 & 1 \\ 0 & 0 & 0 & -\frac{1}{\tau_{\phi W}} & 0 & 0 \\ 0 & 0 & 0 & 0 & -\frac{1}{\tau_{VL}} & 0 \\ 0 & 0 & 0 & 0 & 0 & -\frac{1}{\tau_{\phi L}} \end{bmatrix} \begin{bmatrix} x \\ V_W \\ y \\ \psi_W \\ V_L \\ \psi_L \end{bmatrix} \\ &+ \begin{bmatrix} 0 & \frac{\sin \alpha}{\tau_{\phi W}} \\ \frac{1}{\tau_{VW}} & 0 \\ 0 & -\frac{\cos \alpha}{\tau_{\phi W}} \\ 0 & \frac{1}{\tau_{\phi W}} \\ 0 & 0 \\ 0 & 0 \end{bmatrix} \begin{bmatrix} V_{Wc} \\ \psi_{Wc} \end{bmatrix} + \begin{bmatrix} 0 & 0 \\ 0 & 0 \\ 0 & 0 \\ 0 & 0 \\ \frac{1}{\tau_{VL}} & 0 \\ 0 & \frac{1}{\tau_{\phi L}} \end{bmatrix} \begin{bmatrix} V_{Lc} \\ \psi_{Lc} \end{bmatrix} \end{aligned} \quad (4.25)$$

$$Y = \begin{bmatrix} x \\ V_c \\ y \\ \psi_c \end{bmatrix} = \begin{bmatrix} 1 & 0 & 0 & 0 & 0 & 0 \\ 0 & -1 & 0 & 0 & 1 & 0 \\ 0 & 0 & 1 & 0 & 0 & 0 \\ 0 & 0 & 0 & -1 & 0 & 1 \end{bmatrix} \begin{bmatrix} x \\ V_W \\ y \\ \psi_W \\ V_L \\ \psi_L \end{bmatrix} \quad (4.26)$$

where,

X = state vector

A = plant

Γ = disturbance input matrix

D = disturbance input vector

Y = output vector

C = output matrix

There is almost total decoupling between the x and y -channel. The only coupling between the two occurs due to the disturbance in the x -channel. This is shown in Section 4.1.2.

Due to decoupling, the state vector, $X \in \mathcal{R}^6$, can be partitioned as follows:

$$X = [(x, V_W, V_L), (y, \psi_W, \psi_L)]^T \quad (4.27)$$

4.1.1 Y-Channel. Equations (4.25), (4.26), and (4.27) yield the decoupled y -channel state equation:

$$\begin{bmatrix} \dot{y} \\ \dot{\psi}_W \\ \dot{\psi}_L \end{bmatrix} = \begin{bmatrix} 0 & \left(\frac{\cos \alpha}{\tau_{\psi W}} - 1\right) & 1 \\ 0 & -\frac{1}{\tau_{\psi W}} & 0 \\ 0 & 0 & -\frac{1}{\tau_{\psi L}} \end{bmatrix} \begin{bmatrix} y \\ \psi_W \\ \psi_L \end{bmatrix} + \begin{bmatrix} -\frac{\cos \alpha}{\tau_{\psi W}} \\ \frac{1}{\tau_{\psi W}} \\ 0 \end{bmatrix} \psi_{W_c} + \begin{bmatrix} 0 \\ 0 \\ \frac{1}{\tau_{\psi L}} \end{bmatrix} \psi_{L_c} \quad (4.28)$$

The y -channel control variable is ψ_{W_c} , the wing aircraft's heading command. It responds to formation separation change in the y -channel. Note that the y -channel control system now is augmented to include the new state variable, ψ_L , which was previously treated as a disturbance. Hence, at this level of modelling, an additional output is now available for feedback and employing a mixer as in Dargan's thesis is needed. The role of the disturbance signal is relegated to ψ_{L_c} . Mixer parameters are used to form the generalized y -channel error signal:

$$e_y = k_y y + k_\psi \psi_c \quad (4.29)$$

where,

$\psi_c = \psi_L - \psi_W = \text{heading angle error (radians)}$

$k_y = y\text{-separation error signal mixer gain}$

$k_\psi = \text{heading error signal mixer gain}$

A PI control law operating on the error, e_y , is,

$$\psi_{W_c} = k_{yp} e_y + k_{yi} \int_0^t e_y dt \quad (4.30)$$

where,

k_{yp} = non-dimensional proportional gain operating on the error, e_y

k_{yi} = non-dimensional integral gain operating on the error, e_y

By differentiating Equation (4.30), the following equation is obtained,

$$\dot{\psi}_{W_c} = k_{yp} \dot{e}_y + k_{yi} e_y \quad (4.31)$$

Substituting Equation (4.29) into Equation (4.31) yields,

$$\dot{\psi}_{W_c} = k_{yp}(k_y \dot{y} + k_\phi \dot{\psi}_s) + k_{yi}(k_y y + k_\phi \psi_s) \quad (4.32)$$

The augmented state equations incorporating both the linear mixer and the PI controller are

$$\dot{X}_y = A_y X_y + \Gamma_y d_y \quad (4.33)$$

$$Y_y = C_y X_y \quad (4.34)$$

Therefore,

$$\begin{bmatrix} \dot{y} \\ \dot{\psi}_W \\ \dot{\psi}_L \\ \dot{\psi}_{W_c} \end{bmatrix} = \begin{bmatrix} 0 & \left(\frac{\cos \alpha}{\tau_{\phi W}} - 1\right) & 1 & -\frac{\cos \alpha}{\tau_{\phi W}} \\ 0 & -\frac{1}{\tau_{\phi W}} & 0 & \frac{1}{\tau_{\phi W}} \\ 0 & 0 & -\frac{1}{\tau_{\phi L}} & 0 \\ k_{yi} k_y & C_{\phi W} & C_{\phi L} & C_{\phi W_c} \end{bmatrix} \begin{bmatrix} y \\ \psi_W \\ \psi_L \\ \psi_{W_c} \end{bmatrix} + \begin{bmatrix} 0 \\ 0 \\ \frac{1}{\tau_{\phi L}} \\ k_{yp} k_\phi \frac{1}{\tau_{\phi L}} \end{bmatrix} \psi_{L_c} \quad (4.35)$$

$$Y_y = \begin{bmatrix} 1 & 0 & 0 & 0 \\ 0 & -1 & 1 & 0 \end{bmatrix} \begin{bmatrix} y \\ \psi_w \\ \psi_L \\ \psi_{w_e} \end{bmatrix} = \begin{bmatrix} y \\ \psi_e \end{bmatrix} \quad (4.36)$$

where,

$$C_{\psi_w} = k_{yp}k_y \left(\frac{\cos \alpha}{\tau_{\psi_w}} - 1 \right) + k_{yp}k_\phi \frac{1}{\tau_{\psi_w}} - k_{yi}k_\phi \quad (4.37)$$

$$C_{\psi_L} = k_{yp}k_y - k_{yp}k_\phi \frac{1}{\tau_{\psi_L}} + k_{yi}k_\phi \quad (4.38)$$

$$C_{\psi_{w_e}} = -k_{yp} \frac{1}{\tau_{\psi_w}} (k_y \cos \alpha + k_\phi) \quad (4.39)$$

and

X_y = augmented y-channel state vector

A_y = augmented y-channel plant

Γ_y = augmented y-channel input matrix

D_y = augmented y-channel input vector

Y_y = augmented y-channel output vector

C_y = augmented y-channel output matrix

4.1.1.1 Static Stability Analysis, Y-Channel. It is imperative that the wing aircraft be able to track the lead aircraft with zero steady-state error. This requirement can be stated as follows:

$$\text{As } t \rightarrow \infty, y(\infty) = 0, \text{ and } \psi_w(\infty) = \psi_L(\infty) = \psi_{w_e}(\infty) = \psi_{L_e} = D_y = 1 \quad (4.40)$$

This requirement is met by the y-channel. This is illustrated by observing the y-channel response to a unit step disturbance, $\psi_L(t)$.

$$z(t)_{ss} = \lim_{s \rightarrow 0} s \frac{1}{s} (SI - A_y)^{-1} \Gamma_y = -A_y^{-1} \Gamma_y = \begin{bmatrix} 0 \\ 1 \\ 1 \\ 1 \end{bmatrix} \quad (4.41)$$

The results of Equation (4.41) are true if and only if A_y is invertible. This condition implies the following relation:

$$k_{yi} k_y \neq 0 \quad (4.42)$$

Conclusion: $k_{yi} \neq 0$ and $k_y \neq 0$. Hence, integral control action is necessary. Furthermore, y-feedback is necessary and ψ_e feedback alone will not suffice. Therefore, without loss of generality, assume $k_y = 1$. See Section 4.2 for the rationale to allow $k_y = 1$.

4.1.1.2 Dynamic Stability Analysis, Y-Channel. The dynamic stability analysis consists of 1) obtaining the y-channel characteristic equation, and 2) performing a Routhian stability analysis. The characteristic equation is

$$\det(SI - A_y) = s^4 + as^3 + bs^2 + cs + d \quad (4.43)$$

where the coefficients are,

$$a = \frac{1}{\tau_{\psi_w}} (1 + k_{yp} [\cos \alpha + k_\psi]) + \frac{1}{\tau_{\psi_L}} \quad (4.44)$$

$$b = \frac{1}{\tau_{\psi_w}} (k_{yp} + k_{yi} [k_\psi + \cos \alpha]) + \frac{a}{\tau_{\psi_L}} \quad (4.45)$$

$$c = k_{yi} \frac{1}{\tau_{\psi_w}} + \frac{b}{\tau_{\psi_L}} \quad (4.46)$$

$$d = k_{yi} \frac{1}{\tau_{\psi_w} \tau_{\psi_L}} \quad (4.47)$$

The following relations result from the Routh criterion application of Table 4.1:

Table 4.1 Y-Channel Routhian Array

s^4	1	b	d
s^3	a	c	
s^2	$\frac{ab-c}{a}$	d	
s^1	$c - \frac{a^2d}{ab-c}$		
s^0	d		

row s^3

$$\frac{1}{\tau_{\psi w}} (1 + k_{yp} \cos \alpha + k_{yp} k_{\psi}) + \frac{1}{\tau_{\psi L}} > 0 \quad (4.48)$$

row s^2

$$\begin{aligned} & \frac{1}{\tau_{\psi w}} [(1 + k_{yp} \cos \alpha + k_{yp} k_{\psi}) (k_{yp} + k_{yi} k_{\psi} + k_{yi} \cos \alpha)] \\ & + \frac{1}{\tau_{\psi w} \tau_{\psi L}} (1 + k_{yp} \cos \alpha + k_{yp} k_{\psi})^2 + \frac{1}{\tau_{\psi L}^2} (1 + k_{yp} \cos \alpha + k_{yp} k_{\psi}) - k_{yi} > 0 \end{aligned} \quad (4.49)$$

row s^1

$$\tau_{\psi w} + \tau_{\psi L} (1 + k_{yp} \cos \alpha + k_{yp} k_{\psi}) + \tau_{\psi L}^2 (k_{yp} + k_{yi} k_{\psi} + k_{yi} \cos \alpha) + \tau_{\psi L}^3 k_{yi} > 0 \quad (4.50)$$

row s^0

$$\frac{1}{\tau_{\psi w} \tau_{\psi L}} k_{yi} > 0 \quad (4.51)$$

Similar to Buzogany's thesis, these stability conditions show the relationships between controller and mixer gains, formation geometry, and first-order model time constants. In order to guarantee stability, all of these inequalities must be satisfied.

As in the static stability analysis, the dynamic stability analysis reveals the need for integral control action in order to satisfy stability conditions. Remember, for these stability relations, $k_y = 1$ and as such is not seen in the stability equations. The rationale for this is given in Section 4.2.

4.1.2 X-Channel . Once again, Equations (4.25), (4.26), and (4.27) yield the decoupled x -channel state equation:

$$\begin{bmatrix} \dot{z} \\ \dot{V}_W \\ \dot{V}_L \end{bmatrix} = \begin{bmatrix} 0 & -1 & 1 \\ 0 & -\frac{1}{\tau_{VW}} & 0 \\ 0 & 0 & -\frac{1}{\tau_{VL}} \end{bmatrix} \begin{bmatrix} z \\ V_W \\ V_L \end{bmatrix} + \begin{bmatrix} 0 \\ \frac{1}{\tau_{VW}} \\ 0 \end{bmatrix} V_{Wc} + \begin{bmatrix} 0 & \frac{\sin \alpha}{\tau_{\psi W}} \\ 0 & 0 \\ \frac{1}{\tau_{VL}} & 0 \end{bmatrix} \begin{bmatrix} V_{Lc} \\ d_\psi \end{bmatrix} \quad (4.52)$$

where,

$$d_\psi = \psi_{Wc} - \psi_W$$

There are two disturbances in the x -channel, the lead aircraft's velocity command, V_L , and some coupling of the y -channel into the x -channel due to heading changes, d_ψ . V_{Wc} , the wing aircraft's velocity command, responds to formation separation change in the x -channel. Mixer parameters are used to form the generalized y -channel error signal:

$$e_x = k_x x + k_v V_e \quad (4.53)$$

where,

$$V_e = V_L - V_W = \text{velocity error}$$

$$k_x = \text{x-separation error signal mixer gain}$$

$$k_v = \text{velocity error signal mixer gain}$$

A PI control law operating on the error signal, e_x , is,

$$V_{Wc} = k_{xp} e_x + k_{xi} \int_0^t e_x dt \quad (4.54)$$

where,

k_{sp} = non-dimensional, x-separation error, proportional gain

k_{si} = non-dimensional, x-separation error, integral gain

By differentiating Equation (4.54), the following equation is obtained,

$$\dot{V}_{W_c} = k_{sp}(k_s \dot{x} + k_v \dot{V}_c) + k_{si}(k_s x + k_v V_c) \quad (4.55)$$

The augmented state equations incorporating both the PI controller and the linear mixer are

$$\dot{X}_z = A_z X_z + \Gamma_z d_z \quad (4.56)$$

$$Y_z = C_z X_z \quad (4.57)$$

therefore,

$$\begin{bmatrix} \dot{z} \\ \dot{V}_W \\ \dot{V}_L \\ \dot{V}_{W_c} \end{bmatrix} = \begin{bmatrix} 0 & -1 & 1 & 0 \\ 0 & -\frac{1}{\tau_{VW}} & 0 & \frac{1}{\tau_{VW}} \\ 0 & 0 & -\frac{1}{\tau_{VL}} & 0 \\ k_{si}k_s & C_{VW} & C_{VL} & -k_{sp}k_v \frac{1}{\tau_{VW}} \end{bmatrix} \begin{bmatrix} z \\ V_W \\ V_L \\ V_{W_c} \end{bmatrix} + \begin{bmatrix} 0 & \frac{\sin \alpha}{\tau_{\phi W}} \\ 0 & 0 \\ \frac{1}{\tau_{VL}} & 0 \\ k_{sp}k_v \frac{1}{\tau_{VL}} & k_{sp}k_s \frac{\sin \alpha}{\tau_{\phi W}} \end{bmatrix} \begin{bmatrix} V_{Lc} \\ d_\phi \end{bmatrix} \quad (4.58)$$

$$Y_z = \begin{bmatrix} 1 & 0 & 0 & 0 \\ 0 & -1 & 1 & 0 \end{bmatrix} \begin{bmatrix} z \\ V_W \\ V_L \\ V_{W_c} \end{bmatrix} = \begin{bmatrix} z \\ V_c \end{bmatrix} \quad (4.59)$$

where,

$$C_{VW} = -k_{sp}k_s + k_{sp}k_v \frac{1}{\tau_{VW}} - k_{si}k_v \quad (4.60)$$

$$C_{VL} = k_{sp}k_s - k_{sp}k_v \frac{1}{\tau_{VL}} + k_{si}k_v \quad (4.61)$$

and

- X_z = augmented x-channel state vector
- A_z = augmented x-channel plant
- Γ_z = augmented x-channel input matrix
- D_z = augmented x-channel input vector
- Y_z = augmented x-channel output vector
- C_z = augmented x-channel output matrix

4.1.2.1 Static Stability Analysis, X-Channel. Because it is imperative that the wing be able to track the lead aircraft with zero steady-state error, the conditions of Equation (4.40) can be restated, using x-channel parameters as,

$$As \ t \rightarrow \infty, y(\infty) = 0, \text{ and } V_W(\infty) = V_L(\infty) = V_{W_c}(\infty) = V_{L_c} = 1 \quad (4.62)$$

The requirement of Equation (4.62) is met by the x-channel. This is illustrated by observing the x-channel response to a unit step disturbance, V_{L_c} .

$$x(t)_{ss} = \lim_{s \rightarrow 0} s \frac{1}{s} (SI - A_z)^{-1} \Gamma_z = -A_z^{-1} \Gamma_z = \begin{bmatrix} 0 & \frac{k_x}{k_w} \\ 1 & \frac{\sin \alpha}{r_{\psi w}} \\ 1 & 0 \\ 1 & \frac{\sin \alpha}{r_{\psi w}} \end{bmatrix} \quad (4.63)$$

Since it is proven in the y-channel analysis that $\psi_W \rightarrow \psi_{W_c}$ at steady-state, the disturbance due to the coupling term $\frac{\sin \alpha}{r_{\psi w}} (\psi_{W_c} - \psi_W)$ will $\rightarrow 0$ in steady-state. Therefore, the second column in equation (4.63) does not affect the response in steady state.

The results of Equation (4.63) are true if and only if A_z is invertible. This condition implies the following relation:

$$k_{zi}k_s \neq 0 \quad (4.64)$$

Conclusion: $k_{zi} \neq 0$ and $k_s \neq 0$. Hence, integral control action is necessary. Furthermore, z -feedback is necessary and V_s feedback alone will not suffice. Therefore, without loss of generality, assume $k_s = 1$. See Section 4.2 for the rationale to make $k_s = 1$.

4.1.2.2 Dynamic Stability Analysis, X-Channel. The characteristic equation is

$$\det(SI - A_x) = s^4 + es^3 + fs^2 + gs + h \quad (4.65)$$

where the coefficients are,

$$e = \frac{1}{\tau_{VW}}(1 + k_V) + \frac{1}{\tau_{VL}} \quad (4.66)$$

$$f = \frac{1}{\tau_{VW}}(k_{zp} + k_{zi}k_s) + \frac{e}{\tau_{VL}} \quad (4.67)$$

$$g = \frac{1}{\tau_{VW}}k_{zi} + \frac{f}{\tau_{VL}} \quad (4.68)$$

$$h = \frac{1}{\tau_{VW}\tau_{VL}}k_{zi} \quad (4.69)$$

Table 4.2 X-Channel Routhian Array

s^4	1	f	h
s^3	e	g	
s^2	$\frac{ef-g}{e}$	h	
s^1	$g - \frac{e^2h}{ef-g}$		
s^0	h		

The following relations result from the Routh Criterion application of Table 4.2.

row s^3

$$\frac{1}{\tau_{VW}} (1 + k_{sp}k_v) + \frac{1}{\tau_{VL}} > 0 \quad (4.70)$$

row s^2

$$\frac{1}{\tau_{VW}} \left[(1 + k_{sp}k_v)(k_{sp} + k_{si}k_v) + \frac{1}{\tau_{VL}} (1 + k_{sp}k_v)^2 \right] + \frac{1}{\tau_{VL}^2} (1 + k_{sp}k_v) - k_{si} > 0 \quad (4.71)$$

row s^1

$$\tau_{VW} + \tau_{VL} (1 + k_{sp}k_v) + \tau_{VL}^2 (k_{sp} + k_{si}k_v) + \tau_{VL}^3 k_{si} > 0 \quad (4.72)$$

row s^0

$$\frac{1}{\tau_{VW}\tau_{VL}} k_{si} > 0 \quad (4.73)$$

As in the y -channel, these stability conditions show the relationships between controller and mixer gains, formation geometry, and first-order model time constants. In order to guarantee stability, all of these inequalities must be satisfied.

As in the static stability analysis, the dynamic stability analysis reveals the need for integral control action in order to satisfy stability conditions. Remember for these stability relations that $k_z = 1$ and as such is not seen in the stability equations. The rationale for this is given in Section 4.2.

4.1.2.3 Comparison of Analysis With Prior Work. In order to ensure the previous analysis is correct, it is checked with previous results obtained by Buzogany [2:pages 5-9 and 5-12]. Buzogany's Routhian analysis did not include a mixer in either channel and assumed the lead aircraft states as disturbances. The analysis in Sections

4.1.1 and 4.1.2 includes a mixer and incorporates the lead aircraft states. Therefore, to check the current Routhian analysis with prior analysis, the following conditions must be applied to the inequalities of Equations (4.48) - (4.51) and Equations (4.70) - (4.73):

1. Turn the mixer off (i.e., set $k_y = 1$, $k_\psi = 0$). Therefore, $e_y = y$
2. Lead aircraft states were not available for analysis in the previous thesis. Therefore, terms that include the lead aircraft states are neglected. This is the same as not having sensors that measure lead aircraft parameters.

After applying the previous conditions to the pertinent equations, the resulting inequalities are the same as those found earlier in Buzogany [2:Equations (5.36) - (5.39) and Equations (5.53) - (5.55)]. Therefore, it is shown that the inequalities derived in the this thesis are correct and match the results of previous work.

4.2 Gain Envelopes

The y -channel inequalities in Equations (4.48) - (4.51) and the x -channel inequalities in Equations (4.70) - (4.73) can be employed to graphically portray the resulting stability envelope for the respective gains of each channel. There are four gains in each channel (y -channel: k_{yi} , k_{yp} , k_ψ , and k_y ; x -channel: k_{xi} , k_{xp} , k_θ , and k_x) which influence stability. In order to simplify analysis, $k_y = k_x = 1$. This can be done without loss of generality. To illustrate this point, recall Equation (4.29)

$$e_y = k_y y + k_\psi \psi_e \quad (4.74)$$

k_y can be divided from both sides to yield,

$$\frac{e_y}{k_y} = y + \frac{k_\psi}{k_y} \psi_e \quad (4.75)$$

Equation (4.75) can now be substituted into the equation for the PI controller, Equation (4.30)

$$\psi_{w_c} = \frac{k_{yp}}{k_y} e_y + \frac{k_{yi}}{k_y} \int_0^t e_y dt \quad (4.76)$$

The gains divided by k_y in the previous equations (Equations (4.75) and (4.76)) can be redefined to include k_y in their definitions. Thus

$$k_\psi = \frac{k_\psi}{k_y} \quad k_{yp} = \frac{k_{yp}}{k_y} \quad k_{yi} = \frac{k_{yi}}{k_y} \quad (4.77)$$

Thus allowing $k_y = 1$ can be done without loss of generality, because the gain is absorbed into the remaining gains. This same example can be employed using the x -channel equations to show $k_x = 1$ without loss of generality.

The eight inequalities in Equations (4.48) - (4.51) and (4.70) - (4.73) are difficult to plot. Simplifying the inequalities by employing new variables via a variables transformation will make the inequalities more tractable.

Consider the y -channel first. The inequalities representing stability conditions have been kept in factored form in order that the variables transformation be discerned easily. Upon examination of the inequalities given by Equations (4.48) - (4.51), it is readily apparent that all four stability conditions have three common factored expressions. These are suitable choices for the proposed variables transformation. Hence, the resulting transformed variables for the y -channel are defined.

$$k \triangleq 1 + k_{yp} \cos \alpha + k_{yp} k_\psi \quad (4.78)$$

$$l \triangleq k_{yp} + k_{yi} k_\psi + k_{yi} \cos \alpha \quad (4.79)$$

$$k_{yi} \triangleq k_{yi} \quad (4.80)$$

A similar examination is performed upon the inequalities of the z-channel. The transformed variables for the z-channel are:

$$m \triangleq 1 + k_{zp}k_v \quad (4.81)$$

$$n \triangleq k_{zp} + k_{zi}k_v \quad (4.82)$$

$$k_{zi} \triangleq k_{zi} \quad (4.83)$$

The resulting inequalities with Equations (4.78) - (4.82) substituted into the original factored inequalities given by Equations (4.48) - (4.51) and (4.70) - (4.73) are:

$$\begin{array}{l} \underline{y \text{ row } s^3} \\ \frac{1}{\tau_{\psi w}}k + \frac{1}{\tau_{\psi L}} > 0 \end{array} \quad (4.84)$$

$$\begin{array}{l} \underline{y \text{ row } s^2} \\ \frac{1}{\tau_{\psi w}}kl + \frac{1}{\tau_{\psi w}\tau_{\psi L}}k^2 + \frac{1}{\tau_{\psi L}^2}k - k_{yi} > 0 \end{array} \quad (4.85)$$

$$\begin{array}{l} \underline{y \text{ row } s^1} \\ \tau_{\psi w} + \tau_{\psi L}k + \tau_{\psi L}^2l + \tau_{\psi L}^3k_{yi} > 0 \end{array} \quad (4.86)$$

$$\begin{array}{l} \underline{y \text{ row } s^0} \\ k_{yi} > 0 \end{array} \quad (4.87)$$

Similarly,

$$\begin{array}{l} \underline{z \text{ row } s^3} \\ \frac{1}{\tau_{Vw}}m + \frac{1}{\tau_{VL}} > 0 \end{array} \quad (4.88)$$

$$\begin{array}{l} \underline{z \text{ row } s^2} \\ \frac{1}{\tau_{Vw}}mn + \frac{1}{\tau_{Vw}\tau_{VL}}m^2 + \frac{1}{\tau_{VL}^2}m - k_{zi} > 0 \end{array} \quad (4.89)$$

z row s^1

$$\tau_{VW} + \tau_{VL}m + \tau_{VL}^2n + \tau_{VL}^3k_{zi} > 0 \quad (4.90)$$

y row s^0

$$k_{zi} > 0 \quad (4.91)$$

The transformation of variables for the y and z -channels is a nonlinear transformation in which $K_Y = (k_{yp}, k_{yi}, k_{\phi}) \in \mathcal{R}^3$, is mapped into $G_Y = (k, l, k_{yi}) \in \mathcal{R}^3$, and $K_X = (k_{zp}, k_{zi}, k_{\psi}) \in \mathcal{R}^3$ is mapped into subspace $G_X = (m, n, k_{zi}) \in \mathcal{R}^3$. These nonlinear transformations map the respective gains into a space in which the stability equations become tractable. Once these stability envelopes are plotted, any choice of gains can be transformed into the new space to determine if the gains result in a stable linear system.

The transformed y and z -channel inequalities have a very similar form. The symmetry between the two channels' stability equations shows the elegance of the modelling employed. The differences between the two consist of the pertinent time constants and gains of the respective channel. This simplification allows easier parametric analysis of the stability of the two channels.

The transformed inequalities in Equations (4.84), (4.86), and (4.87) and their corresponding transformed z -channel inequalities, are all equations of planes in a three dimensional space. The inequalities of Equations (4.85) and (4.89) are equations for quadric surfaces [6:page131]. The z and y -channel inequalities are plotted in Figures 4.2 and 4.4. These figures show all of the inequalities plotted on one plot with its associated projection in all three planes. Figures 4.3 and 4.5 show the stability envelopes of the y and z -channel with all other conflicting constraints removed. Notice that for stability, the gains must be between the two surfaces. Therefore, it is now possible to pick gains, parameterize them, and determine if they yield a stable control system by plotting them in the respective gain envelope. The problem of attaining a stable system has been solved. (Appendix C has the individual plots of Equations (4.84) - (4.91))

The relations found by Busogany and presented in Chapter 5 of his thesis, are also plotted in Figures 4.6 and 4.7 (See Busogany [2:Equations (5.36) - (5.39) and (5.53) - (5.55)]). The regions of stability in these plots are shaded for ease of identification.

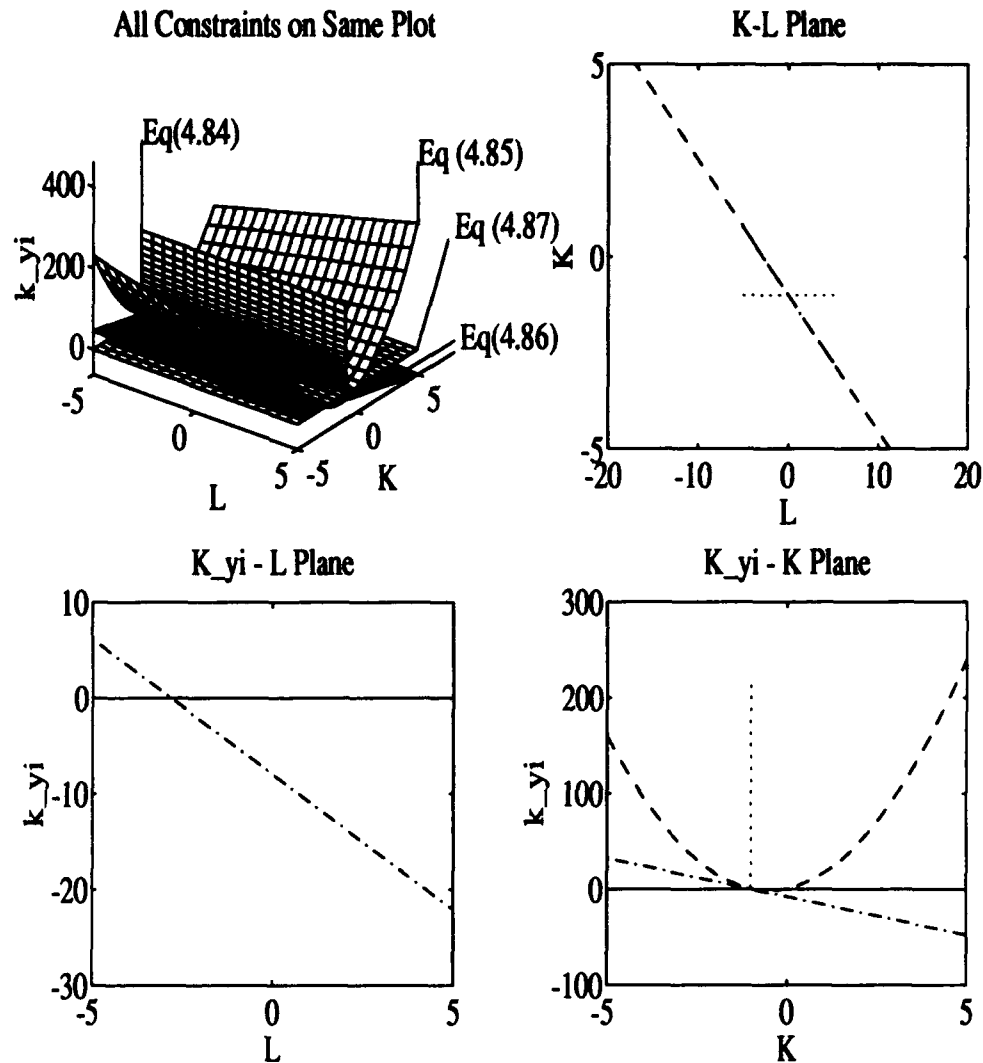


Figure 4.2 Nondimensional Y-Channel Constraints

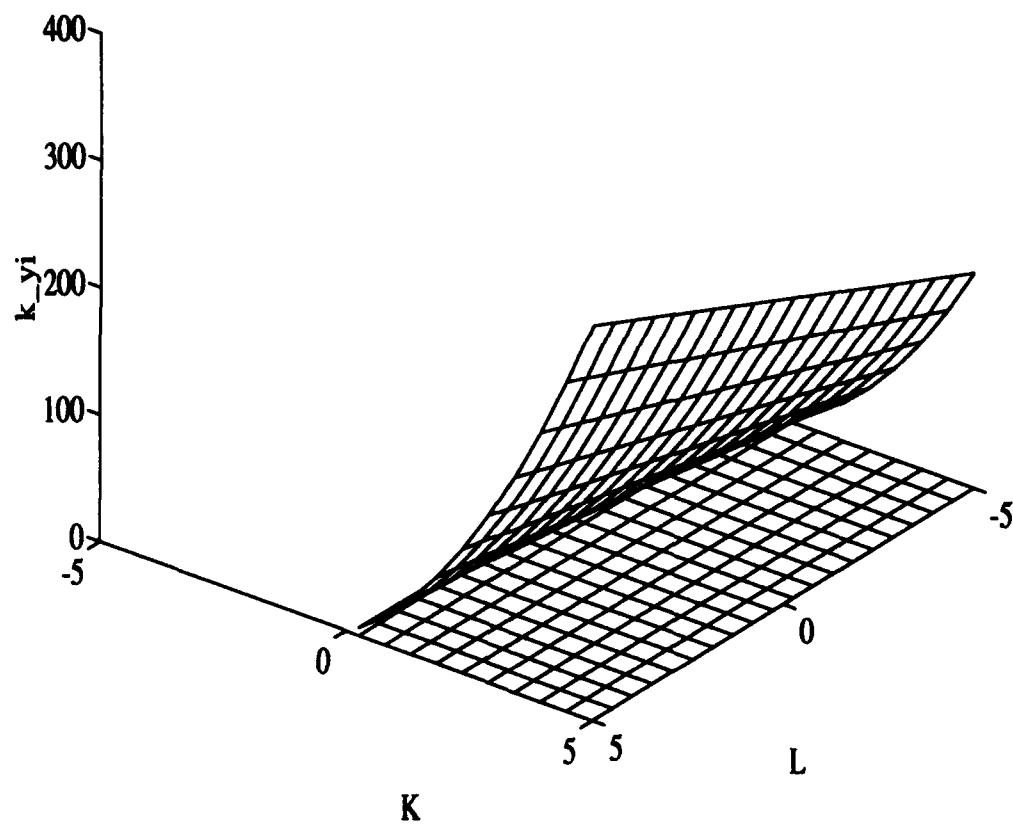


Figure 4.3 Nondimensional Y-Channel Envelope: Stability Between the Surfaces

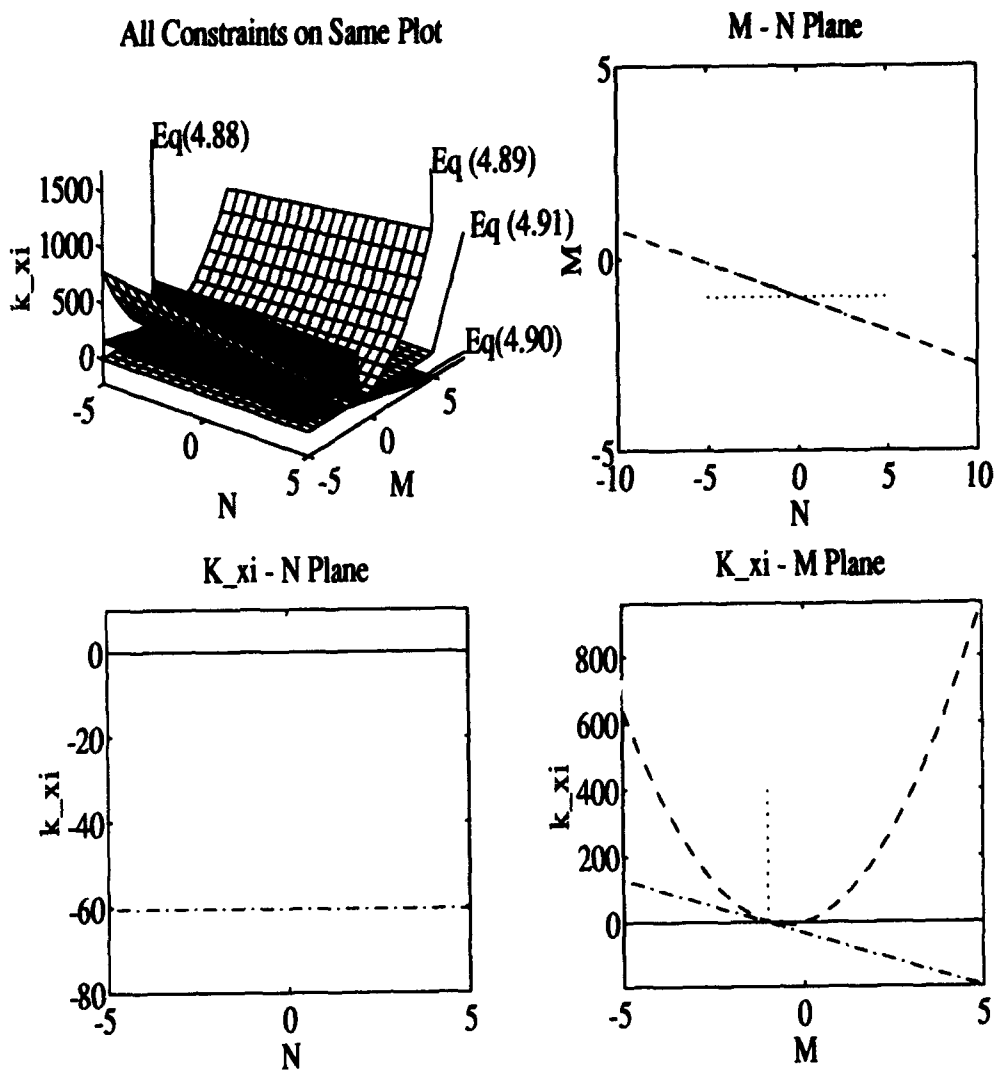


Figure 4.4 Nondimensional X-Channel Constraints

The Stability Envelope for the X-Channel from Another Angle

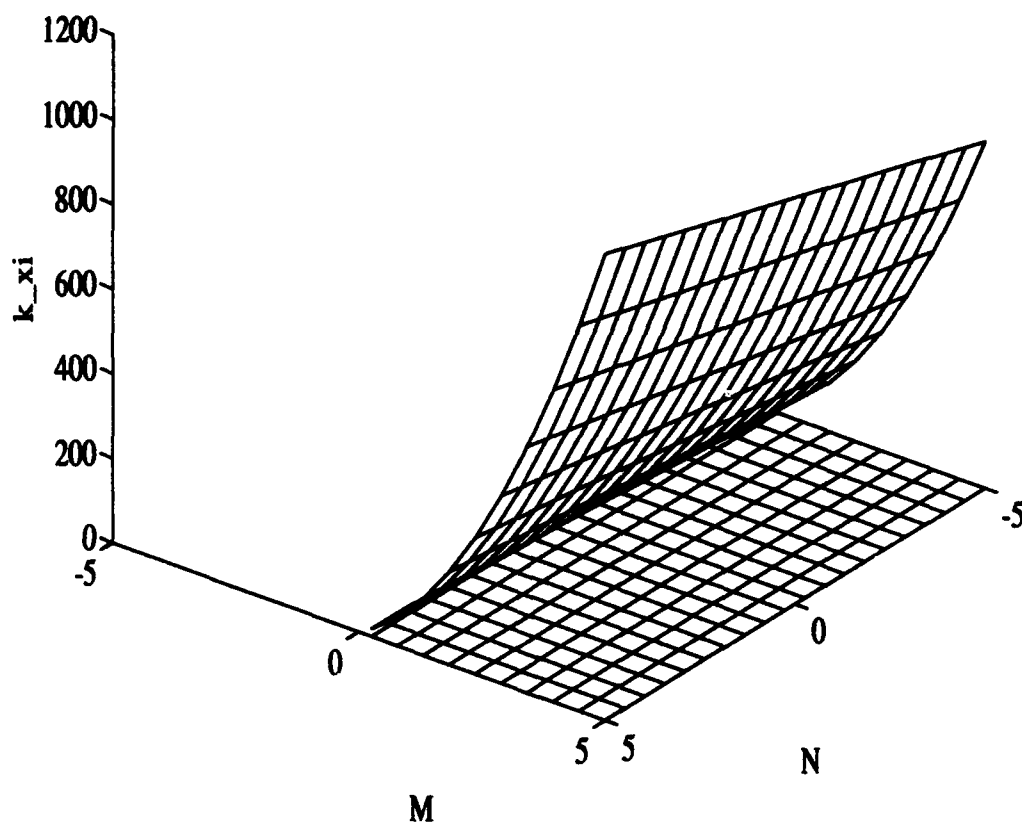


Figure 4.5 Nondimensional X-Channel Envelope: Stability Between the Surfaces

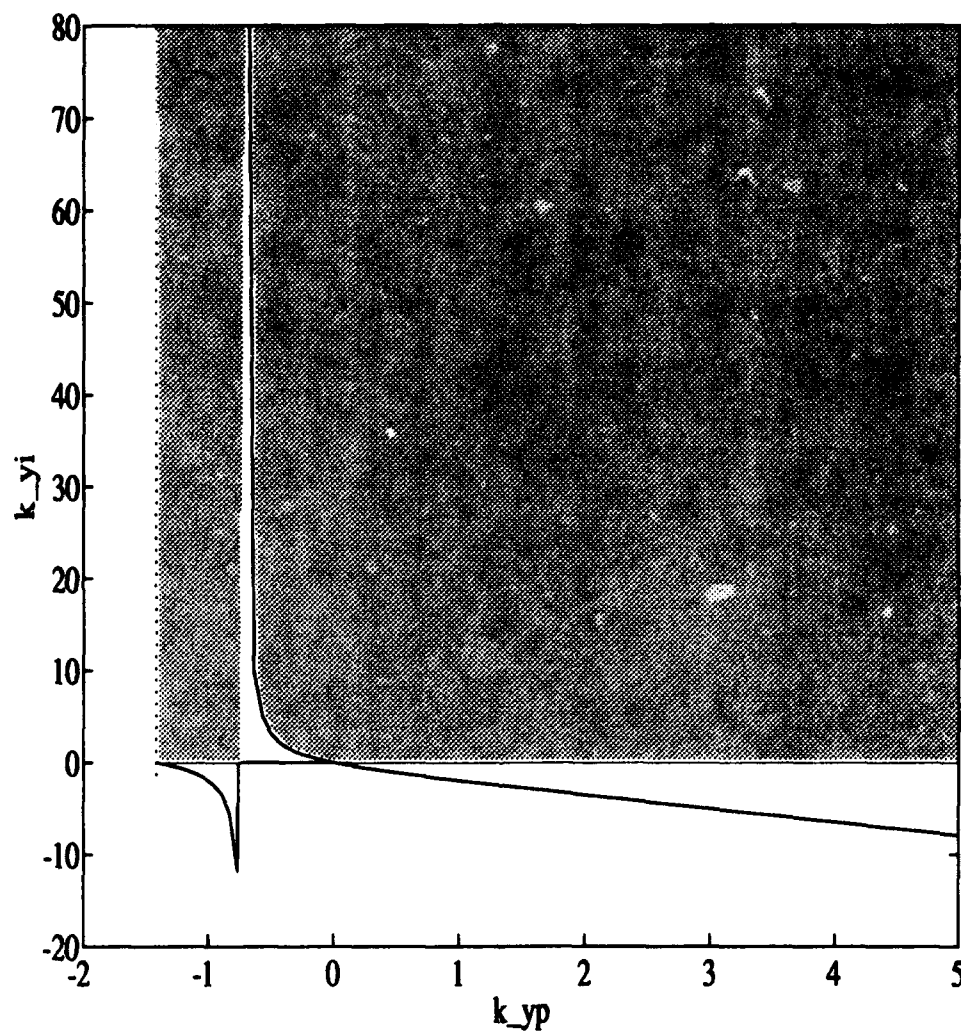


Figure 4.6 Nondimensional Y-Channel, Buzogany's Case: No Mixer, $\alpha = 45^\circ$; Shaded Region Denotes Stability

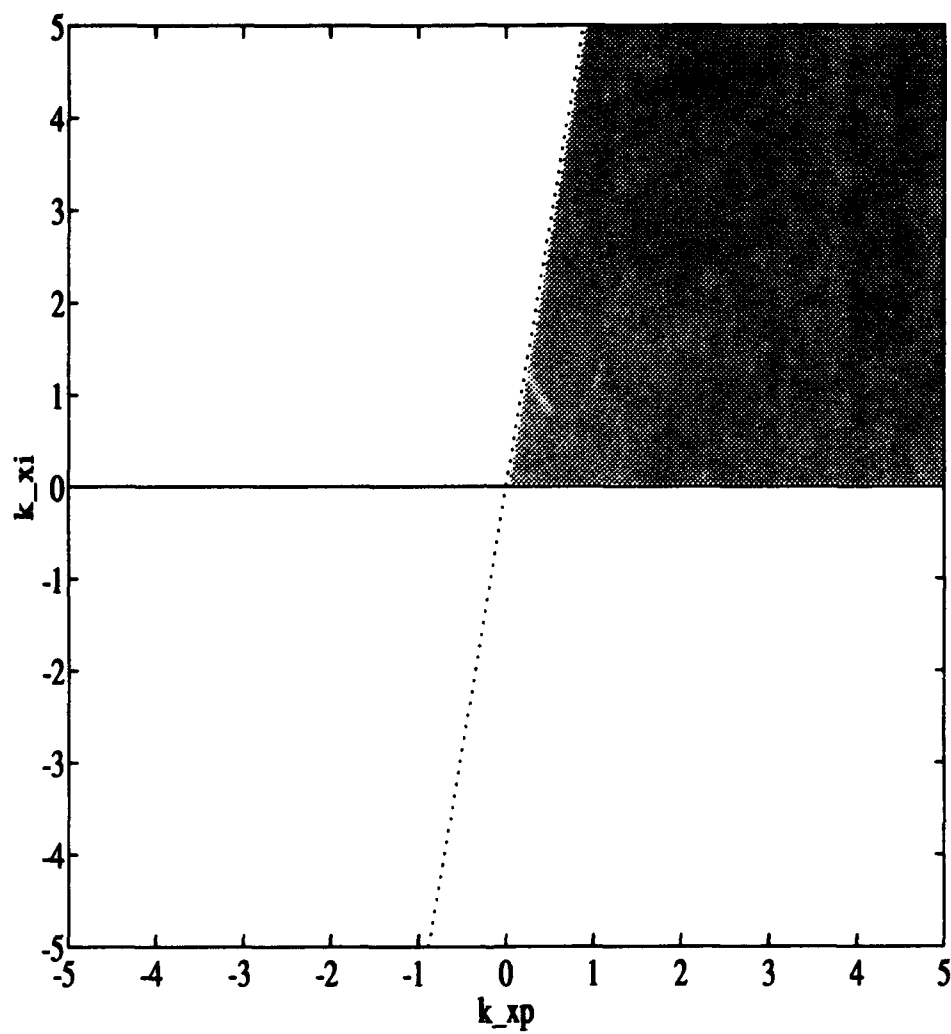


Figure 4.7 Nondimensional X-Channel, Busogany's Case: No Mixer, $\alpha = 45^\circ$; Shaded Region Denotes Stability

4.2.1 Buzogany's Test Case Plotted Inside Stability Envelope. The preceding figures show the stability envelopes for both Buzogany's case (PI controller only, Figures 4.6 and 4.7) and the new case (PI controller and linear mixer, Figures 4.3 and 4.5). In order to insure stability envelopes have been properly defined, the test case used in Buzogany's thesis is plotted inside both the two dimensional envelope and new three dimensional envelope. Table 4.3 defines this test case. Note that the values listed are dimensional. However, the values plotted have all been nondimensionalized.

Using the same gains Buzogany used in his preliminary research (see Table 4.3), the following relations for the transformed variables are determined (remember, no mixer was used in the previous analysis, i.e., $k_\phi = k_v = 0$):

$$k_B = 1 + k_{yp} \cos \alpha \quad (4.92)$$

$$l_B = k_{yp} + k_{yi} \cos \alpha \quad (4.93)$$

$$k_{yiB} = k_{yi} \quad (4.94)$$

and,

$$m_B = 1 \quad (4.95)$$

$$n_B = k_{zp} \quad (4.96)$$

$$k_{ziB} = k_{zi} \quad (4.97)$$

By substituting the values for the test case into Equations (4.92) - (4.97), values can be found which are then plotted inside the stability enveloped developed earlier. Plotting these values yields the plots in Figures 4.8 - 4.10. The values used for the 3-dimensional plots are shown in Table 4.4.

Table 4.3 Test Case: Formation, Aircraft Parameters, and Pertinent Gains

PARAMETER	DESCRIPTION	VALUE (units)	NONDIM. VALUE
V	Nominal Vel	375 (fps)	n/a
x_0	x-Separation	500 (ft)	n/a
y_0	y-Separation	500 (ft)	n/a
α	Formation Angle	45 (deg)	.7854 rad
l	Separation	707 (ft)	n/a
$\tau_{\phi w}$	Wing Hdng Time Constant	$\frac{1}{15}$ (sec)	.35355
τ_{vw}	Wing Vel Time Constant	$\frac{1}{3}$ (sec)	.17660
$\tau_{\phi z}$	Lead Hdng Time Constant	$\frac{1}{1.5}$ (sec)	.5355
τ_{vz}	Lead Velocity Time Constant	$\frac{1}{3}$ (sec)	.17660
BUZOGANY'S GAINS			
k_{yi}	y-Channel Integral Gain	.01 ($\frac{1}{ft \cdot sec}$)	13.333
k_{yp}	y-Channel Proportional Gain	1 ($\frac{1}{ft}$)	707.11
k_{zi}	x-Channel Integral Gain	.0075 ($\frac{1}{sec^2}$)	.026667
k_{zp}	x-Channel Proportional Gain	.75 ($\frac{1}{sec}$)	1.4142
k_{ϕ}	Hdng Errcr Mixer Gain	0 (ft)	0
k_y	y-Separation Error Mixer Gain	1	1
k_v	Vel Error Mixer Gain	0 (sec)	0
k_z	x-Separation Error Mixer Gain	1	1

Table 4.4 Values of Test Case Plotted in 3-Dimensional Nondimensional Stability Envelopes

PARAMETER	NONDIMENSIONAL VALUE
k	501
l	716.53
k_{yi}	13.333
m	1
n	1.4142
k_{xi}	.026667

Figures 4.8 - 4.10 show that using Buzogany's gains yields a point within the stability envelope, as expected. Variations are explored in the next section.

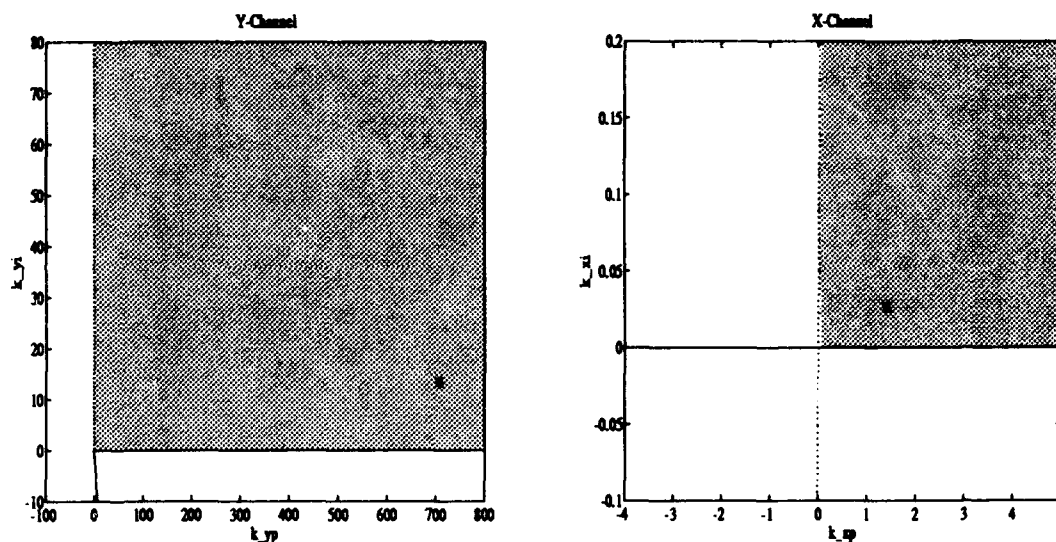


Figure 4.8 Buzogany's Case (No Mixer): Nondimensional Stability Envelopes With Test Case Plotted (See Figure 4.6 to Examine Entire Buzogany Y-Channel Envelope)

4.2.1.1 Varying k_ψ and k_ϕ . Buzogany assumed $k_\psi = 0$. By varying k_ψ , it is useful to see what happens in the stability envelopes. k_ψ and k_ϕ were varied in a manner according to Table 4.5. The resulting plots are in Figures 4.11 and 4.12. As can be seen k_ψ and k_ϕ can be varied and still be within the stability envelope (The X-Channel envelope in this plot looks different due to the magnitude of k_{xi} in the previous plots).

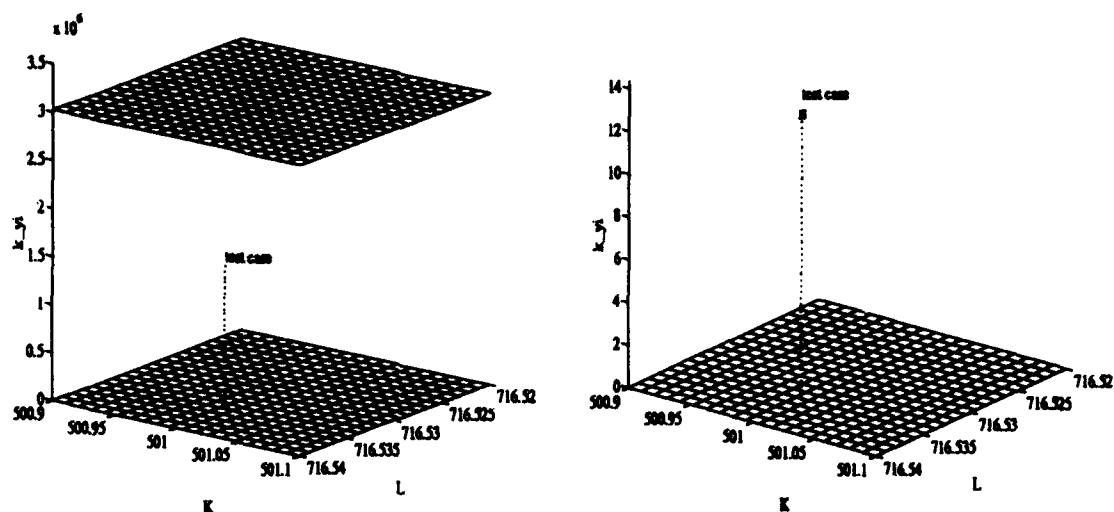


Figure 4.9 Nondimensional Y Stability Envelope With Test Case Plotted (Both Plots are Zoomed In To The Test Case Location: Right Plot Also Has K_{yi} Axis Scaled. See Figure 4.3 To See Whole Envelope Plot)

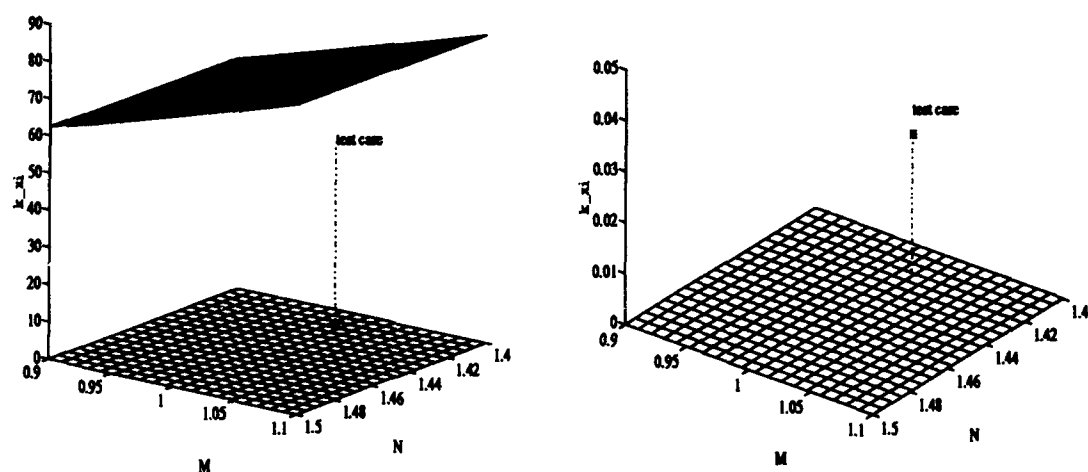


Figure 4.10 Nondimensional X Stability Envelope With Test Case Plotted (Both Plots are Zoomed In To The Test Case Location: Right Plot Also Has K_{xi} Axis Scaled. See Figure 4.5 To See Whole Envelope Plot)

Table 4.5 Variance of Nondimensional Mixer Gains for Plots

PARAMETER	UPPER	LOWER
k_y	.0001	-.0001
k_z	.05	-.05

By exploring the envelope in this way, a designer is allowed to pick stable gains and check to see where they lie inside the envelope.

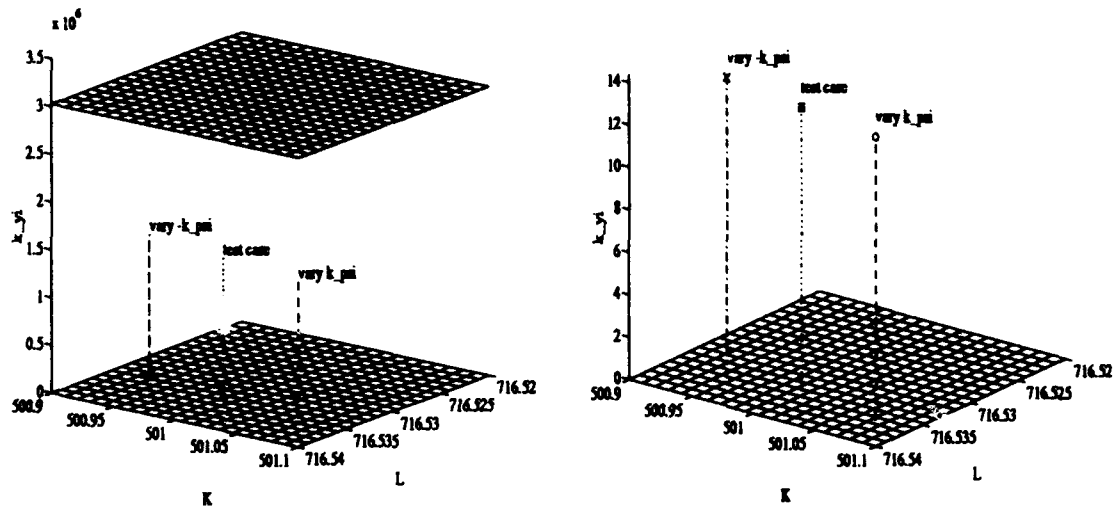


Figure 4.11 Nondimensional Y Stability Envelope With Test Case Plotted and k_y Varied (X Is Associated With $-k_y$ and O Is Associated With k_y ...Right Plot is Zoomed In Further. See Figure 4.3 To See Whole Envelope Plot))

4.2.2 Gain Envelope Conclusion. The stability problem of the x and y -channels is now solved. Picking gains to obtain a stable system can be accomplished easily. However, stability of the system is only one aspect of the control system design. Within these stability envelopes, there are many combinations of gains that will yield a stable system. However, system performance in each of these channels has not been addressed. The performance aspect is the true focus of the research and can now be explored with the knowledge of the stability boundaries.

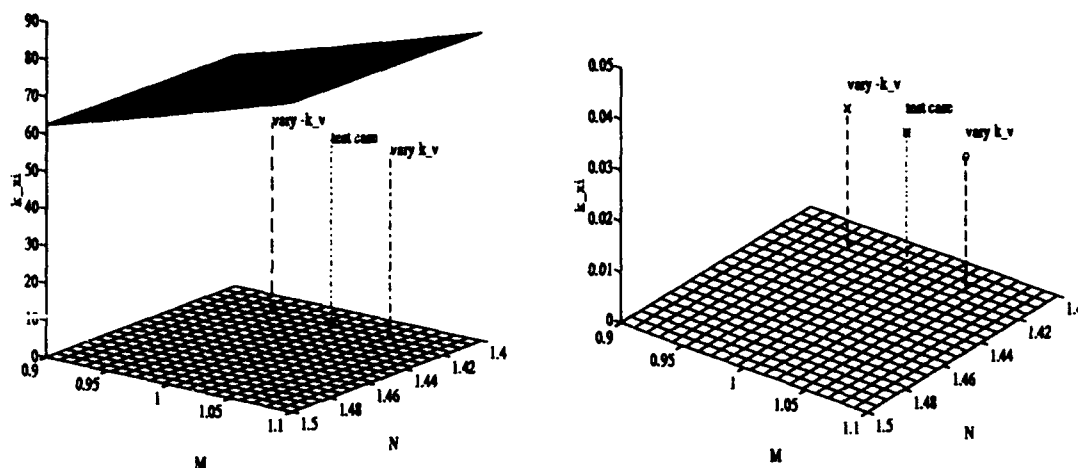


Figure 4.12 Nondimensional X Stability Envelope With Test Case Plotted and k_v Varied (X Is Associated With $-k_v$ and O Is Associated With k_v ...Right Plot is Zoomed In Further. See Figure 4.5 To See Whole Envelope Plot))

A nice result of picking gains and plotting them inside the stability envelope is an indication of system robustness to changes in the gains. A point that is in the middle of the envelope can move about the space defined by the envelope and still yield a stable system. However, a point that is near one of the stability envelope edges is not very tolerant of gain variations. A variation in the wrong direction will result in an unstable system.

The analysis accomplished on gain envelopes for the Automatic Formation Flight Control System modelled in this chapter is very useful when picking gains that yield good performance and robustness. However, this analysis is performed in the linear domain only. It is invalid when the system is nonlinear.

4.3 Pole Placement Through Controller and Linear Mixer Gain Adjustment

The closed-loop MIMO state equations developed in Sections 4.1.1 and 4.1.2 are used to aid in choosing suitable gains for the PI controller and linear mixer in each channel. Using the gains discovered previously through pole placement for the PI controller, the mixer gains are used to place poles that yield a better formation response to lead maneuvers.

These linear mixer gains are used in the nonlinear formation control system model and are refined in order that the best tracking response be obtained. These newly determined mixer gains are then kept constant while the PI controller gains are again used to place the poles of the system. The gains determined through this experimentation are simulated again in the nonlinear formation control model and refined if the tracking response is inadequate [2:page 5-12].

SISO closed-loop transfer functions are obtained for the y and x -channels that relate heading and velocity to their respective commands. They are determined using the following equation:

$$G(s) = C_d [sI - A_d]^{-1} \Gamma_d \quad (4.98)$$

The gain adjustment strategy is to induce the fastest poles corresponding with the largest residues [2:page 5-13]. A first-order response is desired.

Why would someone want a first-order response? In this case, the true system is nonlinear because of rate limiters. A first-order transfer function has the form of

$$Y(s) = \frac{1}{\tau s + 1} \quad (4.99)$$

where τ = time constant (seconds).

The output time response is

$$y(t) = 1 - e^{-\frac{t}{\tau}}. \quad (4.100)$$

Differentiating the output time response yields,

$$\dot{y}(t) = \frac{1}{\tau} e^{-\frac{t}{\tau}}. \quad (4.101)$$

The system in this thesis is nonlinear due to the inclusion of the limiters in the first-order models. However, if the rate values in the model never reach the value of the limiter, then the system is operating in the linear region and is essentially a *linear* system as long as it operates in this region. A rate is equal to $\frac{1}{\tau}$. Now, if a rate limiter in a system limits the output between $\pm 4.7^\circ$, and $\frac{1}{\tau} = 4$, the system will be linear. Therefore, it is in the best interest of the designer to ensure the system is linear by establishing a dominant pole that allows the system to remain in the linear region.

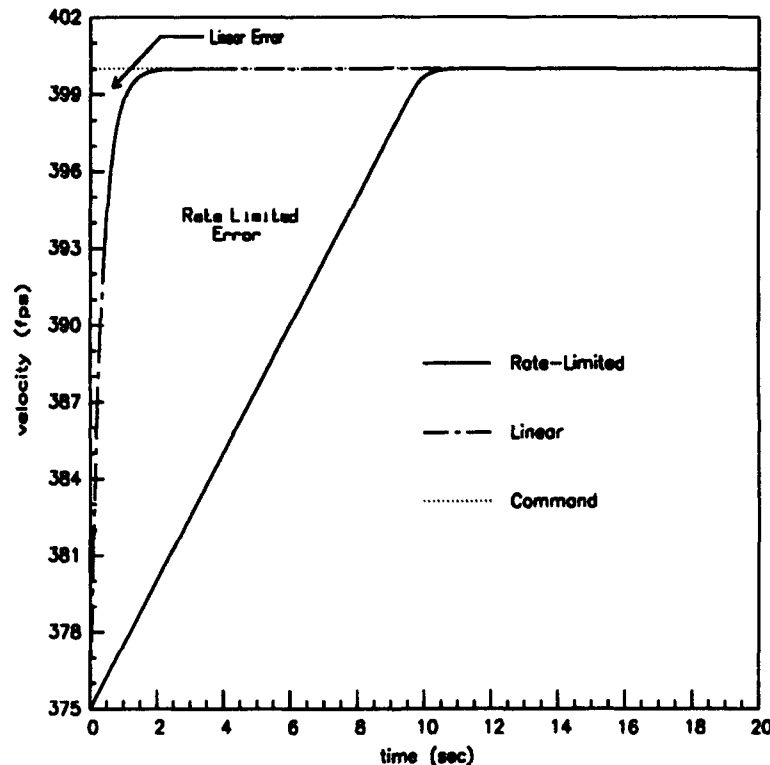


Figure 4.13 Comparison of Linear and Rate-Limited Velocity Responses [2:Figure 5.2]

Buzogany discovered in his thesis that the “rate-limiters in the aircraft [channel] models tend to produce an under-damped oscillatory response for high integral gain values. This response is caused by the increase in tracking error induced by the presence of the rate-limiters [2:page 5-13].” This is shown in Figure 4.13. Since integral control is required for tracking, there is a tradeoff situation existing in which integral control is needed but too much will cause instability.

The formation parameters and gains used in this analysis are provided in Table 4.3. These are the same values used by Buzogany in his analysis. The PI controller gains in Table 4.3 are the gains Buzogany determined through pole placement.

IMPORTANT: The following analysis is performed using dimensional quantities (i.e., time constants, gains, poles, etc). This is done to aid in the comparison of the results in Buzogany's thesis and this research.

It is important to examine how the gains used in this research are nondimensionalized. Using Equations (4.14) and (4.15), the following gains can be nondimensionalized:

$$\begin{aligned} \hat{k}_{yp} &= k_{yp} (l) & \hat{k}_{yi} &= k_{yi} \left(\frac{l^2}{V_o} \right) & \hat{k}_{xp} &= k_{xp} \left(\frac{l}{V_o} \right) & \hat{k}_{xi} &= k_{xi} \left(\frac{l}{V_o} \right)^2 \\ \hat{k}_\psi &= k_\psi \left(\frac{1}{l} \right) & \hat{k}_y &= k_y = 1 & \hat{k}_v &= k_v \left(\frac{V_o}{l} \right) & \hat{k}_z &= k_z = 1 \end{aligned} \quad (4.102)$$

However, the gains used in this section are dimensional.

4.3.1 Linear Mixer Gain Adjustment . The objective of this analysis is to determine a set of linear mixer gains for both the y and z -channels that will result in better formation responses than are possible with a PI controller alone. This is accomplished by keeping separation error signal mixer gains, k_y and k_z , equal to one (see Sections 4.1.1.1 and 4.1.2.1) and varying the remaining mixer gains, k_ψ and k_v , to determine if a dominant pole can be found.

4.3.1.1 Y-Channel Mixer Gains. The Laplace transform of the investigated output response due to a step input is

$$\psi_w(s) = \frac{1}{s} + \frac{r_2}{s + p_2} + \frac{r_3}{s + p_3} + \frac{r_4}{s + p_4} + \frac{r_5}{s + p_5} \quad (4.103)$$

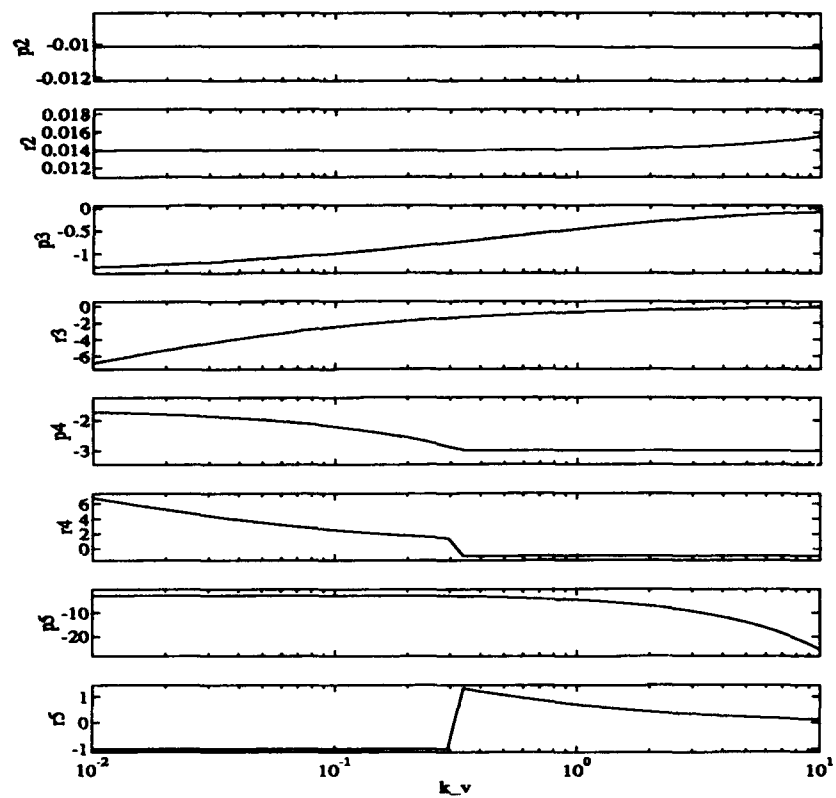


Figure 4.14 Linear System: Y-Channel, ψ_w Heading Step Response, Poles and Residues Versus k_v

This is determined by applying Equation (4.98). Keeping $k_y = 1$ and varying k_ψ results in Figure 4.14. Varying k_ψ does not result in a dominant pole. However, it seems $k_\psi > 2$ yields a better pole/residue response. Therefore, this is the starting point when the nonlinear formation model is simulated.

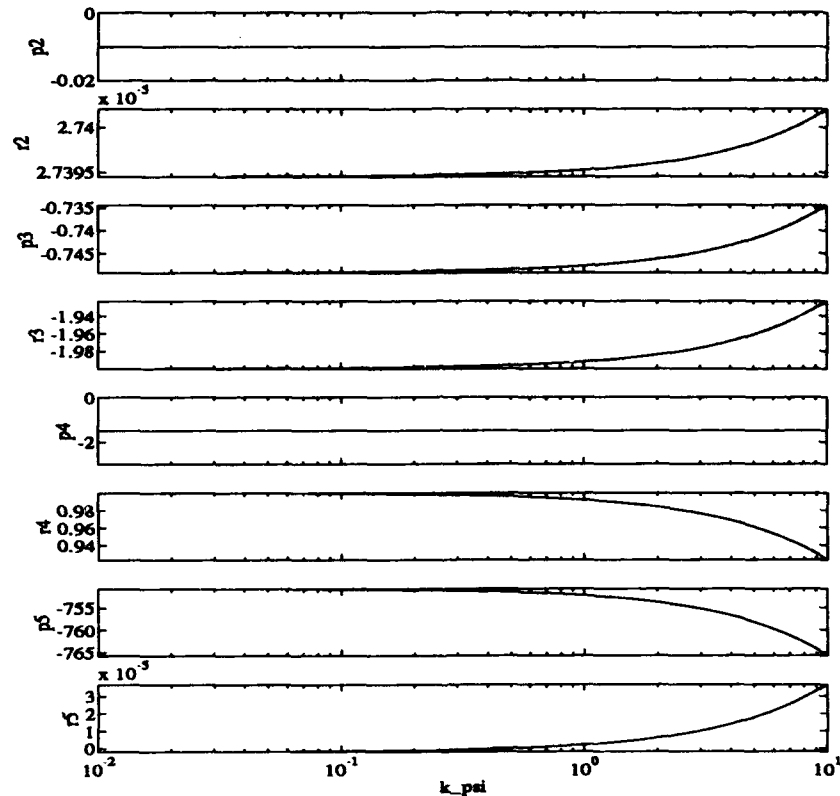


Figure 4.15 Linear System: X-Channel, V_W Velocity Step Response, Poles and Residues Versus k_ψ

4.3.1.2 X-Channel Mixer Gains. The Laplace transform of the investigated output response due to a step input is

$$V_W(s) = \frac{1}{s} + \frac{r_2}{s + p_2} + \frac{r_3}{s + p_3} + \frac{r_4}{s + p_4} + \frac{r_5}{s + p_5} \quad (4.104)$$

This is determined by applying Equation (4.98). Keeping $k_z = 1$ and varying k_v results in Figure 4.15. It seems $k_v > 1$ yields a better pole/residue response. Therefore, this will be the starting point when the nonlinear formation model is simulated.

4.3.2 Trial and Error: Mixer Gains . A heuristic process using the starting point provided by the previous section is initiated with the nonlinear simulation. The maneuvers used to exercise the system are a 10° heading change and a $25 \frac{ft}{sec}$ velocity change shown in Figures 4.16 and 4.17, respectively. Keeping $k_x = k_y = 1$, mixer gains, k_{psi} and k_v , are varied to improve formation performance.

Experimentation with k_{psi} and k_v yields some interesting observations. Varying k_{psi} has no apparent effect on a velocity change. k_{psi} does, however, affect a heading change. Observations concerning k_{psi} reveal:

- Increasing k_{psi} allows wing velocity, V_w , and z separation to peak at lower values than were previously obtainable without the mixer. However, y separation is adversely affected by increasing k_{psi} since it initially decreases before matching the trajectory of the channel without a mixer in place. As k_{psi} is increased, the y separation deviations decrease with greater magnitude before coming back to their nominal value.
- Wing heading, ψ_w or H_w in the plot, has a slightly better response with the mixer in place. It has a slightly quicker rise time.

Observations concerning k_v reveal:

- Increasing k_v allows z separation to peak at lower values than were previously obtainable without the mixer for a velocity change.
- However, as k_v is increased, the plot of z separation during a heading change peaks at a higher value than before. Therefore, k_v has to be chosen to yield good performance for a velocity change and heading change.

The preceding observations agree mathematically with the y and z -channel decoupled state equations, Equations (4.28) and (4.52). The y -channel is completely decoupled from

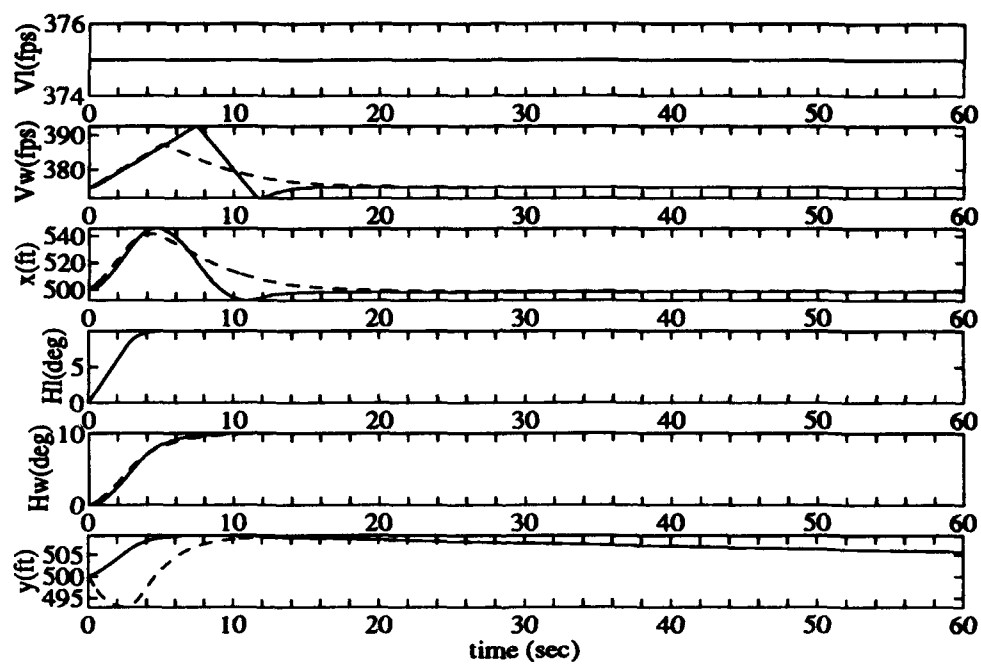


Figure 4.16 C-130A: Diamond Formation, 10 Degree Heading Change, Time Response
Comparison of Buzogany's (solid line) and New Gains (dashed line)

the z -channel. Its only modelled disturbance is the commanded lead heading change (ψ_{L_c}). Therefore, its mixer gains (i.e. k_ψ in this case) should be effective only for a heading disturbance. However, the y -channel is coupled into the z -channel through the disturbance $d_\psi = \psi_{W_c} - \psi_W$. Hence, heading changes cause z separation and wing velocity disturbances as seen in Figure 4.16 and shown mathematically in Equation (4.52), the decoupled z -channel state equation. k_ψ affects the coupling into the z -channel, or more distinctly, k_ψ affects the disturbance into the z -channel. Therefore, k_ψ must not be too large since it directly impacts the magnitude of the disturbance in the z -channel.

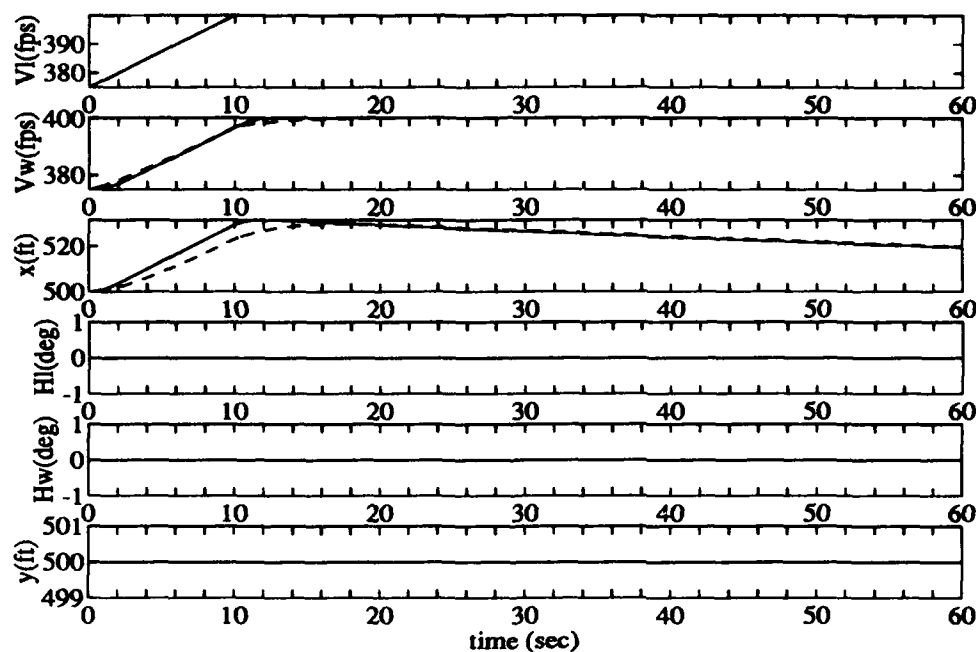


Figure 4.17 C-130A: Diamond Formation, 25 $\frac{ft}{sec}$ Velocity Change, Time Response Comparison of Buzogany's (solid line) and New Gains (dashed line)

Table 4.6 Dimensional Mixer Gains		
PARAMETER	NEW	PREVIOUS
k_ψ	4	0
k_ϕ	2	0

Table 4.7 Dimensional PI Controller Gains Used In Simulations

k_{yi}	k_{yp}	k_{zi}	k_{zp}
.01	1	.0075	.75

In the same manner, k_z must also be chosen for better performance in response to commands in both channels. It has to yield better performance during a velocity change, while allowing the z separation during a heading change to be small. The gains used for k_y and k_z are listed in Table 4.6.

It can now be concluded that the addition of a linear mixer improved aircraft performance.

(NOTE: It is an interesting observation that k_y only has an effect during a heading change, while k_z has effects both during heading and velocity changes due to the coupling of the y -channel into the z -channel.)

4.3.3 Varying Y-Channel PI Controller Gains Only. The PI controller gains affecting the y -channel, k_{yi} and k_{yp} , are now varied to determine if a dominant pole can be found. The Laplace transform of the output response being investigated is

$$\psi_w(s) = \frac{1}{s} + \frac{r_2}{s + p_2} + \frac{r_3}{s + p_3} + \frac{r_4}{s + p_4} + \frac{r_5}{s + p_5} \quad (4.105)$$

As in Buzogany's thesis, the PI controller gains are varied while the pole and residues are determined. The mixer gains are the same as in Table 4.6. The ratio $\frac{k_{yz}}{k_{yi}}$ is fixed while k_{yp} is varied from 10^{-3} to 10. Figure 4.18 shows how varying the PI controller gains affects the poles and residues of the output response. There is not a gain range that allows a dominant pole. The problem lies with including the lead states into the model. It contributes a pole at -1.5 with residue at approximately 1. This pole interferes with other poles' dominance. Therefore, varying the PI controller gains alone does not yield a dominant pole.

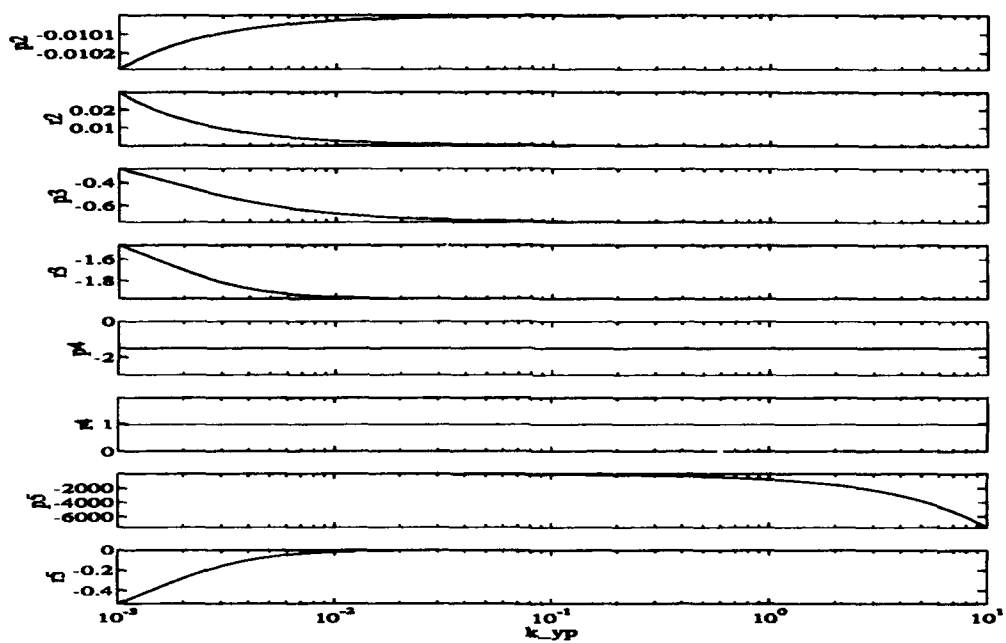


Figure 4.18 Linear System: Y-Channel, ψ_w Heading Step Response, Poles and Residues Versus Controller Gains, $\frac{k_{yz}}{k_{yi}} = 100$

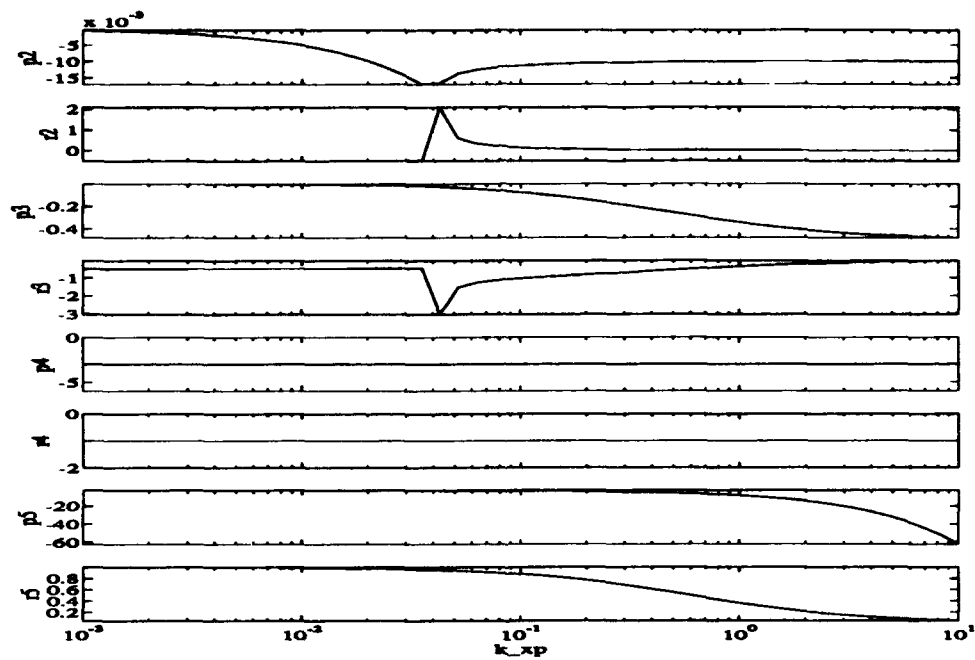


Figure 4.19 Linear System: X-Channel, V_w Heading Step Response, Poles and Residues Versus Controller Gains, $\frac{k_{xp}}{k_{xi}} = 100$

4.3.4 Varying X-Channel PI Controller Gains Only. The gains affecting the z-channel, k_{zi} and k_{zp} , are now varied to determine if a dominant pole can be found. The Laplace transform of the output response being investigated is

$$V_W(s) = \frac{1}{s} + \frac{r_2}{s + p_2} + \frac{r_3}{s + p_3} + \frac{r_4}{s + p_4} + \frac{r_5}{s + p_5} \quad (4.106)$$

Like the y-channel, the PI controller gains are varied while the poles and residues of the system are determined. The mixer gains are those used in Table 4.6. The ratio $\frac{k_{z2}}{k_{zi}}$ is fixed while k_{zp} is varied from 10^{-3} to 10. Figure 4.19 shows how varying the PI controller gains affect the poles and zeros of the output response. Once again there is not a gain range that yields a dominant pole.

Since no dominant pole can be found, a trial and error process is used to determine the best formation response. Buzogany's PI controller gains listed in Table 4.3 are used as a baseline.

4.3.5 Trial and Error: PI Controller Gains. After determining the mixer gains in the previous section, attention is now focused on the PI controller. A trial and error approach is used once again to investigate the possibility of improving the formation performance.

Using Buzogany's PI controller and the linear mixer determined in the previous section as a starting point, the PI controller gains in both channels are changed while the mixer is kept constant. The gains in Table 4.8 yield better performance than that of Section 4.3.2 when implemented in the simulation. (See Figures 4.20 and 4.21).

Table 4.8 Adjusted Dimensional PI Controller Gains Used In Simulations To Achieve Better Performance

k_{yi}	k_{yp}	k_{zi}	k_{zp}
.1	1	.1	1

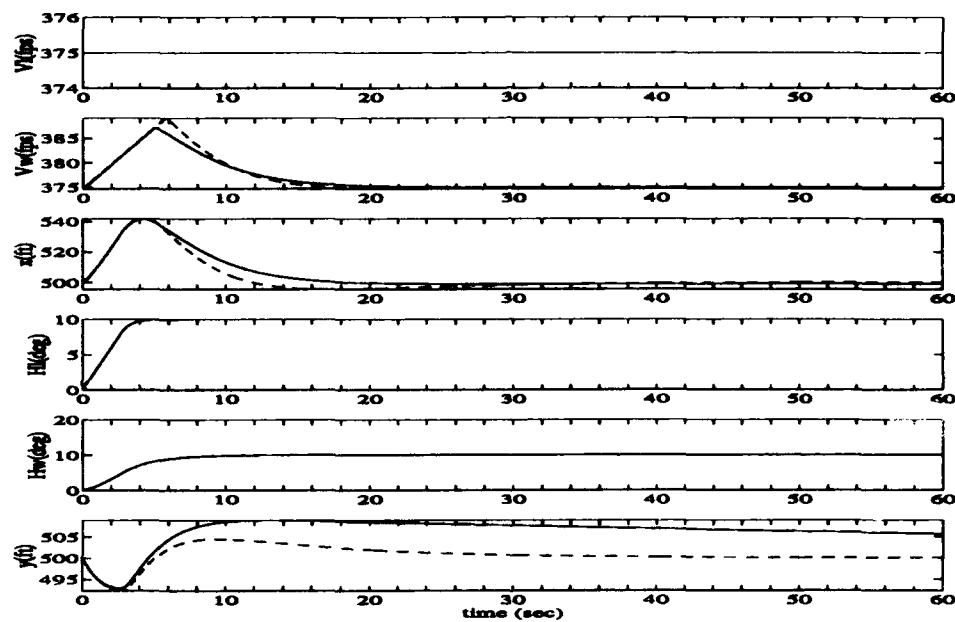


Figure 4.20 C-130A: Diamond Formation, 10 Degree Heading Change, Time Response Comparison of Figure 4.16 (solid line) and New PI Gains (dashed line)

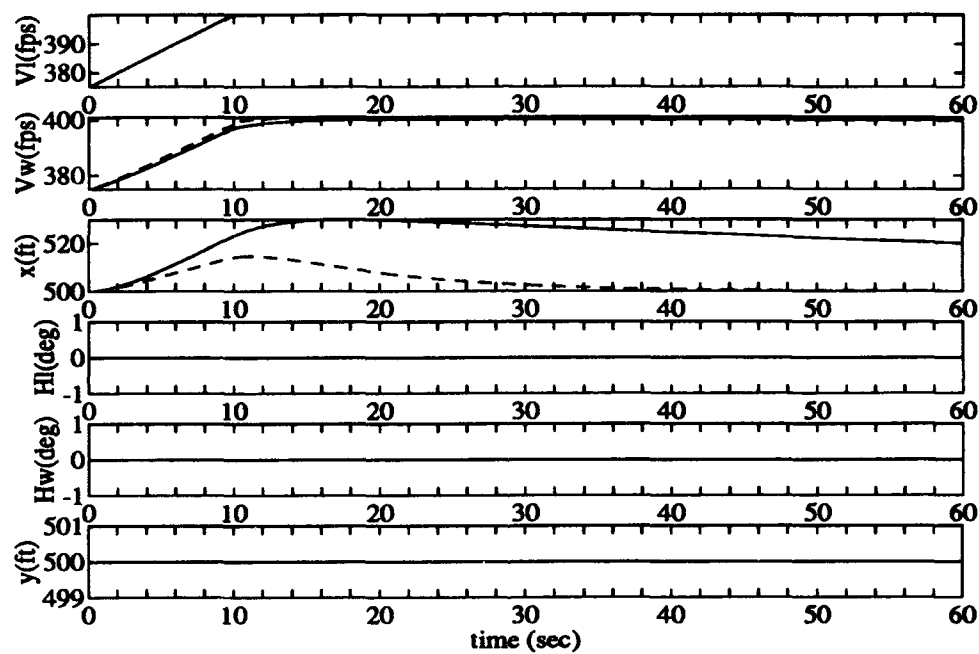


Figure 4.21 C-130A: Diamond Formation, 25 $\frac{ft}{sec}$ Velocity Change, Time Response Comparison of Figure 4.17 (solid line) and New Gains (dashed line)

Similar to Section 4.3.2, the y -channel gains only affect a heading change while the x -channel gains affect both heading and velocity changes. Once again, this is due to the disturbance in the x -channel due to the y -channel coupling into the x -channel.

4.3.6 Comparison of New Dimensional Gains With Those of Dargan's. The gains determined by Dargan were found empirically, like the new gains listed in Tables 4.6 and 4.7. The gains Dargan used are in Table 4.9. These same gains were used by Buzogany in Chapter 7 of his thesis when using first-order models. C-130B models are now used to compare to simulation runs accomplished by Buzogany in Chapter 7 of his thesis.

Table 4.9 Dargan's Dimensional Gains (See Also Table 4.10 For Adjusted k_v)

<i>Dimensional Gains</i>	<i>Value</i>
k_{yp}	.5
k_{yi}	.05
k_{xp}	.17
k_{xi}	.02
k_x	2
k_v	5
k_y	1
k_ψ	10

As can be seen by examination of Figures 4.22 and 4.23, the new gains provide a better response for all states of the system with the notable exception of V_w when a 30° heading change is commanded as in Figure 4.22. The gains used by Dargan and Buzogany have a much better response for V_w than the new gains found. The question to ask is which provides the best overall performance. The constraint most important to formation flying is that of maintaining an adequate separation distance. No matter what the maneuver is, if the aircraft involved cannot perform it in a timely manner due to their formation separation response then the formation flight control system is not adequate. The new gains yield a much better separation response for both heading changes and velocity changes. The increase in wing velocity for a 30° heading change in Figure 4.22 is approximately $14 \frac{mi}{hr}$ more than the response of the Buzogany/Dargan gains. This is a minimal change.

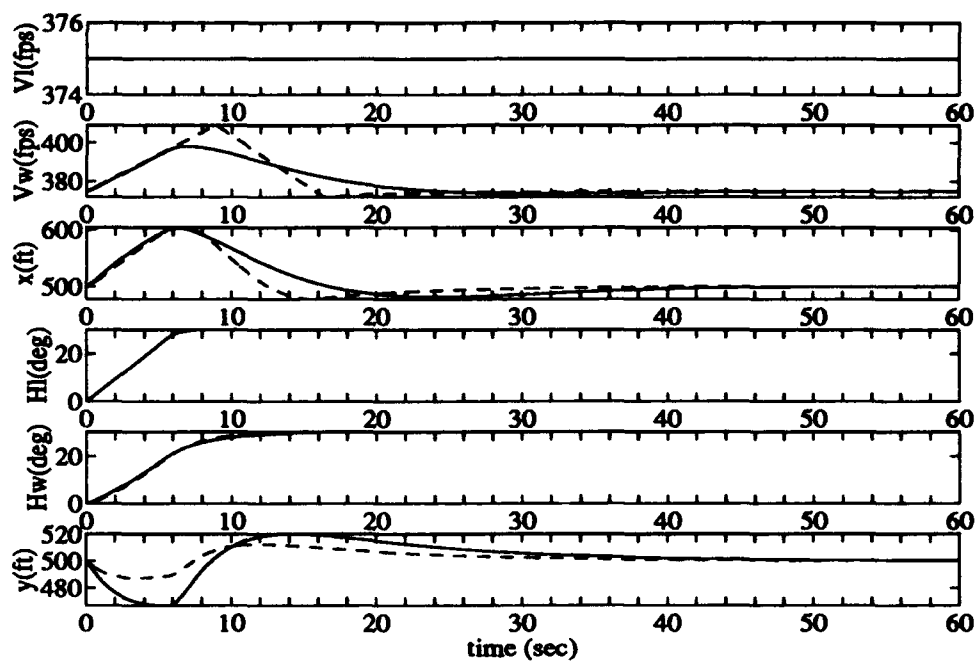


Figure 4.22 C-130B: Diamond Formation, 30 Degree Heading Change, Time Response Comparison Of Dargan/Busogany Gains For Mixer And PI Controller (solid line) And New PI Gains (dashed line). First-Order Models Are Used

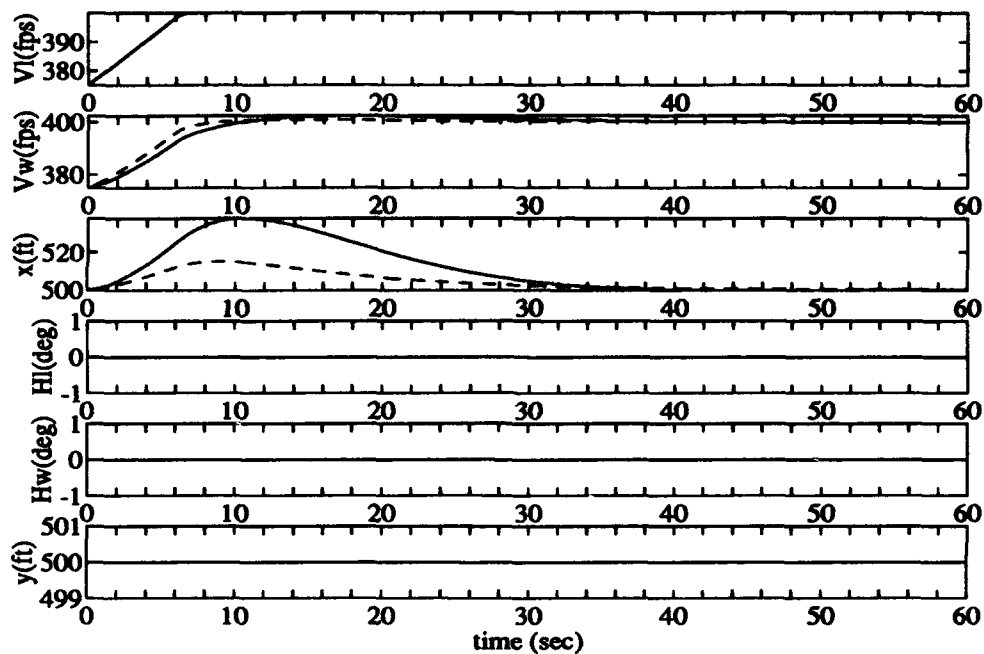


Figure 4.23 C-130B: Diamond Formation, 25 $\frac{ft}{sec}$ Velocity Change, Time Response Comparison Of Dargan/Buzogany Gains For Mixer And PI Controller (solid line) And New PI Gains (dashed line). First-Order Models Are Used

Examining the y -separation response deviation in the same figure shows it to be much better (approximately 20 ft). Separation between aircraft is the more important of the two indicators.

Even though the new gains give a better overall response, it seems the responses can be refined slightly more. Therefore, following additional trial and error approach, the only gain that needs to be changed is k_v . The new k_v is listed in Table 4.10.

Table 4.10 Adjusted Gain To Refine Response of Figure 4.22

Adjusted Dimensional Parameter	Value
k_v	3

Examining Figure 4.24 it is seen that the response is slightly better than that of Figure 4.22. During simulations it is seen that there is a tradeoff between V_w , wing velocity, and z -separation. As V_w increases there is less deviation from the nominal z -separation distance and vice-versa. This makes physical sense. If a diamond formation composed of two aircraft makes a heading change, the wing aircraft will have to increase speed if it is on the outside of the turn. If wing speed is increased, there should be less deviation in the nominal z -separation (following this same argument, the converse is also true). An additional benefit is the operation of the wing velocity stays longer in the linear region of operation than previously.

4.4 Dimensional Eigenvalue Comparison

(See Appendix A for *dimensional* plant models) Applying Equation (4.98) to the dimensionalized y -channel yields the y -channel closed-loop transfer functions which when disturbed by the lead aircraft heading command results in the Laplace output response below.

$$\psi_w(s) = G(s)\psi_{Lc}(s) = \begin{bmatrix} 0 & 1 & 0 & 0 \end{bmatrix} [sI - A_v]^{-1} \Gamma_v \frac{1}{s} \quad (4.107)$$

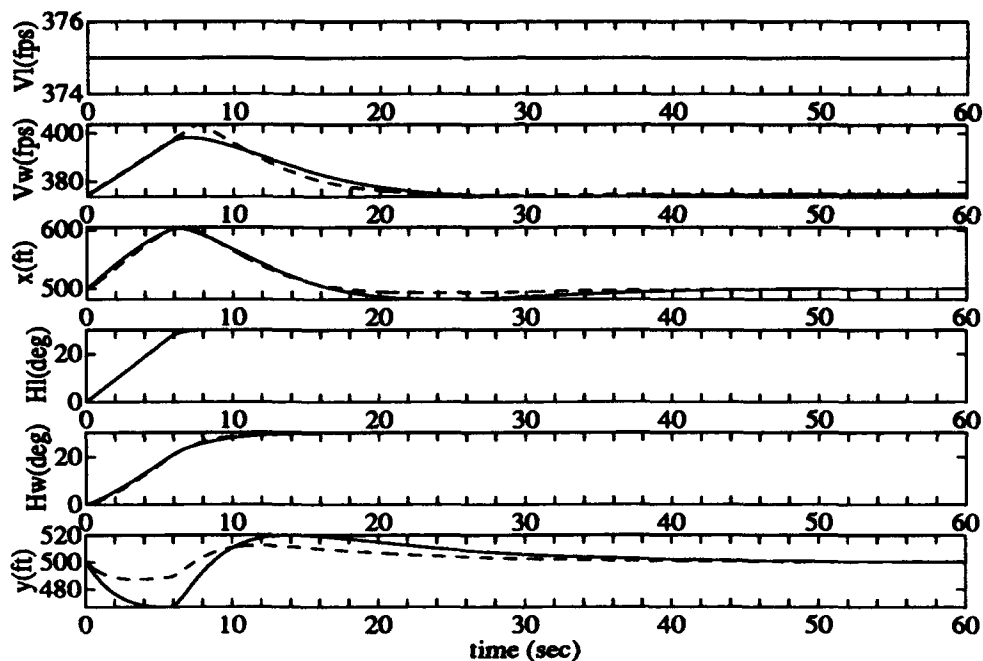


Figure 4.24 C-130B: Diamond Formation, 30 Degree Heading Change, Time Response Comparison Of Dargan/Buzogany Gains For Mixer And PI Controller (solid line) And New PI Gains (dashed line). First-Order Models Are Used. $k_v = 3$.

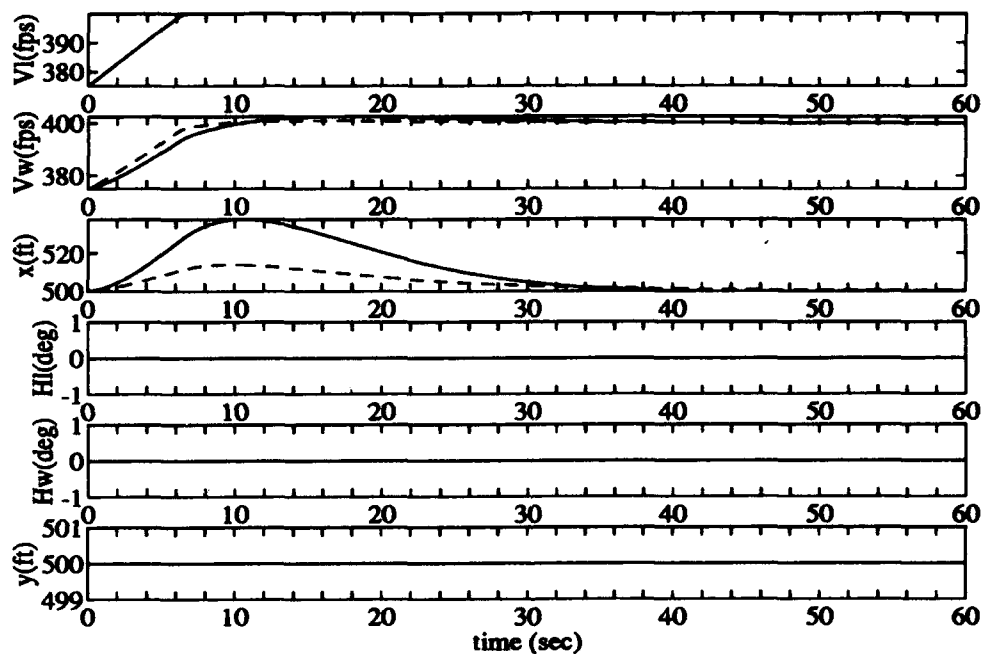


Figure 4.25 C-130B: Diamond Formation, $25 \frac{ft}{sec}$ Velocity Change, Time Response Comparison Of Dargan/Buzogany Gains For Mixer And PI Controller (solid line) And New PI Gains (dashed line). First-Order Models Are Used. $k_v = 3$.

where, the mixer and PI controller gains are those specified in Table 4.11.

Table 4.11 Mixer and PI Controller Gains Used In Dimensional Eigenvalue Comparisons

Parameter	k_{yi}	k_{yp}	k_{ϕ}	k_y	k_{zi}	k_{zp}	k_v	k_s
Dimensional Value	.1	1	4	1	.1	1	3	1

Now,

$$A_y = \begin{bmatrix} 0 & 375 & 375 & -750 \\ 0 & -1.5 & 0 & 1.5 \\ 0 & 0 & -1.5 & 0 \\ .1 & 380.6 & 369.4 & -756 \end{bmatrix}, \Gamma_y = \begin{bmatrix} 0 \\ 0 \\ 1.5 \\ 6 \end{bmatrix}, C_y = \begin{bmatrix} 0 & 1 & 0 & 0 \end{bmatrix} \quad (4.108)$$

therefore,

$$\psi_w(s) = \frac{1}{s} + \frac{.00035587}{s + .10003} + \frac{-1.9689}{s + .74319} + \frac{.9685}{s + 1.5} + \frac{.000013813}{s + 756.66} \quad (4.109)$$

Buzogany's Laplace output response is (see Buzogany [2], Equation (5.58))

$$\psi_w(s) = G(s)\psi_L(s) = \overbrace{\frac{1}{s} + \frac{.0001}{s + .01} + \frac{-1.0010}{s + .7492} + \frac{.0010}{s + 750.7408}}^{\text{Buzogany's Response}} \quad (4.110)$$

dominant

As can be seen in Equation (4.109), there is not any one pole that is dominant as in Equation (4.110). Therefore, its behavior will not be a classical first-order response when disturbed by a step input.

An interesting observation can be made by comparing the new eigenvalues and residues (Equation(4.109)) to those of Buzogany (Equation (4.110)). There is a close correspondence between the eigenvalues, but not the residues, however. The eigenvalue that does not correspond to Buzogany's response is due to the inclusion of the lead aircraft states into the Formation Flight Control problem formulation. Another observation is that

since the sum of the residues equals 0, the denominator is two or more degrees higher than the numerator [5:page 117]. (This last statement was proven to be true using the ss2tf (state-space-2-transfer-function) command in Matlab)

Applying Equation (4.98) to the x -channel, where

$$A_x = \begin{bmatrix} 0 & -1 & 1 & 0 \\ 0 & -3 & 0 & 3 \\ 0 & 0 & -3 & 0 \\ .1 & 7.7 & -7.7 & -9 \end{bmatrix}, \Gamma_x = \begin{bmatrix} 0 & 750 \\ 0 & 0 \\ 3 & 0 \\ 9 & 750 \end{bmatrix}, C_x = \begin{bmatrix} 0 & 1 & 0 & 0 \end{bmatrix} \quad (4.111)$$

results in the following Laplace transform of the output response

$$V_W(s) = G(s) \begin{bmatrix} V_{L_c}(s) \\ D_\Psi(s) \end{bmatrix} = \begin{bmatrix} 0 & 1 & 0 & 0 \end{bmatrix} [sI - A_x]^{-1} \Gamma_x \frac{1}{s} \quad (4.112)$$

therefore, with V_{L_c} as the input,

$$V_W(s) = \frac{1}{s} + \frac{.37130}{s + .12299} + \frac{-.63590}{s + .20906} + \frac{-1}{s + 3} + \frac{.26459}{s + 11.668} \quad (4.113)$$

and, with d_Ψ as the input,

$$V_W(s) = \frac{750}{s} + \frac{423.21}{s + .12299} + \frac{-1190.1}{s + .20906} + \frac{5.9348 \times 10^{-14}}{s + 3} + \frac{16.862}{s + 11.668} \quad (4.114)$$

Buzogany's Laplace output is (see Buzogany [2], Equation (5.59)),

$$V_W(s) = G_x(s)D_x(s) = \overbrace{\frac{1}{s} + \frac{.0138}{s + .0101} + \frac{-6.6677}{s + 1.3719} + \frac{5.6538}{s + 1.6179}}^{\text{Buzogany's Response}} \quad (4.115)$$

Once again, there are some interesting observations that can be made by comparing the eigenvalues and residues of the two responses. There is not a close correspondence between the eigenvalues of the different approaches as there is in the y -channel. There is no dominant pole in the new response and Buzogany's response. The residues approximately add up to zero, thus the denominator is two or more degrees higher than the numerator [5:page 117]. (This last statement was proven to be true using the `ss2tf` (state-space-2-transfer-function) command in Matlab). Once again, the first order-model pole shows up in the response. This pole is not allowing any other pole to become dominant.

The disturbance response is also interesting. It has a large magnitude and no true dominant pole. Its step response will not exactly be a first order response, but will be closer than the velocity and heading step responses. It is of no immediate concern to the Formation Flight Control system since it is the response of the disturbance, $\psi_w - \psi_w$, which goes to zero in steady-state.

4.4.1 Plots of Linear System Response To A Unit Step. The linearised model responses are simulated in order to compare the newly derived model with Buzogany's model. Figure 4.26 shows the ψ_w response to a unit step disturbance for both the new system and Buzogany's, Figure 4.27 shows the V_w response to a unit step disturbance for both systems, and Figure 4.28 shows the V_w response to the y -channel coupling into the x -channel.

As can be seen from these figures, the addition of the lead aircraft states into the linearized plant model has resulted in slower rise times for the different responses. This makes physical sense. With addition of more dynamics into the system, additional phase lag is introduced, thus slowing the responses.

4.5 Conclusion

This chapter develops a linearized and parameterized MIMO plant. It then presents a thorough investigation of x and y -channel stability and their stability envelopes. The

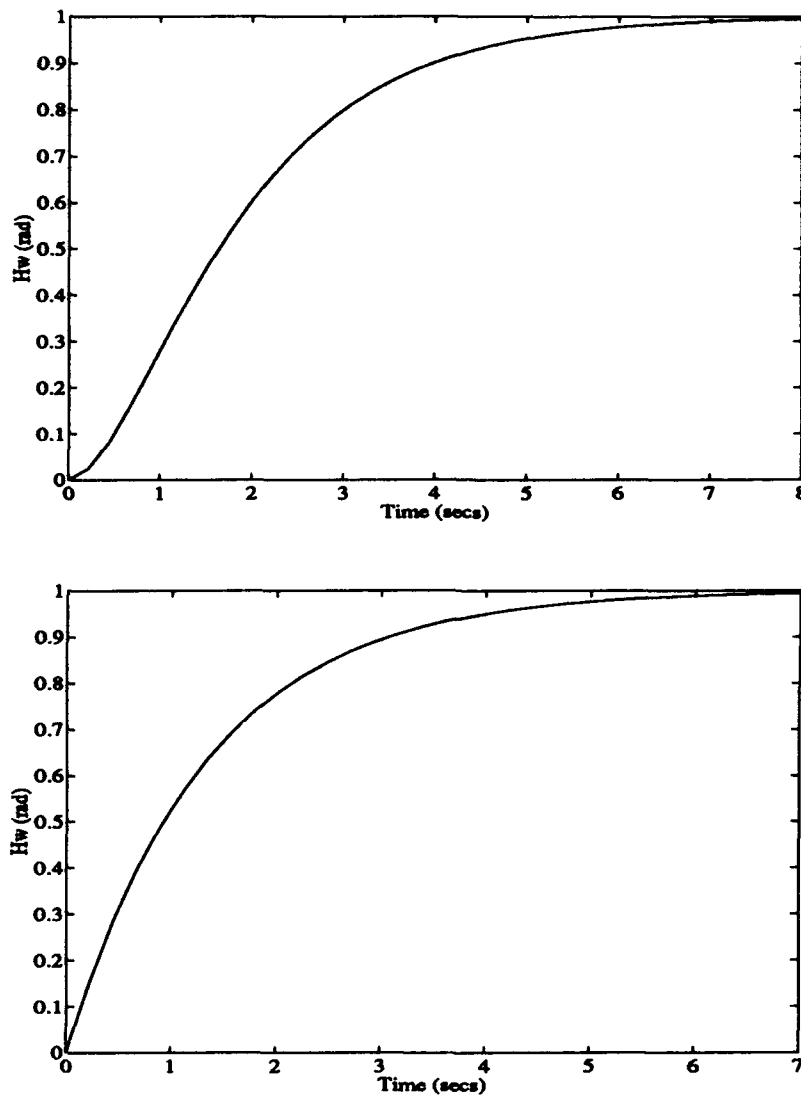


Figure 4.26 (Linear System) TOP: New ψ_W Response to a Unit Step Disturbance (ψ_L) with Mixer and PI Controller; BOTTOM: Buzogany's ψ_W Response to a Unit Step Disturbance (ψ_L) with Mixer Only

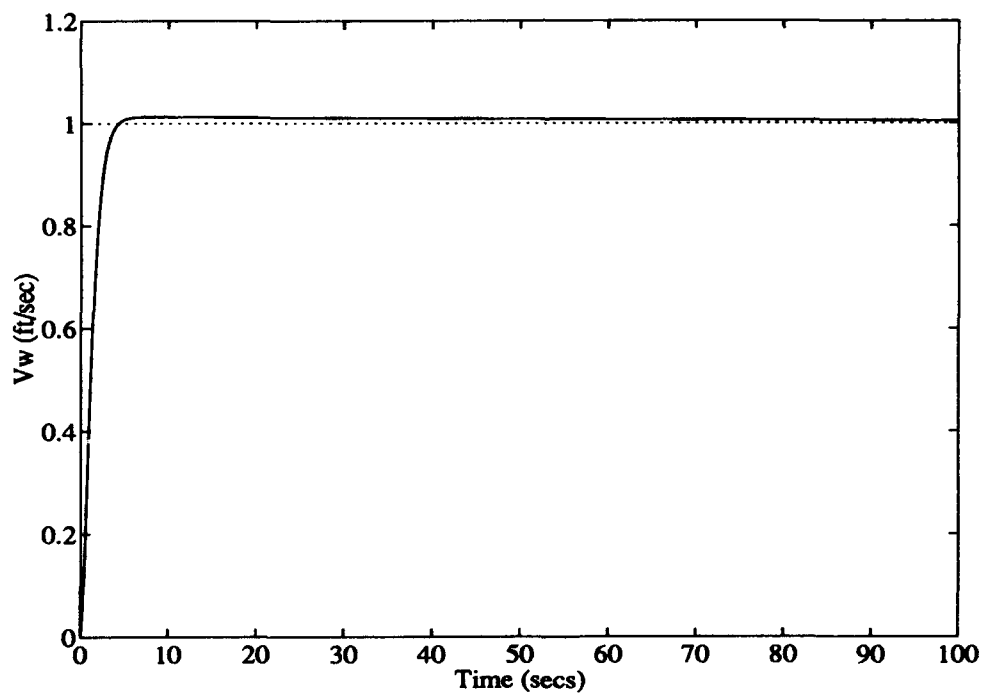
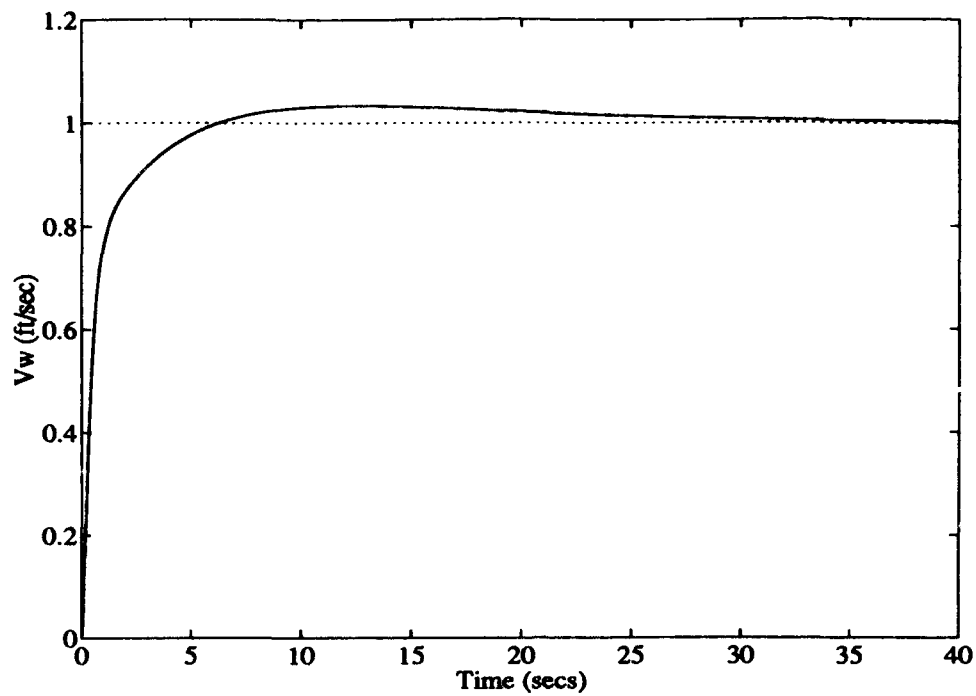


Figure 4.27 (Linear System) TOP: New V_w Response to a Unit Step Disturbance (V_{L_c}) with Mixer and PI Controller; BOTTOM: Buzogany's V_w Response to a Unit Step Disturbance (V_L) with Mixer Only

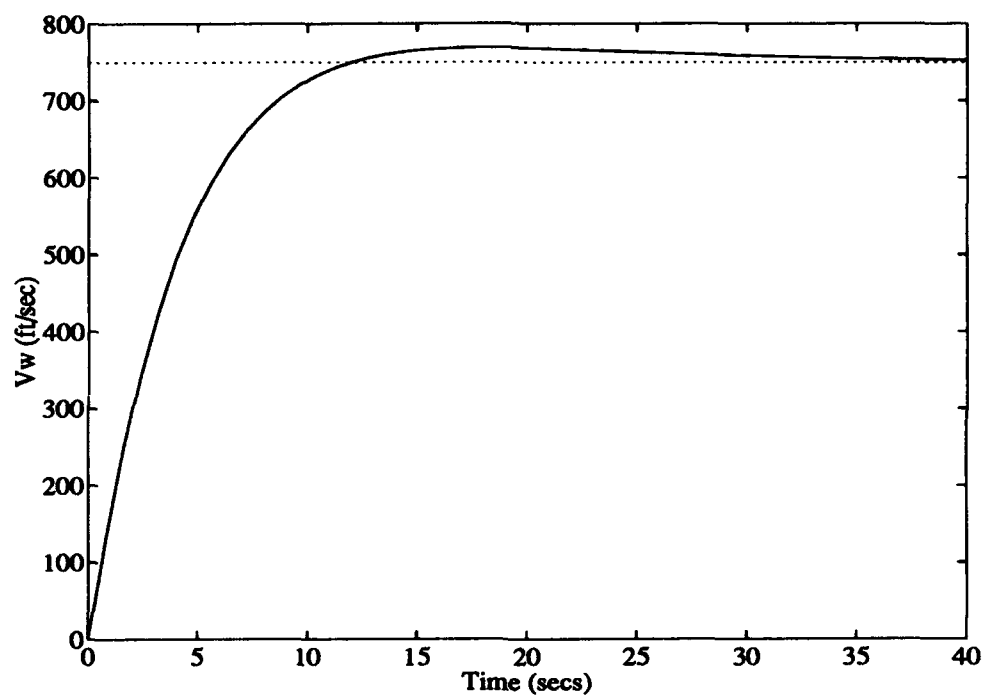


Figure 4.28 Linear System: V_w Response to a Unit Step Disturbance ($d\psi$)

performance of the new system and previous work is compared. Finally, an eigenvalue comparison between present and previous work is accomplished.

The final and overall result of the previous analysis is that the addition of a linear mixer does indeed improve system performance.

V. Three Dimensional Energy Excursion Minimizing Maneuvers

In Chapter IV, formation velocity and heading changes accomplished in the plane (i.e., they are two dimensional maneuvers) are considered. Consequently, the wing aircraft has a smaller or larger turn radius than the lead aircraft during a heading change, due to the constraint of two dimensional maneuvers. This necessitates a wing acceleration/deceleration sequence. This chapter investigates the possibility of performing three dimensional maneuvers and maintaining formation integrity in steady-state. This research is a continuation of the research begun by Buzogany in 1992 [2:Chapter 6]. Buzogany's thesis formulation only considered automatic flight control heading change maneuvers. This research is extended to include the design of a formation hold autopilot using energy minimizing maneuvers which will allow velocity and altitude change maneuvers in addition to heading change maneuvers.

Three Dimensional Maneuvers afford the possibility of conserving the wing aircraft's energy. Instead of accelerating/decelerating to maintain formation integrity as in the two dimensional problem, the wing aircraft now has the ability to accelerate/decelerate by decreasing/increasing altitude, respectively, without, however, having to change its energy state. The latter is most intimately connected to throttle activity, which is reduced. This is done at the expense of separation requirements. Therefore, maintaining the vertical separation requirement between the lead and wing aircraft is relaxed in order to accommodate maneuvers outside of the lead aircraft's flight plane. Also as a result, the h -channel is coupled into the x -channel.

The analysis of three dimensional maneuvers is accomplished in this chapter with first-order aircraft models.

5.1 Development

Following the same initial theoretical development as in Buzogany, Chapter 6, the (total) specific energy of an object is the sum of its kinetic and potential energy per unit mass. Therefore, the total specific energy for the wing aircraft is

$$e_W = gh_W + \frac{1}{2}V_W^2 \quad (5.1)$$

where

g = acceleration of gravity

e_W = wing aircraft's specific energy

h_W = wing aircraft's altitude

Differentiating Equation (5.1) and setting \dot{e}_W equal to zero leads to the fundamental relationship for energy conservation,

$$\dot{e}_W = V_o \dot{V}_W + g \dot{h}_W = 0 \quad (5.2)$$

Using the first-order aircraft altitude response model from Buzogany's thesis [2:Equation (6.3)],

$$\dot{h}_W = -\frac{1}{\tau_{h_W}} h_W + \frac{1}{\tau_{h_W}} h_{W_c}, \quad (5.3)$$

and substituting Equation (4.3), the first-order aircraft velocity response model, into Equation (5.2) yields the following equation,

$$\dot{e}_W = -\frac{g}{\tau_{h_W}} h_W - \frac{V_o}{\tau_{V_W}} V_W + \frac{g}{\tau_{h_W}} h_{W_c} + \frac{V_o}{\tau_{V_W}} V_{W_c}, \quad (5.4)$$

which shows the total specific energy development when it is controlled by an altitude change and/or a velocity change.

Like Chapter IV, it is desirable to nondimensionalize and parameterize Equation (5.4). Once again, Equations (4.14), (4.15), and V_o will be used to nondimensionalize Equations (5.3) and (5.4) (Equation (4.3) has already been nondimensionalized, See Equation (4.18)). Therefore, the additional nondimensional variables are:

$$\begin{aligned} \hat{h}_W &= \frac{h_W}{l}; & \hat{h}_{W_o} &= \frac{h_{W_o}}{l}; & \hat{\tau}_{h_W} &= \frac{\tau_{h_W}}{t}; \\ \hat{e}_W &= \frac{e_W}{V_o^2}; & \hat{e}_{W_o} &= \frac{e_{W_o}}{V_o^2} \end{aligned} \quad (5.5)$$

(The “~” symbol is now dropped for convenience. All variables are nondimensional unless otherwise noted.)

The nondimensional form of Equation 5.4 is ,

$$\dot{e}_W = -\frac{gl}{V_o^2} \frac{1}{\tau_{h_W}} h_W + \frac{1}{\tau_{V_W}} V_W + \frac{gl}{V_o^2} \frac{1}{\tau_{h_W}} h_{W_o} + \frac{1}{\tau_{V_W}} V_{W_o} \quad (5.6)$$

A common factor in Equation (5.6) is $\frac{gl}{V_o^2}$. This expression is nondimensional. Therefore,

$$\xi \triangleq \frac{gl}{V_o^2} \quad (5.7)$$

where,

ξ = nondimensional altitude to velocity proportionality constant [2:page 6-2].

Substituting ξ for $\frac{gl}{V_o^2}$ yields,

$$\dot{e}_W = -\xi \frac{1}{\tau_{h_W}} h_W + \frac{1}{\tau_{V_W}} V_W + \xi \frac{1}{\tau_{h_W}} h_{W_o} + \frac{1}{\tau_{V_W}} V_{W_o} \quad (5.8)$$

With a slight abuse of notation, the derivative states of Equation (5.2), can be assumed to be perturbations, and V_o is the unperturbed formation speed. Equation (5.2) now becomes

$$\underbrace{e_w = gh_w + V_o V_w}_{\text{dimensional equation}} \quad (5.9)$$

Rearranging Equation (5.9) and isolating V_w yields,

$$\underbrace{V_w = \frac{1}{V_o} e_w - \frac{g}{V_o} h_w}_{\text{dimensional equation}} \quad (5.10)$$

In nondimensional form,

$$V_w = e_w - \xi h_w \quad (5.11)$$

Now, Equation (5.11) is substituted into Equation (5.8). The resulting equation is

$$\dot{e}_w = -\frac{1}{\tau_{V_w}} e_w + \xi \left(\frac{1}{\tau_{V_w}} - \frac{1}{\tau_{h_w}} \right) h_w + \xi \frac{1}{\tau_{h_w}} h_{w_o} + \frac{1}{\tau_{V_w}} V_{w_o} \quad (5.12)$$

Taking Equation (4.17), the nondimensionalized \dot{z} separation equation of Chapter IV, and substituting Equation (5.11) for V_w results in the following:

$$\dot{z} = \xi h_w - e_w + d \quad (5.13)$$

where,

$$d = V_L + \frac{\sin \alpha}{\tau_{\psi_w}} (\psi_{w_o} - \psi_w) \quad (5.14)$$

In addition, the lead aircraft altitude state is available:

$$\dot{h}_L = -\frac{1}{\tau_{h_L}} + \frac{1}{\tau_{h_L}} h_{L_o} \quad (5.15)$$

Therefore, h_e , the altitude error signal can be generated.

Equations (5.3), (5.12), (5.13), and (5.15) can now be put into state space form,

$$\dot{X}_{zs} = A_{zs}X_{zs} + B_{zs}U_{zs} + \Gamma_{zs}D_{zs} \quad (5.16)$$

hence,

$$\begin{aligned} \begin{bmatrix} \dot{z} \\ \dot{h}_w \\ \dot{e}_w \\ \dot{h}_L \end{bmatrix} &= \begin{bmatrix} 0 & \xi & -1 & 0 \\ 0 & -\frac{1}{\tau_{h_w}} & 0 & 0 \\ 0 & \xi \left(\frac{1}{\tau_{v_w}} - \frac{1}{\tau_{h_w}} \right) & -\frac{1}{\tau_{v_w}} & 0 \\ 0 & 0 & 0 & -\frac{1}{\tau_{h_L}} \end{bmatrix} \begin{bmatrix} z \\ h_w \\ e_w \\ h_L \end{bmatrix} \\ &+ \begin{bmatrix} 0 & 0 \\ 0 & \frac{1}{\tau_{h_w}} \\ \frac{1}{\tau_{v_w}} & \xi \frac{1}{\tau_{h_w}} \\ 0 & 0 \end{bmatrix} \begin{bmatrix} V_{w_c} \\ h_{w_c} \end{bmatrix} + \begin{bmatrix} 1 & 0 & \frac{\sin \alpha}{\tau_{\phi_w}} \\ 0 & 0 & 0 \\ 0 & 0 & 0 \\ 0 & \frac{1}{\tau_{h_L}} & 0 \end{bmatrix} \begin{bmatrix} V_L \\ h_{L_c} \\ d_\phi \end{bmatrix} \end{aligned} \quad (5.17)$$

where, $d_\phi = \psi_{w_c} - \psi_w$, as in Chapter IV, Section 4.1.2.

As in Buzogany's thesis, there is a need for a PI controller to be designed to command the wing's altitude response to a change in z -separation [2:page 6-2]. Hence, the PI controller is

$$h_{w_c} = k_{zsp}x + k_{zsi} \int_0^t x \, dt \quad (5.18)$$

where,

k_{zsp} = nondimensional, three dimensional z -separation error, proportional gain

k_{zsi} = nondimensional, three dimensional z -separation error, integral gain

Differentiating Equation (5.18) results in

$$\dot{h}_{w_c} = k_{zsp}\dot{x} + k_{zsi}x \quad (5.19)$$

Substituting Equation (5.13) into Equation (5.18) yields a result similar to Busogany [2:Equation (6.10)],

$$\dot{h}_{W_e} = k_{ssp}\xi h_W - k_{ssp}e_W + k_{ssp}d + k_{ssi}x \quad (5.20)$$

Now a new control concept is needed to relate energy conservation and commanded velocities. This new control concept is based on using V_{W_e} as a control to conserve the wing's total specific energy during a formation maneuver. Conserving the wing aircraft's total specific energy implies moderate throttle usage. Therefore,

$$\dot{e}_W = \frac{V(T - D)}{m}, \quad (5.21)$$

where,

T = aircraft's thrust

D = aircraft's drag

m = aircraft's mass

Using a PI control law as before,

$$V_{W_e} = k_{ssp_v} h_e + k_{ssi_v} \int_0^t h_e dt \quad (5.22)$$

where,

$h_e = h_L - h_W$ = altitude error

k_{ssp_v} = nondimensional, three dimensional altitude error, proportional gain

k_{ssi_v} = nondimensional, three dimensional altitude error, integral gain

However, Equation (5.22) does not conserve the wing aircraft's energy. If \dot{e}_W is set equal to zero in Equation (5.12), the equation is solved for V_{W_e} , and the new relation for V_{W_e} is added to Equation (5.22), the following control law is obtained:

$$V_{W_c} = \underbrace{\tau_{V_w} \left(\frac{1}{\tau_{V_w}} e_w + \xi \left[\frac{1}{\tau_{h_w}} - \frac{1}{\tau_{V_w}} \right] h_w - \xi \frac{1}{\tau_{h_w}} h_{W_c} \right)}_{\text{Energy Conserving} = \text{elevator usage}} + \underbrace{k_{ssp_v} h_e + k_{ssi_v} \int_0^t h_e dt}_{\text{Energy Changing} = \text{throttle usage}} \quad (5.23)$$

This control law is a contradiction in terms, because there are two distinct and different parts. The part determined by setting $\dot{e}_w = 0$ conserves the wing aircraft specific energy, and thus works the elevator of the wing aircraft. In contrast, the PI controller, contingent upon altitude error, changes the wing specific energy. It is actually commanding the throttle usage of the wing aircraft. The two pieces form an energy minimising control law. Differentiating Equation (5.23) yields:

$$\dot{V}_{W_c} = \tau_{V_w} \left(\frac{1}{\tau_{V_w}} \dot{e}_w + \xi \left[\frac{1}{\tau_{h_w}} - \frac{1}{\tau_{V_w}} \right] \dot{h}_w - \xi \frac{1}{\tau_{h_w}} \dot{h}_{W_c} \right) + k_{ssp_v} \dot{h}_e + k_{ssi_v} h_e \quad (5.24)$$

The closed loop zz -channel is found by augmenting the open loop state space, Equation (5.17), with V_{W_c} and h_{W_c} . The resulting closed loop state space is:

$$\dot{X}_{zsc} = A_{zsc} X_{zsc} + \Gamma_{zsc} D_{zsc} \quad (5.25)$$

$$Y_{zsc} = C_{zsc} X_{zsc} \quad (5.26)$$

hence,

$$\begin{bmatrix} \dot{x} \\ \dot{h}_w \\ \dot{e}_w \\ \dot{h}_L \\ \dot{V}_w \\ \dot{h}_w \end{bmatrix} = \begin{bmatrix} 0 & \xi & -1 & 0 & 0 & 0 \\ 0 & -\frac{1}{\tau_{hw}} & 0 & 0 & 0 & \frac{1}{\tau_{hw}} \\ 0 & \xi \left(\frac{1}{\tau_{vw}} - \frac{1}{\tau_{hw}} \right) & -\frac{1}{\tau_{vw}} & 0 & \frac{1}{\tau_{vw}} & \xi \frac{1}{\tau_{hw}} \\ 0 & 0 & 0 & -\frac{1}{\tau_{hl}} & 0 & 0 \\ -\tau_{vw} \xi \frac{1}{\tau_{hw}} k_{zsi} & D_{hw} & D_{ew} & D_{hl} & \frac{1}{\tau_{vw}} & D_{hw_c} \\ k_{zsi} & k_{zsp} \xi & -k_{zsp} & 0 & 0 & 0 \end{bmatrix} \begin{bmatrix} x \\ h_w \\ e_w \\ h_L \\ V_w \\ h_w \end{bmatrix} \\
+ \begin{bmatrix} 1 & 0 & 0 & 0 & 0 & 0 \\ 0 & 0 & 0 & 0 & 0 & 0 \\ 0 & 0 & 0 & 0 & 0 & 0 \\ 0 & \frac{1}{\tau_{hl}} & 0 & 0 & 0 & 0 \\ -\tau_{vw} \xi \frac{1}{\tau_{hw}} k_{zsp} & k_{zsp} \frac{1}{\tau_{hl}} & -\tau_{vw} \xi \frac{1}{\tau_{hw}} k_{zsp} \frac{\sin \alpha}{\tau_{vw}} & 0 & 0 & 0 \\ k_{zsp} & 0 & k_{zsp} \frac{\sin \alpha}{\tau_{vw}} & 0 & 0 & 0 \end{bmatrix} \begin{bmatrix} V_L \\ h_{Lc} \\ d_\phi \end{bmatrix} \quad (5.27)$$

$$Y_{zz} = \begin{bmatrix} 1 & 0 & 0 & 0 & 0 & 0 \\ 0 & -1 & 0 & 1 & 0 & 0 \end{bmatrix} = \begin{bmatrix} x \\ h_c \end{bmatrix} \quad (5.28)$$

where,

$$D_{hw} = \xi \left(\frac{1}{\tau_{vw}} - \frac{1}{\tau_{hw}} \right) - \tau_{vw} \xi \frac{1}{\tau_{hw}} \left(\frac{1}{\tau_{hw}} - \frac{1}{\tau_{vw}} \right) - \tau_{vw} \xi^2 \frac{1}{\tau_{hw}} k_{zsp} + k_{zspv} \frac{1}{\tau_{hw}} - k_{zsi v} \quad (5.29)$$

$$D_{ew} = -\frac{1}{\tau_{vw}} + \tau_{vw} \xi \frac{1}{\tau_{hw}} k_{zsp} \quad (5.30)$$

$$D_{hl} = -\frac{1}{\tau_{hl}} k_{zspv} + k_{zsi v} \quad (5.31)$$

$$D_{hw_c} = \xi \frac{1}{\tau_{hw}} + \tau_{vw} \xi \frac{1}{\tau_{hw}} \left(\frac{1}{\tau_{hw}} - \frac{1}{\tau_{vw}} \right) - k_{zspv} \frac{1}{\tau_{hw}} \quad (5.32)$$

and,

X_{zsc} = augmented zz -channel state vector

A_{zsc} = augmented zz -channel plant matrix

Γ_{zsc} = augmented zz -channel input matrix

$D_{zz,d}$ = augmented zz -channel input vector

$Y_{zz,d}$ = augmented zz -channel output vector

$C_{zz,d}$ = augmented zz -channel output matrix

5.1.1 *Difference Between The New Approach and Previous (Buzogany's) Approach.*

In Chapter 6 of Buzogany's thesis, energy conserving maneuvers were considered. They were accomplished by using the control h_w , and feeding back x separation. In the new formulation, energy excursion minimization is investigated. h_w is still a control and x -separation is fed back, however, h_e , the altitude error, is also fed back and an additional control, $V_{w,e}$, is implemented.

Previously, during a heading change, wing aircraft velocity changes were made by changing altitude during a turn. Once the turn was completed the wing aircraft used its kinetic energy to return to the lead's flight plane. However, if the lead aircraft actually changed speed, then the wing aircraft would increase or decrease its own velocity by changing its altitude and thus maintaining constant specific energy, e_w . Therefore, the previous system was satisfactory during formation heading changes but not for formation energy changes, where changing velocity or altitude meant a corresponding change in the other.

The concept of energy excursion minimizing, presented in this chapter, tries to conserve energy but also allows the wing aircraft to track the lead aircraft through both heading and velocity changes. This is accomplished by keeping Buzogany's approach in place and augmenting it with a PI control law. Equation (5.23) without the PI controller is $\dot{e}_w = 0$. Therefore, by including the PI controller in Equation (5.23) the requirement for keeping the $\dot{e}_w = 0$ has been relaxed. No longer does energy conservation apply. The object of the zz -control system is to minimize the energy swings, namely throttle usage. Therefore, during a heading change, the aircraft will still alter its x -separation by changing its altitude, but it will return back to its flight plane quicker due to moderate throttle usage. However, energy changes can now be accommodated. Hence, the energy minimizing is more capable than energy conserving maneuvers. However, it is not as energy efficient

during formation maneuvers. Thus, wing aircraft capability has been increased at the expense of wing aircraft energy.

5.1.1.1 Why The Addition of The PI Controller Works. Looking at Equations (5.18) and (5.23), one might wonder how a control scheme can be effective in which one control law commands an altitude change in response to x-separation, while another control law commands a velocity change based upon altitude error. This is accomplished due to the time constants of the two controlled states. The velocity time constant is smaller than the altitude time constant. Therefore, the velocity response will be quicker responding to a command than the altitude response. Examining Equations (3.1) and (3.3), and inserting their respective time constants yields the following transfer functions:

First-order velocity transfer function and time response equation,

$$V(s) = \frac{3}{s + 3} \quad (5.33)$$

$$v(t) = 3e^{-3t} \quad (5.34)$$

First-order altitude transfer function and time response equation,

$$H(s) = \frac{.5}{s + .5} \quad (5.35)$$

$$h(t) = .5e^{-.5t} \quad (5.36)$$

By looking at Equations (5.33) and (5.35) or Equations (5.34) and (5.36), it is obvious that the velocity equations will reach steady-state faster than the altitude equations. To illustrate this further, look at Figure 5.1.

Theoretically, the sequence of events for a velocity change should appear in this order:

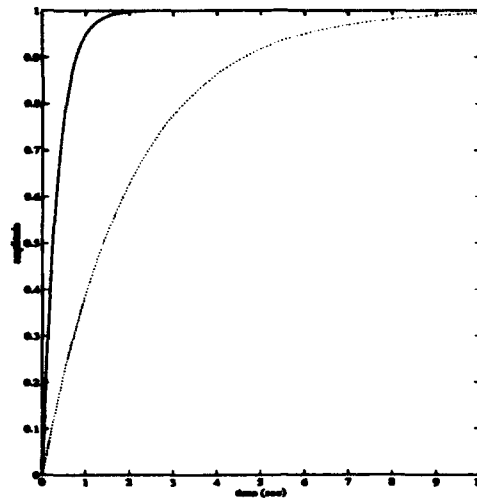


Figure 5.1 Comparison of $v(t)$ (solid line) and $h(t)$ (dotted line)

1. During a maneuver, the x separation response will deviate from its nominal value
2. An altitude command based on the x -separation error will be issued. This command also is included with wing altitude perturbation, h_w , to command the velocity channel first order model to increase speed in order that the x -separation error will return to zero. This is the energy conserving part of the control law
3. In addition to this, a PI controller is included in the wing velocity command control law that is active once there is an altitude error between the lead and wing aircraft. Therefore, in addition to the energy conserving part of the control law, there is a energy changing part which commands more velocity as the altitude error increases
4. Because of the time constants of the two channels, the altitude response should generally be slower than the velocity response to the respective commands. Therefore, one can expect an initial change in altitude but less altitude loss due to the increase of velocity during an energy minimizing maneuver

This is validated by simulation.

5.1.2 Static Stability Analysis. As in Chapter IV, Section 4.1.2, the linear system is investigated to determine if the system is able to track a step disturbance input in V_L or h_{Lc} (Remember $d_\psi \rightarrow 0$ at steady state, See Section 4.1.2). It is imperative that the aircraft be able to track an altitude or velocity command. Like the two dimensional case, this requirement can be stated as follows:

for disturbance $h_{Lc}(s) = \frac{1}{s}$,

$$\begin{aligned} \text{As } t \rightarrow \infty, \quad x(\infty) = V_{Wc} = 0, \text{ and } h_W(\infty) = h_L(\infty) = h_{Wc} = D_{zs} = 1, \\ \text{and } e_W(\infty) = \xi \end{aligned} \quad (5.37)$$

for disturbance $V_L = \frac{1}{s}$,

$$\begin{aligned} \text{As } t \rightarrow \infty, \quad x(\infty) = h_W(\infty) = h_L(\infty) = h_{Wc}(\infty) = 0, \\ \text{and } e_W(\infty) = V_{Wc}(\infty) = V_L(\infty) = 1; \end{aligned} \quad (5.38)$$

The requirements of Equations (5.37) and (5.38) are verified by observing the zx -channel response to unit step disturbances, V_L , h_{Lc} , and d_ψ (the mathematics in this section are accomplished with Mathematica [7]):

$$x(t)_{ss} = \lim_{s \rightarrow 0} s \frac{1}{s} (SI - A_{zz})^{-1} \Gamma_{zs} = -A_{zz}^{-1} \Gamma_{zs} = \begin{bmatrix} 0 & 0 & 0 \\ 0 & 1 & 0 \\ 1 & \xi & \frac{\sin \alpha}{\tau_{\psi W}} \\ 0 & 1 & 0 \\ 1 & 0 & \frac{\sin \alpha}{\tau_{\psi W}} \\ 0 & 1 & 0 \end{bmatrix} \quad (5.39)$$

Since $d_\psi \rightarrow 0$ in steady state, the third column of Equation (5.39) is of no consequence and is disregarded in analysis. However, the first two columns are the expected results from the conditions of Equations (5.37) and (5.38). The results of Equation (5.39) are true if A_{zz} is invertible. This implies the following relation:

$$k_{zzi} \neq 0 \quad (5.40)$$

Conclusion: Once again (see Chapter IV, Sections 4.1.2 and 4.1.1), integral control is necessary for this technique to work. Furthermore, x feedback is necessary.

5.1.3 *Dynamic Stability Analysis* . The characteristic equation is

$$\det(SI - A_{zzcl}) = s^6 + is^5 + js^4 + ks^3 + ls^2 + ms + n \quad (5.41)$$

where the coefficients are,

$$i = \frac{1}{\tau_{hL}} + \frac{1}{\tau_{hW}} \quad (5.42)$$

$$j = \frac{1}{\tau_{hW}} \left(\frac{1}{\tau_{hL}} - k_{zsp}\xi \right) \quad (5.43)$$

$$k = \frac{1}{\tau_{hW}} \left(-\frac{k_{zsp}k_{zspv}}{\tau_{VW}} - k_{zzi}\xi - \frac{k_{zsp}\xi}{\tau_{hL}} \right) \quad (5.44)$$

$$l = \frac{1}{\tau_{hW}} \left(-\frac{k_{zziV}k_{zsp}}{\tau_{VW}} - \frac{k_{zzi}k_{zspv}}{\tau_{VW}} - \frac{k_{zsp}k_{zspv}}{\tau_{hL}\tau_{VW}} - \frac{k_{zzi}\xi}{\tau_{hL}} \right) \quad (5.45)$$

$$m = \frac{1}{\tau_{hW}} \left(-\frac{k_{zzi}k_{zziV}}{\tau_{VW}} - \frac{k_{zziV}k_{zsp}}{\tau_{hL}\tau_{VW}} - \frac{k_{zzi}k_{zspv}}{\tau_{hL}\tau_{VW}} \right) \quad (5.46)$$

$$n = -\frac{k_{zzi}k_{zziV}}{\tau_{hL}\tau_{hW}\tau_{VW}} \quad (5.47)$$

The Routhian array for Equation (5.41) is in Table 5.1.

The following relations result from the Routh criterion application of Table 5.1:

row s^5

$$\tau_{hL} + \tau_{hW} > 0 \quad (5.48)$$

Table 5.1 XZ-Channel Routhian Array

s^6	1	j	l	n
s^5	i	k	m	
s^4	$\frac{ij-k}{i}$	$\frac{il-m}{i}$	n	
s^3	$\frac{ijk-h^2-i^2l+im}{ij-k}$	$\frac{ijm-km-i^2n}{ij-k}$		
s^2	$\frac{ijhl-k^2l-i^2l^2-ij^2m+jkm+2ilm-m^2+i^2jn-ikn}{ij-k-h^2-i^2l+im}$	n		
s^1	$\frac{ijkilm-h^2lm-i^2l^2m-ij^2m^2+jkm^2+2ilm^2-m^3-ijh^2n+h^3n+i^2hln+2i^2jmn-3ikmn-i^4n^2}{ijhl-k^2l-i^2l^2-ij^2m+jkm+2ilm-m^2+i^2jn-ikn}$			
s^0	n			

row s^4

$$k_{zsp}k_{zspv}\tau_{hL}^2\tau_{hw} + \tau_{hL}\tau_{VW} + \tau_{hw}\tau_{VW} - k_{zsp}\tau_{hL}^2\tau_{VW}\xi + k_{zzi}\tau_{hL}^2\tau_{hw}\tau_{VW}\xi > 0 \quad (5.49)$$

row s^3

$$\begin{aligned} & -(k_{zsp}^2k_{zspv}^2\tau_{hL}^3\tau_{hw}) + k_{zzi}k_{zsp}\tau_{hL}^3\tau_{VW} + k_{zzi}k_{zspv}\tau_{hL}^3\tau_{VW} + k_{zsp}k_{zspv}\tau_{hL}\tau_{hw}\tau_{VW} \\ & + k_{zzi}k_{zsp}\tau_{hL}^2\tau_{hw}\tau_{VW} + k_{zzi}k_{zspv}\tau_{hL}^2\tau_{hw}\tau_{VW} - k_{zzi}k_{zzi}v\tau_{hL}^3\tau_{hw}\tau_{VW} + k_{zsp}k_{zspv}\tau_{hL}^2\tau_{VW} \\ & - k_{zzi}k_{zzi}v\tau_{hL}^2\tau_{hw}\tau_{VW} + k_{zsp}^2k_{zspv}\tau_{hL}^3\tau_{VW}\xi - k_{zsp}^2k_{zspv}\tau_{hL}^2\tau_{hw}\tau_{VW}\xi \\ & - 2k_{zzi}k_{zsp}k_{zspv}\tau_{hL}^3\tau_{hw}\tau_{VW}\xi - k_{zsp}\tau_{hL}\tau_{VW}^2\xi - k_{zsp}\tau_{hw}\tau_{VW}^2\xi + k_{zzi}\tau_{hL}\tau_{hw}\tau_{VW}^2\xi \\ & + k_{zzi}\tau_{hw}^2\tau_{VW}^2\xi + k_{zsp}^2\tau_{hL}^2\tau_{VW}^2\xi^2 + k_{zzi}k_{zsp}\tau_{hL}^3\tau_{VW}^2\xi^2 - k_{zzi}k_{zsp}\tau_{hL}^2\tau_{hw}\tau_{VW}^2\xi^2 \\ & - k_{zzi}^2\tau_{hL}^3\tau_{hw}\tau_{VW}^2\xi^2 > 0 \end{aligned} \quad (5.50)$$

rows $s^2 - s^1$ are in Appendix B

row s^0

$$k_{zzi}k_{zzi}v > 0 \quad (5.51)$$

Equations (5.48) - (5.51) were found in part through the use of Mathematica [7]. The equations for rows s^3 - s^1 are very large and difficult to analyze. Due to time constraints, the stability envelopes of these stability relations will not be explored in this thesis effort.

These stability relations show the interrelationships between the controller and mixer gains, first-order aircraft model time constants, and stability. It is interesting to note that this analysis agrees with the static stability analysis and demonstrates integral control action is once again required for stability. Equation 5.51 shows that $k_{ssi} \neq 0$ and $k_{ssiv} \neq 0$. Therefore, it is a requirement for Energy Excursion Minimizing Maneuvers to have integral control action in both the h_{w_c} and the V_{w_c} control laws.

5.2 Mathematical Analysis of Three Dimensional Maneuvers

Buzogany's thesis effort did not calculate V_{w_c} . Instead, V_w was determined directly through the physics of the problem (i.e, V_w was found by assuming $e_w = 0$ and solving for V_w in Equation (5.11)). It is useful to calculate Buzogany's actual velocity control law.

Beginning with the first-order equation for the aircraft velocity [Equation (4.18)]

$$\dot{V}_w = -\frac{1}{\tau_{V_w}} V_w + \frac{1}{\tau_{V_w}} V_{w_c} \quad (5.52)$$

Substitute the relation for V_w , when $e_w = 0$ from Equation (5.11),

$$V_w = -\xi h_w \quad (5.53)$$

Equation (5.52) becomes,

$$-\xi \dot{h}_w = \xi \frac{1}{\tau_{V_w}} h_w + \frac{1}{\tau_{V_w}} V_{w_c} \quad (5.54)$$

Substitute the nondimensional form of Equation (5.3) into Equation (5.54) and solve for V_{w_c} to obtain

$$V_{W_e} = \xi h_w \left(\frac{\tau_{V_w}}{\tau_{h_w}} - 1 \right) - \xi \frac{\tau_{V_w}}{\tau_{h_w}} h_{W_e} \quad (5.55)$$

This differs from Equation (5.23) in two ways:

1. The PI controller utilizing altitude error is absent. This was not in Buzogany's formulation of the problem
2. ξe_w term is also absent. This is because Buzogany assumed $e_w = 0$

Thus,

Preposition V.1 *In the linear case, the new control law in Equation (5.23) with the PI controller gains set to zero will be the same velocity control law Buzogany had previously in his thesis.*

However, there is a problem with Equation (5.55). This was Buzogany's V_{W_e} if he commanded the first-order velocity model given in Equation (5.52). However, he did not do that. Instead, he used Equation (5.53) to find velocity. In order to determine what his actual V_{W_e} was, Equation (5.55) needs to be reexamined and all terms containing τ_{V_w} should be neglected. This leaves the following equation:

$$V_{W_e} = -\xi h_w \quad (5.56)$$

Which is the same as Equation (5.53). This equation is Buzogany's true V_{W_e} since he did not have the first-order velocity model included in his simulation.

The differences in implementation between Buzogany's and the new simulation are illustrated in Figures 5.2 and 5.3, respectively.

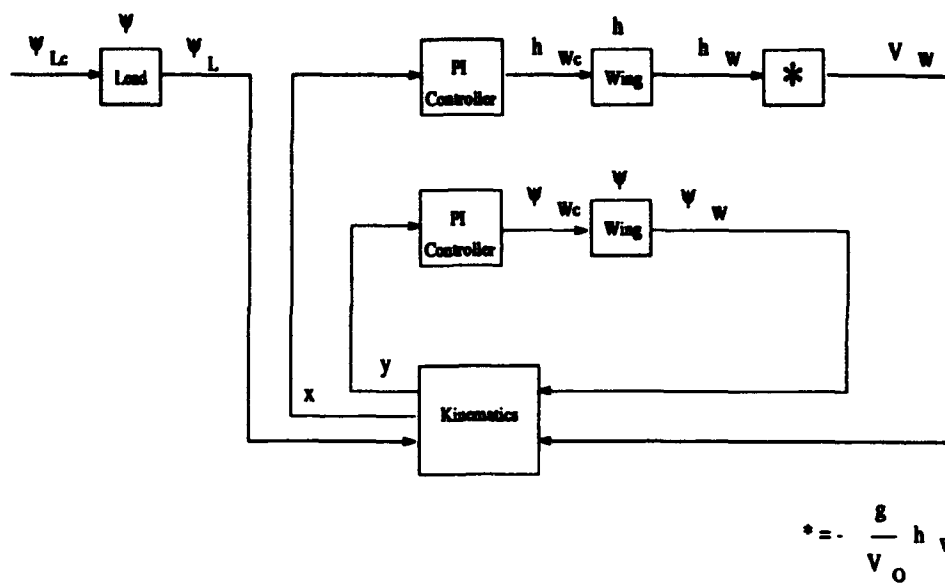


Figure 5.2 Energy Conservation: Buzogany's Three Dimensional Maneuvers Simulation Formulation, With the Aircraft Specific Energy Rate = 0

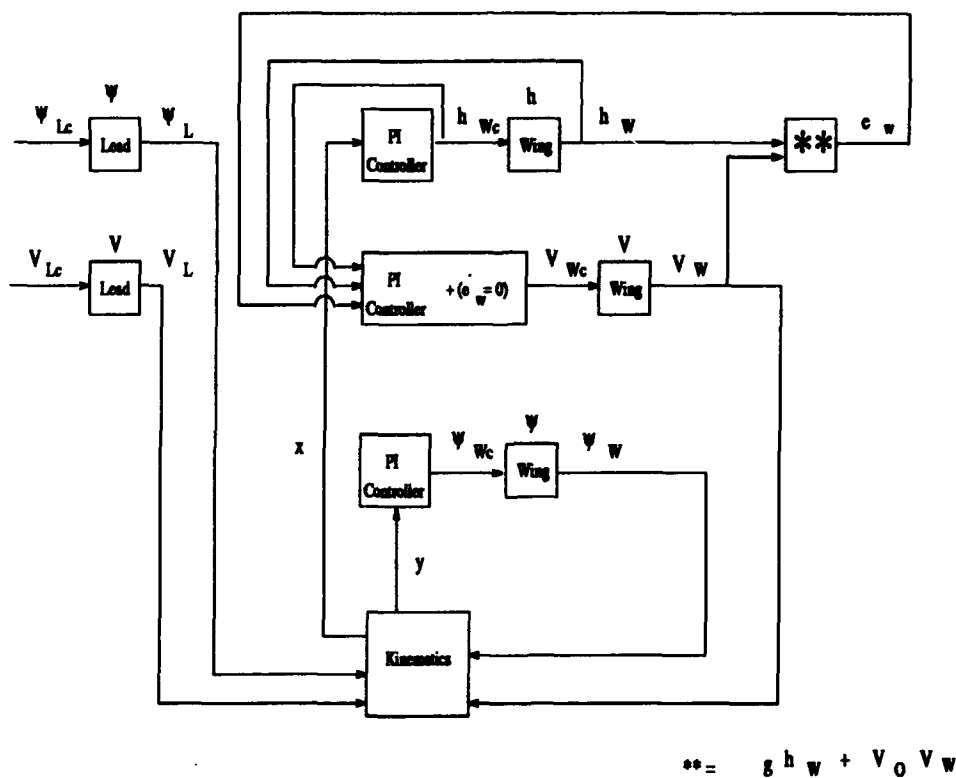


Figure 5.3 Energy Excursion Minimization: New Three Dimensional Maneuvers Simulation Formulation

5.3 Graphical Comparison of Implementations: Energy Excursion Minimizing and Energy Conserving

According to Section 5.2, the only difference between energy excursion minimizing and conserving is the addition of the PI controller and the e_w term into the V_w . This is verifiable by "turning the PI controller off", i.e. set PI gains equal to zero, and simulating energy conserving and energy minimizing maneuver control techniques. The implementations are depicted in Figures 5.2 and 5.3. The simulations are shown in Figure 5.4. As can be seen, the time responses do not match. Evidently, the nonlinear simulation's limiters are interfering with the responses. As a check, the interfering limiters are eliminated and the resulting responses are inspected. Looking at Figure 5.5, the simulations do agree when they remain within the linear region of operation. Therefore, Proposition V.1 has been proven correct experimentally.

This comparison of implementations shows that energy conservation is really just a special case of energy minimizing with the PI controller gains set equal to zero. The remainder of this chapter compares the two methods. In the remainder of this thesis, the term "energy conservation" denotes energy minimization with the PI controller gains set equal to zero.

5.4 Energy Excursion Minimizing Maneuvers Simulation

Once again the simulations are accomplished with dimensional gains. Therefore, it is useful to determine how the nondimensional PI controller gains in Equation (5.23) are related to their dimensional counterparts.

$$\hat{k}_{zspv} = k_{zspv} \bar{t} \quad \hat{k}_{zsi v} = k_{zsi v} \bar{t}^2 \quad (5.57)$$

The "~" notation is dropped in the rest of this chapter. The reader will be told when equations are dimensional or nondimensional. This section deals

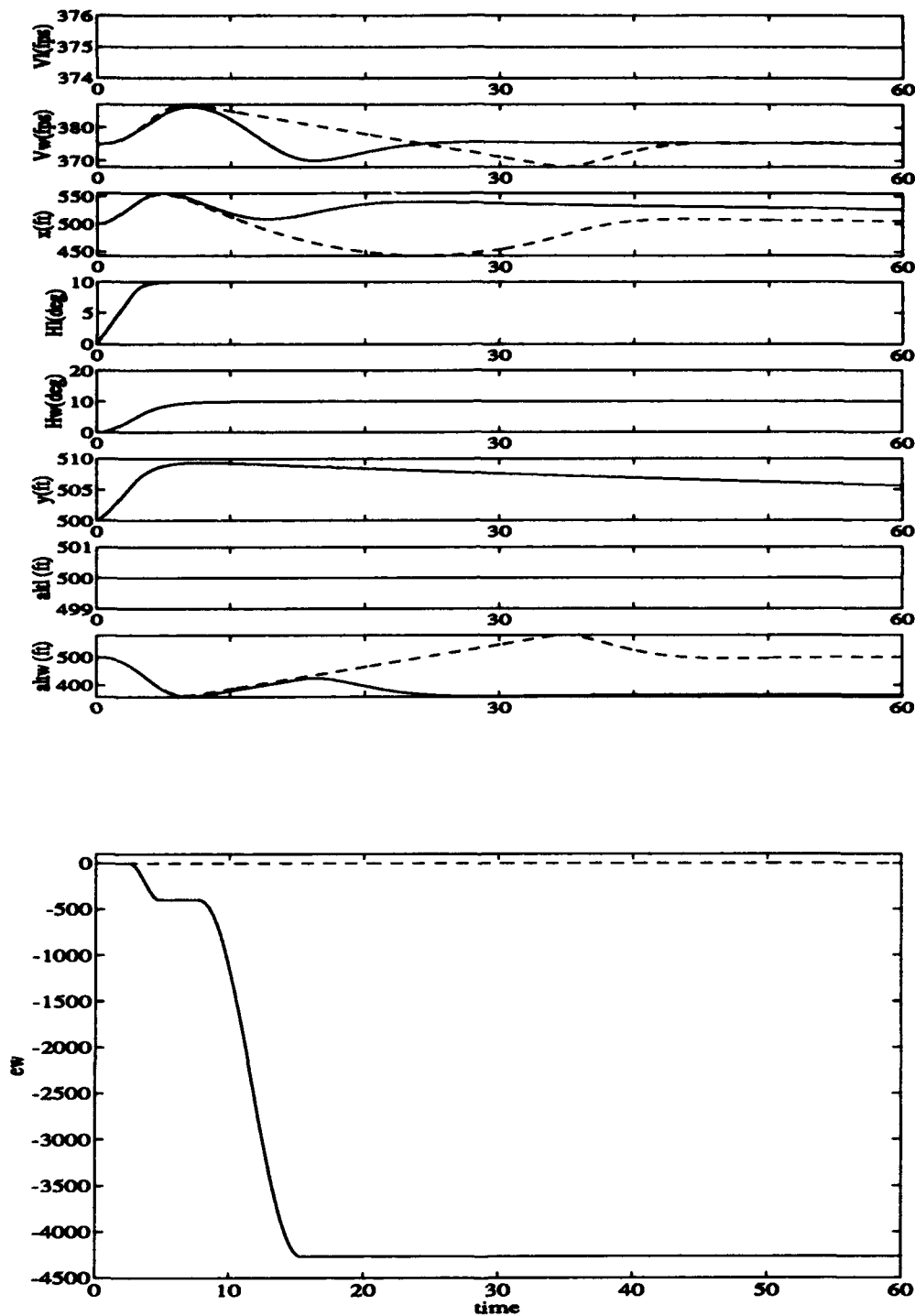


Figure 5.4 Nonlinear Simulation, C-130A Aircraft: Comparison of Buzogany's Implementation (solid line) and New Implementation (dashed line) in Equation (5.23)

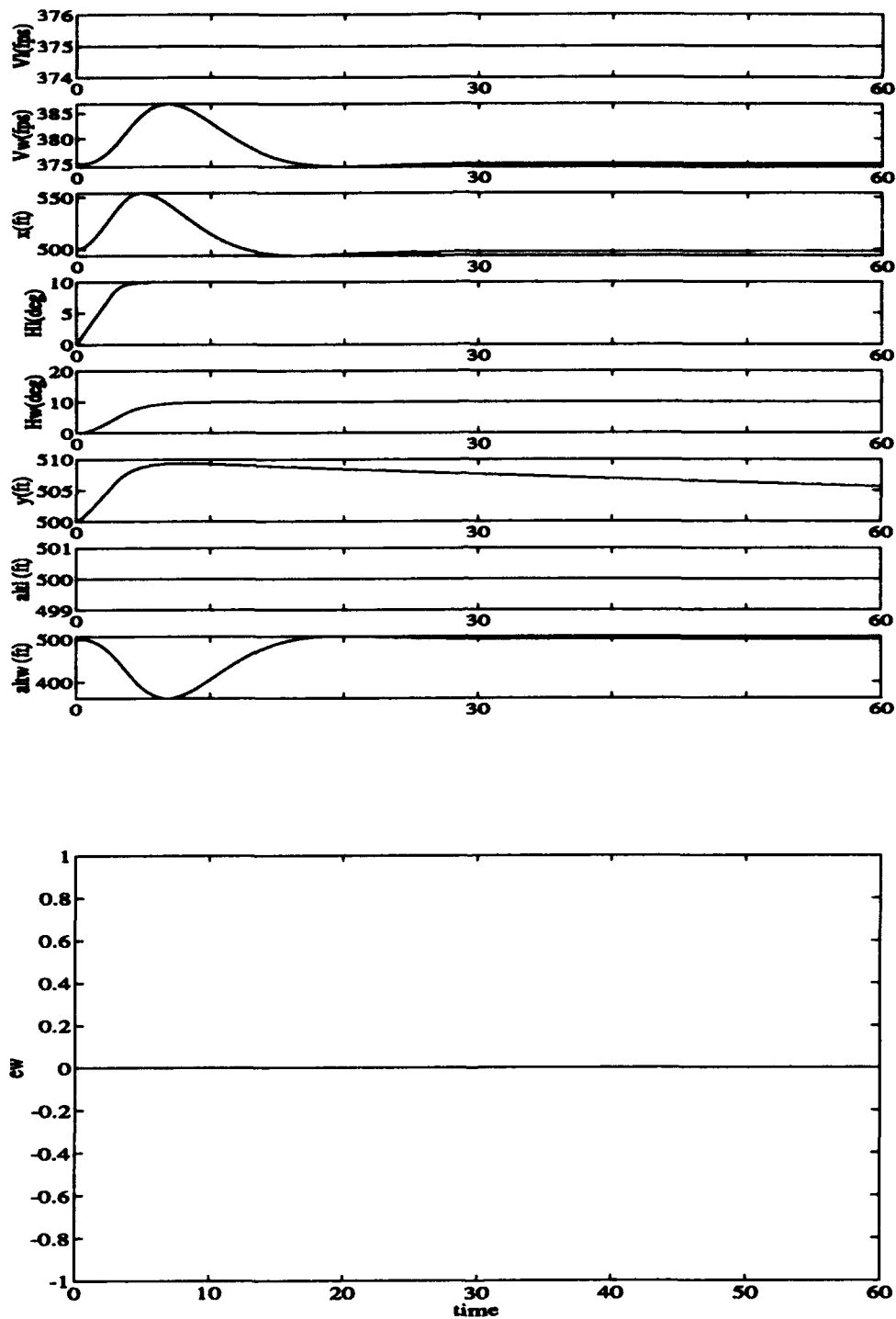


Figure 5.5 Nonlinear Simulation, C-130A Aircraft, With Velocity and Altitude Error Signal Limiters Eliminated: Comparison of Buzogany's Implementation (solid line) and New Implementation (dashed line) in Equation (5.23)

with dimensional simulation runs. Therefore, the gains are *dimensional* in this section.

The initial conditions for the three dimensional, energy conserving maneuvers is the same as Table 4.3. The PI controller gains for V_w , are in their respective sections.

5.5 Dimensional Eigenvalue Analysis

(See Appendix A for *dimensional* plant models) Using Busogany's results as a starting point, only the PI controller gains associated with V_w , k_{sspv} and k_{ssiv} , are varied. The objective of this section is to compare the new Laplace Transform of the step response with Busogany's response [2:page 6-5]. In order to do this, the output matrix, C_{ss} has been changed to reflect Busogany's output, and thus examine the wing velocity response. Therefore, the nondimensional wing velocity's Laplace output step response is:

$$V_w(s) = \underbrace{[0 \quad -\xi \quad 1 \quad 0 \quad 0 \quad 0]}_{\text{Nondimensional}} [sI - A_{ss}]^{-1} \Gamma_{ss} \frac{1}{s} \quad (5.58)$$

Correspondingly, the dimensional wing velocity's step response is:

$$V_w(s) = \underbrace{\left[0 \quad -\frac{g}{V_0} V_0 \quad 0 \quad 0 \quad 0\right]}_{\text{Dimensional}} [sI - A_{ss}]^{-1} \Gamma_{ss} \frac{1}{s} \quad (5.59)$$

$$V_w(s) = \frac{1}{s} + \frac{r_2}{s+p_2} + \frac{r_3}{s+p_3} + \frac{r_4}{s+p_4} + \frac{r_5}{s+p_5} + \frac{r_6}{s+p_6} + \frac{r_7}{s+p_7} \quad (5.60)$$

As in the previous chapter, it is desired to perform an eigenvalue analysis to determine if a fast response is possible for V_w . This is accomplished experimentally by keeping the ratio of $\frac{k_{sspv}}{k_{ssiv}} = 100$ while varying their respective values. Keeping this ratio equal to 100 is an engineering "rule of thumb." Keeping the ratio equal to 100 is not a proven

mathematical concept. However, this has demonstrated good performance in the past. Therefore, it is used in this analysis.

Examining Figure 5.6 shows that picking gains at $k_{ssp_v} = .0005$ and $k_{ssiv} = .000005$ yields a response where the poles p4 and p5 are dominant (they are complex conjugates of each other). These gains allow for tracking of a step input, dominance of a complex conjugate pair, and stability. $k_{ssp_v} < .005$ for stability (See poles p4 and p5).

Previously, Buzogany found the wing velocity response to be:

$$V_w(s) = \underbrace{\frac{1}{s} + \frac{.043}{s + 0.0104}}_{\text{Buzogany's Response}} + \overbrace{\frac{.72592 \angle -135.92^\circ}{s + .2448 - j.252} + \frac{.72592 \angle 135.92^\circ}{s + .2448 + j.252}}^{\text{Dominant Poles}} \quad (5.61)$$

(This is different from Equation (6.21) page 6-5 of Buzogany's thesis. The expression in that thesis is incorrect. The residues do not add up to zero, which is a requirement for a partial fraction expansion whose denominator is 3 degrees higher than the numerator [5:page 117]).

Transfer function and Partial Fraction expansion of the step response with $k_{ssp_v} = .0005$ and $k_{ssiv} = .000005$ yields:

$$\frac{V_w(s)}{V_L(s)} = \frac{.1287(s + .5)(s + .00874 \pm j.00992)(s + .01)}{(s + .5)(s + .235 \pm j.243)(s + .00942 \pm j.00997)(s + .0104)} \quad (5.62)$$

$$V_w(s) = \frac{1}{s} + \frac{.050670}{s + .0104} + \frac{.040758 - j.040545}{s + .00942 + j.00997} + \frac{.040758 + j.040545}{s + .00942 - j.00997} + \underbrace{\frac{-.56609 - j.54353}{s + .235 + j.243} + \frac{-.56609 + j.54353}{s + .235 - j.243}}_{\text{Dominant Poles}} + \frac{0}{s + .5} \quad (5.63)$$

These gains can now be utilized by the nonlinear simulation to determine if they produce desirable results.

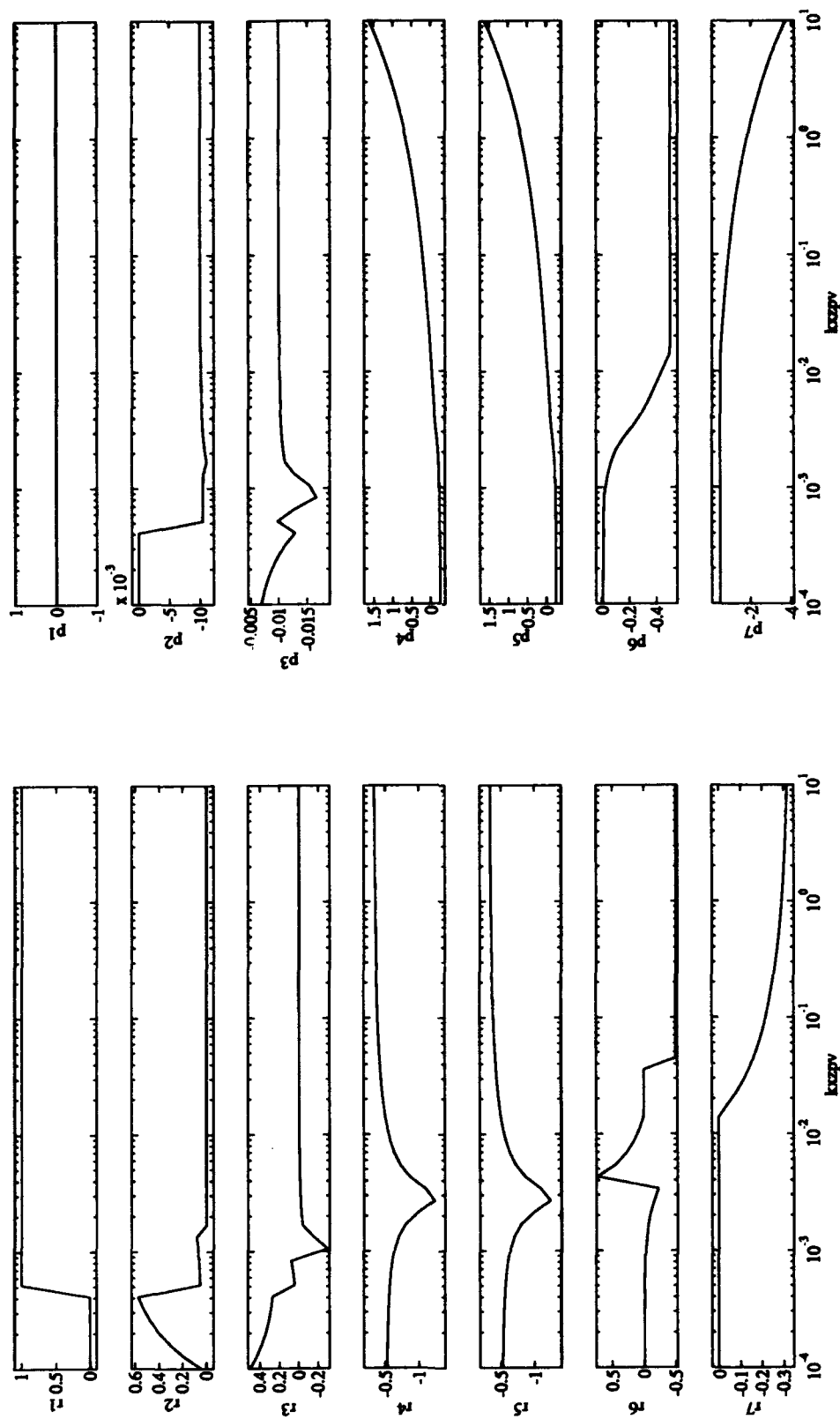


Figure 5.6 XZ-Channel, Wing Velocity Response, Dimensional Poles and Residues versus Controller Gains, $\frac{k_{zpy}}{k_{zpy}} = 100$

5.5.1 Nonlinear Three Dimensional Maneuvers Simulation. The gains used for the full nonlinear simulation are in Table 5.2. These were determined by the eigenvalue analysis in the previous section. Included are the values used by the other gains in the simulation.

Table 5.2 PI Controller Values For Equation (5.23) and Nonlinear Simulation Shown in Figures 5.7 - 5.9

Parameter	Dimensional Value
k_{zspv}	.0005
$k_{zsi v}$.000005
k_{yp}	1
k_{yi}	.01
k_{zp}	.75
k_{zi}	.0075
k_y	1
k_ψ	0
k_z	1
k_v	0

The values from Table 5.2 are implemented in the nonlinear simulation resulting in Figures 5.7 - 5.9. Examining Figure 5.9, where a $25 \frac{ft}{sec}$ velocity command has been issued, shows the reason for adding the PI controller to the energy conservation part of the velocity control law. Keeping e_w constant causes the wing aircraft in the energy conservation response to decrease altitude when a velocity change has been commanded. Allowing e_w to fluctuate causes the wing aircraft utilizing energy minimization to recover back to its nominal altitude. The PI controller is commanding the throttle and changing the wing aircraft energy state. This results in less deviation in z -separation than the energy conservation approach. In Figure 5.9, the specific energy of the wing aircraft for both methods has been plotted as a function of time.

The heading changes in Figures 5.7 and 5.8 show that some performance is traded for more capability. The rate limiters impact the response here dramatically. The energy conservation responses are better than the energy minimizing responses.

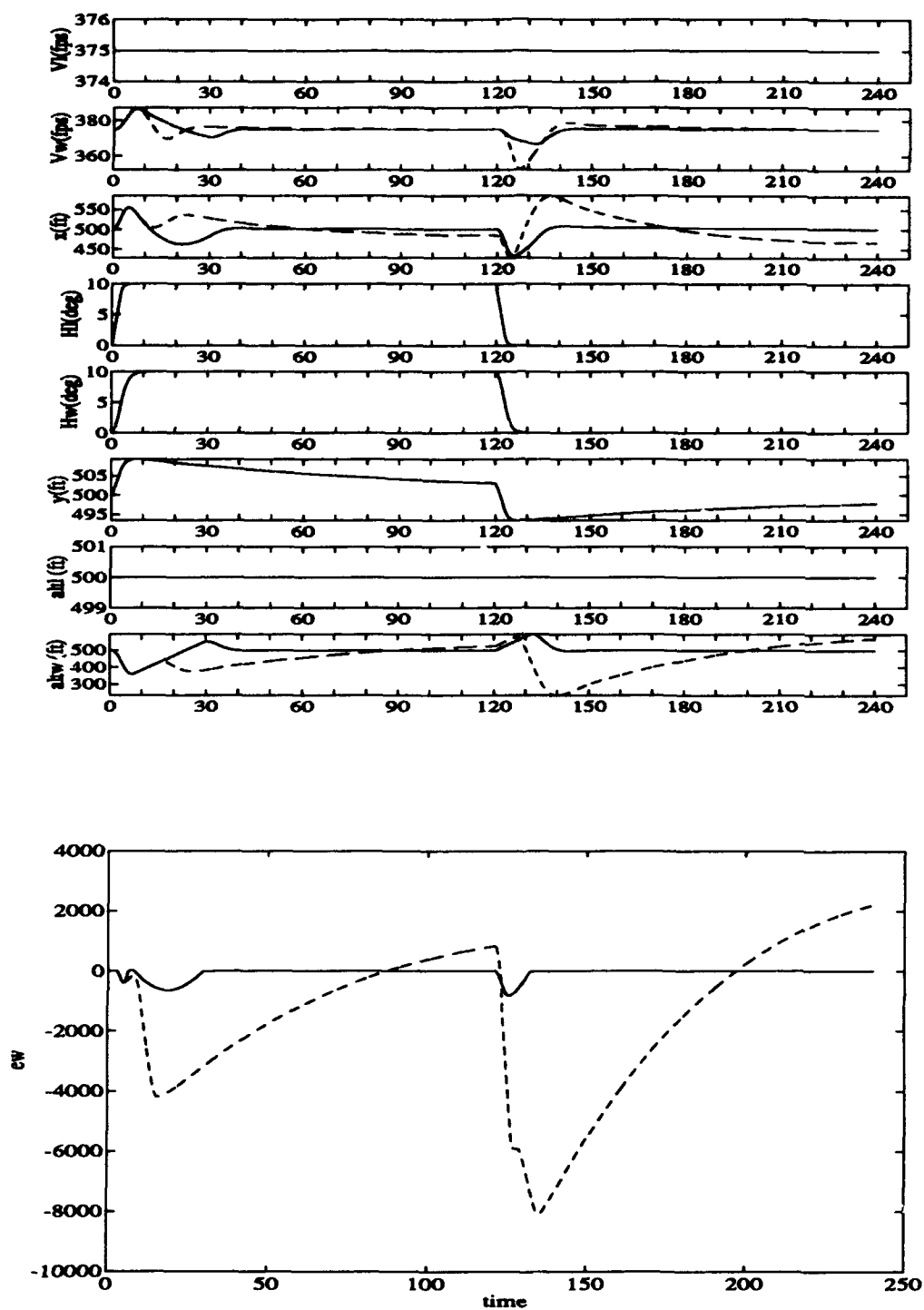


Figure 5.7 C-130A: Diamond Formation, 10° Side Step Heading Change. Nonlinear Simulation: Energy Conserving Implementation (solid line) and Energy Excursion Minimizing Implementation (dashed line)

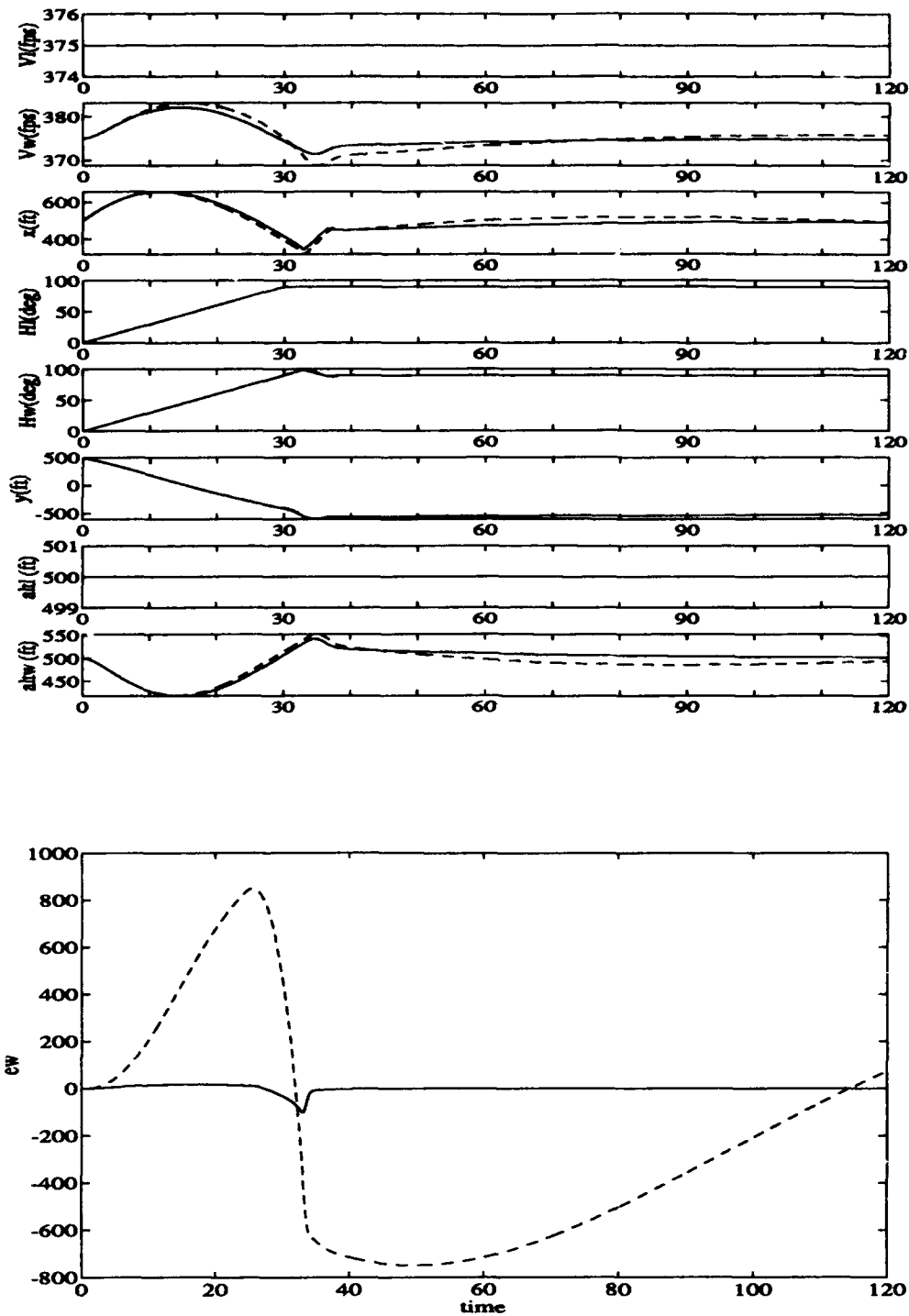


Figure 5.8 C-130A: Diamond Formation, 90° Heading Change. Nonlinear Simulation: Energy Conserving Implementation (solid line) and Energy Excursion Minimizing Implementation (dashed line)

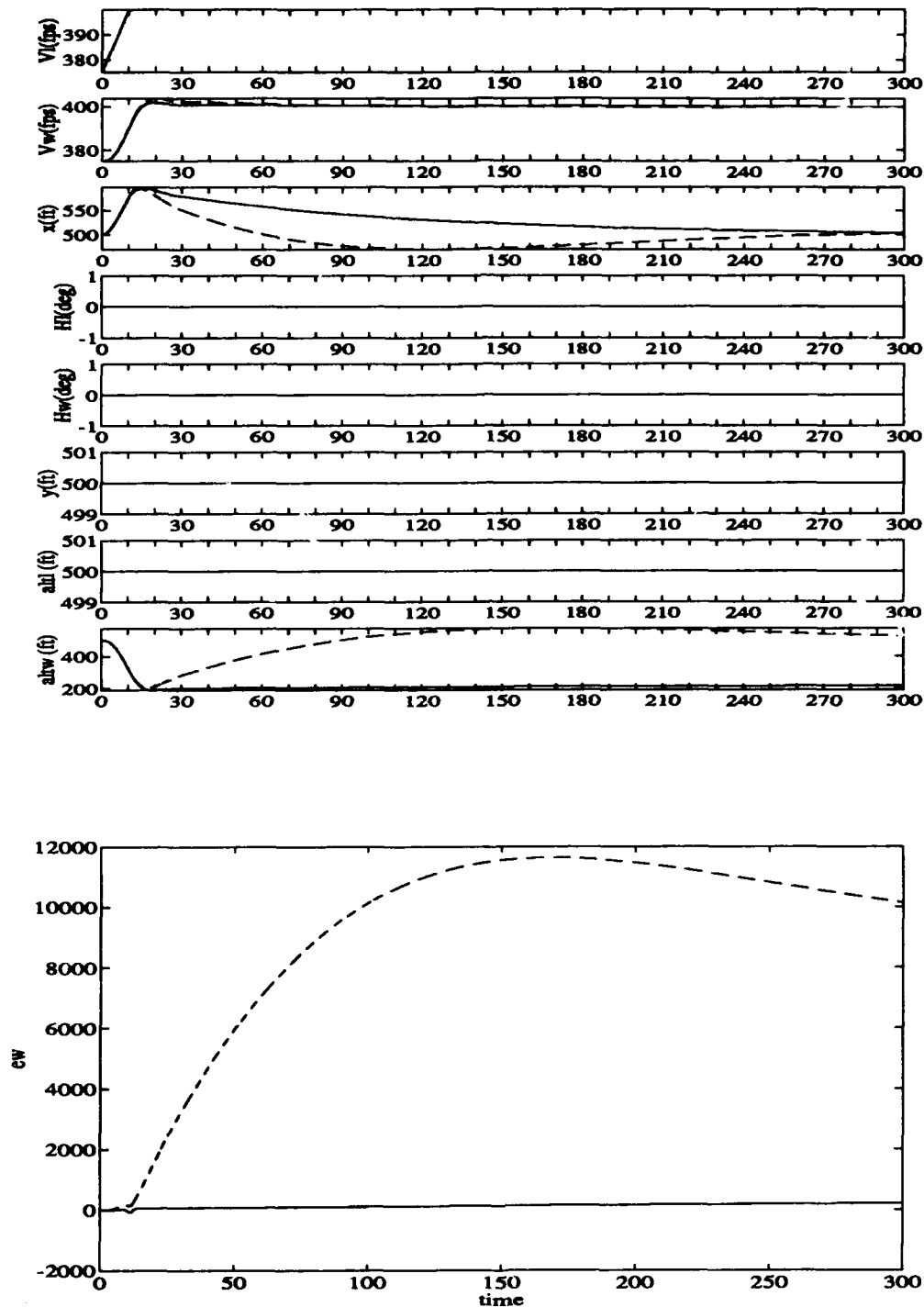


Figure 5.9 C-130A: Diamond Formation, 25 $\frac{ft}{sec}$ Velocity Change. Nonlinear Simulation: Energy Conserving Implementation (solid line) and Energy Excursion Minimizing Implementation (dashed line)

As seen in Figures 5.7 - 5.9, allowing the specific energy of the wing aircraft to make excursions away from its nominal value through the addition of a PI controller in the V_{W_c} command yields two conflicting results when no other parameters are changed:

- Heading changes have worse responses (i.e., there is undershoot in the x separation response that results in decreasing aircraft separation)
- Velocity changes have much better responses (i.e., x separation response away from nominal is less and the aircraft are at the same altitude in steady- state unlike energy conserving maneuvers

5.6 New Approach To V_{W_c}

Theoretically, energy excursion minimization should result in more aggressive wing aircraft response to lead maneuvers and better performance than energy conserving maneuvers. A better response can be found in velocity changes for the new formulation, however, there is a worse response for heading changes. Obviously, the present formulation for energy minimizing maneuvers is not as good as was previously hoped. The concept needs to be reexamined.

The whole premise of energy conserving maneuvers is to have zero rate of change in the perturbation of the specific energy of the wing aircraft. Energy excursion minimizing maneuvers allow the wing aircraft specific energy perturbation to make excursions away from nominal value and change the energy state of the aircraft. This energy change should be lower than two dimensional maneuvers. In order to accomplish this, a new control law governing V_{W_c} has been determined. In its most basic sense, the control law has two parts: 1) energy conservation part 2) energy changing part. As a new or modified way of accomplishing energy excursion minimizing maneuvers, allow the e_W term in Equation (5.23) to be zero. This is mathematically correct, since \dot{e}_W is a perturbation quantity and is set to zero to obtain the energy conserving part of V_{W_c} . Setting the derivative of a perturbation to zero is the same as setting the perturbation to zero because a perturbation

is zero at time equals zero. therefore, the wing aircraft specific energy perturbation, e_w , must equal zero. In equation form,

$$V_{W_e} = \tau_{VW} \left(\xi \left[\frac{1}{\tau_{hW}} - \frac{1}{\tau_{VW}} \right] h_W - \xi \frac{1}{\tau_{hW}} h_{W_e} \right) + k_{zspv} h_e + k_{zsiV} \int_0^t h_e dt \quad (5.64)$$

This is now implemented to check the results. The state space representation of the system including this new V_{W_e} is listed in Appendix D.

5.7 Dimensional Eigenvalue Analysis For New V_{W_e}

(See Appendix A for *dimensional* plant models) Like Section 5.5, the objective of this section is to compare the new Laplace transform of the step response with Buzogany's response [2:page 6-5]. However, in this analysis energy excursion minimizing with no e_w in V_{W_e} is used. In order to do this, the output matrix, C_{zz} has been changed to reflect Buzogany's output, and thus examine the wing velocity response (See Section 5.5)

The dimensional wing velocity's step response is:

$$V_W(s) = \underbrace{\left[0 - \frac{g}{V_0} V_0 \ 0 \ 0 \ 0 \right]}_{\text{Dimensional}} [sI - A_{zz}]^{-1} \Gamma_{zz} \frac{1}{s} \quad (5.65)$$

$$V_W(s) = \frac{1}{s} + \frac{r_2}{s + p_2} + \frac{r_3}{s + p_3} + \frac{r_4}{s + p_4} + \frac{r_5}{s + p_5} + \frac{r_6}{s + p_6} + \frac{r_7}{s + p_7} \quad (5.66)$$

As in Section 5.5, it is desired to perform an eigenvalue analysis to determine if a fast response is possible for V_W . This is accomplished experimentally by keeping the ratio of $\frac{k_{zspv}}{k_{zsiV}} = 100$ while varying their respective values. This is shown in Figure 5.10.

Figure 5.10 yields some interesting observations. In order to track a step, k_{zspv} must be $\geq .01$. k_{zspv} must also be < 1 so that p_4 and p_5 do not go unstable. The fastest

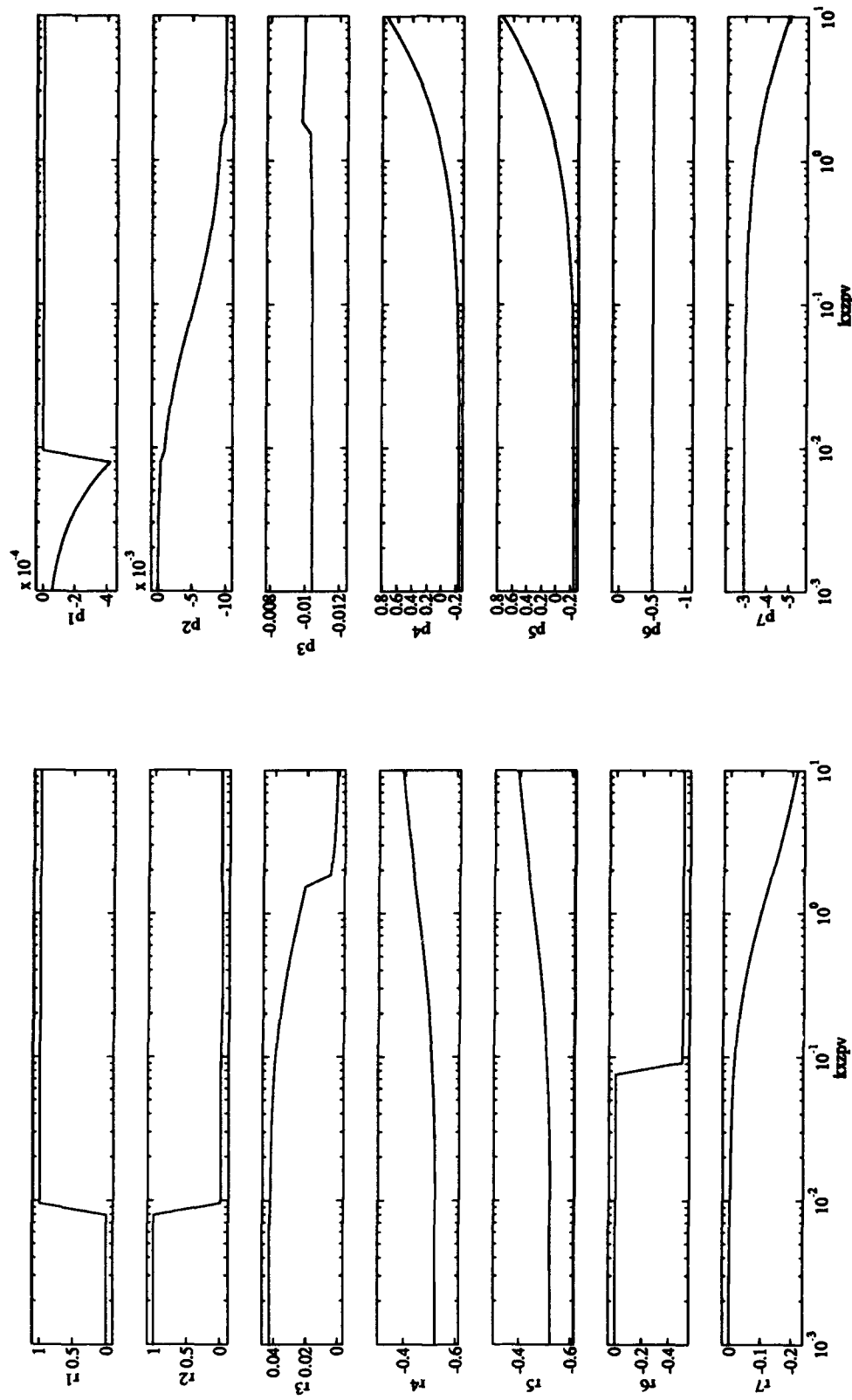


Figure 5.10 XZ-Channel, Wing Velocity Response, Dimensional Poles and Residues versus Controller Gains, $\frac{k_{xzpv}}{k_{xzpv}} = 100$

pole is p7. It remains at -3 until $k_{zspv} = .1$, however, its residue is very small (≈ 0) until $k_{zspv} = .1$. Yet, its residue becomes approximately -.1 at $k_{zspv} = 1$. This is still 5 times less than the residue for poles 4 and 5. Its contribution would be negligible and would make poles 4 and 5 slower (i.e. closer to the imaginary axis). Therefore, the fastest poles with the possibility of having a dominant response are poles 4 and 5, which are complex conjugates. They are the fastest poles with the largest residues. Therefore, picking $k_{zspv} = .01$ and $k_{zsi_v} = .0001$ results in

- V_W is able to track step inputs
- Poles p2, p3, and p6 have small residues \therefore they do not contribute much to the output response
- Poles p4 and p5 are complex conjugates of each other and are dominant
- Pole p7 is the fastest pole but its residue is never large enough to have an impact on the output response

This chapter has explored two ways of energy minimizing maneuvers. One had e_W in the formulation for V_{Wc} , while the other disregarded e_W . Comparing eigenvalue analyses of both formulations will show the differences.

Transfer function and Partial Fraction expansion of the step response of system without e_W :

$$\frac{V_W(s)}{V_L(s)} = \frac{.1287(s + .5)(s + 3.3486)(s + .0010441)(s + .01)}{(s + .5)(s + .24136 \pm j.28202)(s + .01041)(s + .0010437)(s + 3.0058)} \quad (5.67)$$

$$V_W(s) = \frac{1}{s} + \frac{-4.2185 \times 10^{-4}}{s + .0010437} + \frac{.042551}{s + .01041} + \underbrace{\frac{-.52011 - j.45447}{s + .24136 + j.28202} + \frac{-.52011 + j.45447}{s + .24136 - j.28202}}_{\text{Dominant Poles}} + \frac{0}{s + .5} + \frac{-1.9009 \times 10^{-3}}{s + 3.0058} \quad (5.68)$$

Examining Equations (5.62) and (5.67), shows V_{w_c} without e_w in its formulation should yield superior performance due to the fact that the system without e_w will respond quicker than the other system since its dominant poles are faster (i.e., farther to the left in the Real-Imaginary Plane). In addition, the poles in Equation (5.68) are faster overall than those of Equation (5.67), and Equation (5.68) has only one pair of complex poles versus two. The extra pair of complex poles in Equation (5.63) are very slow (i.e. very close to the imaginary axis) and their residues are larger than the residues of the corresponding real poles (p2 and p7). Since the denominator has 3 more poles than zeros, the residues should and do add up to 0 [5:page 117].

It is interesting to note that the newer formulation for V_{w_c} has poles close to Buzo-gany's response. Also, leaving e_w out of V_{w_c} allows the integral and proportional gain to be increased.

5.7.1 Nonlinear Simulations With New V_{w_c} . The gains for the heading changes are listed in Table 5.3, and the responses are in Figures 5.11 and 5.12. The gains were determined in the previous section. The heading changes are very good. The responses are almost as good as in energy conserving maneuvers. There is a slightly worse response in x separation. However, this response is much better than previously shown when e_w was included in the feedback control law. A 90° heading change using energy conserving/excursion minimizing maneuvers using transposition is depicted in Figure 5.13. The transposition allows lower energy usage during large heading changes.

Table 5.3 PI Controller Values For Equation (5.64) and Nonlinear Simulations Using New V_{w_c} : Heading Changes In Figures 5.11 and 5.12

Parameter	Dimensional Value
k_{ssp_v}	.01
k_{ssi_v}	.0001

The gains for the velocity change are given in Table 5.4. The 25 $\frac{ft}{sec}$ velocity command response is shown in Figure 5.14.

Table 5.4 PI Controller Values For Equation (5.64) and Nonlinear Simulation Using New V_{w_c} : Velocity Change In Figure 5.14

Parameter	Dimensional Value
k_{ssp_v}	.02
k_{ssiv}	.002

An interesting observation can be discerned concerning the velocity change. The proportional and integral gains cannot be chosen such that the ratio between proportional and integral gains equals 100, if a quick response is desired. The integral gain had to be increased in order that the recovery from the altitude change would occur in a reasonable amount of time. Otherwise, recovery is on the order of 600 - 800 seconds. The values in Table 5.4 are determined heuristically. Using the gains determined in Section 5.7, the gains were modified in a trial and error process until a desirable response was attained. Increasing integral gain allows the altitude to respond much quicker.

In addition, altitude responses are investigated in this section. Like velocity changes, Buzogany's formulation could not handle altitude changes. Buzogany's control in energy conservation consisted of controlling altitude through x -separation and velocity through altitude. If the lead aircraft changed altitude, there was no way for the formation to follow using energy conservation because there was no controller dependent on altitude error. The new formulation addresses this through the PI controller augmented to the V_{w_c} in Equation (5.64). This controller operates on altitude error and thus increases the speed of the wing by throttle usage when there is an altitude differential. This is seen in Figure 5.15. The gains used for the PI controller in V_{w_c} are larger than those in Table 5.4. They are listed in Table 5.5.

Table 5.5 PI Controller Values For Equation (5.64) and Nonlinear Simulation Using New V_{w_c} : Altitude Change In Figure 5.15

Parameter	Dimensional Value
k_{ssp_v}	.07
k_{ssiv}	.007

As in the velocity response, the integral gain had to be increased in order to allow recovery from an altitude change in 100 seconds.

5.8 Conclusions

This chapter has introduced the concept of energy excursion minimising maneuvers. It explored two methods of minimizing energy excursion during maneuvers. Based on the results presented, the wing velocity control law that sets $e_w = 0$ results in better responses (See Equation (5.64)). Therefore, it is the preferred method of achieving energy excursion minimising maneuvers.

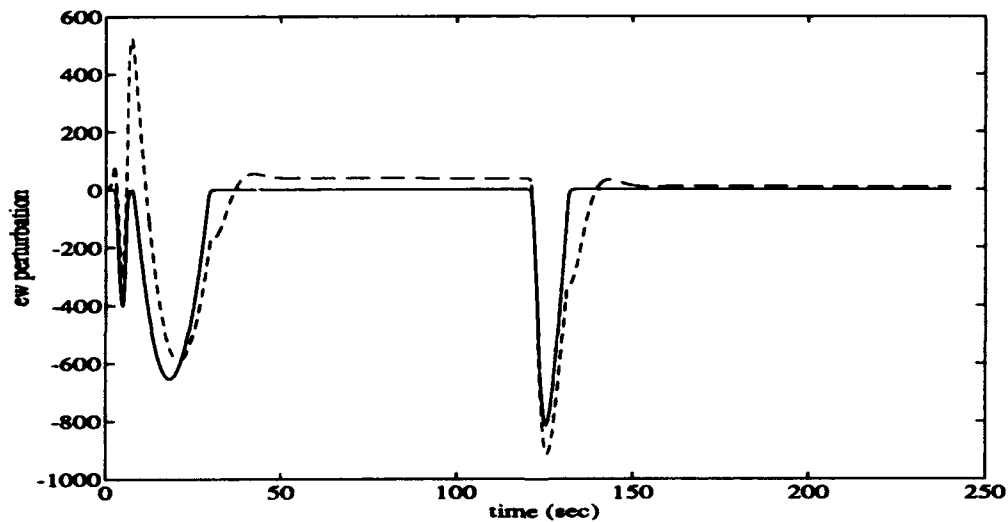
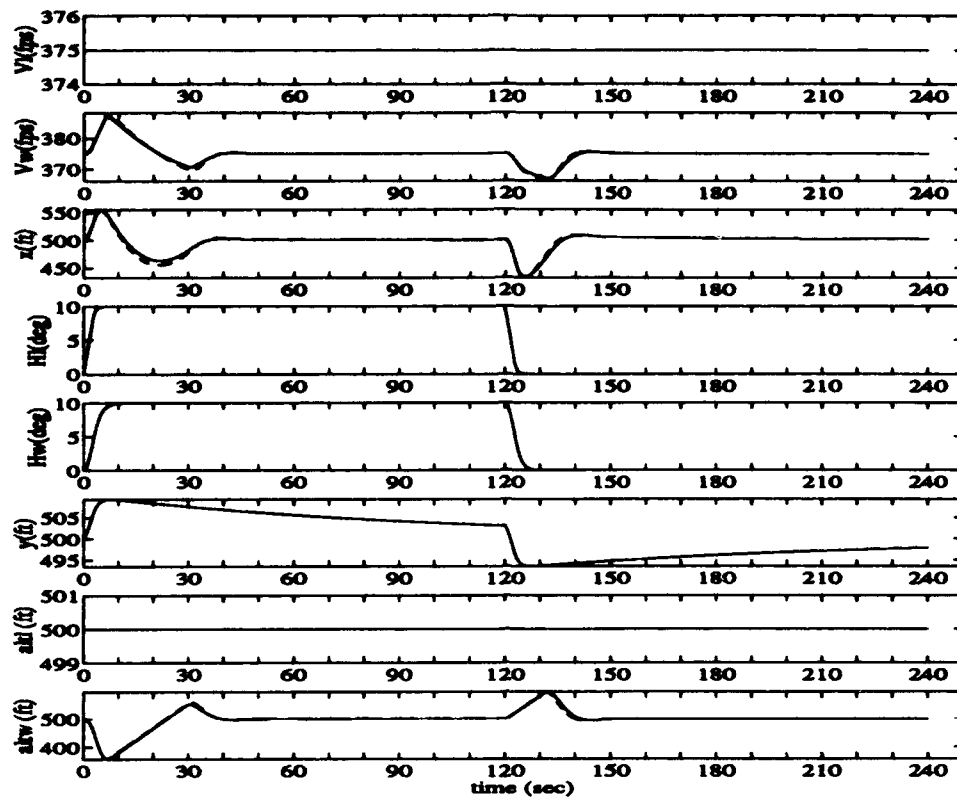


Figure 5.11 C-130A: Nonlinear Simulation, Response To A 10° Side Step Heading Change: Energy Conserving Implementation (solid line) and Energy Excurtion Minimizing Implementation (dashed line)

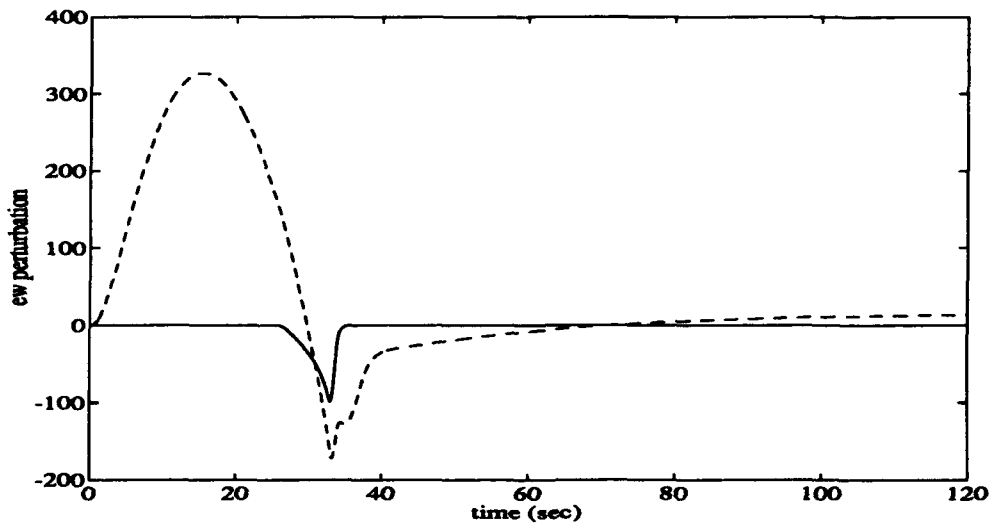
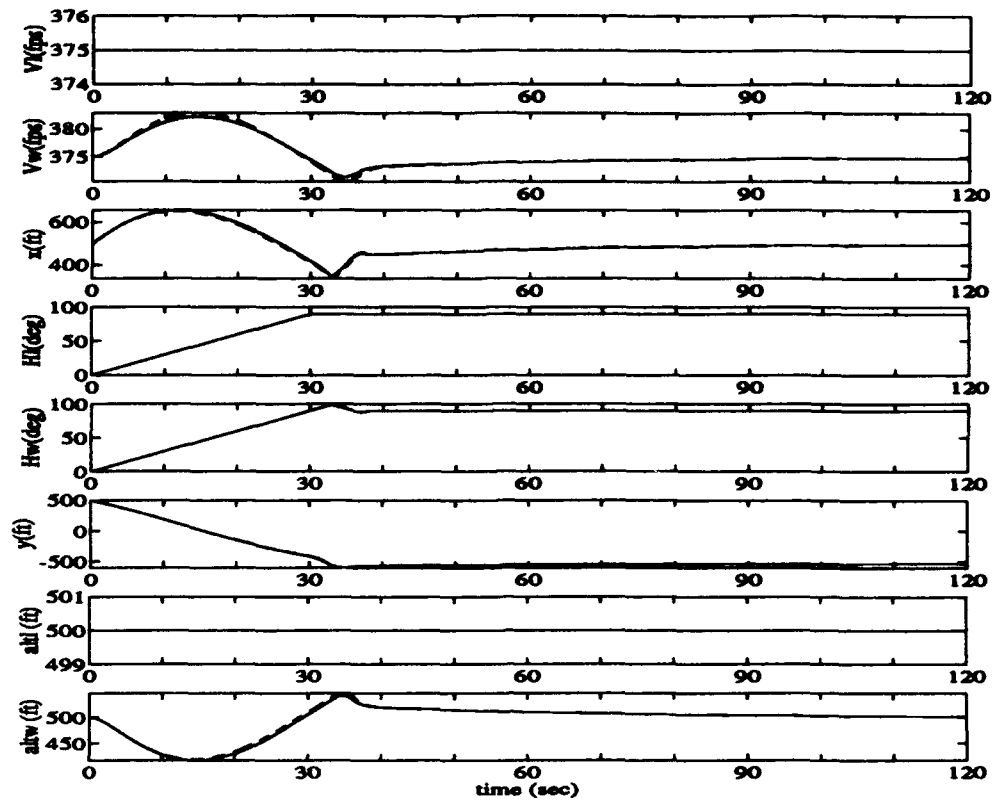


Figure 5.12 C-130A: Nonlinear Simulation, Response To A 90° Step Heading Change: Energy Conserving Implementation (solid line) and Energy Excursion Minimizing Implementation (dashed line)

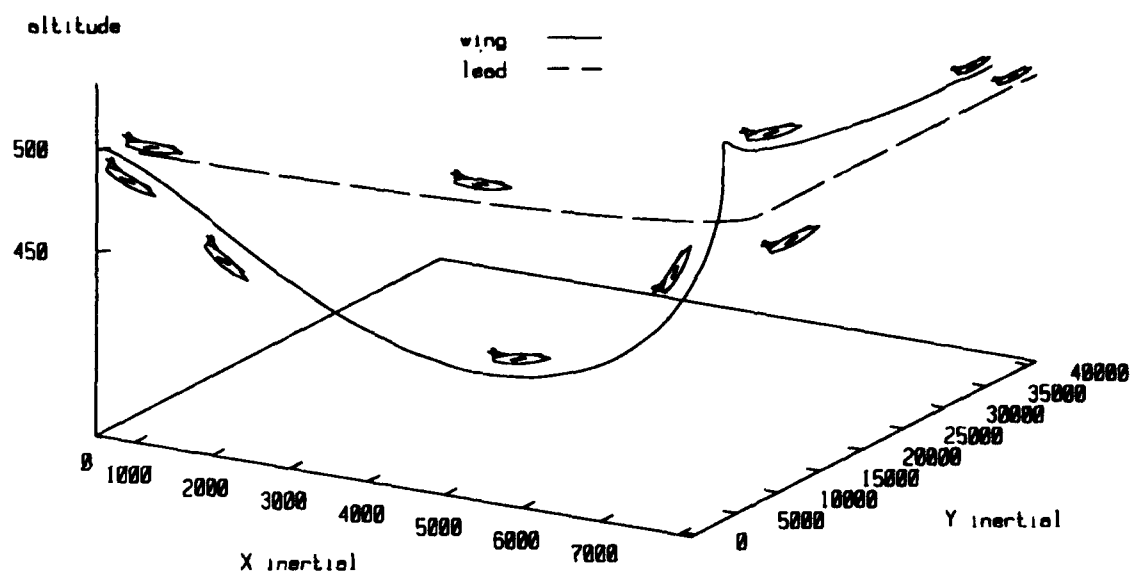


Figure 5.13 Diamond Formation 90° Heading and Formation Change Utilizing Energy Conserving/Excursion Minimizing [2:Figure 6.6]

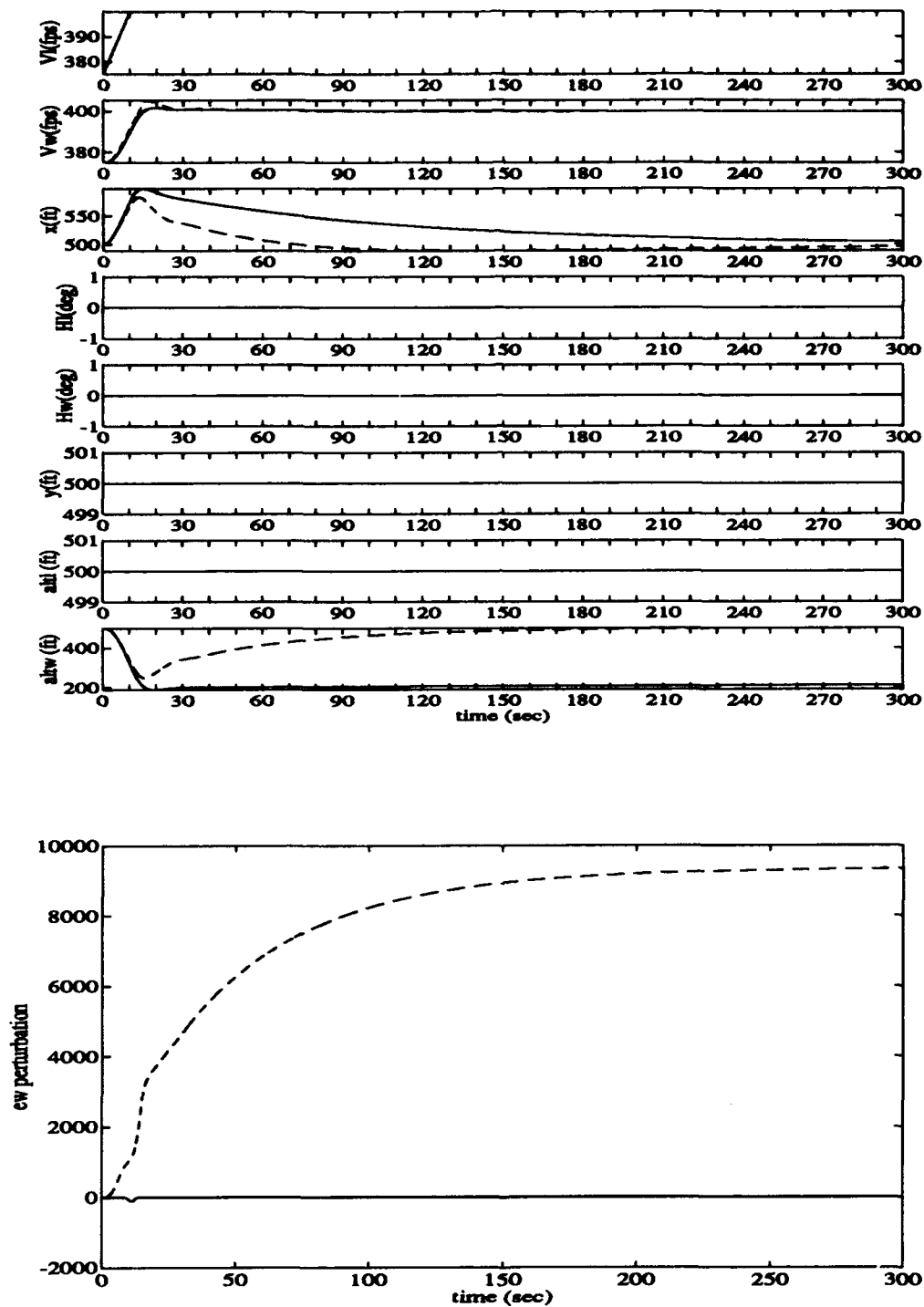


Figure 5.14 C-130A: Nonlinear Simulation, Response To A 25 $\frac{ft}{sec}$ Step Velocity Change: Energy Conserving Implementation (solid line) and Energy Excursion Minimizing Implementation (dashed line)

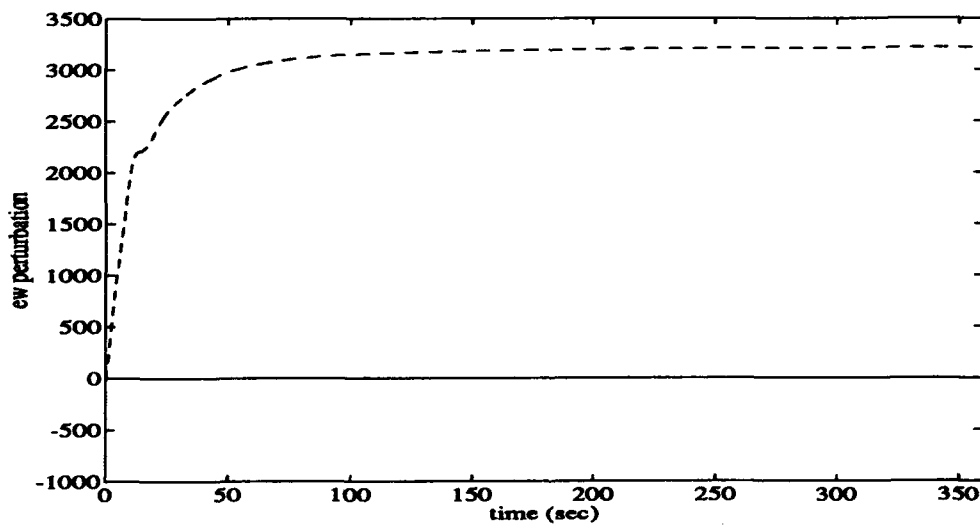
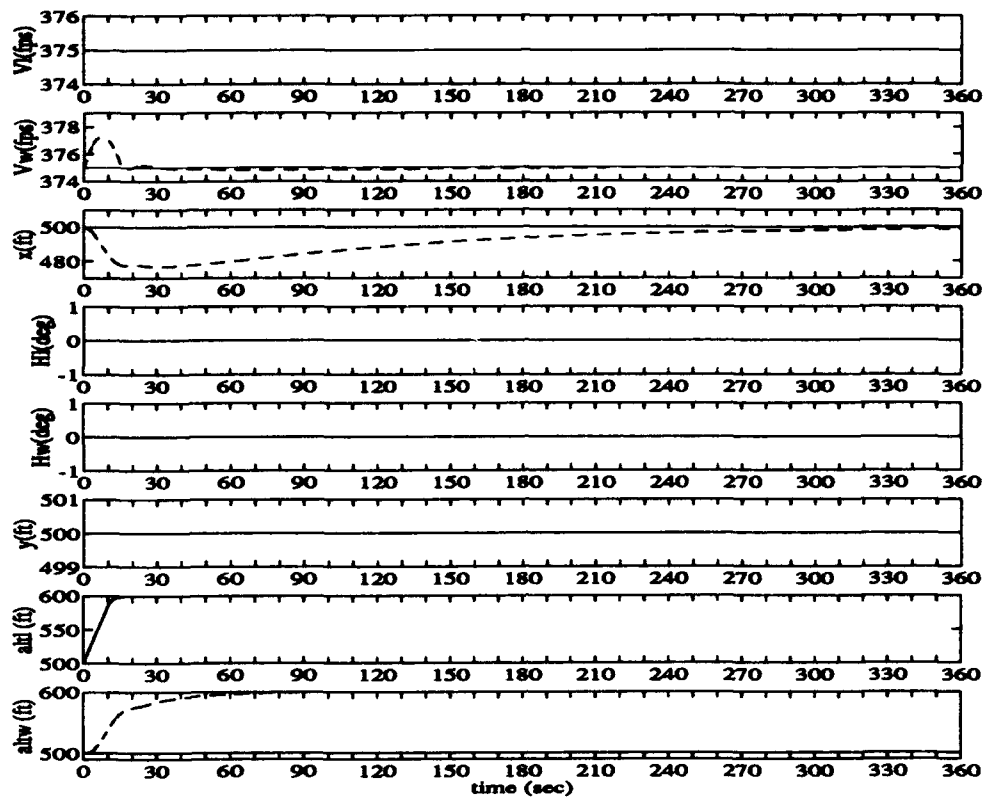


Figure 5.15 C-130A: Nonlinear Simulation, Response To A 100 ft Step Altitude Change: Energy Conserving Implementation (solid line) and Energy Excursion Minimizing Implementation (dashed line)

VI. Comparison of Two Dimensional and Three Dimensional Maneuvers

Two Dimensional Maneuvers and Three Dimensional Maneuvers are explored in Chapters IV and V, respectively. The objective of this chapter is to simulate and compare the following methods:

1. Two dimensional maneuvers (i.e., all maneuvers occur in the same plane of flight)
2. Energy conserving maneuvers (i.e., all maneuvers occur with constant aircraft specific energy, in and out of the same plane of flight)
3. Energy excursion minimizing maneuvers (i.e., all maneuvers occur without constant aircraft specific energy, in and out of the same plane of flight)

The results of this comparison are evaluated and a recommendation for further study is stated.

6.1 Nonlinear Simulations

This section compares the responses for the nonlinear simulations of the three methods outlined in the introduction of this chapter. The gains used are listed in Table 6.1. Once again, these are the gains used by Buzogany in Chapters 5 and 6 of his thesis. This is done to show the effect of including the PI controller into the V_{W_c} of energy minimizing maneuvers. In all the plots, solid line indicates energy conserving maneuvers, dashed line indicates energy excursion minimizing maneuvers, and dotted line indicates two dimensional maneuvers.

6.2 Discussion

Figures 6.1 - 6.4 yield the following observations:

1. The two dimensional maneuvers provide the best response in x-separation overall. The deviations away from nominal are smaller than the energy conserving and energy excursion minimizing maneuvers

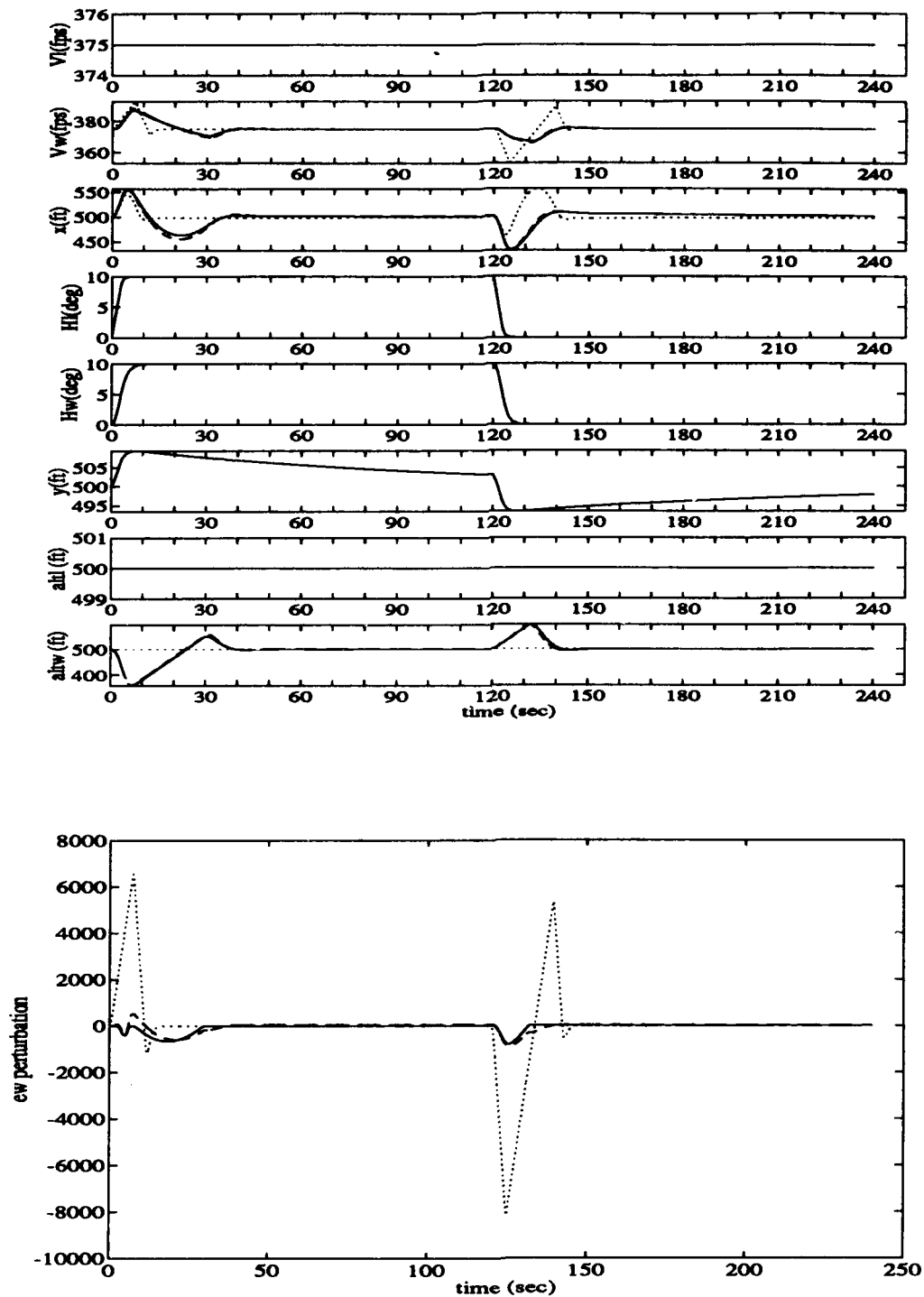


Figure 6.1 C-130A: Diamond Formation, 10° Side Step Heading Change. Nonlinear Simulation: Energy Conserving Implementation (solid line), Energy Minimizing Implementation (dashed line), and Two Dimensional Implementation (dotted line)

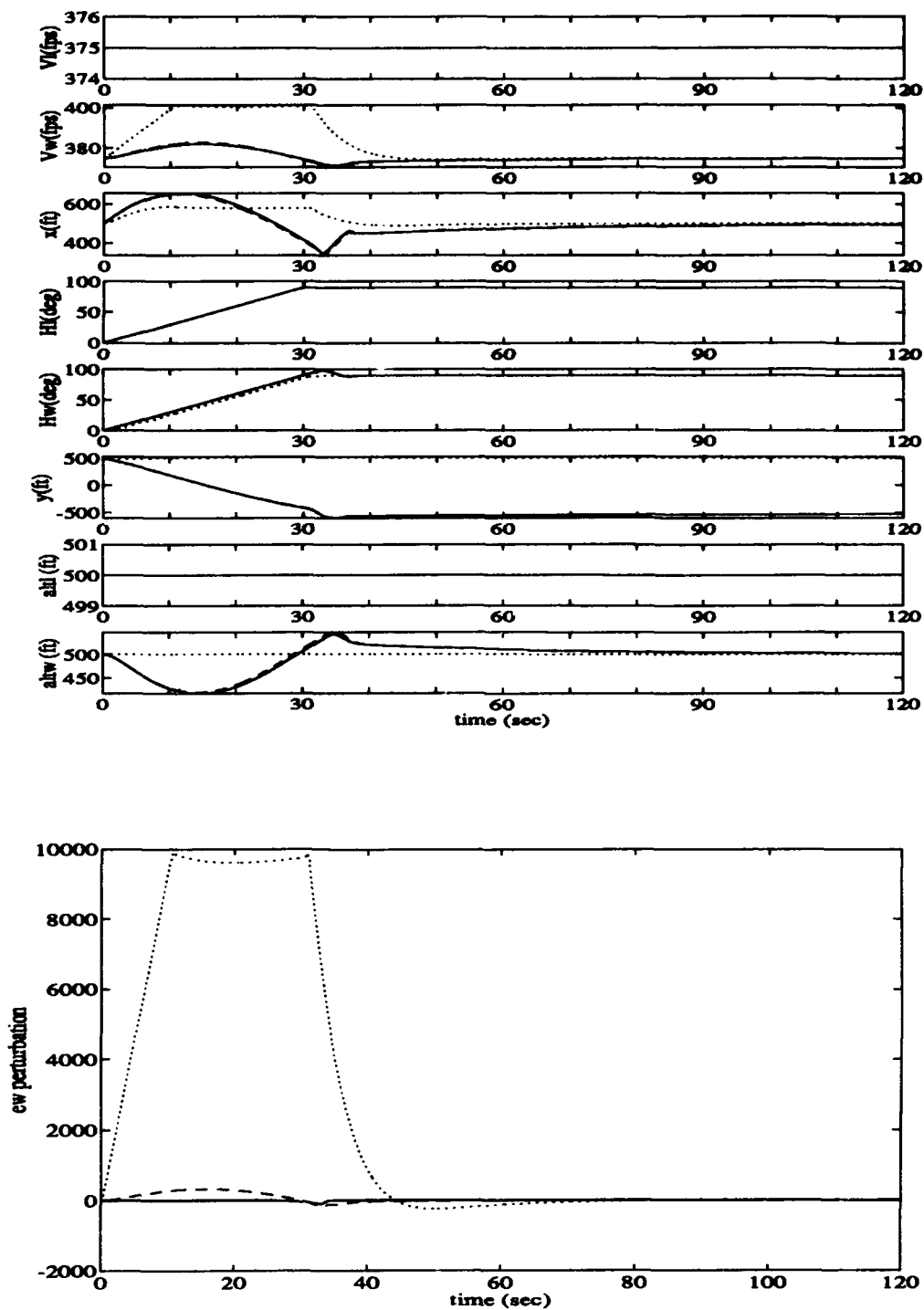


Figure 6.2 C-130A: Diamond Formation, 90° Heading Change. Nonlinear Simulation: Energy Conserving Implementation (solid line), Energy Minimizing Implementation (dashed line), and Two Dimensional Implementation (dotted line)

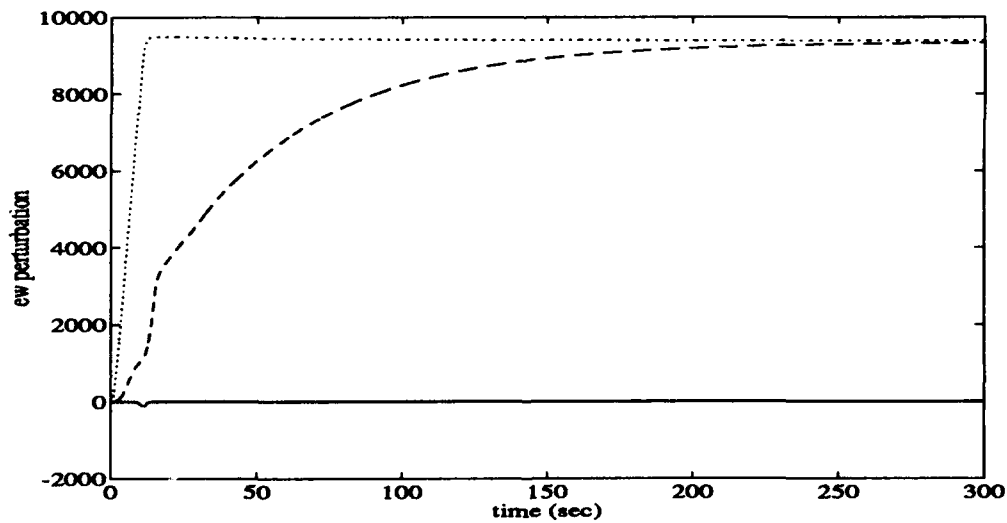
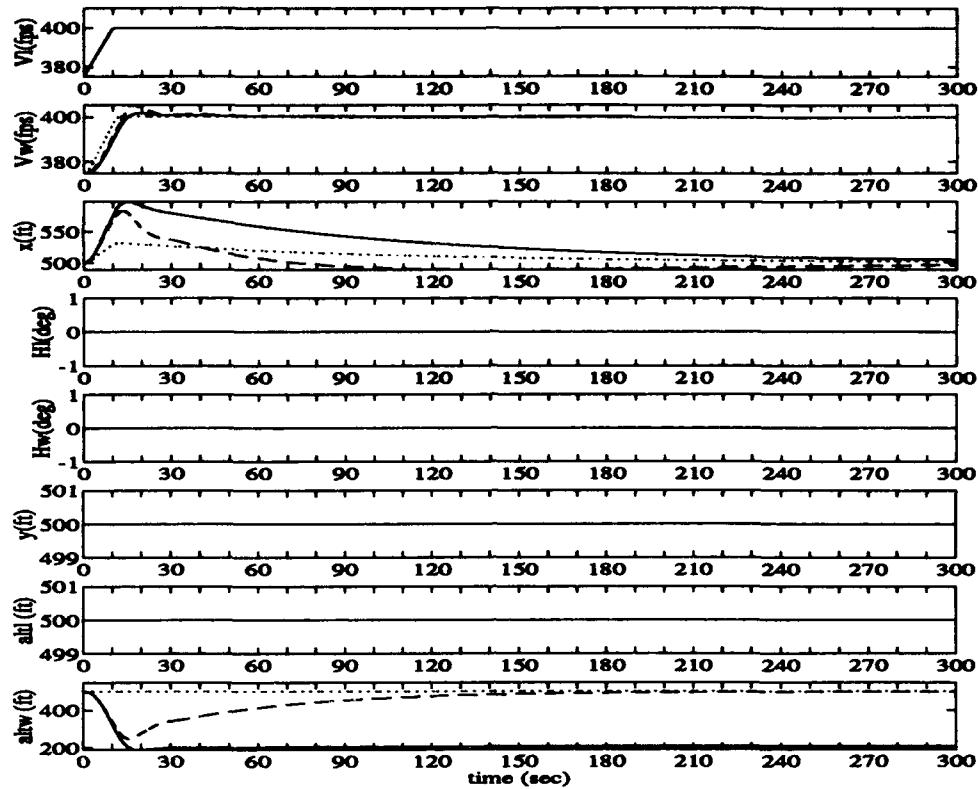


Figure 6.3 C-130A: Diamond Formation, 25 $\frac{ft}{sec}$ Velocity Change. Nonlinear Simulation: Energy Conserving Implementation (solid line), Energy Minimizing Implementation (dashed line), and Two Dimensional Implementation (dotted line)

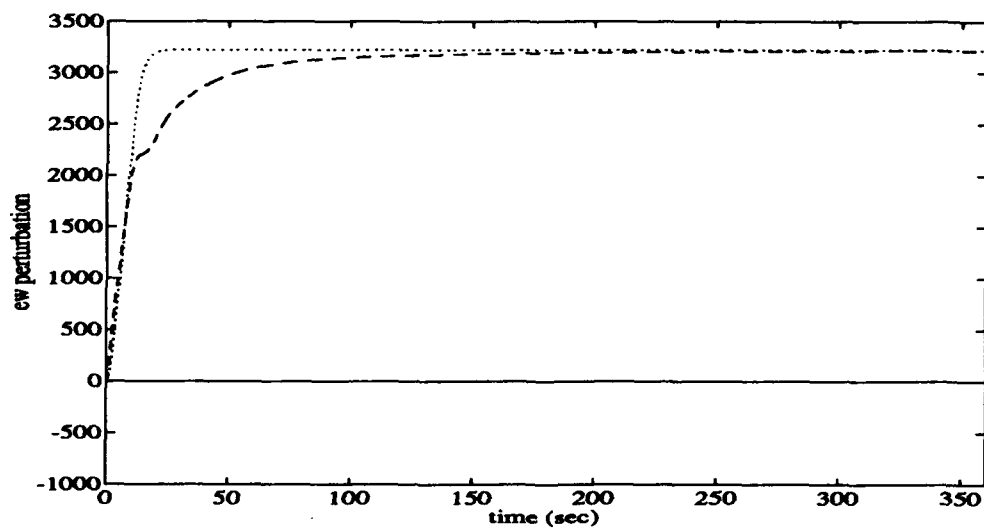
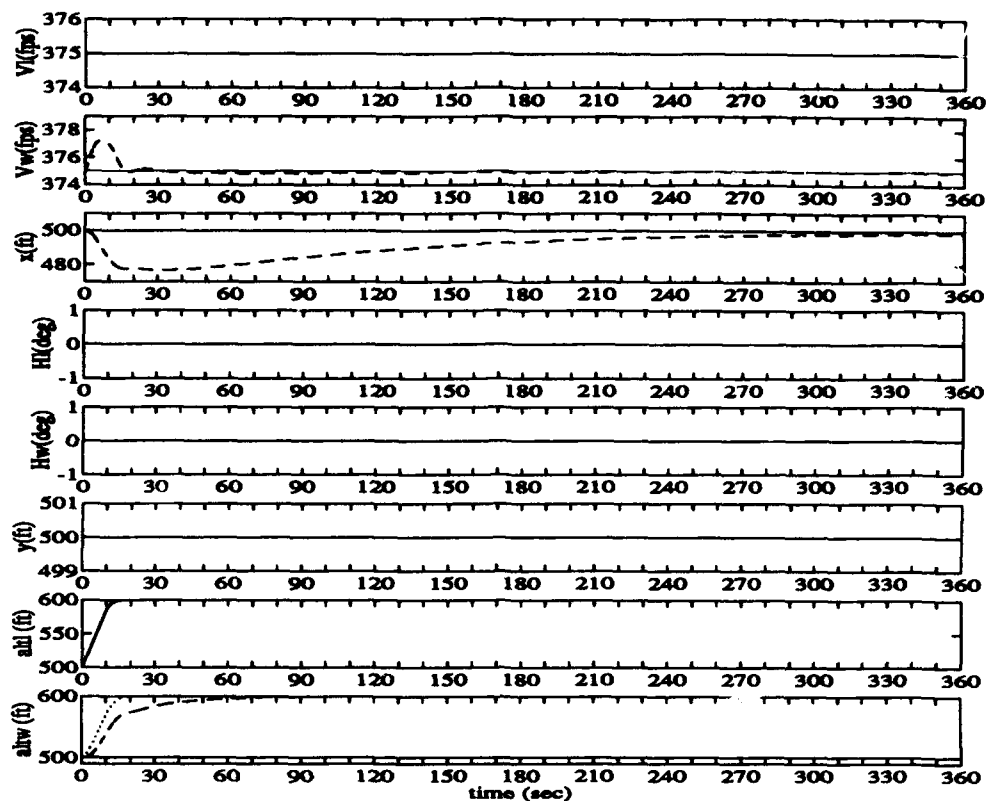


Figure 6.4 C-130A: Nonlinear Simulation, Response To A 100 ft Step Altitude Change: Energy Conserving Implementation (solid line), Energy Minimizing Implementation (dashed line), and Two Dimensional Implementation (dotted line)

Table 6.1 Gains Used In Nonlinear Simulations To Compare All Three Methods For Heading, Velocity, and Altitude Changes In Figures 6.1 - 6.4

Parameter	Dimensional Value							
	Two Dimensional Maneuvers				Energy Conserving	Energy Minimizing		
	10° Δ	90° Δ	Velocity Δ	Altitude Δ	All Maneuver Δ s	Heading Δ	Velocity Δ	Altitude Δ
k_{zpv}						.01	.02	.07
k_{zsv}						.0001	.002	.007
k_z	1	1	1	1	1	1	1	1
k_v	0	3	0	0	0	0	0	0
k_{zp}	.75	1	.75	.75	.75	.75	.75	.75
k_{zi}	.0075	.1	.0075	.0075	.0075	.0075	.0075	.0075
k_y	1	1	1	1	1	1	1	1
k_{ψ}	0	4	0	0	0	0	0	0
k_{yp}	1	1	1	1	1	1	1	1
k_{yi}	.01	.1	.01	.01	.01	.01	.01	.01
k_{sp}				1				
k_{si}				.5				

2. There are no wing aircraft altitude changes using two dimensional maneuvers for heading and velocity changes
3. Two dimensional maneuvers cause the largest amount of wing specific energy excursions \triangleq throttle usage
4. Energy conserving maneuvers allow heading changes that have a worse response in x-separation (i.e., there are larger deviations away from nominal)
5. Energy conserving maneuvers use the least amount of energy during heading changes. The specific energy of the wing aircraft is not exactly constant. Due to rate limiters in the nonlinear simulation, the specific energy of the wing aircraft do not remain at their nominal value. However, the excursions away from nominal are small and negative
6. Energy conserving maneuvers have a worse x-separation response. They also have altitude drops associated with their accomplishment. In addition, the velocity perturbs farther away from nominal than in two dimensional maneuvers

7. **Energy excursion minimizing maneuvers cause the second largest amount of energy excursions during maneuvers. This is expected. It should be between energy conserving maneuvers and two dimensional maneuvers.**
8. **Energy excursion minimizing maneuvers also yield x-separation performance between two dimensional and energy conserving maneuvers. Additionally, the velocity response shows much larger excursions away from nominal during maneuvers**
9. **Energy excursion minimizing maneuvers largest advantage over energy conserving maneuvers is its recovery from velocity and altitude changes. It also has a smaller altitude change than energy conserving maneuvers**

Observations 1 - 9 show that there are distinct differences between the three methods. Two dimensional maneuvers are good if it is unwise for wing aircraft in the formation to track the lead aircraft without altitude deviations and large x-separation deviations. However, these maneuvers cause significant energy excursions more so than other maneuvers, resulting in more fuel use by the wing aircraft. Energy conserving maneuvers are good if only interested in heading changes. Wing aircraft would use less fuel and would have the same energy consumption as the lead aircraft. Energy excursion minimizing maneuvers provide the best overall capabilities and energy usage if altitude changes do not cause any problem within the formation.

There are times when each of these methods is appropriate for a formation. Two dimensional maneuvers use the most energy. However, the characteristics of no altitude changes and smaller deviations in x-separation would benefit a low altitude formation penetrating hostile territory.

Both energy conserving maneuvers and energy excursion minimizing maneuvers provide good characteristics for a formation in friendly skies at cruising altitude. Altitude changes of a few hundred feet are of no consequence at 20,000 feet above ground level (AGL). Separation requirements can also be relaxed since detection by enemy forces is not a threat. The question is what kind of performance is desired. Heading changes are

definitely better when done with energy conserving maneuvers. The aircraft energy is preserved and fuel use is kept consistent with the lead aircraft. However, velocity changes cannot be performed using constant energy maneuvers. Energy excursion minimizing maneuvers are capable of performing velocity changes with less energy consumption than two dimensional maneuvers. Their only disadvantage is they are not as efficient as energy conserving maneuvers during heading changes. If one or the other must be chosen, energy excursion minimizing maneuvers definitely provide the most capabilities with lower use of energy than two dimensional maneuvers.

A logical extension of these observations can be determined by examining the "flight phases" of aircraft. Nelson divides the flight phases of an aircraft into the following:

1. Nonterminal Flight Phase

- (a) **Category A :** "Nonterminal flight phases that require rapid maneuvering, precision tracking, or precise flight-path control. Included in the category are air-to-air combat ground attack, weapon delivery/launch, aerial recovery, reconnaissance, in-flight refueling (receiver), terrain-following, antisubmarine search, and close-formation flying"
- (b) **Category B :** "Nonterminal flight phases that are normally accomplished using gradual maneuvers and without precision tracking, although accurate flight-path control may be required. Included in the category are climb, cruise, loiter, in-flight refueling (tanker), descent, emergency descent, emergency deceleration, and aerial delivery"

2. Terminal Flight Phase

- (a) **Category C :** "Terminal flight phases are normally accomplished using gradual maneuvers and usually require accurate flight-path control. Included in this category are takeoff, catapult takeoff, approach, wave-off/go-around, and landing"

[8]

These definitions of flight phase concern individual aircraft. However, they can be extended to a formation of aircraft also. Two dimensional maneuvers would be ideal for Category A flying. This application could very easily be used for reconnaissance, terrain-following, and close-formation flying. Category B could be handled by energy excursion minimising maneuvers especially cruising, loitering, climb, or descent. Obviously, the appropriate form of control would need to be used for the corresponding flight phase. Category C flight phase will probably never be used with this kind of control system.

6.3 Conclusion

All three maneuvering methods compared in this chapter are useful concepts of automatic formation flight control, however, each has its advantage and disadvantage. Different flight phases experienced by the formation would determine which concept to use.

VII. Analysis and Conclusions

7.1 Objectives of Research Met

The objective of this research is to continue the previous work accomplished by Rohs, Dargan, and Busogany, by enhancing the Automatic Formation Flight Control System with the inclusion of a linear mixer, which blends velocity and heading rate with the longitudinal and lateral formation spacing, and investigating energy excursion minimizing maneuvers. These objectives have been accomplished.

7.1.1 Horizontal Formation Flight Control - Analysis. The inclusion of a linear mixer into the Automated Flight Control System is accomplished in Chapter IV for both the x and y channels. Two dimensional maneuvers are considered. The difference between the previous effort accomplished by Busogany [2] and the new effort is the inclusion of the linear mixer gains and lead aircraft states in the analysis. Busogany's analysis fed back only separation errors while the new formulation feeds back separation errors, heading error (ψ_e , y -channel), and velocity error (V_e , x -channel). Previously, the lead aircraft states were considered to be disturbances into the system. Now, the disturbances into the system are the lead aircraft commands. The lead aircraft states augment the plant's state vector. Because the six state model is used with first-order aircraft channel models, the characteristic polynomials for each channel are of fourth-order. Performing a Routhian stability analysis on each channel results in conditions for system stability. A gain parameter stability envelope in three dimensional space is determined by performing a linear transformation on the gain parameters of interest. The gains of interest for each channel are: k_{yi} , k_{yp} , and k_ψ for the y -channel and k_{xi} , k_{xp} , and k_v for the x -channel (recall: $k_y = k_x = 1$). There are some quadratic terms in each channel that make plotting the envelope difficult. By analyzing the stability equations, a nonlinear transformation of variables is determined between the $K_Y = (k_{yp}, k_{yi}, k_\psi) \in \mathcal{R}^3$ and $G_Y = (k, l, k_{yi}) \in \mathcal{R}^3$, and $K_X = (k_{xp}, k_{xi}, k_v) \in \mathcal{R}^3$ and $G_X = (m, n, k_{xi})$ parameter vectors. These nonlinear transformations map the respective gains into a space in which the stability equations become more tractable and thus easier

to plot. With these stability envelopes, any choice of gains can be transformed into the new space to graphically gauge the stability of the system.

Simulations with the mixer in place showed better response characteristics in velocity and separation error. Thus, including mixers and lead aircraft states into the new Formation Flight Control model has successfully been completed and validated.

7.1.2 Three Dimensional Energy Excursion Minimizing Maneuvers. Previously, energy conserving maneuvers were accomplished by keeping the specific energy of the wing aircraft constant. Thus, any increase in lead aircraft velocity results in a corresponding decrease in wing aircraft altitude, and vice-versa. Hence, energy conserving maneuvers are fine during formation heading changes, however, velocity or altitude changes result in loss of formation integrity. This research effort allows the specific energy of the wing aircraft to deviate from its nominal value by including a PI controller for V_{W_e} . Thus, a PI controller commands the throttle (V_{W_e}) which causes excursions in specific energy. Therefore, formation energy changes can be made and formation integrity will be maintained.

7.1.3 Comparison Of Formulations. The three formulations for Automatic Formation investigated in this thesis are:

- Two dimensional formation maneuvers
- Energy conserving maneuvers (i.e., specific energy is kept constant)
- Energy excursion minimizing maneuvers (i.e., specific energy is allowed to make excursions away from its nominal value)

As expected, the energy conserving maneuvers provided heading changes with minimal excursions in specific energy due to aircraft rate limiters. However, they do not provide good response characteristics for velocity changes or altitude changes. Both two dimensional and energy excursion minimizing maneuvers provide formation energy change capabilities in addition to heading change capability. The two dimensional maneuvers provide better

performance overall in x separation, y separation, wing velocity, and wing altitude. However, this is done at the cost of requiring more wing aircraft specific energy excursions than the energy minimizing maneuvers, which change the altitude in order to compensate for velocity changes.

These formulations for Automatic Flight Control provide different degrees of performance and energy use. There is a tradeoff between capability and energy use. This is a useful finding because it forms the foundation for a control system that provides desirable characteristics in Flight Phases A - C [8]. In cruise, a blend of energy conserving and energy excursion minimizing would provide sufficient formation capabilities. However, penetrating enemy airspace would obviate the need for two dimensional maneuvers, where tighter formations and lower altitudes could be flown.

Concept	Maneuvers									
	Heading				Velocity			Altitude		
	x	y	h _w	e _w	x	h _w	e _w	x	h _w	e _w
Planar	+	o	+	-	+	+	-	+	+	-
Energy Conserving	o	o	-	+	n/c	n/c	n/c	n/c	n/c	n/c
Energy Exc. Min.	-	o	o	o	-	-	+	-	-	-

where,

+ = best response

o = good response

- = worst response

n/c = not capable

7.2 Conclusions and Lessons Learned

The following conclusions are drawn from this research effort:

- In accordance with research accomplished by Buzogany in December, 1992, analysis proves the necessary and sufficient condition of integral control action to achieve zero

steady-state error for a formation of aircraft. Additionally, a parameter stability envelope can be plotted to show regions of guaranteed stability for the gains of interest.

- Using the linearized, state space MIMO plant model, PI controller gains can be determined through pole placement techniques. These gains provide good response characteristics in the linear case, however, they need to be adjusted using a heuristic process, due to the rate limiters in the nonlinear aircraft channel models.
- Adding a linear mixer, which blends velocity and heading rate with formation spacing, into the analysis yields a better overall response.
- Analysis of energy excursion minimizing maneuvers also proved the necessary and sufficient condition of integral control action. Due to time constraints, stability envelopes were not researched. However, the linearized MIMO plant model allowed the use of pole placement techniques to provide values of the PI controller parameters. Once again, a heuristic/experimentation process is required to determine the best gains for the full nonlinear simulation.
- Comparison of the three concepts for Automatic Formation Flight Control show the relative capabilities of each method. These capabilities can be used to synthesize a flexible control system optimized for different phases of flight.

7.3 Recommendations For Further Study

As stated in Chapter I, this thesis is a stepping stone. Some recommendations for further study are:

1. Include sensor models into the simulation. Additionally, sensor noise should be incorporated to evaluate its effect on system stability [2:page 8-5].
2. Investigate incorporating air-refueling capabilities into Automatic Formation Flight Control

3. Determine a method to quantify the effect of nonlinear rate limiters on the control system response in order to remove the heuristic process of selecting "good" controller and mixer gains
4. Include second order models developed by Buzogany and perform analytic analyses to determine the pertinent parametric stability envelopes
5. Time delays representing update data rates/sampling rates should be incorporated into the model and simulation in order to quantify the effects on system stability
[4:page 6-4]
6. Investigate energy conserving and excursion minimizing maneuvers with dissimilar aircraft
7. Energy excursion minimizing maneuvers should be utilized with multiple wing aircraft to investigate its effect on formation integrity
8. A robustness investigation applying the Routh Stability Criterion for both two dimensional and energy minimizing maneuvers should be explored
9. Optimal control techniques should be applied to energy minimization maneuvers in order that the optimal energy use during maneuvers is determined

This concept can also be applied to other vehicles that move in large groups. Some future applications are:

1. Extend this research to helicopters. Rotorblades make flying in tight formation dangerous
2. Explore formations composed of fighter aircraft, to explore high performance considerations
3. Explore formations composed of hovercraft, which are used for beach assaults

7.4 Summary

As the research performed by Buzogany and Dargan showed [2] [4], a PI controller can successfully maintain a multiple aircraft formation through different maneuvers. Analysis reaffirmed the necessary and sufficient condition of integral control action for maintaining formation integrity during maneuvers. Parameter stability envelopes can be determined in the two dimensional case. Two dimensional and energy excursion minimizing maneuvers provide desirable formation response characteristics for the appropriate flight phase.

Appendix A. Dimensional Plant Matrices

Through the course of this thesis, analysis is performed on the linearized state space MIMO model and the dimensional eigenvalues. Chapters IV and V interchange between dimensional and nondimensional discussions. In order to avoid confusion, the MIMO state space models in these chapters are presented in their dimensional form

A.1 Chapter IV Dimensional Models

A.1.1 Y-Channel.

$$\begin{bmatrix} \dot{y} \\ \dot{\psi}_W \\ \dot{\psi}_L \\ \dot{\psi}_{Wc} \end{bmatrix} = \begin{bmatrix} 0 & \left(\frac{l \cos \alpha}{\tau_{\psi W}} - V_0\right) & V_0 & -\frac{l \cos \alpha}{\tau_{\psi W}} \\ 0 & -\frac{1}{\tau_{\psi W}} & 0 & \frac{1}{\tau_{\psi W}} \\ 0 & 0 & -\frac{1}{\tau_{\psi L}} & 0 \\ k_{yi}k_y & C_{\psi W} & C_{\psi L} & C_{\psi Wc} \end{bmatrix} \begin{bmatrix} y \\ \psi_W \\ \psi_L \\ \psi_{Wc} \end{bmatrix} + \begin{bmatrix} 0 \\ 0 \\ \frac{1}{\tau_{\psi L}} \\ k_{yp}k_\psi \frac{1}{\tau_{\psi L}} \end{bmatrix} \psi_{Lc} \quad (A.1)$$

$$Y_y = \begin{bmatrix} 1 & 0 & 0 & 0 \\ 0 & -1 & 1 & 0 \end{bmatrix} \begin{bmatrix} y \\ \psi_W \\ \psi_L \\ \psi_{Wc} \end{bmatrix} = \begin{bmatrix} y \\ \psi_c \end{bmatrix} \quad (A.2)$$

where,

$$C_{\psi W} = k_{yp}k_y \left(\frac{l \cos \alpha}{\tau_{\psi W}} - V_0 \right) + k_{yp}k_\psi \frac{1}{\tau_{\psi W}} - k_{yi}k_\psi \quad (A.3)$$

$$C_{\psi L} = k_{yp}k_y V_0 - k_{yp}k_\psi \frac{1}{\tau_{\psi L}} + k_{yi}k_\psi \quad (A.4)$$

$$C_{\psi Wc} = -k_{yp} \frac{1}{\tau_{\psi W}} (lk_y \cos \alpha + k_\psi) \quad (A.5)$$

A.1.2 X-Channel.

$$\begin{bmatrix} \dot{z} \\ \dot{V}_W \\ \dot{V}_L \\ \dot{V}_{Wc} \end{bmatrix} = \begin{bmatrix} 0 & -\frac{1}{\tau_{VW}} & 1 & 0 \\ 0 & -\frac{1}{\tau_{VW}} & 0 & \frac{1}{\tau_{VW}} \\ 0 & 0 & -\frac{1}{\tau_{VL}} & 0 \\ k_{zi}k_z & C_{VW} & C_{VL} & -k_{zp}k_V \frac{1}{\tau_{VW}} \end{bmatrix} \begin{bmatrix} z \\ V_W \\ V_L \\ V_{Wc} \end{bmatrix} + \begin{bmatrix} 0 & \frac{l \sin \alpha}{\tau_{\psi W}} \\ 0 & 0 \\ \frac{1}{\tau_{VL}} & 0 \\ k_{zp}k_v \frac{1}{\tau_{VL}} & k_{zp}k_z \frac{l \sin \alpha}{\tau_{\psi W}} \end{bmatrix} \begin{bmatrix} V_{Lc} \\ d_\psi \end{bmatrix} \quad (A.6)$$

$$Y_z = \begin{bmatrix} 1 & 0 & 0 & 0 \\ 0 & -1 & 1 & 0 \end{bmatrix} \begin{bmatrix} z \\ V_W \\ V_L \\ V_{W_c} \end{bmatrix} = \begin{bmatrix} z \\ V_c \end{bmatrix} \quad (\text{A.7})$$

where,

$$C_{V_W} = -k_{zp}k_z + k_{zp}k_v \frac{1}{\tau_{V_W}} - k_{zi}k_v \quad (\text{A.8})$$

$$C_{V_L} = k_{zp}k_z - k_{zp}k_v \frac{1}{\tau_{V_L}} + k_{zi}k_v \quad (\text{A.9})$$

A.2 Chapter V Dimensional Model

$$\begin{bmatrix} \dot{z} \\ \dot{h}_W \\ \dot{e}_W \\ \dot{h}_L \\ \dot{V}_{W_c} \\ \dot{h}_{W_c} \end{bmatrix} = \begin{bmatrix} 0 & \frac{g}{V_0} & -\frac{1}{V_0} & 0 & 0 & 0 \\ 0 & -\frac{1}{\tau_{h_W}} & 0 & 0 & 0 & \frac{1}{\tau_{h_W}} \\ 0 & g \left(\frac{1}{\tau_{V_W}} - \frac{1}{\tau_{h_W}} \right) & -\frac{1}{\tau_{V_W}} & 0 & V_0 \frac{1}{\tau_{V_W}} & g \frac{1}{\tau_{h_W}} \\ 0 & 0 & 0 & -\frac{1}{\tau_{h_L}} & 0 & 0 \\ -\frac{g}{V_0} \tau_{V_W} \frac{1}{\tau_{h_W}} k_{zsi} & D_{h_W} & D_{e_W} & D_{h_L} & \frac{1}{\tau_{V_W}} & D_{h_{W_c}} \\ k_{zsi} & \frac{g}{V_0} k_{zsp} & -k_{zsp} \frac{1}{V_0} & 0 & 0 & 0 \end{bmatrix} \begin{bmatrix} z \\ h_W \\ e_W \\ h_L \\ V_{W_c} \\ h_{W_c} \end{bmatrix} + \begin{bmatrix} 1 & 0 & \frac{l \sin \alpha}{\tau_{\phi_W}} \\ 0 & 0 & 0 \\ 0 & 0 & 0 \\ 0 & \frac{1}{\tau_{h_L}} & 0 \\ -\frac{g}{V_0} \tau_{V_W} \frac{1}{\tau_{h_W}} k_{zsp} & k_{zsp} \frac{1}{\tau_{h_L}} & -\frac{g}{V_0} \tau_{V_W} \frac{1}{\tau_{h_W}} k_{zsp} \frac{l \sin \alpha}{\tau_{\phi_W}} \\ k_{zsp} & 0 & k_{zsp} \frac{l \sin \alpha}{\tau_{\phi_W}} \end{bmatrix} \begin{bmatrix} V_L \\ L_c \\ d\phi \end{bmatrix} \quad (\text{A.10})$$

$$Y_{zs} = \begin{bmatrix} 1 & 0 & 0 & 0 & 0 & 0 \\ 0 & -1 & 0 & 1 & 0 & 0 \end{bmatrix} = \begin{bmatrix} z \\ h_c \end{bmatrix} \quad (\text{A.11})$$

where,

$$D_{h_W} = \frac{g}{V_0} \left(\frac{1}{\tau_{V_W}} - \frac{1}{\tau_{h_W}} \right) - \frac{g}{V_0} \tau_{V_W} \frac{1}{\tau_{h_W}} \left(\frac{1}{\tau_{h_W}} - \frac{1}{\tau_{V_W}} \right) - \frac{g^2}{V_0^2} \tau_{V_W} \frac{1}{\tau_{h_W}} k_{zsp} + k_{zsp} \frac{1}{\tau_{h_W}} - k_{zsi} \quad (\text{A.12})$$

$$D_{ew} = -\frac{1}{V_0} \frac{1}{\tau_{vw}} + \frac{g}{V_0^2} \tau_{vw} \frac{1}{\tau_{hw}} k_{ssp} \quad (\text{A.13})$$

$$D_{hL} = -\frac{1}{\tau_{hL}} k_{sspV} + k_{ssiv} \quad (\text{A.14})$$

$$D_{hw} = \frac{g}{V_0} \frac{1}{\tau_{hw}} + \frac{g}{V_0} \tau_{vw} \frac{1}{\tau_{hw}} \left(\frac{1}{\tau_{hw}} - \frac{1}{\tau_{vw}} \right) - k_{sspV} \frac{1}{\tau_{hw}} \quad (\text{A.15})$$

Appendix B. Stability Equations From Chapter V

The following stability equations are from Section 5.1.3. They are derived from a Routhian array in the same section. Due to the complexity of the algebra, Mathematica was used to derive the larger inequalities in this appendix. For more information, see Section 5.1.3.

row s^5

$$\tau_{hL} + \tau_{hW} > 0 \quad (B.1)$$

row s^4

$$k_{zsp}k_{zspv}\tau_{hL}^2\tau_{hW} + \tau_{hL}\tau_{VW} + \tau_{hW}\tau_{VW} - k_{zsp}\tau_{hL}^2\tau_{VW}\xi + k_{zsi}\tau_{hL}^2\tau_{hW}\tau_{VW}\xi > 0 \quad (B.2)$$

row s^3

$$\begin{aligned} & -(k_{zsp}^2k_{zspv}^2\tau_{hL}^3\tau_{hW}) + k_{zsi}k_{zsp}\tau_{hL}^3\tau_{VW} + k_{zsi}k_{zspv}\tau_{hL}^3\tau_{VW} + k_{zsp}k_{zspv}\tau_{hL}\tau_{hW}\tau_{VW} \\ & + k_{zsi}k_{zsp}\tau_{hL}^2\tau_{hW}\tau_{VW} + k_{zsi}k_{zspv}\tau_{hL}^2\tau_{hW}\tau_{VW} - k_{zsi}k_{zsi}v\tau_{hL}^3\tau_{hW}\tau_{VW} + k_{zsp}k_{zspv}\tau_{hL}^2\tau_{hW}\tau_{VW} \\ & - k_{zsi}k_{zsi}v\tau_{hL}^2\tau_{hW}^2\tau_{VW} + k_{zsp}^2k_{zspv}\tau_{hL}^3\tau_{VW}\xi - k_{zsp}^2k_{zspv}\tau_{hL}^2\tau_{hW}\tau_{VW}\xi \\ & - 2k_{zsi}k_{zsp}k_{zspv}\tau_{hL}^3\tau_{hW}\tau_{VW}\xi - k_{zsp}\tau_{hL}^2\tau_{VW}^2\xi - k_{zsp}\tau_{hW}\tau_{VW}^2\xi + k_{zsi}\tau_{hL}\tau_{hW}\tau_{VW}^2\xi \\ & + k_{zsi}\tau_{hW}^2\tau_{VW}^2\xi + k_{zsp}^2\tau_{hL}^2\tau_{VW}^2\xi^2 + k_{zsi}k_{zsp}\tau_{hL}^3\tau_{VW}^2\xi^2 - k_{zsi}k_{zsp}\tau_{hL}^2\tau_{hW}\tau_{VW}^2\xi^2 \\ & - k_{zsi}^2\tau_{hL}^3\tau_{hW}\tau_{VW}^2\xi^2 > 0 \end{aligned} \quad (B.3)$$

row s^2

$$\begin{aligned}
& k_{ssp}^3 k_{spp}^3 \tau_{hL}^3 \tau_{hW} + k_{ssiv} k_{ssp}^3 k_{spp}^2 \tau_{hL}^4 \tau_{hW} + k_{ssi} k_{ssp}^2 k_{spp}^3 \tau_{hL}^4 \tau_{hW} - k_{ssiv} k_{ssp}^2 k_{spp} \tau_{hL}^3 \tau_{VW} \\
& - k_{ssi} k_{ssp} k_{spp}^2 \tau_{hL}^3 \tau_{VW} - k_{ssiv}^2 k_{ssp}^2 \tau_{hL}^4 \tau_{VW} - 2k_{ssi} k_{ssiv} k_{ssp} k_{spp} \tau_{hL}^4 \tau_{VW} - k_{ssi}^2 k_{spp}^2 \tau_{hL}^4 \tau_{VW} \\
& - k_{ssp}^2 k_{spp}^2 \tau_{hL} \tau_{hW} \tau_{VW} + 2k_{ssi} k_{ssiv} k_{ssp} k_{spp} \tau_{hL}^3 \tau_{hW} \tau_{VW} + 2k_{ssi} k_{ssiv}^2 k_{ssp} \tau_{hL}^4 \tau_{hW} \tau_{VW} \\
& + 2k_{ssi}^2 k_{ssiv} k_{spp} \tau_{hL}^4 \tau_{hW} \tau_{VW} - k_{ssp}^2 k_{spp}^2 \tau_{hW}^2 \tau_{VW} \\
& + k_{ssi} k_{ssiv} k_{ssp} k_{spp} \tau_{hL}^2 \tau_{hW}^2 \tau_{VW} - k_{ssi}^2 k_{ssiv}^2 \tau_{hL}^4 \tau_{hW}^2 \tau_{VW} + k_{ssiv} k_{ssp} \tau_{hL} \tau_{VW}^2 \\
& + k_{ssi} k_{spp} \tau_{hL} \tau_{VW}^2 + k_{ssiv} k_{ssp} \tau_{hW} \tau_{VW}^2 + k_{ssi} k_{spp} \tau_{hW} \tau_{VW}^2 - k_{ssi} k_{ssiv} \tau_{hL} \tau_{hW} \tau_{VW}^2 \\
& - k_{ssi} k_{ssiv} \tau_{hW}^2 \tau_{VW}^2 - k_{ssp}^3 k_{spp}^2 \tau_{hL}^3 \tau_{VW} \xi - k_{ssiv} k_{ssp}^3 k_{spp} \tau_{hL}^4 \tau_{VW} \xi \\
& - k_{ssi} k_{ssp}^2 k_{spp}^2 \tau_{hL}^4 \tau_{VW} \xi + k_{ssp}^3 k_{spp}^2 \tau_{hL}^2 \tau_{hW} \tau_{VW} \xi \\
& + 3k_{ssi} k_{ssp}^2 k_{spp}^2 \tau_{hL}^3 \tau_{hW} \tau_{VW} \xi + k_{ssi} k_{ssiv} k_{ssp}^2 k_{spp} \tau_{hL}^4 \tau_{hW} \tau_{VW} \xi \\
& + 2k_{ssi}^2 k_{ssp}^2 k_{spp}^2 \tau_{hL}^4 \tau_{hW} \tau_{VW} \xi + k_{ssp}^2 k_{spp} \tau_{hL} \tau_{VW}^2 \xi - k_{ssiv} k_{ssp}^2 \tau_{hL}^2 \tau_{VW}^2 \xi - k_{ssi} k_{ssp} k_{spp} \tau_{hL}^2 \tau_{VW}^2 \xi \\
& - 2k_{ssi} k_{ssiv} k_{ssp} \tau_{hL}^3 \tau_{VW}^2 \xi - k_{ssi}^2 k_{spp} \tau_{hL}^3 \tau_{VW}^2 \xi + k_{ssp}^2 k_{spp} \tau_{hW} \tau_{VW}^2 \xi \\
& - 2k_{ssi} k_{ssp} k_{spp} \tau_{hL} \tau_{hW} \tau_{VW}^2 \xi + 2k_{ssi}^2 k_{ssiv} \tau_{hL}^3 \tau_{hW} \tau_{VW}^2 \xi \\
& - 2k_{ssi} k_{ssp} k_{spp} \tau_{hW}^2 \tau_{VW}^2 \xi + k_{ssi}^2 k_{ssiv} \tau_{hL}^2 \tau_{hW}^2 \tau_{VW}^2 \xi \\
& - k_{ssp}^3 k_{spp} \tau_{hL}^2 \tau_{VW}^2 \xi^2 - 2k_{ssi} k_{ssp}^2 k_{spp} \tau_{hL}^3 \tau_{VW}^2 \xi^2 \\
& - k_{ssi}^2 k_{ssp} k_{spp} \tau_{hL}^4 \tau_{VW}^2 \xi^2 + 2k_{ssi} k_{ssp}^2 k_{spp} \tau_{hL}^2 \tau_{hW} \tau_{VW}^2 \xi^2 + 3k_{ssi}^2 k_{ssp} k_{spp} \tau_{hL}^3 \tau_{hW} \tau_{VW}^2 \xi^2 \\
& + k_{ssi}^3 k_{spp} \tau_{hL}^4 \tau_{hW} \tau_{VW}^2 \xi^2 \\
& + k_{ssi} k_{ssp} \tau_{hL} \tau_{VW}^3 \xi^2 + k_{ssi} k_{ssp} \tau_{hW} \tau_{VW}^3 \xi^2 - k_{ssi}^2 \tau_{hL} \tau_{hW} \tau_{VW}^3 \xi^2 \\
& - k_{ssi}^2 \tau_{hW}^2 \tau_{VW}^3 \xi^2 - k_{ssi} k_{ssp}^2 \tau_{hL}^2 \tau_{VW}^3 \xi^3 \\
& - k_{ssi}^2 k_{ssp} \tau_{hL}^3 \tau_{VW}^3 \xi^3 + k_{ssi}^2 k_{ssp} \tau_{hL}^2 \tau_{hW} \tau_{VW}^3 \xi^3 + k_{ssi}^3 \tau_{hL} \tau_{hW} \tau_{VW}^3 \xi^3 > 0
\end{aligned}$$

(B.4)

$$\begin{aligned}
& -(k_{zzi}k_{zsp}^4k_{zspv}^3\tau_{hL}^3\tau_{hw}) - k_{zzi}k_{zsp}^3k_{zspv}^4\tau_{hL}^3\tau_{hw} - k_{zsi}^2k_{zsp}^4k_{zspv}^2\tau_{hL}^4\tau_{hw} \\
& - 2k_{zzi}k_{zsi}k_{zsp}^3k_{zspv}^3\tau_{hL}^4\tau_{hw} - k_{zzi}^2k_{zsp}^2k_{zspv}^4\tau_{hL}^4\tau_{hw} - k_{zzi}k_{zsi}^2k_{zsp}^3k_{zspv}^2\tau_{hL}^5\tau_{hw} \\
& - k_{zzi}^2k_{zsi}k_{zsp}^2k_{zspv}^3\tau_{hL}^5\tau_{hw} + k_{zsi}^2k_{zsp}^3k_{zspv}^3\tau_{hL}^3\tau_{vw} + 2k_{zzi}k_{zsi}k_{zsp}^2k_{zspv}^2\tau_{hL}^3\tau_{vw} \\
& + k_{zzi}^2k_{zsp}^3k_{zspv}^3\tau_{hL}^3\tau_{vw} + k_{zsi}^3k_{zsp}^3\tau_{hL}^4\tau_{vw} + 3k_{zzi}k_{zsi}^2k_{zsp}^2k_{zspv}^4\tau_{hL}^4\tau_{vw} \\
& + 3k_{zzi}^2k_{zsi}k_{zsp}^2k_{zspv}^4\tau_{hL}^4\tau_{vw} + k_{zzi}^3k_{zsp}^3\tau_{hL}^4\tau_{vw} \\
& + k_{zzi}k_{zsi}^3k_{zsp}^2\tau_{hL}^5\tau_{vw} + 2k_{zzi}^2k_{zsi}^2k_{zsp}k_{zspv}^5\tau_{hL}^5\tau_{vw} \\
& + k_{zzi}^3k_{zsi}k_{zsp}^2\tau_{hL}^5\tau_{vw} + k_{zsi}^3k_{zsp}^3k_{zspv}^2\tau_{hL}^4\tau_{hw}\tau_{vw} + k_{zzi}k_{zsp}^2k_{zspv}^3\tau_{hL}^4\tau_{hw}\tau_{vw} \\
& - 2k_{zzi}k_{zsi}^2k_{zsp}^2k_{zspv}^3\tau_{hL}^3\tau_{hw}\tau_{vw} - 2k_{zzi}^2k_{zsi}k_{zsp}^2k_{zspv}^3\tau_{hL}^3\tau_{hw}\tau_{vw} - 2k_{zzi}k_{zsi}^3k_{zsp}^2\tau_{hL}^4\tau_{hw}\tau_{vw} \\
& - 4k_{zzi}^2k_{zsi}^2k_{zsp}k_{zspv}^4\tau_{hL}^4\tau_{hw}\tau_{vw} - 2k_{zzi}^3k_{zsi}k_{zsp}^2\tau_{hL}^4\tau_{hw}\tau_{vw} - 2k_{zzi}^2k_{zsi}^3k_{zsp}\tau_{hL}^5\tau_{hw}\tau_{vw} \\
& - 2k_{zzi}^3k_{zsi}^2k_{zspv}^5\tau_{hL}^5\tau_{hw}\tau_{vw} + k_{zsi}^3k_{zsp}^3k_{zspv}^2\tau_{hL}^2\tau_{vw} + k_{zzi}k_{zsp}^2k_{zspv}^3\tau_{hL}^2\tau_{vw} \\
& + k_{zzi}^2k_{zsi}^2k_{zsp}k_{zspv}^3\tau_{hL}^3\tau_{hw}\tau_{vw} + k_{zzi}^2k_{zsi}^3k_{zsp}\tau_{hL}^4\tau_{hw}\tau_{vw} + k_{zzi}^3k_{zsi}^2k_{zspv}^4\tau_{hL}^4\tau_{hw}\tau_{vw} \\
& + k_{zzi}^3k_{zsi}^3\tau_{hL}^5\tau_{hw}\tau_{vw} - k_{zsi}^2k_{zsp}^2\tau_{hL}^2\tau_{vw}^2 \\
& - 2k_{zzi}k_{zsi}k_{zsp}k_{zspv}^2\tau_{hL}^2\tau_{vw}^2 \\
& - k_{zzi}^2k_{zspv}^2\tau_{hL}^2\tau_{vw}^2 - k_{zsi}^2k_{zsp}^2\tau_{hw}\tau_{vw}^2 - 2k_{zzi}k_{zsi}k_{zsp}k_{zspv}^2\tau_{hw}\tau_{vw}^2 \\
& - k_{zzi}^2k_{zspv}^2\tau_{hw}\tau_{vw}^2 + 2k_{zzi}k_{zsi}^2k_{zsp}\tau_{hL}^2\tau_{hw}\tau_{vw}^2 + 2k_{zzi}^2k_{zsi}k_{zspv}^2\tau_{hL}^2\tau_{hw}\tau_{vw}^2 \\
& + 2k_{zzi}k_{zsi}^2k_{zsp}\tau_{hw}^2\tau_{vw}^2 + 2k_{zzi}^2k_{zsi}k_{zspv}^2\tau_{hw}^2\tau_{vw}^2 \\
& - k_{zzi}^2k_{zsi}^2\tau_{hL}^2\tau_{hw}^2\tau_{vw}^2 - k_{zzi}^2k_{zsi}^2\tau_{hw}^3\tau_{vw}^2 \\
& + k_{zsi}k_{zsp}^4k_{zspv}^2\tau_{hL}^3\tau_{vw}\xi + k_{zzi}k_{zsp}^3k_{zspv}^3\tau_{hL}^3\tau_{vw}\xi \\
& + k_{zsi}^2k_{zsp}^4k_{zspv}^4\tau_{hL}^4\tau_{vw}\xi + 2k_{zzi}k_{zsi}k_{zsp}^3k_{zspv}^2\tau_{hL}^4\tau_{vw}\xi \\
& + k_{zzi}^2k_{zsp}^2k_{zspv}^3\tau_{hL}^4\tau_{vw}\xi + k_{zzi}k_{zsi}^2k_{zsp}^3k_{zspv}^5\tau_{hL}^5\tau_{vw}\xi \\
& + k_{zzi}^2k_{zsi}k_{zsp}^2k_{zspv}^5\tau_{hL}^5\tau_{vw}\xi - k_{zsi}k_{zsp}^4k_{zspv}^2\tau_{hL}^2\tau_{hw}\tau_{vw}\xi \\
& - k_{zzi}k_{zsp}^3k_{zspv}^3\tau_{hL}^2\tau_{hw}\tau_{vw}\xi - 2k_{zzi}k_{zsi}k_{zsp}^3k_{zspv}^2\tau_{hL}^3\tau_{hw}\tau_{vw}\xi
\end{aligned}$$

$$\begin{aligned}
& -3k_{zzi}^2 k_{zsp}^2 k_{zspv}^3 \tau_{hL}^3 \tau_{hw} \tau_{Vw} \xi - k_{zzi} k_{zsi}^2 k_{zsp}^3 k_{zspv} \tau_{hL}^4 \tau_{hw} \tau_{Vw} \xi \\
& -3k_{zzi}^2 k_{zsi} k_{zsp}^2 k_{zspv}^2 \tau_{hL}^4 \tau_{hw} \tau_{Vw} \xi \\
& -2k_{zzi}^3 k_{zsp}^2 k_{zspv}^3 \tau_{hL}^4 \tau_{hw} \tau_{Vw} \xi - k_{zzi}^2 k_{zsi}^2 k_{zsp}^2 k_{zspv}^3 \tau_{hL}^5 \tau_{hw} \tau_{Vw} \xi \\
& -2k_{zzi}^3 k_{zsi} k_{zsp}^2 k_{zspv}^3 \tau_{hL}^5 \tau_{hw} \tau_{Vw} \xi - k_{zsi} k_{zsp}^3 k_{zspv}^2 \tau_{hL}^2 \tau_{Vw}^2 \xi \\
& -k_{zzi} k_{zsp}^2 k_{zspv}^2 \tau_{hL}^2 \tau_{Vw}^2 \xi + k_{zsi}^2 k_{zsp}^3 \tau_{hL}^2 \tau_{Vw}^2 \xi \\
& +2k_{zzi} k_{zsi} k_{zsp}^2 k_{zspv}^2 \tau_{hL}^2 \tau_{Vw}^2 \xi + k_{zzi}^2 k_{zsp}^2 k_{zspv}^2 \tau_{hL}^2 \tau_{Vw}^2 \xi \\
& +k_{zzi} k_{zsi}^2 k_{zsp}^2 \tau_{hL}^3 \tau_{Vw}^2 \xi + 2k_{zzi}^2 k_{zsi} k_{zsp}^2 k_{zspv}^2 \tau_{hL}^3 \tau_{Vw}^2 \xi \\
& +k_{zzi}^3 k_{zsp}^2 \tau_{hL}^3 \tau_{Vw}^2 \xi - k_{zsi} k_{zsp}^3 k_{zspv}^2 \tau_{hw} \tau_{Vw}^2 \xi \\
& -k_{zzi} k_{zsp}^2 k_{zspv}^2 \tau_{hw} \tau_{Vw}^2 \xi + k_{zzi} k_{zsi} k_{zsp}^2 k_{zspv}^2 \tau_{hL} \tau_{hw} \tau_{Vw}^2 \xi \\
& +2k_{zzi}^2 k_{zsp}^2 k_{zspv}^2 \tau_{hL} \tau_{hw} \tau_{Vw}^2 \xi - 2k_{zzi} k_{zsi}^2 k_{zsp}^2 \tau_{hL}^2 \tau_{hw} \tau_{Vw}^2 \xi \\
& -2k_{zzi}^2 k_{zsi} k_{zsp}^2 k_{zspv}^2 \tau_{hL}^2 \tau_{hw} \tau_{Vw}^2 \xi - 2k_{zzi}^2 k_{zsi}^2 k_{zsp}^3 \tau_{hL}^2 \tau_{hw} \tau_{Vw}^2 \xi - 2k_{zzi}^3 k_{zsi} k_{zsp}^2 \tau_{hL}^3 \tau_{hw} \tau_{Vw}^2 \xi \\
& +k_{zzi} k_{zsi} k_{zsp}^2 k_{zspv}^2 \tau_{hw}^2 \tau_{Vw}^2 \xi + 2k_{zzi}^2 k_{zsp}^2 k_{zspv}^2 \tau_{hw}^2 \tau_{Vw}^2 \xi \\
& +k_{zzi}^2 k_{zsi}^2 k_{zsp}^2 \tau_{hL}^2 \tau_{hw}^2 \tau_{Vw}^2 \xi + k_{zzi}^3 k_{zsi}^2 \tau_{hL}^3 \tau_{hw}^2 \tau_{Vw}^2 \xi \\
& +k_{zsi} k_{zsp}^4 k_{zspv}^2 \tau_{hL}^2 \tau_{Vw}^2 \xi^2 + k_{zzi} k_{zsp}^3 k_{zspv}^2 \tau_{hL}^2 \tau_{Vw}^2 \xi^2 \\
& +k_{zzi} k_{zsi} k_{zsp}^3 k_{zspv}^2 \tau_{hL}^3 \tau_{Vw}^2 \xi^2 + 2k_{zzi}^2 k_{zsp}^2 k_{zspv}^2 \tau_{hL}^3 \tau_{Vw}^2 \xi^2 \\
& +k_{zzi}^2 k_{zsi} k_{zsp}^2 k_{zspv}^2 \tau_{hL}^4 \tau_{Vw}^2 \xi^2 + k_{zzi}^3 k_{zsp}^2 k_{zspv}^2 \tau_{hL}^4 \tau_{Vw}^2 \xi^2 \\
& +k_{zzi}^3 k_{zsi} k_{zsp}^2 k_{zspv}^2 \tau_{hL}^5 \tau_{Vw}^2 \xi^2 - k_{zzi} k_{zsi} k_{zsp}^3 k_{zspv}^2 \tau_{hL}^2 \tau_{hw} \tau_{Vw}^2 \xi^2 \\
& -2k_{zzi}^2 k_{zsp}^2 k_{zspv}^2 \tau_{hL}^2 \tau_{hw} \tau_{Vw}^2 \xi^2 - k_{zzi}^2 k_{zsi} k_{zsp}^2 k_{zspv}^2 \tau_{hL}^3 \tau_{hw} \tau_{Vw}^2 \xi^2 \\
& -3k_{zzi}^3 k_{zsp}^2 k_{zspv}^2 \tau_{hL}^3 \tau_{hw} \tau_{Vw}^2 \xi^2 - k_{zzi}^3 k_{zsi} k_{zsp}^2 k_{zspv}^2 \tau_{hL}^4 \tau_{hw} \tau_{Vw}^2 \xi^2 \\
& -k_{zzi}^4 k_{zsp}^2 \tau_{hL}^4 \tau_{hw} \tau_{Vw}^2 \xi^2 - k_{zzi} k_{zsi} k_{zsp}^3 \tau_{hL}^5 \tau_{hw} \tau_{Vw}^2 \xi^2 \\
& -k_{zzi}^2 k_{zsp}^2 k_{zspv}^2 \tau_{hL}^3 \tau_{Vw}^3 \xi^2 - k_{zzi}^2 k_{zsp}^2 k_{zspv}^2 \tau_{hw} \tau_{Vw}^3 \xi^2 \\
& +k_{zzi}^3 k_{zsp}^2 \tau_{hL} \tau_{hw} \tau_{Vw}^3 \xi^2 + k_{zzi}^3 k_{zspv}^2 \tau_{hw}^2 \tau_{Vw}^3 \xi^2 \\
& +k_{zzi}^2 k_{zsp}^2 k_{zspv}^2 \tau_{hL}^2 \tau_{Vw}^3 \xi^3 + k_{zzi}^3 k_{zsp}^2 k_{zspv}^2 \tau_{hL}^3 \tau_{Vw}^3 \xi^3 \\
& -k_{zzi}^3 k_{zsp}^2 k_{zspv}^2 \tau_{hL}^2 \tau_{hw} \tau_{Vw}^3 \xi^3 - k_{zzi}^4 k_{zspv}^2 \tau_{hL}^3 \tau_{hw} \tau_{Vw}^3 \xi^3 > 0
\end{aligned}$$

(B.5)

row s^0

$$k_{ss}k_{ssv} > 0$$

(B.6)

Appendix C. Y and X Channel Stability Constraints Plotted Separately

The stability constraints of Equations (4.84) - (4.87) for the y -channel and Equations (4.88) - (4.91) for the z -channel are plotted individually and then together on the same plot in this appendix. Figures 4.3 and 4.5 show the stability envelopes of the y and z -channel, respectively. This appendix shows all of the intermediate plots that were used to derive the final stability envelopes.

- Figures C.1 - C.5 and Figures C.7 - C.11 show the intermediate plots of the pertinent stability constraints. The corresponding equation number is listed in the caption of each figure
- Figures C.6 and C.12 show the final stability envelopes of the y and z -channels, as in Chapter IV. They are included here to show the complete process, from beginning to end

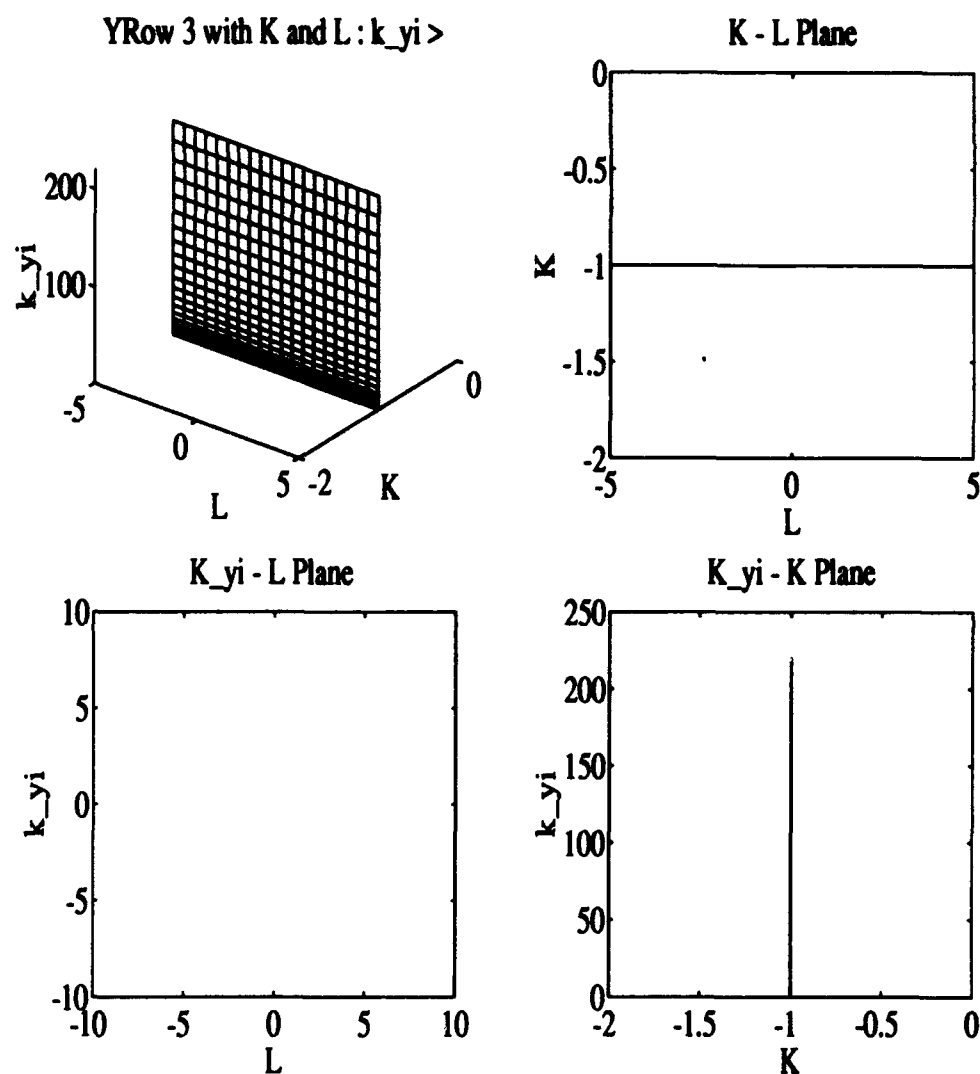


Figure C.1 Plot of the Nondimensional Y-Channel Stability Constraint for Row s^3 of the Routhian Array (Equation (4.84))

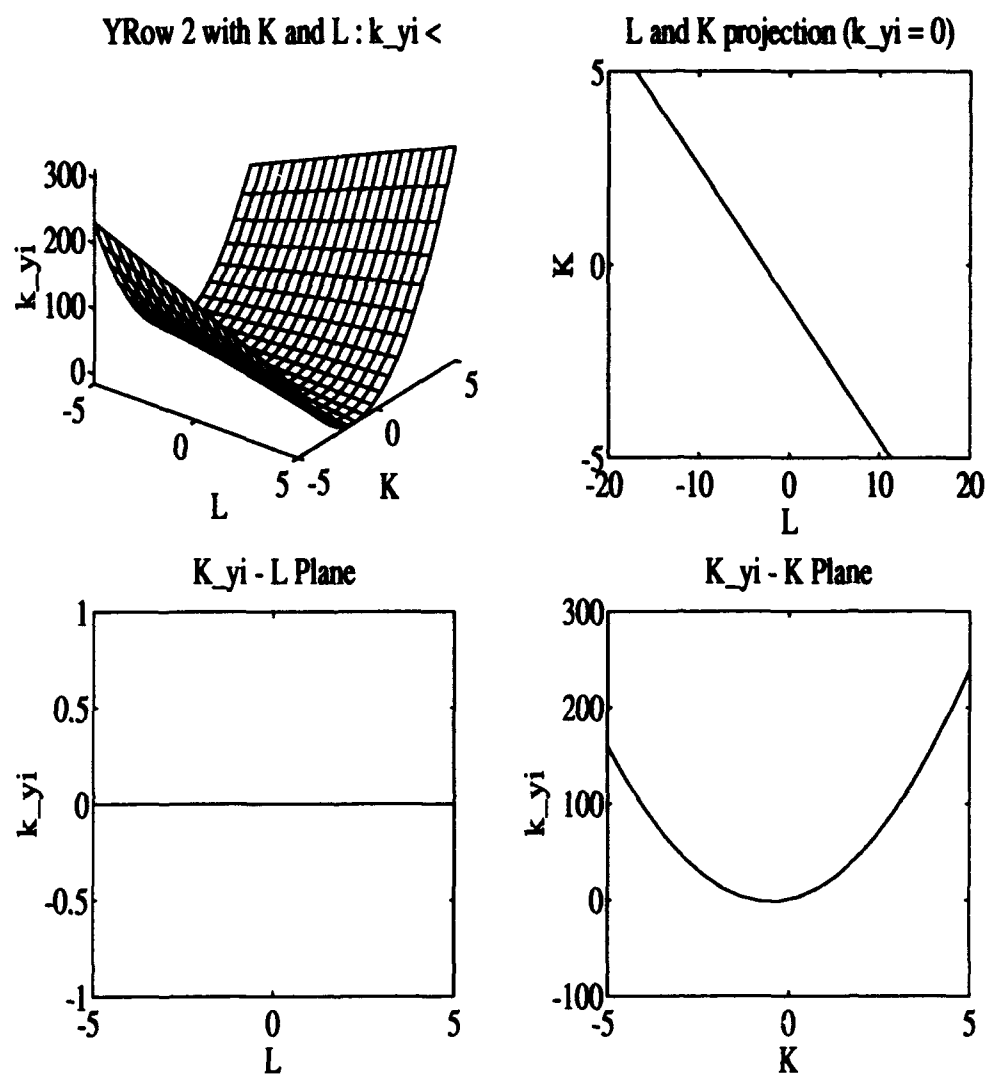


Figure C.2 Plot of the Nondimensional Y-Channel Stability Constraint for Row s^2 of the Routhian Array (Equation (4.85))

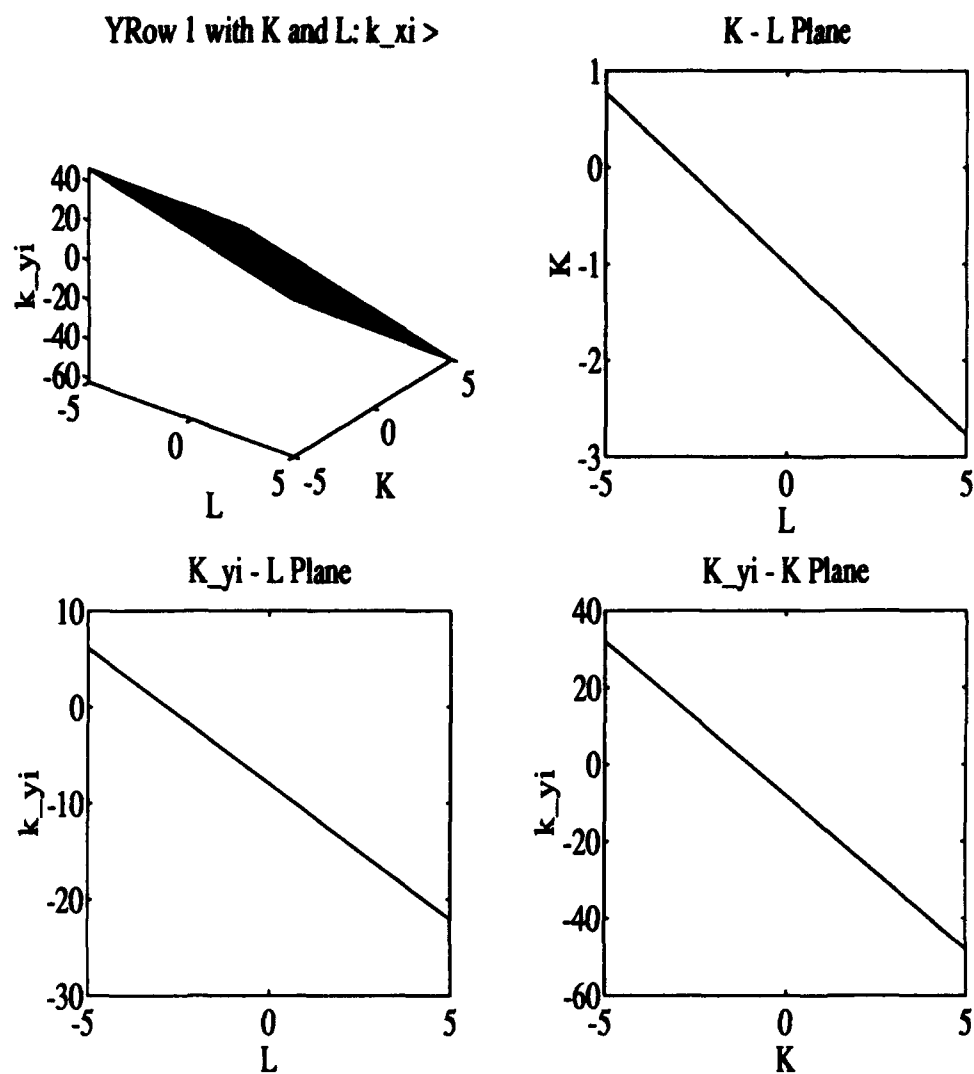


Figure C.3 Plot of the Nondimensional Y-Channel Stability Constraint for Row s^1 of the Routhian Array (Equation (4.86))

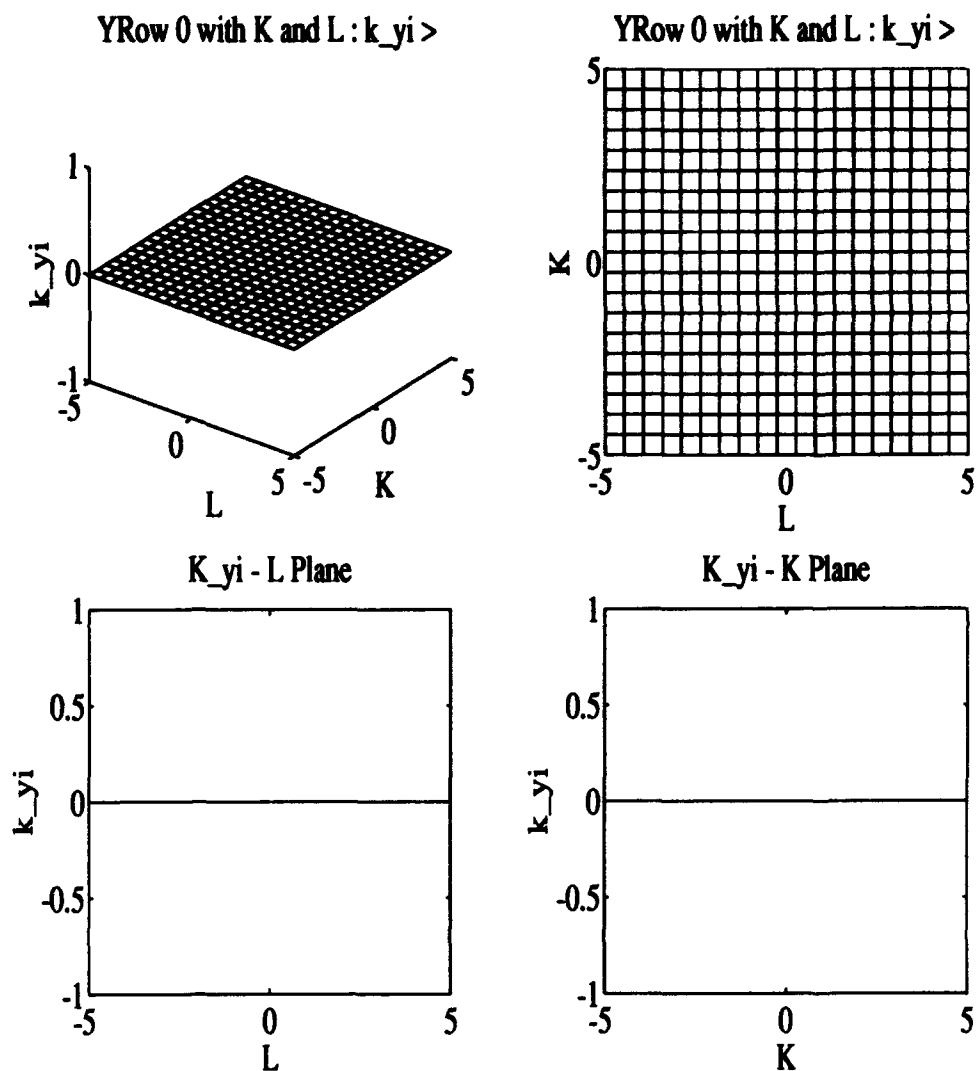


Figure C.4 Plot of the Nondimensional Y-Channel Stability Constraint for Row s^0 of the Routhian Array (Equation (4.87))

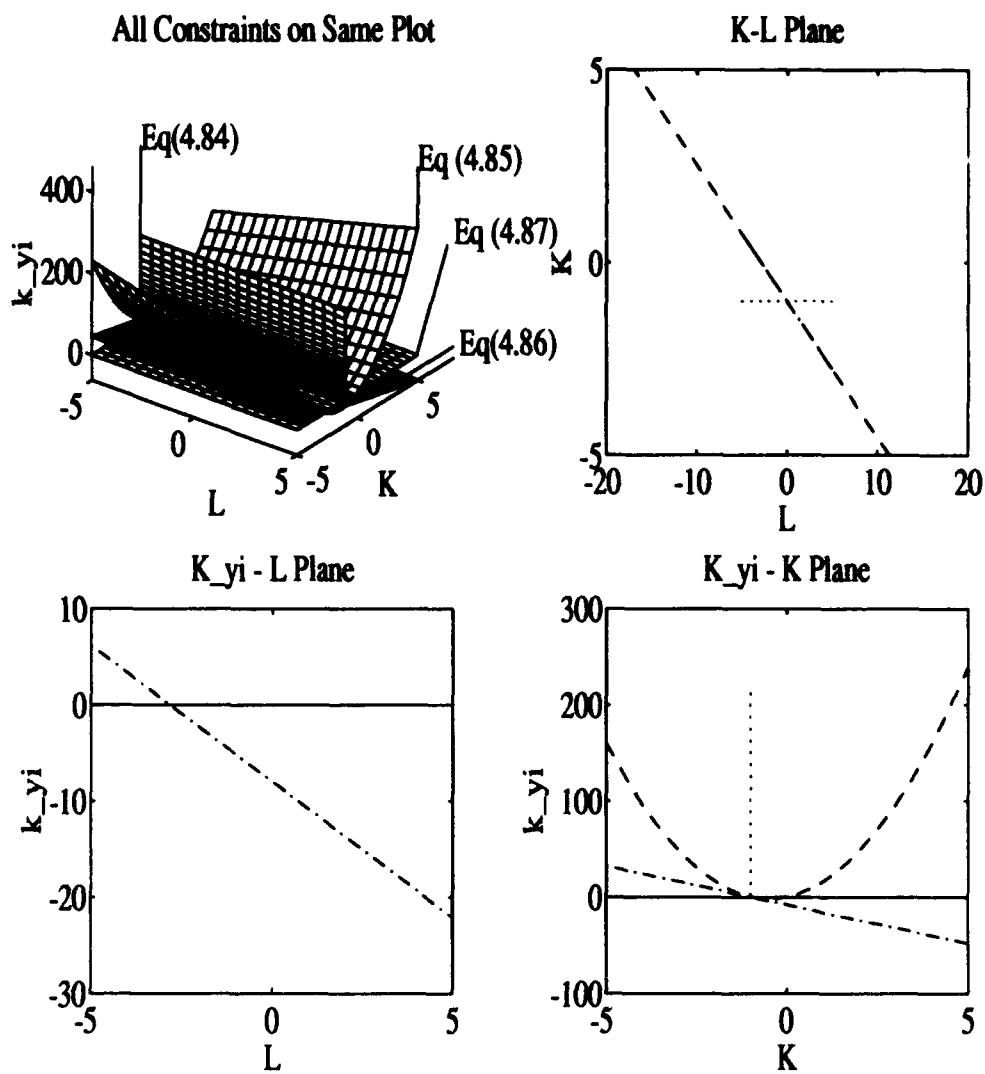


Figure C.5 All of the Nondimensional Y-Channel Stability Constraints

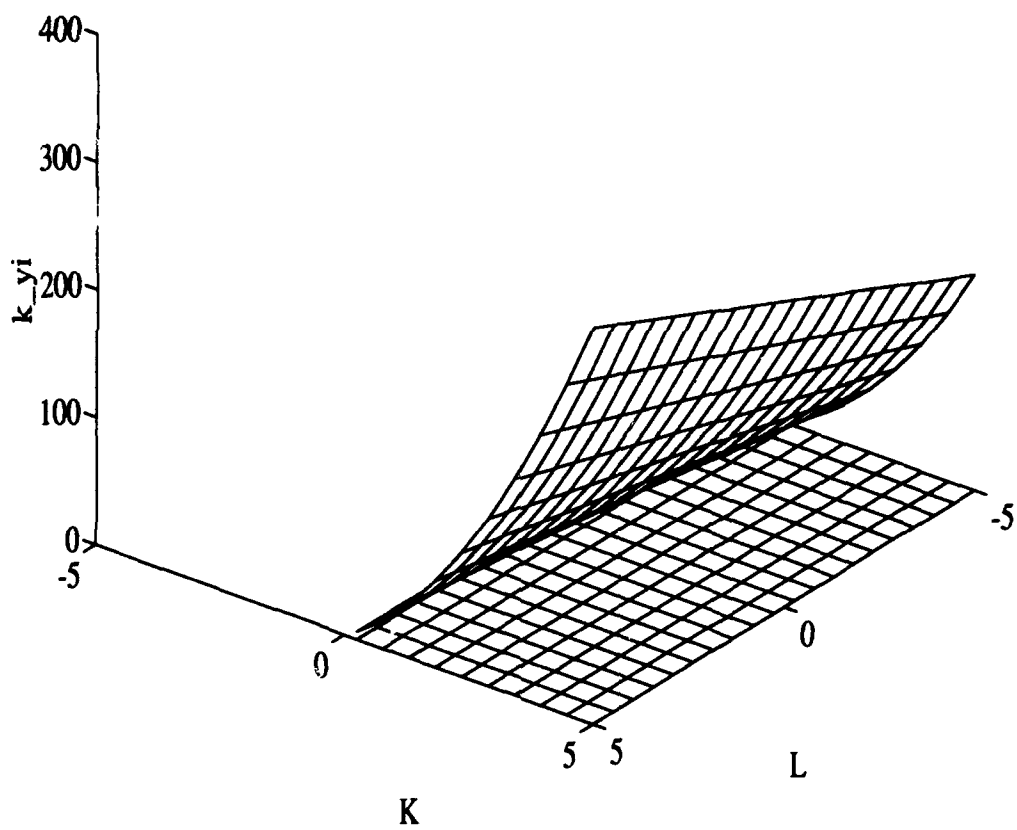


Figure C.6 Nondimensional Y-Channel Envelope: Stability Between the Surfaces

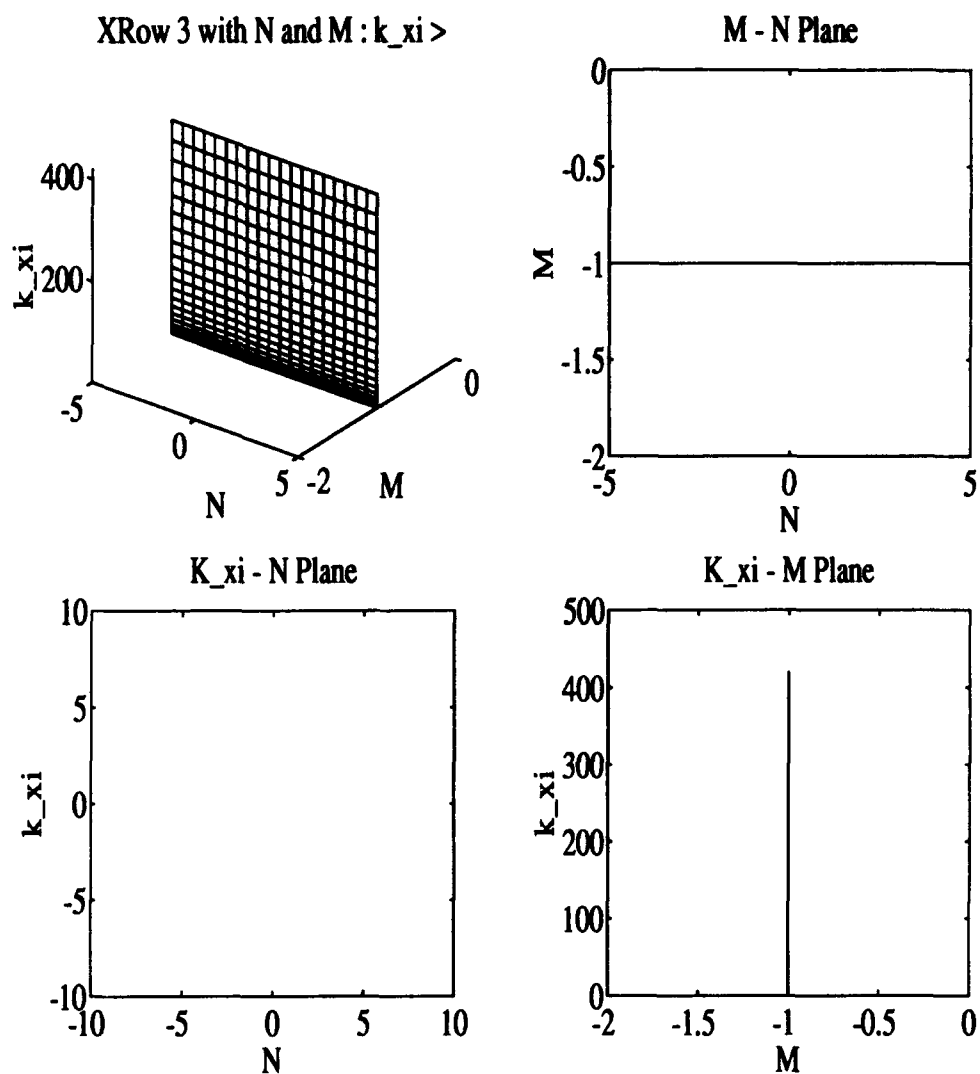


Figure C.7 Plot of the Nondimensional X-Channel Stability Constraint for Row 3 of the Routhian Array (Equation (4.88))

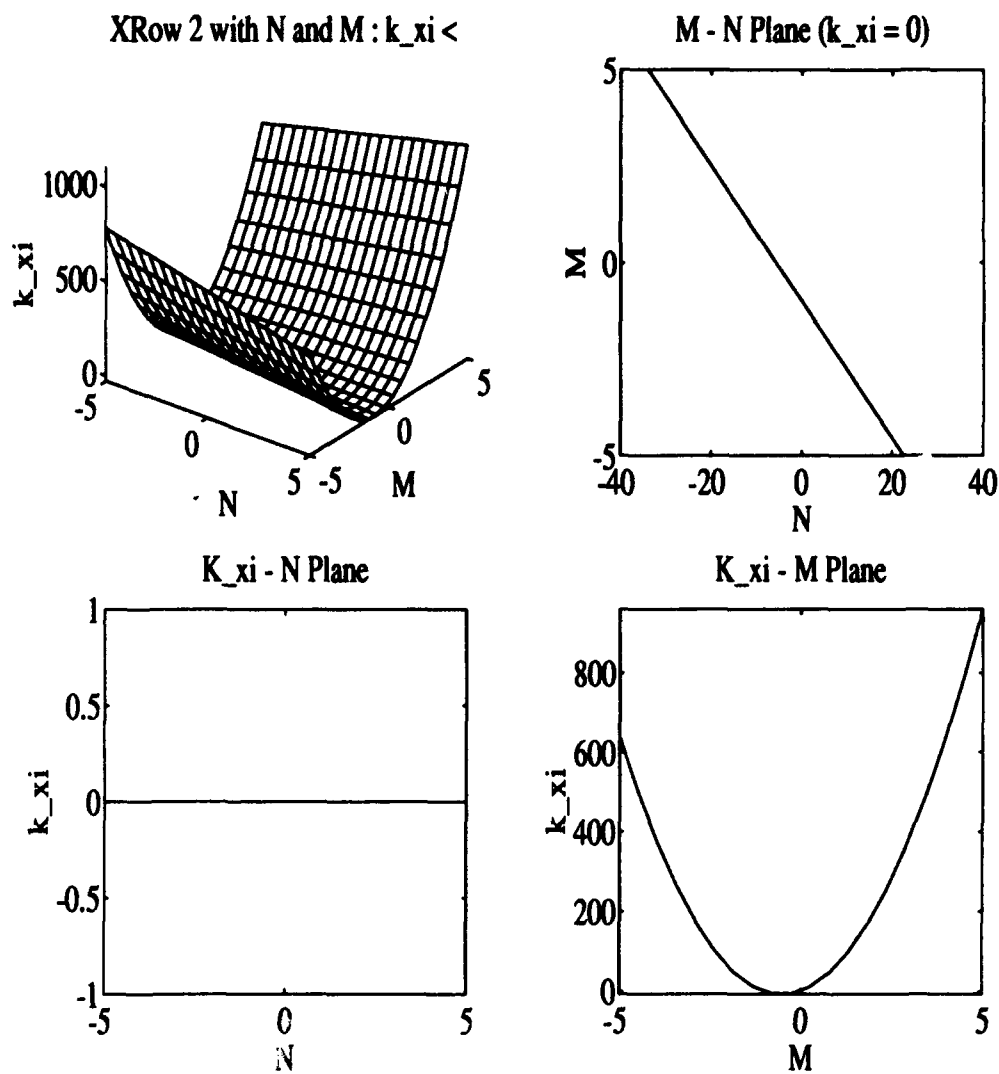


Figure C.8 Plot of the Nondimensional X-Channel Stability Constraint for Row s^2 of the Routhian Array (Equation (4.89))

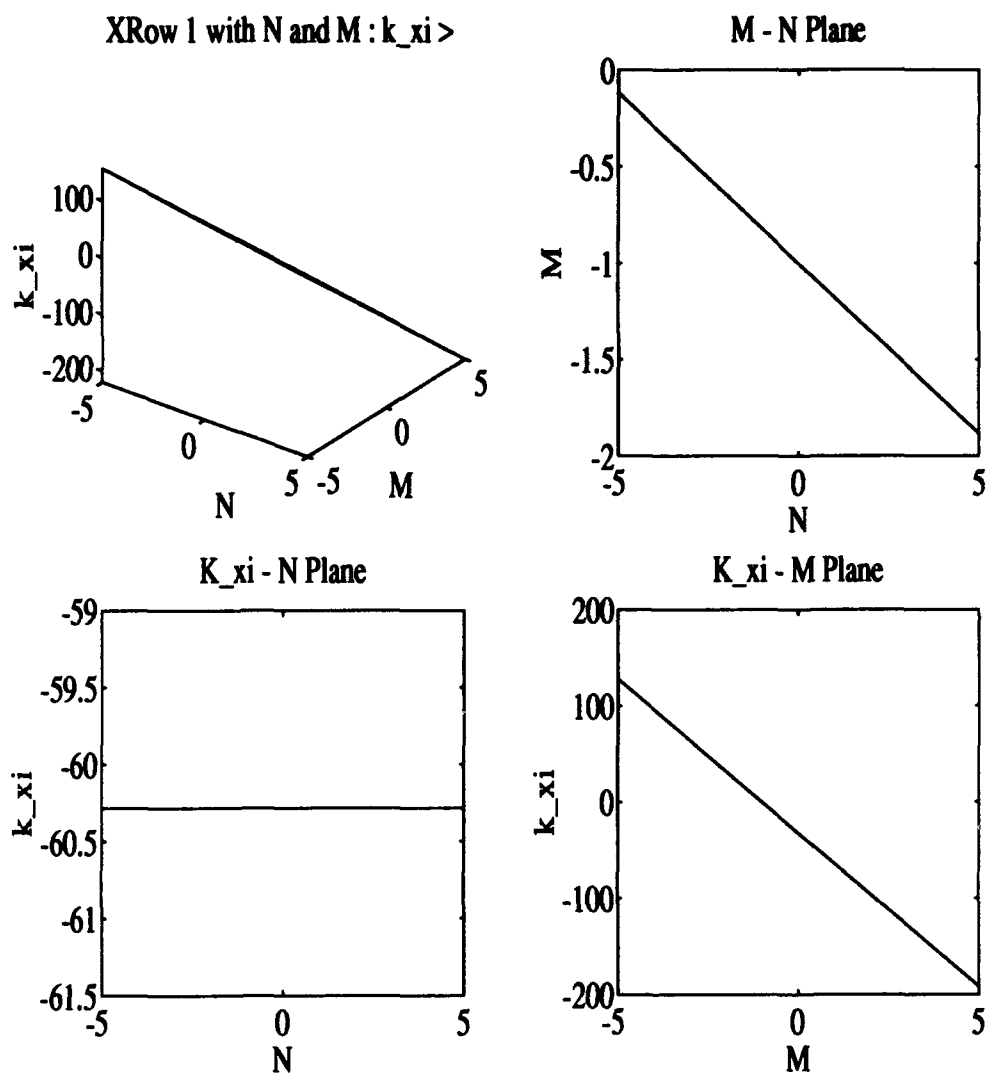


Figure C.9 Plot of the Nondimensional X-Channel Stability Constraint for Row s^1 of the Routhian Array (Equation (4.90))

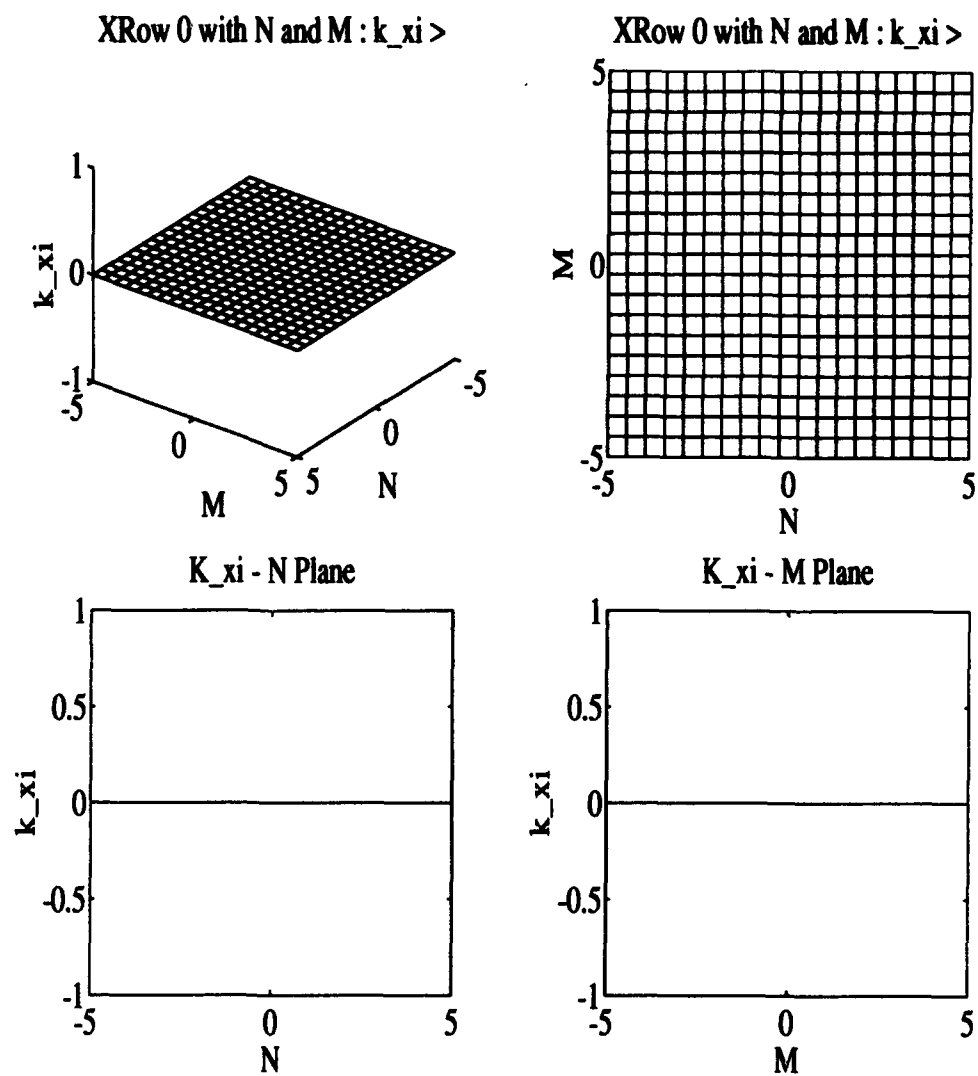


Figure C.10 Plot of the Nondimensional X-Channel Stability Constraint for Row s^0 of the Routhian Array (Equation (4.91))

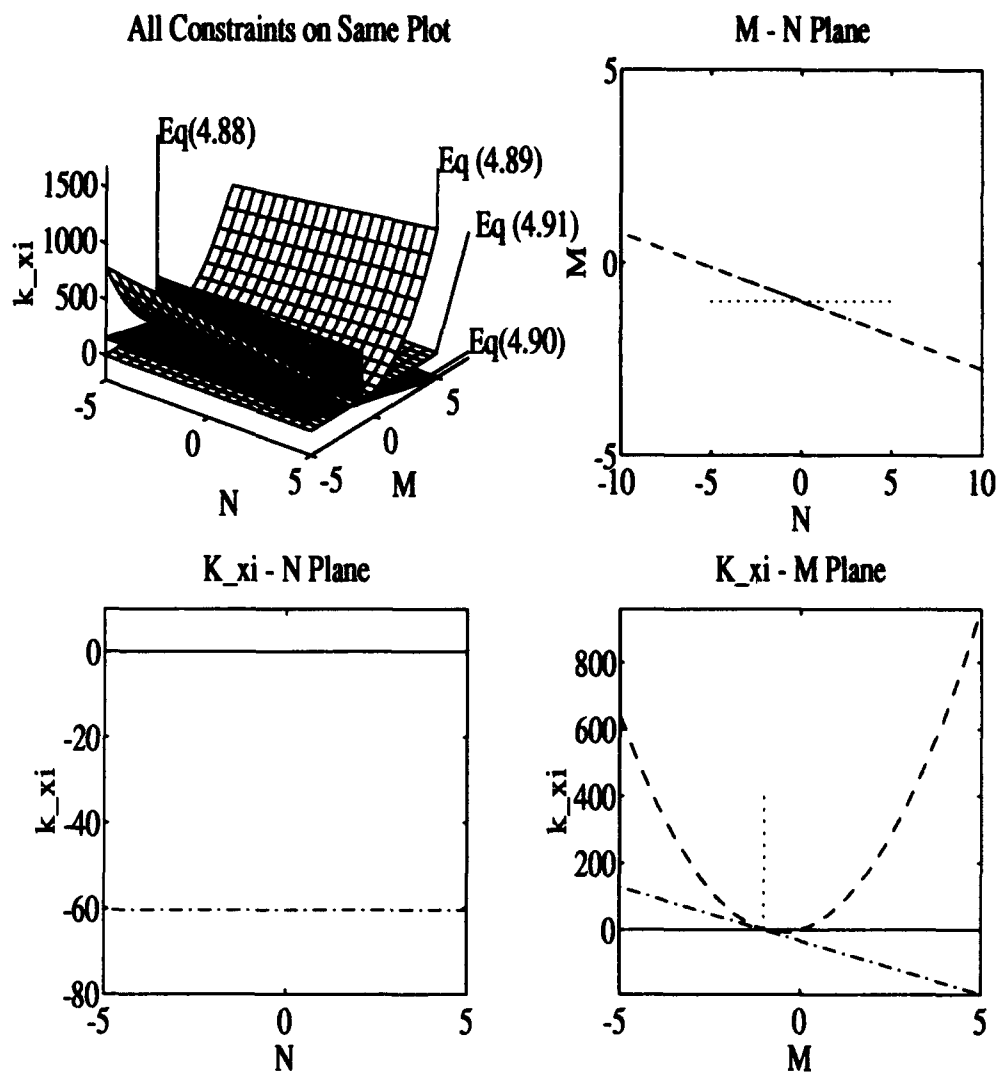


Figure C.11 All of the Nondimensional X-Channel Constraints

The Stability Envelope for the X-Channel from Another Angle

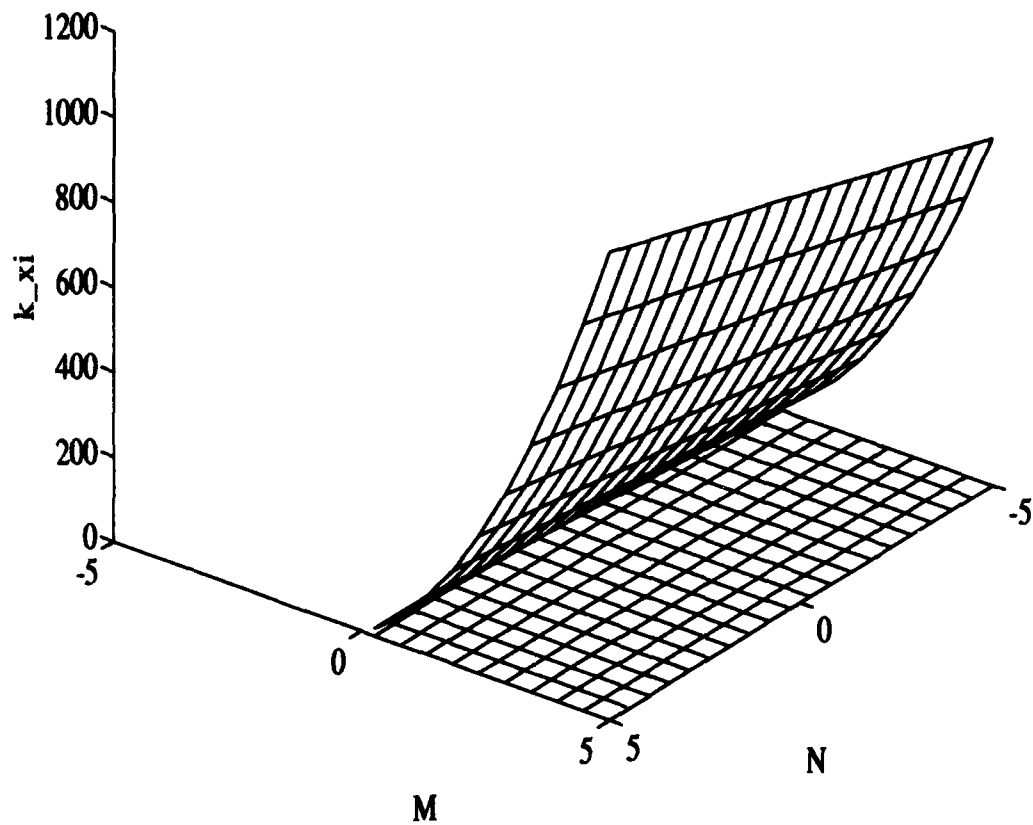


Figure C.12 Nondimensional Y-Channel Envelope: Stability Between the Surfaces

Appendix D. Energy Minimizing Maneuvers Without e_w in V_{w_c}

In Chapter V, it was determined V_{w_c} formulated without e_w provided better transient time responses and energy usage than the system including e_w . This is attributed to the assumption that there are two different parts of V_{w_c} : an energy conserving part and an energy using part. Together, they yield an energy minimizing control law. The energy conserving portion of the control law is derived with the assumption that the specific energy perturbation, e_w , is zero. However, when the PI controller is added to this energy conserving control law, the assumption that e_w remains at zero is violated since the PI controller is directly driving the e_w perturbation. Thus, the resulting model is:

$$\begin{bmatrix} \dot{x} \\ \dot{h}_w \\ \dot{e}_w \\ \dot{h}_L \\ \dot{V}_{w_c} \\ \dot{h}_{w_c} \end{bmatrix} = \begin{bmatrix} 0 & \xi & -1 & 0 & 0 & 0 \\ 0 & -\frac{1}{\tau_{hw}} & 0 & 0 & 0 & \frac{1}{\tau_{hw}} \\ 0 & \xi \left(\frac{1}{\tau_{vw}} - \frac{1}{\tau_{hw}} \right) & -\frac{1}{\tau_{vw}} & 0 & \frac{1}{\tau_{vw}} & \xi \frac{1}{\tau_{hw}} \\ 0 & 0 & 0 & -\frac{1}{\tau_{hL}} & 0 & 0 \\ -\tau_{Vw} \xi \frac{1}{\tau_{hw}} k_{zzi} & D_{hw} & D_{ew} & D_{hL} & 0 & D_{hw_c} \\ k_{zzi} & k_{zsp} \xi & -k_{zsp} \frac{\sin \alpha}{\tau_{\phi w}} & 0 & 0 & 0 \end{bmatrix} \begin{bmatrix} x \\ h_w \\ e_w \\ h_L \\ V_{w_c} \\ h_{w_c} \end{bmatrix} + \begin{bmatrix} 1 & 0 & 0 & 0 \\ 0 & 0 & 0 & 0 \\ 0 & 0 & 0 & 0 \\ 0 & \frac{1}{\tau_{hL}} & 0 & 0 \\ -\tau_{Vw} \xi \frac{1}{\tau_{hw}} k_{zsp} & k_{zsp} \frac{1}{\tau_{hL}} & -\tau_{Vw} \xi \frac{1}{\tau_{hw}} k_{zsp} \frac{\sin \alpha}{\tau_{\phi w}} & k_{zsp} \frac{\sin \alpha}{\tau_{\phi w}} \end{bmatrix} \begin{bmatrix} V_L \\ h_{Lc} \\ d_\phi \end{bmatrix} \quad (D.1)$$

$$Y_{zs} = \begin{bmatrix} 1 & 0 & 0 & 0 & 0 & 0 \\ 0 & -1 & 0 & 1 & 0 & 0 \end{bmatrix} = \begin{bmatrix} x \\ h_c \end{bmatrix} \quad (D.2)$$

where,

$$\begin{aligned} D_{hw} = & -\tau_{Vw} \xi \frac{1}{\tau_{hw}} \left(\frac{1}{\tau_{hw}} - \frac{1}{\tau_{Vw}} \right) - \tau_{Vw} \xi^2 \frac{1}{\tau_{hw}} k_{zsp} \\ & + k_{zsp} \frac{1}{\tau_{hw}} - k_{zsi} \end{aligned} \quad (D.3)$$

$$D_{e_w} = \tau_{V_w} \xi \frac{1}{\tau_{h_w}} k_{ssp} \quad (D.4)$$

$$D_{h_L} = -\frac{1}{\tau_{h_L}} k_{ssp_v} + k_{ssi_v} \quad (D.5)$$

$$D_{h_{w_c}} = \tau_{V_w} \xi \frac{1}{\tau_{h_w}} \left(\frac{1}{\tau_{h_w}} - \frac{1}{\tau_{V_w}} \right) - k_{ssp_v} \frac{1}{\tau_{h_w}} \quad (D.6)$$

and,

$X_{zz_{cl}}$ = augmented zz -channel state vector

$A_{zz_{cl}}$ = augmented zz -channel plant matrix

$\Gamma_{zz_{cl}}$ = augmented zz -channel disturbance input matrix

$D_{zz_{cl}}$ = augmented zz -channel disturbance input vector

$Y_{zz_{cl}}$ = augmented zz -channel output vector

$C_{zz_{cl}}$ = augmented zz -channel output matrix

The only difference between this model and the one in Chapter V is the coefficients D_{h_w} , D_{e_w} , D_{h_L} , and $D_{h_{w_c}}$. These are the terms which contain those expressions related to the derivative of e_w .

D.1 Static Stability Analysis

A static stability analysis has been performed upon the system with no e_w included in the V_{w_c} . This analysis is the same as in Section 5.1.2. The determined result is the same answer that the previous analysis yielded. See Equation (5.39).

D.2 Dynamic Stability Analysis

The characteristic equation is:

$$\det(SI - A_{zz_{cl}}) = s^6 + ps^5 + qs^4 + rs^3 + ts^2 + us + v \quad (D.7)$$

where the coefficients are,

$$p = \frac{1}{\tau_{hL}} + \frac{1}{\tau_{hW}} + \frac{1}{\tau_{VW}} \quad (D.8)$$

$$q = \frac{1}{\tau_{hL}\tau_{hW}} + \frac{1}{\tau_{VW}^2} + \frac{1}{\tau_{hL}\tau_{VW}} + \frac{1}{\tau_{hW}\tau_{VW}} - \frac{k_{asp}\zeta}{\tau_{hW}} \quad (D.9)$$

$$r = \frac{1}{\tau_{hL}\tau_{VW}^2} + \frac{1}{\tau_{hW}\tau_{VW}^2} - \frac{k_{asp}k_{aspv}}{\tau_{hW}\tau_{VW}} + \frac{1}{\tau_{hL}\tau_{hW}\tau_{VW}} - \frac{k_{ssi}\zeta}{\tau_{hW}} - \frac{k_{asp}\zeta}{\tau_{hL}\tau_{hW}} \quad (D.10)$$

$$t = \frac{1}{\tau_{hL}\tau_{hW}\tau_{VW}^2} - \frac{k_{ssiv}k_{asp}}{\tau_{hW}\tau_{VW}} - \frac{k_{ssi}k_{aspv}}{\tau_{hW}\tau_{VW}} - \frac{k_{asp}k_{aspv}}{\tau_{hL}\tau_{hW}\tau_{VW}} - \frac{k_{ssi}\zeta}{\tau_{hL}\tau_{hW}} \quad (D.11)$$

$$u = -\frac{k_{ssi}k_{ssiv}}{\tau_{hW}\tau_{VW}} - \frac{k_{ssiv}k_{asp}}{\tau_{hL}\tau_{hW}\tau_{VW}} - \frac{k_{ssi}k_{aspv}}{\tau_{hL}\tau_{hW}\tau_{VW}} \quad (D.12)$$

$$v = -\frac{k_{ssi}k_{ssiv}}{\tau_{hL}\tau_{hW}\tau_{VW}} \quad (D.13)$$

The Routhian array resulting from this characteristic equation is shown in Table D.1.

Table D.1 XZ-Channel Routhian Array

s^6	1	q	t	v
s^5	p	r	u	
s^4	$\frac{pq-r}{p}$	$\frac{pt-u}{p}$	v	
s^3	$\frac{pqr-r^2-p^2t+pu}{pq-r}$	$\frac{pqu-ru-p^2v}{pq-r}$		
s^2	$\frac{pqrt-r^2t-p^2t^2-pq^2u+qr^2u+2ptu-u^2+p^2qu-pru}{pqr-r^2-p^2t+pu}$	v		
s^1	$\frac{pqrtu-r^2tu-p^2t^2u-pq^2u^2+qr^2u^2+2ptu^2-u^3-pqr^2u+r^2u+p^2rtu+2p^2quu-3pruu-p^3u^2}{pqrt-r^2t-p^2t^2-pq^2u+qr^2u+2ptu-u^2+p^2qu-pru}$			
s^0	v			

The resulting stability equations resulting from applying the Routh Stability Criterion to Table D.1 are:

row s^5

$$\tau_{hL}\tau_{hW} + \tau_{hL}\tau_{VW} + \tau_{hW}\tau_{VW} > 0 \quad (D.14)$$

row s^4

$$\begin{aligned}
 & \tau_{h_L}^2 \tau_{h_W}^2 + \tau_{h_L}^2 \tau_{h_W} \tau_{V_W} + \tau_{h_L} \tau_{h_W}^2 \tau_{V_W} + \tau_{h_L}^2 \tau_{V_W}^2 \\
 & + 2\tau_{h_L} \tau_{h_W} \tau_{V_W}^2 + k_{ssp} k_{ssiv} \tau_{h_L}^2 \tau_{h_W} \tau_{V_W}^2 + \tau_{h_W}^2 \tau_{V_W}^2 \\
 & + \tau_{h_L} \tau_{V_W}^3 + \tau_{h_W} \tau_{V_W}^3 - k_{ssp} \tau_{h_L}^2 \tau_{h_W} \tau_{V_W}^2 \xi \\
 & - k_{ssp} \tau_{h_L}^2 \tau_{V_W}^3 \xi + k_{ssi} \tau_{h_L}^2 \tau_{h_W} \tau_{V_W}^3 \xi > 0
 \end{aligned} \tag{D.15}$$

rows $s^3 - s^1$ are too complex and large to include

row s^0

$$k_{ssi} k_{ssiv} > 0 \tag{D.16}$$

In this case, where e_W is absent from V_{W_c} , integral control action is required for both zero steady-state error and transient or dynamic stability.

Bibliography

1. Blakelock, John H. *Automatic Control of Aircraft and Missiles* (Second Edition). John Wiley & Sons, Inc., 1991.
2. Buzogany, Louis E. *Automated Control of Aircraft in Formation Flight*. MS thesis, School of Engineering, Air Force Institute of Technology (AU), Wright-Patterson AFB OH, December 1992.
3. Buzogany, Louis E., M. Pachter and J.J. D'Azzo. *Automated Control of Aircraft in Formation Flight*. 1993 AIAA Guidance, Navigation, and Control Conference, Monterrey, Ca.
4. Dargan, John L. *Proportional Plus Integral Control of Aircraft for Automated Maneuvering Formation Flight*. MS thesis, School of Engineering, Air Force Institute of Technology (AU), Wright-Patterson AFB OH, December 1991.
5. D'Azzo, John J. and Constantine H. Houpis. *Linear Control System Analysis and Design* (Third Edition). McGraw-Hill Book Company, 1988.
6. Kindle, Joseph H. *Schaum's Outline Series: Theory and Problems of Plane and Solid Analytic Geometry*. Schaum Publishing Company, 1950.
7. Mathematica 2.0 for SPARC. Copyright 1988-91. Wolfram Research, Inc.
8. Nelson, Robert C. *Flight Stability and Automatic Control*. McGraw-Hill Book Company, 1989.
9. Personal Interviews with Dr. Meir Pachter, Associate Professor of Electrical Engineering, Department of Electrical and Wright-Patterson Air Force Base Oh. February AFIT/ENG Computer Engineering, Air Force Institute of Technology.
10. Rohs, Paul R. *A Fully Coupled, Automated Formation Control System for Dissimilar Aircraft in Maneuvering, Formation Flight*. MS thesis, School of Engineering, Air Force Institute of Technology (AU), Wright-Patterson AFB OH, March 1991.
11. Telephone Interview with Mr Bill Young, WL/FIGX, February 1993.

Vita

Vince Reyna was born in San Antonio, Texas. He grew up there and attended high school at Antonian College Preparatory. Upon graduation he attended the United States Air Force Academy and received a Bachelor of Science in Astronautical Engineering. His first duty station was Wright-Patterson Air Force Base. He was assigned to the Flight Stability and Control Branch, Flight Technology Division, Flight Systems Directorate, DCS Engineering from 1 September 1990 to 21 May 1992. While there, he worked several flight control issues concerning F-16, B-1B, C-141B, and VISTA NF-16 aircraft. He married Lorraine Haley in November of 1991. In May of 1992, he entered the Air Force Institute of Technology, Wright-Patterson Air Force Base, in pursuance of a Master of Science Degree in Electrical Engineering.

Permanent address: 4953D Westmoreland Ct.
Riverside, Oh, 45431

REPORT DOCUMENTATION PAGE			REPORT NUMBER AFIT/GE/ENG/94M-01	
1. AGENCY USE ONLY (Leave blank)		2. REPORT DATE December 1993		3. REPORT TYPE AND DATES COVERED Master's Thesis
4. TITLE AND SUBTITLE AUTOMATION OF FORMATION FLIGHT CONTROL				5. FUNDING NUMBERS
6. AUTHOR(s) Vincent P. Reyna, First Lieutenant, USAF				
7. PERFORMING ORGANIZATION NAME(S) AND ADDRESS(ES) Air Force Institute of Technology, WPAFB OH 45433-6583				8. PERFORMING ORGANIZATION REPORT NUMBER AFIT/GE/ENG/94M-01
9. SPONSORING MONITORING AGENCY NAME(S) AND ADDRESS(ES) Capt. Steve Rasmussen WL/FIGS 2210 Eighth St Ste 11 Wright-Paterson AFB, OH 45433				10. SPONSORING MONITORING AGENCY REPORT NUMBER
11. SUPPLEMENTARY NOTES				
12a. DISTRIBUTION AVAILABILITY STATEMENT Approved for public release; distribution unlimited				12b. DISTRIBUTION CODE
13. ABSTRACT (Maximum length) The research contained in this thesis explores the concepts of Automated Formation Flight Control documented in three previous AFIT theses. The generic formation analyzed consists of a Leader and Wingman, with the Wingman referencing its maneuvers off of Leader maneuvers. Specifically, planar formation flight control concerning only heading and velocity changes is considered. Next, the vertical separation constraint is relaxed to allow wing maneuvers outside of the flight plane of the lead in order to minimize the energy expended by the wing in a maneuver. Analysis of the two forms of formation flight control investigated in this thesis reveals the close relationship between formation geometry, aircraft time constants, controller gains, formation performance, and control system stability. Integral control action is determined to be necessary for formation flight control. Nonlinear simulations are accomplished on a digital computer to validate the analysis of the automated formation flight control system. Comparisons are made between the two forms of formation flight control considered, and a third, energy conserving maneuvers, in order to determine which is best for each phase of flight.				
14. SUBJECT TERMS Formation Flight Control, Energy Minimizing Maneuvers, Energy Excursion Minimizing Maneuvers, Planar Maneuvers, Two Dimensional Maneuvers				15. NUMBER OF PAGES 191 16. PRICE CODE
17. SECURITY CLASSIFICATION OF REPORT Unclassified	18. SECURITY CLASSIFICATION OF THIS PAGE Unclassified	19. SECURITY CLASSIFICATION OF ABSTRACT Unclassified	20. LIMITATION OF ABSTRACT UL	